Regulation of type IV pili localization in *Myxococcus xanthus*

Dissertation
zur Erlangung des Doktorgrades
der Naturwissenschaften
(Dr. rer. nat.)

dem
Fachbereich Biologie
der Philipps-Universität Marburg
vorgelegt von

Iryna Bulyha
aus Minsk, Weißrussland

Marburg / Lahn, April 2010

Die Untersuchungen zur vorliegenden Arbeit wurden von Oktober 2006 bis Februar 2010 am Max-Planck-Institut für terrestrische Mikrobiologie unter der Leitung von Prof. MD, PhD Lotte Søgaard-Andersen durchgeführt.

Vom Fachbereich Biologie der Philipps-Universität Marburg als
Dissertation am:
_____ angenommen

Erstgutachter: Prof. MD, PhD Lotte Søgaard-Andersen
Zweitgutachter: Prof. Dr. Martin Thanbichler

Tag der mündlichen Prüfung:

Die während der Promotion erzielten Ergebnisse sind zum Teil in folgender Orginalpublikationen veröffentlicht:

Bulyha I., Schmidt C., Lenz P., Jakovljevic V., Höne A., Maier B., Hoppert M., , Søgaard-Andersen L., (2009) Regulation of the type IV pili molecular machine by dynamic localization of two motor proteins. *Mol Microbiol.* **74**: 691-706.

Leonardy S., Miertzschke M., **Bulyha I**., Sperling E., Wittinghofer A., Søgaard-Andersen L., (2010) Regulation of dynamic polarity switching in bacteria by a Ras-like G-protein and its cognate GAP. *in review*

Die Ergebnisse dieser Arbeit, wie auch anderer Arbeiten auf demselben Gebiet, wurden während der Dissertation in folgendem Review diskutiert:

Leonardy, S., **Bulyha I.,** Søgaard-Andersen L., (2008) Reversing cells and oscillating motility proteins. *Mol Biosyst* **4**: 1009-1014.

Table of contents

Abstract

Myxococcus xanthus cells are rod-shaped and move in the direction of their long axis, using two distinct motility systems. The S-motility system is type IV pili (T4P)-dependent. T4P are dynamic structures, localized at the leading cell pole and undergo extension/retraction oscillations. Upon retraction T4P generate a mechanical force, large enough to pull a cell forward. Regulation of T4P extension/retraction dynamics relies on two motor proteins, PilB and PilT, which are members of the superfamily of secretion ATPases. PilT is the only protein required for retraction. Genetic and biochemical analyses suggest that PilB and PilT function antagonistically and that ATP hydrolysis by PilB provides the energy for T4P extension, while the energy for T4P retraction is provided by ATP hydrolysis by PilT. How the activities of PilB and PilT are regulated to provide temporal separation of T4P extension and retraction is not known. Although several models have been proposed, it is still not clear how mechanical force is generated in the second motility system, the A-motility system.

As *M. xanthus* cells move over a surface, they occasionally stop and then resume gliding in opposite direction, with the old lagging pole becoming the new leading pole and *vice versa*. The Frz chemosensory system regulates the reversal frequency. Importantly, during reversals the two motility systems change their polarity synchronously. To investigate the molecular mechanisms underlying T4P extension/retraction and T4P pole-to-pole oscillations during a reversal, the cellular localization of six conserved T4P proteins (PilB, PilT, PilQ, PilC, PilN and PilM) was determined. These six proteins in combination localize to three different subcellular compartments – the outer membrane, inner memrane and cytoplasm. We found that PilB, PilT, PilQ, PilC, PilN and PilM localized in three distinct polar patterns. The outer membrane secretin PilQ, the inner membrane proteins PilC and PilN and the MreB/FtsA-like cytoplasmic protein PilM localized to both poles in a symmetric pattern. Notably, this pattern did not change during reversals. Moreover, no differences in the localization of PilQ, PilC, PilN and PilM were observed in the absence of an active Frz system. Thus, we propose that PilQ, PilC, PilN and PilM are stationary T4P components, which do not oscillate from pole to pole during cellular reversal. Furthermore, we found that the cytoplasmic proteins PilB and PilT localized to the opposite poles. PilB, the extension motor, localized predominantly at the piliated cell pole, whereas PilT, the retraction motor, predominantly at the non-piliated cell pole. Using time-lapse microscopy, we directly observed pole-to-pole relocation of YFP-PilT during cellular reversals, which did not occur in the absence of the Frz system. We also

observed clear differences in the PilB localization in the WT and in a *frz* mutant. In WT, three distinct PilB localization patterns were observed in immunofluorescence microscopy with anti-PilB antibodies: unipolar (40% of cells), bipolar asymmetric (35%) and bipolar symmetric (25%). In a *frz* mutant, however, the ratio shifted towards bipolar symmetric localization. We conclude that the molecular motors PilB and PilT are dynamic T4P components and oscillate between poles during reversals. Hence, T4P pole-to-pole oscillations in *M. xanthus* involve the disassembly of T4P machinery at one pole and reassembly of this machinery at the opposite pole. In addition, YFP-PilT displayed noisy accumulation at the piliated pole between reversals, and FRAP experiments revealed rapid turnover of YFP-PilT in the polar clusters between reversals. Taken together, these observations suggest that the spatial separation of PilB and PilT in combination with the noisy PilT accumulation at the piliated pole allow the temporal separation of extension and retraction.

The Frz system regulates the dynamic localization of PilB and PilT during reversals. In addition, we found that the Ras-like GTPase MglA and its paralog SofG regulate the correct polarity of PilB and PilT. Specifically, we found that MglA is a nucleotide-dependent molecular switch that establishes correct PilT polarity and regulates its dynamic localization during reversals. SofG is required for establishing the correct localization/polarity of PilB and PilT and also inhibits T4P assembly at the lagging cell pole.

Zusammenfassung (German)

Die stäbchenförmigen Zellen des Bakteriums *Myxococcus xanthus* bewegen sich mit Hilfe zweier verschiedener Fortbewegungssysteme entlang ihrer Längsachse. Die S-Bewegung stellt eine Type IV Pili (T4P)-abhängige Bewegung dar. T4P sind sehr dynamische Strukturen, welche an dem vorderen Pol der Zelle lokalisieren und dort Zyklen der Extension/Retraktion vollziehen. Die Retraktion der T4P erzeugt genügend Energie um eine Zelle vorwärts zu ziehen. Die Extensions/Retraktions Zyklen werden über die zwei Motorproteine, PilB und PilT reguliert. Beide Proteine gehören zu der Superfamilie von Sekretions ATPasen. Für die Retraktion von T4P wird ausschließlich die PilT ATPase benötigt. Genetische und biochemische Analysen deuten darauf hin, dass PilB und PilT antagonistisch arbeiten, wobei die ATP Hydrolyse von PilB die Energie für die T4P Extension liefert, während die ATP Hydrolyse von PilT die Energie für die T4P die Retraktion bereitstellt. Die A-Bewegung befähigt die Zellen eine individuelle und von anderen Zellen unabhängige Vorwärtsbewegung auszuführen. Der molekulare Mechanismus, mit dem die Bewegung mittels des A-Systems generiert wird, ist weitgehend unbekannt. Derzeit sind zwei verschiedene Modelle für das A-Bewegungssystem beschrieben.

M. xanthus Zellen wechseln regelmäßig die Richtung ihrer Bewegung, wobei der alte vordere Pol zum neuen hinteren Zellpol wird und umgekehrt. Die Frequenz der Richtungswechsel wird durch das chemosensorische Frz System geregelt. Während eines Richtungswechsels müssen die beiden Bewegungsmaschinerien synchron ihre Polarität innerhalb der Zelle ändern, um eine erneute Vorwärtsbewegung in die entgegengesetzte Richtung zu garantieren. Um den molekularen Mechanismus, welcher die T4P Extensions/Retraktions Zyklen und den Polaritätswechsel der T4P während eines Richtungswechsels reguliert, zu erforschen wurde die Lokalisierung von sechs konservierten T4P Proteinen (PilB, PilT, PilQ, PilC, PilN und PilM) analysiert. Diese Proteine weisen eine subzelluläre Lokalisierung in drei verschiedenen Kompartimenten auf: in der äußeren Membran, der inneren Membran und im Zytoplasma. In dieser Arbeit konnte gezeigt werden, dass die sechs Proteine jeweils drei verschiedene Lokalisierungsmuster aufweisen.

Das in der äußeren Membran sitzende Sekretin PilQ, die Proteine PilC und PilN in der inneren Membran, wie auch das cytoplasmatische MreB/FtsA-ähnliche PilM lokalisieren alle symmetrisch an beiden Zellpolen. Wird das Frz System inaktiviert, so ändert sich die Lokalisierung der Proteine nicht. Aus diesem Grund vermuten wir, dass PilQ, PilC, PilN und PilM stationäre T4P Komponenten darstellen, welche ihre Lokalisierung zwischen den Polen während eines Richtungswechsels nicht verändern.

Interessanterweise zeigten die Lokalisierungsstudien von PilB und PilT, dass die beiden Proteine an gegenüberliegenden Polen lokalisieren. Während die PilB ATPase, welche die Extension der T4P vermittelt, hauptsächlich am vorderen Zellpol lokalisiert, an dem sich ebenfalls die T4P befinden, lokalisiert die für die Retraktion verantwortliche PilT ATPase hauptsächlich am hinteren Pol, welcher keine T4P aufweist. Mithilfe von Timelapse-Mikroskopie konnte gezeigt werden, dass die Lokalisierung von YFP-PilT zwischen den Polen während eines Richtungswechsels ebenfalls wechselt. Des Weiteren konnte gezeigt werden, dass dieser Lokalisierungswechsel nicht in Abwesenheit des Frz Systems erfolgt. Der Vergleich der Lokalisierung von PilB in WT Zellen mit der in einer Frz Mutante weist deutliche Unterschiede auf. In mit WT Zellen durchgeführten Immunfluoreszenz-Analysen weist PilB drei verschiedene Lokalisierungsmuster auf: eine unipolare Lokalisierung (40% der Zellen), eine asymmetrische Lokalisierung an beiden Polen (35% der Zellen), wie auch eine symmetrische Lokalisierung an beiden Zellpolen (25% der Zellen). In der Frz Mutante hingegen tendiert PilB vermehrt dazu symmetrisch an beiden Polen zu lokalisieren. Zusammengefasst, lässt sich schlussfolgern, dass die beiden molekularen Motorproteine PilT und PilB die dynamische T4P Komponente darstellen und beide eine dynamische Lokalisierung zwischen den Polen während eines Richtungswechsels vollziehen. Demnach lokalisieren einige Komponenten der T4P stationär an beiden Polen, während andere Komponenten (PilT und PilB) dynamisch zwischen den Polen lokalisieren. Dementsprechend würde die Relokalisierung der T4P zwischen den Polen auf der dynamischen Lokalisierung von T4P Komponenten PilB und PilT basieren. Des Weiteren konnte in dieser Arbeit gezeigt werden, dass YFP-PilT ebenfalls eine schwankende Lokalisierung an dem T4P befindlichen Pol zwischen zwei Richtungswechseln aufweist. FRAP Experimente zeigten, dass es einen rasanten Ausstausch von YFP-PilT zwischen den Polen während eines Richtungswechsels gibt. Die genannten Beobachtungen deuten darauf hin, dass die zeitliche Trennung von Retraktion und Extension der T4P auf der räumlichen Trennung von PilT und PilB basiert, wie auch auf der schwankenden Lokalisierung von PilT am vorderen Pol.

In dieser Arbeit konnte gezeigt werden, dass das Frz System die dynamische Lokalisierung von PilB und PilT beeinflusst. Jedoch gibt es weitere Proteine die diesen Prozess regulieren. Zu nennen sind hierbei die kleine Ras-ähnliche GTPase MglA und sein Paralog SofG, welche die korrekte Polarität von T4P Komponenten und auch die T4P Relokalisierung zwischen den Polen regulieren. Des Weiteren deuten unsere Ergebnisse darauf hin, dass SofG die unipolare T4P Lokalisierung an dem vorderen Zellpol inhibiert.

Abbreviations

bp	Base pairs
BSA	Bovine serum albumin
cDNA	Single-stranded complementary DNA
Cm	Chloramphenicol
CTT	Casitone Tris medium
ECM	Extracellular matrix
EPEC	Enteropathogenic *E. coli*
EPS	Exopolysaccharides
FRAP	Fluorescence recovery after photobleaching
GDP/GTP	Guanosine di- /Guanosine triphosphate
h	Hours
IPTG	Isopropyl β-D-1-thiogalaktopyranoside
Km	Kanamycin
min	Minutes
s	seconds
SDS-PAGE	Sodium dodecyl sulfate polyacrilamide gel electrophoresis
T4P	Type IV pili
YFP	Yellow fluorescent protein
WT	Wild type

1 Introduction

The emergence of a complex multicellular organism requires the ability of millions of cells to cooperate. One fascinating example of such cooperation is coordinated cell migration which is essential in processes such as development of the neural system during embryogenesis, establishment of immunity/development and maturation of the immune system (Laird *et al.*, 2008), or pathologies such as tumorogenesis and metastasis. Coordinated cell migration in simple organisms has been extensively studied in an attempt to extract principles that could be applied to more complex systems. An example is provided by the studies of the slime mold *Dictyostelium discoidum*, which have established the principles of motility and chemotaxis applicable to mammalian leukocyte migration (Insall and Andrew, 2007).

Prokaryotes are also capable of complex multicellular behaviors. One example is bacterial biofilms, in which bacteria differentiate into specialized cell types contributing distinct functions to the microcommunity (Vlamakis *et al*., 2008). A different example of prokaryotic multicellular morphogenesis is found in the myxobacteria, which form multicellular fruiting bodies in response to starvation. *Myxococcus xanthus* has emerged as the model organism to understand the mechanisms underlying fruiting body formation. *M. xanthus* is a Gram-negative, soil *δ*-proteobacterium and has a complex life cycle that includes vegetative growth, predatory behavior and differentiation culminating in the production of spores inside mature fruiting bodies (Figure 1-2). All these processes require that cells are motile and that thousands of cells coordinate their motility. Thus, *M. xanthus* represents a powerful model system to study coordinated cell migration in a prokaryotic system. This study focuses on the regulation of directed cell movement in *M. xanthus* and how this is accomplished through the tight regulation of the localization of molecular machines.

1.1 Life cycle of *Myxococcus xanthus*

M. xanthus cells grow by scavenging nutrients from decomposing detritus or by predation on other microorganisms (Kaiser, 2003, 2006; Shimkets, 1999). Clustering of cells into organized groups facilitates predation and food gathering, because numerous bacterial cells can cooperate to produce antibiotics and digestive enzymes (Rosenberg *et al*., 1977). These antibiotics and lytic enzymes kill and digest prokaryotic and eukaryotic microorganisms (Zusman *et al*., 2007). The social lifestyle of *M. xanthus* crucially depends on the ability of cells to display active movements. *M. xanthus* cells move by gliding motility (described in details in Chapter 1.2). If present on a solid surface at a high cell density, *M. xanthus* cells self-organize into three morphologically

distinct spatial patterns, known as spreading colonies, ripples and fruiting bodies (Dworkin, 1996; Konovalova *et al*., 2010) (Figure 1). The pattern formed largely depends on the nutritional status of cells.

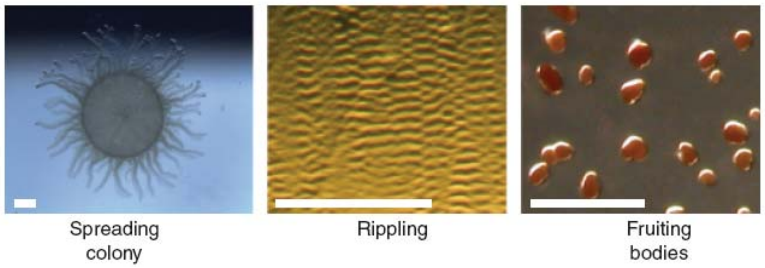

Figure 1. The three cellular patterns formed by *M. xanthus* cells.

Scale bars=1 mm.

The figure is reproduced from Konovalova *et al*. (Konovalova *et al.*, 2010)

In the presence of nutrients, the motile, rod-shaped cells grow, divide and form spreading colonies. At the edge of the colony cells spread coordinately over the surface, forming a thin, film-like structure. Once nutrients are depleted, the spreading behavior is constrained, cells start to aggregate and initiate the developmental programme that culminates in the formation of spore-filled fruiting bodies. Fruiting body formation proceeds in distinct morphological stages that are separated in time and space. During this process, the patterns of cell movements are highly regulated. The first signs of fruiting bodies formation are evident after 4-6 h of starvation as cells aggregate to form small aggregation centres (Figure 2). As they accumulate more cells, the centres increase in size and eventually become mound-shaped (Figure 2).

By 24 h, the aggregation process is complete and each nascent fruiting body contains approximately 10^5-10^6 densely packed cells (Konovalova *et al.*, 2010; Zusman *et al.*, 2007). Inside fruiting bodies rod-shaped cells undergo morphological and physiological differentiation into spherical myxospores, leading to the formation of mature fruiting bodies. Spore maturation is finished approximately 72 h after onset of starvation. Interestingly, only 1 to 3% of cells from the initial starving population differentiate into spores inside fruiting bodies (Sogaard-Andersen *et al.*, 1996). However, some rod-shaped cells (up to 30%), referred to as peripheral rods, are present around and between fruiting bodies (O'Connor and Zusman, 1991a, b) (Figure 2). The remaining cells (around 80% of the population) undergo cell lysis (Nariya and Inouye, 2008; Rosenbluh *et al.*, 1989; Wireman and Dworkin, 1977).

Aggregation and sporulation are two invariable morphological processes in fruiting body formation. Under less stringent starvation conditions (Shimkets and Kaiser, 1982) or in the presence of prey (Berleman *et al.*, 2006; Berleman and Kirby, 2007), *M. xanthus* cells organize into a third cellular pattern referred to as rippling.

Rippling is coordinated rhythmic movement of cells that creates “accordion waves”, in which cells seem to form travelling waves (Figure 1). Microscopic examination of rippling cells has shown that individual cells essentially oscillate back and forth, suggesting that colliding waves reflect off of each other (Sager and Kaiser, 1994; Sliusarenko *et al.*, 2006; Welch and Kaiser, 2001). Rippling is typically initiated before aggregation. Later, during the aggregation process, the wave structure disintegrates and cells aggregate into the nascent fruiting bodies (Konovalova *et al.*, 2010).

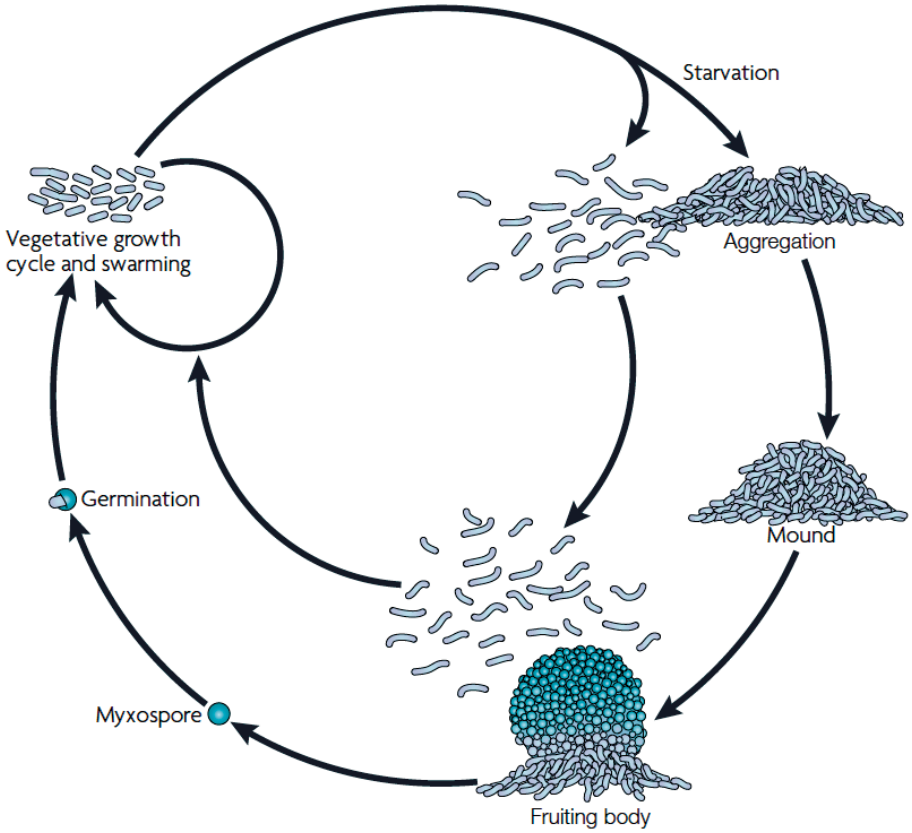

Figure 2. Life cycle of *Myxococcus xanthus*

Schematic representation of the individual stages in the *M. xanthus* life cycle. Various stages are described in the main text. The figure is reproduced from Zusman *et al*., 2007.

Fruiting body formation depends extensively on intercellular signaling between *M. xanthus* cells. Two signals, the A- and C-signals, have been characterized biochemically and functionally to some detail. These two systems have different functions. The A-signal becomes important after 2 h of starvation (Kuspa *et al.*, 1986) and functions to ensure that fruiting body formation does not initiate unless a sufficiently high number of cells are starved (Konovalova *et al.*, 2010). The C-signaling system functions to ensure the correct temporal order of rippling, aggregation and sporulation. The C-signal also provides cells with positional information, ensuring the

spatial coupling of aggregation of cells into fruiting bodies and sporulation of cells that have accumulated inside fruiting bodies (Konovalova *et al.*, 2010). The C-signal becomes important after 6 h of starvation (Kroos and Kaiser, 1987) and is absolutely required for rippling, aggregation and sporulation (Shimkets *et al.*, 1983). The C-signal is a 17 kDa protein, anchored in the outer membrane and thus not diffusible (Lobedanz and Sogaard-Andersen, 2003). Therefore, C-signal transmission requires active motility and proper cell alignment (Kim and Kaiser, 1990a, b; Kroos *et al.*, 1988).

1.2 Gliding motility

Surfaces are important features of many environments, offering high amounts of nutrients and therefore being attractive sites for bacterial colonization (McBride, 2001). Bacteria have evolved efficient strategies to move over surface. *Proteus mirabilis*, *Vibrio parahaemoliticus*, *Serratia marcescens*, and many other bacteria employ numerous flagella to spread over moist surfaces in a process known as swarming motility (Harshey, 1994). Other bacteria, such as *Pseudomonas aeruginosa* and *Neisseria gonorrhoeae* use type IV pili to move in a process called twitching motility (Henrichsen, 1983). Finally, diverse bacteria such as *M. xanthus*, *Flavobacterium johnsoniae*, *Phormidium uncinatum*, *Mycoplasma mobile,* and many others move over surfaces by gliding motility (Hoiczyk, 2000; Spormann, 1999). Historically, bacterial gliding motility is defined as smooth translocation of cells over a surface by an active process requiring energy consumption; gliding does not require flagella, and cell movement generally follows the long axis of the cell (Henrichsen, 1972). This definition does not specify a molecular apparatus or a mode of force generation and has been used to describe movements by many phylogenetically unrelated bacteria (Spormann, 1999).

Over the years, several models have been proposed to explain bacterial gliding motility; however, recent studies suggest that it is unlikely that any single mechanism will be able to explain all forms of bacterial gliding. Instead, it appears that there are several different types of gliding motility “motors” (Mignot, 2007; Wolgemuth and Oster, 2004). Nevertheless, it has become clear that some forms of gliding motility require type IV pili (Bhaya *et al.*, 2000; Mattick, 2002; Wall and Kaiser, 1999).

M. xanthus cells are non-motile in liquid growth media due to the lack of flagella, but can move on solid growth substrates at speeds of 2-4 μm per minute. This is extremely slow compared with other species such as *Escherichia coli*, which swims at a rate of ~50 μm per second (Baker *et al.*, 2006), and *F. johnsoniae*, which glides at 5-10 μm per second (McBride, 2001). Nevertheless, most of the research on gliding motility has been conducted with *M. xanthus* (Hartzell and Youderian, 1995; Ward and

Zusman, 1997; Youderian, 1998; Zusman and McBride, 1991). Genetic and molecular approaches in combination with high-resolution motion analysis have been extensively used to understand the mechanism of gliding motility in *M. xanthus*. The first genetic screens of chemical and UV-induced mutants with visible defects in colony swarming, performed by Hodgkin and Kaiser in 1979, revealed that gliding motility in *M. xanthus* is controlled by two multigene systems: the A-(adventurous) system, which controls gliding motility of single, isolated cells, and the S-(social) motility system, which is contact-dependent (Hodgkin and Kaiser, 1979a, b). The A- and S-motility systems work independently of each other, as a mutation that inactivates one of the systems leaves the second system still functional (Hodgkin and Kaiser, 1979a). However, if both systems are inactivated, motility is completely abolished. Moreover, based on the measurements of colony expansion rates of A^+S^+, A^-S^+ and A^+S^- cells it has been argued that the A- and S-motility systems act synergistically to generate force in the same direction (Kaiser and Crosby, 1983). Thus, *M. xanthus* harbors mechanisms, which ensure that the two motility systems generate force in the same direction.

1.3 A-motility

Single cells are visible at the edge of A-motile colonies (Figure 3). In contrast, colonies of A^-S^+ cells have flares with a smooth edge, where no isolated, individual cells are visible (Figure 3, middle panel) (Spormann, 1999).

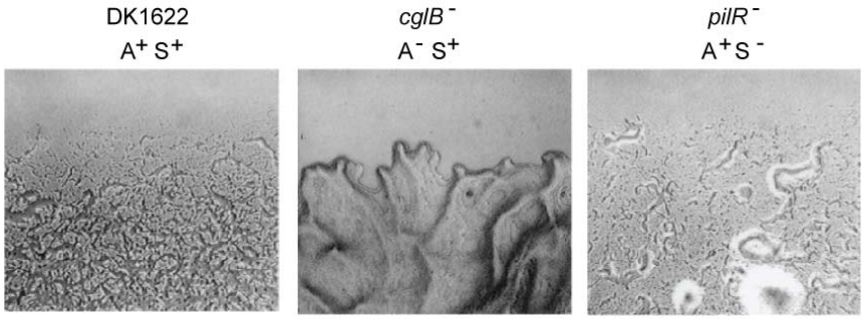

Figure 3. Colony morphology of A^+S^+, A^-S^+ and A^+S^- cells

A^+S^+ cells are WT cells, moving with both A- and S-motility; A^-S^+ move exclusively by means of S-motility, and A^+S^- cells exclusively by A-motility. Modified from Spormann, 1999.

Currently, however, it is not clear how motive force is generated in the A-system. The engine for A-motility has been especially difficult to characterize due to the absence of A-motility specific appendages on *M. xanthus* cells. Two models have been proposed for the A-motility system. In one model, A-motility depends on the secretion and subsequent hydration of the polyelectrolyte gel from nozzle-like structures embedded in the cell envelope (Wolgemuth *et al.*, 2002). According to a mathematical

model, hydration of the polyelectrolyte gel could produce a force sufficient to push an *M. xanthus* cell forward (Wolgemuth *et al.*, 2002). Interestingly, nozzle-like structures were observed by electron microscopy at both poles in *M. xanthus,* but the polyelectrolyte secretion has been suggested to only occur at the lagging cell pole. This model is supported by the finding that a large number of genes required for A-motility encode proteins involved in polymer synthesis and export (Youderian *et al.*, 2003; Yu and Kaiser, 2007). Recently it was reported that RomR response regulator, absolutely required for A-motility, is localized in a bipolar asymmetric pattern with a large cluster at the lagging cell pole (Leonardy *et al.*, 2007), suggesting that part of the A-motility machinery is localized and activated at the lagging cell pole.

In an alternative model, proposed by Mignot *et al*. (Mignot, 2007; Mignot *et al.*, 2007), force generation depends on multiple adhesion complexes distributed along the cell body. These complexes are defined by the AglZ protein, which is absolutely required for A-motility (Yang *et al.*, 2004). Using an active AglZ-YFP fusion, Mignot and colleagues (Mignot *et al.*, 2007) observed that AglZ localized in clusters along the cell body, that remained fixed relative to the substratum as cells moved forward. The clusters were proposed to be assembled from a large AglZ cluster at the leading cell pole and then disperse towards the lagging cell pole. According to this model, motive force would be generated by a protein complex, which includes AglZ, spans the cell envelope, adheres to the substratum, and pulls on a cytoskeletal structure. The motors, attached to AglZ, are hypothesized to move on helical cytoskeletal filaments, possibly the actin homolog MreB (Zusman *et al.*, 2007). Indeed, recently MreB in *M. xanthus* was shown to be essential for both A- and S-motility (Mauriello *et al.*, 2010). A model, involving multiple motors located along the cell body, is supported by the observation that cells which move by means of the A-motility system only, move with the same speed irrespectively of their cell length (Sliusarenko *et al.*, 2007).

Nevertheless, both models for A-motility system suffer from lack of experimental evidence on how motive force is generated. The different localization patterns of the two A-motility proteins AglZ and RomR suggest that the A-motility machinery is composed of distinct units (Leonardy *et al.*, 2007), with RomR stimulating polyelectrolyte secretion at the lagging cell pole and AglZ-containing focal adhesion complexes along the cell body. Given that both *aglZ* and *romR* mutations result in loss of A-motility, two units are suggested to be functionally interconnected (Leonardy *et al.*, 2007).

1.4 S-motility

S-motility involves movement of cells in groups and generally requires cell-cell

contact (Hodgkin and Kaiser, 1979a, b). S-motile colonies show a clearly defined, undulating edge (Spormann, 1999) (Figure 3, middle panel). S-motility is the equivalent of twitching motility in *Neisseria* and *Pseudomonas* species and depends on type IV pil (T4P) (Kaiser, 1979; Wu and Kaiser, 1995). T4P are highly dynamic structures, which undergo cycles of extension, attachment to the substratum or other cells, and retraction. During retractions a force sufficient to pull a bacterial cell forward is generated (Clausen *et al.*, 2009; Maier *et al.*, 2002). *M. xanthus* contains 5-10 T4P per cell (Kaiser, 1979), which are localized only at the leading cell pole (Sun *et al.*, 2000) In *M. xanthus* the T4P-dependent motility system is generally active only when cells are within contact distance of each other (Hodgkin and Kaiser, 1979b; Li *et al.*, 2003). This partial dependency on cell-cell contact has been attributed to the presence of polysaccharides in the extracellular matrix (ECM) that stimulate T4P retraction (Li *et al.*, 2003). Finally, the lipopolysaccharide O-antigen was demonstrated to be required for T4P-dependent motility (Bowden and Kaplan, 1998).

1.4.1 Type IV pili

T4P are one of the most widespread bacterial cell-surface structures and the only pili found in both Gram-negative and Gram-positive bacteria (Pelicic, 2008). T4P have essential functions in pathogenesis caused by several human pathogens by mediating attachment to and microcolony formation on host cells (Craig et al., 2004), cell motility (Mattick, 2002), biofilm formation (Klausen *et al.*, 2003; O'Toole and Kolter, 1998) and natural transformation (Dubnau, 1999). T4P are thin (5-8 nm) and flexible filaments, several microns in length and primarily composed of a single protein generically named pilin (Craig *et al.*, 2004; Soto and Hultgren, 1999). T4P from different species share many sequence and structural properties (Craig and Li, 2008).

- The pilin subunits and pilus filaments

The pilin subunits, while extremely variable in sequence and length, always display a consensus N-terminal motif (Pugsley, 1993). They are synthesized as precursors (prepilins) with a hydrophilic leader peptide ending with a glycine, which is cleaved by a unique leader peptidase. Type IV pili are separated into type IVa (T4aP) and type IVb (T4bP) subclasses based on pilin amino acid sequence. Type IVa pilins are characterized by a short leader sequence length (5-6 residues), a methylated N-terminal phenylalanine, and an approximate length of 145-160 residues after prepilin peptidase processing (Hansen and Forest, 2006). The best-studied bacteria producing T4aP are *P. aeruginosa*, *Neisseria* species and *M. xanthus*. The first crystal structure of a type IVa pilin was solved for PilE from *N. gonorrhoeae* strain MS11 in 1995 (Parge *et al.*, 1995), followed by the crystal structures of the truncated and full-length PilA from

P. aeruginosa strains K (PAK) and K122-4 (Audette *et al.*, 2004; Craig *et al.*, 2003; Hazes *et al.*, 2000). Comparisons of these structures revealed that type IVa pilins share a general architecture of a four-stranded anti-parallel *β*-sheet that forms a buried hydrophobic core with the N-terminal *α*-helix (*α*1) to create a *αβ*-roll. In both full-length MS11 PilE and full-length PAK PilA crystal structures the N-terminal half of the *α*1 helix protrudes out from the globular head domain as an exposed tail (Figure 4A and B). The protruding half of *α*1, *α*1-N, is primarily hydrophobic, whereas the buried half, *α*1-C, is amphipathic. Two regions flanking the *β*-sheet show substantial sequence, length and structural variations: the *αβ*-loop, which connects N-terminal *α*-helix to the *β*-sheet; and the disulfide-bridged or D-region, which is adjacent to the *β*-sheet and is delineated by the conserved cysteines (Figure 4A and B) (Craig *et al.*, 2004). On basis of the available type IVa pilin crystal structures different computational models of the type IVa pilus fiber were generated. The MS11 pilus was modeled as a right-handed one-start helix with five PilE monomers per turn, an outer diameter of 60 Å, and a pitch of 41 Å. In this model, the N-terminal *α*1 helices are nearly parallel to the fiber axis in the center of the filament creating a hydrophobic core (Parge *et al.*, 1995). The PAK fiber model is slightly different from MS11 model, comprising a right-handed one-start helix with a 41 Å pitch, an outer diameter of 58 Å, but only four PilA subunits per turn. However, in the PAK model the N-terminal *α*1 helices also generate a hydrophobic core in the centre of the filament (Craig *et al.*, 2004). Thus, both computational models of the type IVa pilus fiber demonstrate that the pilin monomer is able to assemble into a filament using conserved N-terminal *α*1 helices for hydrophobic packing and stabilization, predicting a general scheme for other type IVa pilins.

The b subclass of type IV pilins has amino acid homology over 30 N-terminal residues to type IVa pilins. However, it differs from the type IVa class in leader sequence length (15-30 residues), N-terminal residue of the mature protein (no conserved phenylalanine), and overall size (either long around 180-200 residues or surprisingly short, only 40-50 residues) (Hansen and Forest, 2006; Pelicic, 2008). Nevertheless, the 3D structures of several types IVb pilins reveal the same conserved architecture consisting of an extended N-terminal *α*-helix and a globular head (Craig *et al.*, 2004). The best-studied type IVb pili are the bundle-forming pilus (Bfp) of enteropathogenic *E. coli* (EPEC) (Ramer *et al.*, 2002), the toxin co-regulated pilus (Tcp) of *Vibrio cholerae* (Kirn et al., 2003) and the R64 plasmid thin pilus (R64 Pil) of *E. coli* (Yoshida *et al.*, 1999). An example of the crystal structure of *V. cholerae* TcpA is represented in Figure 4C. Interestingly, an alternative computational model, proposed for the bundle-forming pilus (Bfp) of EPEC based on BfpA NMR structure, suggests

that EPEC pilus fiber comprises a three-start helix, suggesting a different filament assembly strategy (Craig and Li, 2008; Ramboarina *et al.*, 2005).

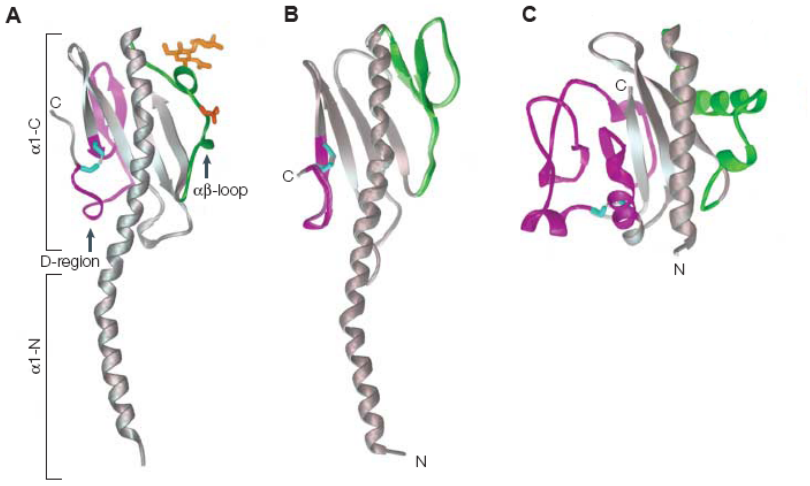

Figure 4. Structural comparisons of type IV pilins

A) Structure of *N. gonorrhoeae* pilin, showing the covalently attached carbohydrate at Ser63 (orange) and phosphate at Ser68 (red). In each of the structures the *αβ*-loop is colored green, the D-region is colored magenta and the disulphides are colored cyan. **B)** Structure of full-length *P. aeruginosa* PAK pilin. **C)**. Structure of N-terminally truncated *V. cholerae* TcpA. Modified from Craig *et al*. (Craig *et al.*, 2004).

- The T4P biogenesis machinery

In Gram-negative bacteria T4P biogenesis machineries comprise a conserved core of proteins that includes: (i) a pilin subunit; (ii) a specific peptidase that processes prepilins and prepilin-like proteins; (iii) a traffic ATPase that powers T4P assembly; (iv) an integral inner membrane protein of unknown function, and (v) an outer membrane protein, named secretin, necessary for the passage of T4P through outer membrane (Figure 5) (Pelicic, 2008). Deletion of any of the core components leads to the inability of bacterial cells to assemble T4P. The names of the pilus assembly components differ depending on the organism, and are listed in Table 1 for the most-studied systems. Many T4P systems also possess a “retraction” ATPase (PilT) that drives depolymerization of the pilus filament (Craig and Li, 2008; Pelicic, 2008). It is important to note that *pilT* mutants still assemble T4P, in some organisms these mutants are even hyper-piliated (Wolfgang *et al.*, 1998; Wu *et al.*, 1997). However, T4P of *pilT* mutants generally do not retract (Merz *et al.*, 2000; Sun *et al.*, 2000).

Strikingly, proteins similar to T4P assembly proteins are found in the type II secretion machinery that mediates the passage of folded proteins through the outer membrane in Gram-negative bacteria, and also in machineries involved in the biogenesis of filamentous phage and archaeal flagella or in DNA uptake in Gram-positive bacteria (Peabody *et al.*, 2003).

Systematic genetic studies have defined the complete set of genes encoding the proteins specifically dedicated to T4P biogenesis in several model systems, including both T4aP and T4bP systems. These studies showed that T4P machineries are composed of 10 (*V. cholerae*) to 18 (*P. aeruginosa*) proteins. Importantly, these studies revealed the differences that are consistent with the subdivision into T4aP and T4bP pili systems (Pelicic, 2008). Generally, both T4aP and T4bP pili machineries include a universally conserved core of 5-6 proteins, described above, and a set of additional, non-core proteins (Figure 5). Importantly, the core proteins are found in all T4aP and T4bP pili systems of Gram-negative bacteria (Craig and Li, 2008; Pelicic, 2008). It should be noted that many but not all of the non-core T4P proteins in T4aP pili systems are also highly conserved (Figure 5), e.g. PilM, PilN, PilO and PilP proteins of unknown function, PilC adhesins and PilW lipoprotein (Tgl in *M. xanthus*) (Pelicic, 2008). Furthermore, in bacteria producing T4aP T4P biogenesis genes are mostly scattered throughout the genome (Pelicic, 2008) with *M. xanthus* being a notable exception, as depicted in Figure 6. Another exception is the *pilMNOPQ* gene cluster, which is conserved among T4aP-producing species in respect to both gene order and sequence identity (Pelicic, 2008).

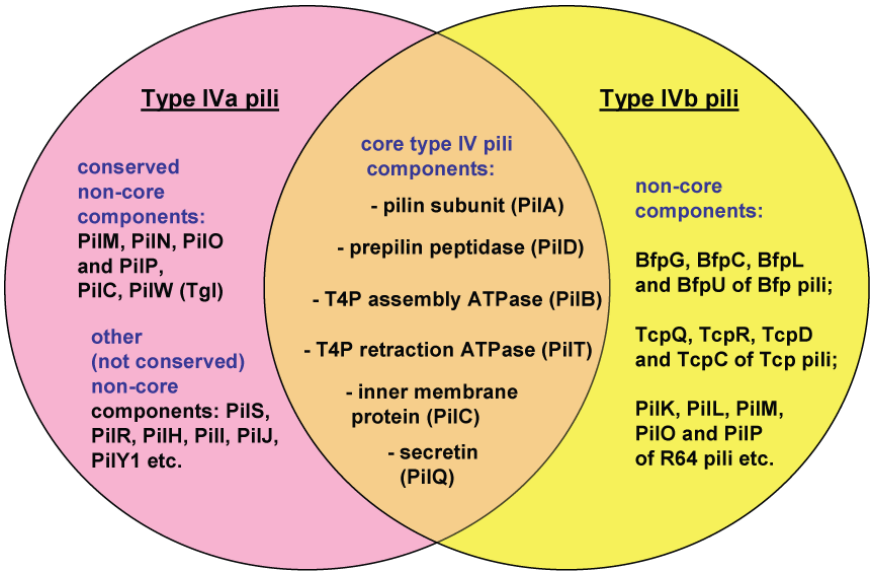

Figure 5. Core and non-core components of T4aP and T4bP pili systems

For the core T4P components *M. xanthus* protein names have been used.

On the contrary, the picture in bacteria producing T4bP is very different. None of the non-core components in T4bP machineries are conserved between species (Figure 5) (Pelicic, 2008). In addition, T4bP biogenesis proteins are less numerous (10 to 12 proteins in comparison to 16-18 proteins in T4a pili machineries) (Kirn *et al.*, 2003; Ramer *et al.*, 2002; Yoshida *et al.*, 1999), and the corresponding genes are mainly

clustered, suggesting that T4b pili-encoding genes could be part of pathogenecity islands, which is in fact the case for the *tcp* cluster in *V. cholerae* (Pelicic, 2008).

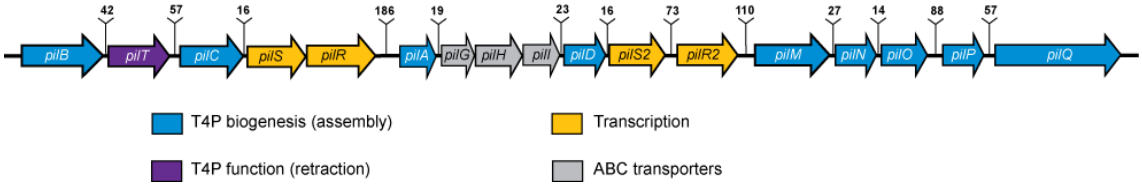

Figure 6. Genetic map of *pil* cluster in *M. xanthus*

All 17 ORFs are transcribed from left to right. Most of the genes were named after their orthologs in *P. aeruginosa*, except for *pilGHI*, which are unique to *M. xanthus*. Numbers indicate distances between stop and start codons of contiguous genes in base pairs. The *tgl* gene, which is not located in *pil* operon, is not shown.

It is particularly interesting that none of the non-core T4P components are conserved between T4aP and T4bP-producing bacteria, given that non-core proteins in both systems account for up to 40% of the proteins essential for T4P biogenesis (Pelicic, 2008). These observations suggest that mechanisms of T4P assembly might differ between the species (Pelicic, 2008). These mechanisms remain to be elucidated.

Table 1. Nomenclature of key T4P biogenesis components

Bacteria	Pilin subunit	Prepilin peptidase	Assembly ATPase	Retraction ATPase	Inner membrane protein	Secretin
T4a pili						
Pseudomonas aeruginosa	PilA, PilE	PilD	PilB	PilT, PilU	PilG	PilQ
Neisseria gonorrhoeae	PilE	PilD	PilF	PilT	PilG	PilQ
N. meningitidis	PilE	PilD	PilF	PilT	PilG	PilQ
Francisella tularensis	PilE	PilD	PilF	PilT	PilG	PilQ
Myxococcus xanthus	PilA	PilD	PilB	PilT	PilC	PilQ
Haemophilus influenzae	PilA	PilD	PilB			ComE
Clostridium perfringens	PilA1, PilA2	PilD	PilB	PilT		None
T4b pili						
Vibrio cholerae	TcpA, MshA	TcpJ	TcpT		TcpE	TcpC
Enteropathogenic *Escherichia coli* (EPEC)	BfpA	BfpP	BfpD	BfpF	BfpE	BfpB
Enterotoxigenic *E. coli* (ETEC)	CofA	CofP	CofH		CofI	CofD
Salmonella typhi	PilS	PilU			PilR	

In contrast to the progress made on the T4P filament structure, the mechanism by which these filaments are assembled is still poorly understood. Genetic and biochemical evidence suggest that the polymerization of the filament requires ATP hydrolysis by a cytosolic hexameric ATPase, which is recruited to the cytosolic face of the inner membrane by an integral membrane protein (Crowther *et al.*, 2004; Tripathi and Taylor, 2007). For retractile pili, a retraction ATPase is required to rapidly depolymerize the pili, which allows bacteria to move over solid surfaces, to transduce phage and transform DNA (Burrows, 2005). Both the assembly and the retraction ATPases belong to the large superfamily of type II/IV secretion NTPases (Craig and Li, 2008).

The analysis of the crystal structures of the type II secretion ATPase EpsE from *V. cholerae* (Robien *et al.*, 2003), the type IV secretion ATPases HP0525, VirB11 from *Helicobacter pylori* (Savvides *et al.*, 2003; Yeo *et al.*, 2000), and the T4P retraction ATPase PilT from *Aquifex aeolicus* (Satyshur *et al.*, 2007) revealed some intriguing details. First, the subunits of all these ATPases share a bilobed structure, with an N-terminal domain (NTD) and a C-terminal domain (CTD) connected by a hinge region (Figure 7A). Subunits bind nucleotide in the cleft between the two domains via canonical Walker A, Walker B, Asp box and His box ATPase motifs of the CTD, and basic side chains on the NTD (Figure 7B). Second, subunits are arranged in hexameric rings. Within a single hexamer subunits can exist in different conformational and active states, as would be expected for a biological motor (Craig and Li, 2008; Satyshur *et al.*, 2007). Finally, the analysis of these structures suggested that binding and hydrolysis of ATP induce major conformational changes that could provide a mechanical force that drives secretion/polymerization (Savvides, 2007). Some of the secretion/assembly ATPases, e.g. PulE from *Klebsiella oxytoca* and PilB from *M. xanthus* additionally contain a relatively well-conserved N-terminal extension, which is not present in the T4P retraction ATPases (Peabody *et al.*, 2003) (Figure 7A).

Several lines of experimental evidence support the observations above. Two secretion ATPases, EpsE of *V. cholerae* (Camberg and Sandkvist, 2005) and its ortholog XpsE of *Xanthomonas campestris* (Shiue *et al.*, 2006) have been shown to have ATPase activity and to form oligomers *in vitro.* Replacement of the conserved lysine residue in the Walker A box (Figure 7B) led to the reduction in the ATPase activity in both proteins and to the inability of mutants to support secretion (Camberg and Sandkvist, 2005; Sandkvist *et al.*, 1995; Shiue *et al.*, 2006). Similar observations were made for the T4P assembly ATPases PilQ from the conjugative R64 pilus system in *E. coli* (Sakai *et al.*, 2001) and BfpD of bundle-forming pilus system of EPEC

(Crowther *et al.*, 2005). Moreover, ATPase activities were reported *in vitro* for PilT of cyanobacteria *Synechocystis* sp. strain PCC 6803 (Okamoto and Ohmori, 2002) and *Microcystis aeruginosa* (Nakasugi *et al.*, 2007), and for hexameric PilT from *A. aeolicus* (Herdendorf *et al.*, 2002). Additionally, for PilT from *A. aeolicus* replacement of the conserved lysine residue in the Walker A abolished ATP hydrolysis (Herdendorf *et al.*, 2002). Recently it has been shown that both PilB and PilT ATPases from *M. xanthus* have ATPase activities *in vitro*, which depend on the intact Walker A and Walker B boxes (Jakovljevic *et al.*, 2008). Furthermore, the mutated PilB and PilT ATPases containing either replacement of the conserved lysine residue in the Walker A box (predicted to be important for the ATP binding) or of the conserved glutamate residue in the Walker B box (predicted to be important for the ATP hydrolysis) were also non-functional *in vivo* (Jakovljevic *et al.*, 2008).

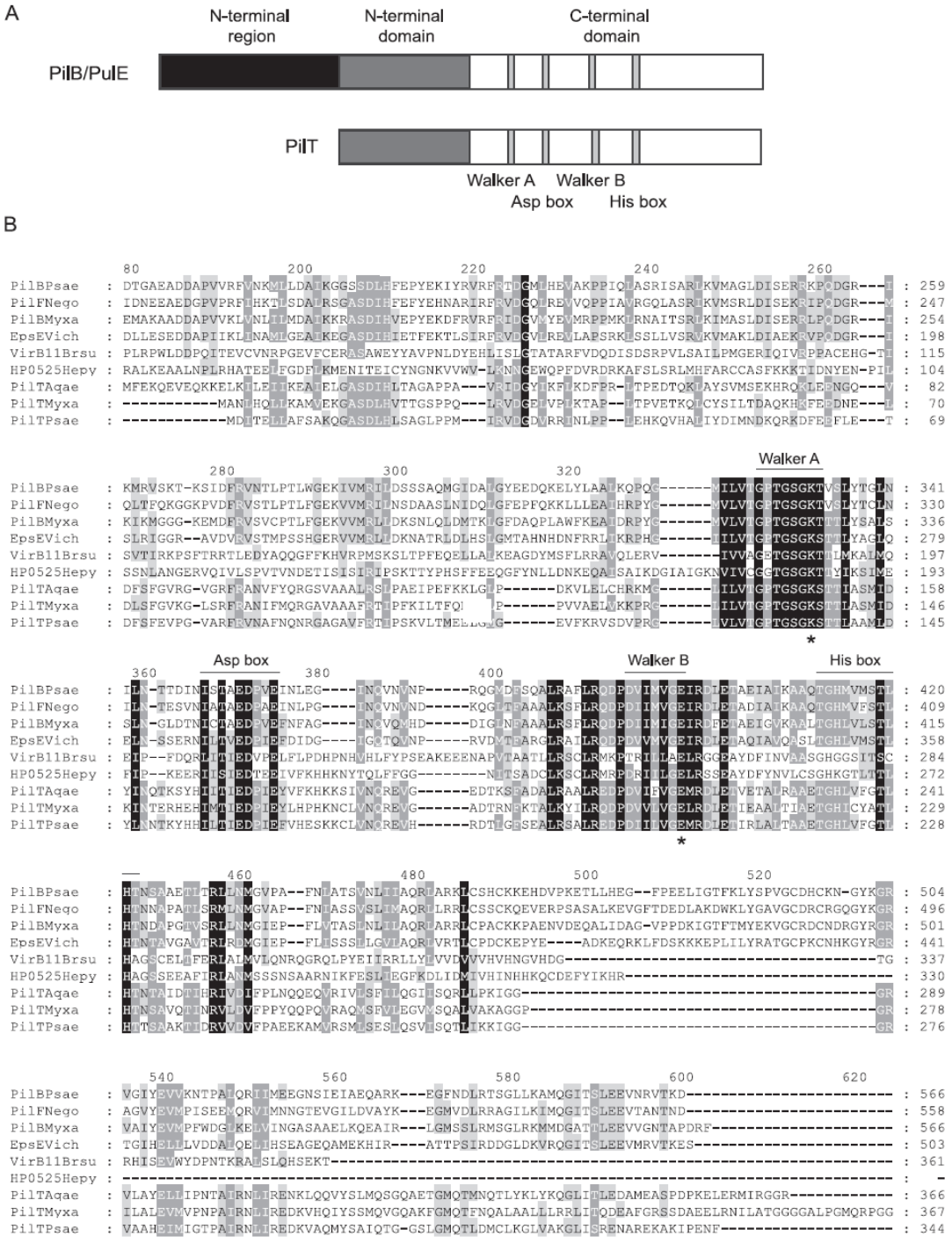

Figure 7. Domain structure of secretion ATPases

A) Scheme of the domain strusture of PulE, PilB and PilT ATPases. The conserved N-terminal region in PulE and PilB proteins, the N-terminal conseved domain (NTD) and the C-terminal conserved domain (CTD) are indicated. Vertical gray bars in the CTD indicate the four conserved sequence motifs in secretion ATPases: Walker A box, Asp box, Walker B box and His box. **B)** Alignment of PilB and PilT of *M. xanthus* with well-studied secretion ATPpases. PilBMyxa and PilTMyxa stand for PilB and PilT of *M. xanthus*, respectively; PilBPsae and PilTPsae for PilB and PilT of *P.aeruginosa*, respectively; PilFNego for PilF (PilB ortholog) of *N. gonorrhoeae*, EpsEVich for EpsE of *V. cholerae*, VirB11Brsu for VirB11 of *Brucella suis,* HP0525 for HP0525 from *H. pylori* and PilTAqae for PilT from *A. aeolicus*. Walker A, Asp, Walker B and His boxes are indicated. The conserved lysine in the Walker A box and the conserved glutamate in the Walker B box, described in text, are indicated with asterisks. White-on-black residues are 100% conserved, white-on-gray residues are 80% conserved, and black-

on-gray residues are 60% conserved. The N-terminal extensions of PilB, EspE, VirB11 and HP0525 are not included. The figure is reproduced from Jakovljevic *et al*. (Jakovljevic *et al.*, 2008).

The assembly/secretion ATPases have not been shown to interact directly with their corresponding pili (in T4P systems) or pseudopili (in type II secretion systems), but they do interact with inner membrane partners: the EpsE NTD forms a complex with a cytoplasmic N-terminal segment of the inner membrane protein EpsL (Abendroth *et al.*, 2005); EPEC assembly ATPase BfpD interacts with the N-terminus of an inner membrane protein BfpE (Crowther *et al.*, 2005). The analysis of the reconstructed inner membrane protein PilG structure of *N. meningitidis* using negative stain electron microscopy suggests that PilG forms a tetramer (Collins *et al.*, 2007). Importantly, the PilG architecture provides substantial cytoplasmic and periplasmic domains for the interaction with the assembly/retraction ATPases and periplasmic proteins, including the pilin subunit (Craig and Li, 2008).

Lastly, the outer membrane protein belongs to the secretin superfamily complexes, which are utilized not only in T4P systems, but also in type II and III secretion systems and filamentous phage release (Craig and Li, 2008). Secretins are homooligomers of integral membrane proteins with a conserved C-terminal domain that is predicted to span the outer membrane and mediate the oligomerization (Craig and Li, 2008). The analysis of the PilQ complex from *N. meningitidis* revealed a long cavity inside that is 90 Å in height and approximately 87 Å in diameter, i.e. large enough to accommodate an assembled pilus, which is 60 Å in diameter (Craig and Li, 2008). *In vitro* assays demonstrated a direct interaction between PilQ complexes and one end of the purified T4P, which fills the large central cavity and induces significant structural changes in PilQ (Collins *et al.*, 2005). The strongest evidence that T4P pass through this cavity is the finding that piliation can be restored in *Neisseria* secretin mutants in the absence of pilus retraction, but the filaments remain trapped within the periplasm (Carbonnelle *et al.*, 2005; Wolfgang *et al.*, 2000). It seems that T4P secretins do not require additional non-core (pilot) proteins for oligomerization and targeting to the outer membrane (Carbonnelle *et al.*, 2005; Pelicic, 2008) as do type II secretion secretins, but stability of PilQ complexes is dependent on a partner non-core lipoprotein, such as PilW in *N. meningitidis* (Pelicic, 2008) and its ortholog TgI in *M. xanthus* (Nudleman *et al.*, 2006). A peculiarity of TgI in *M. xanthus* is that *tgl*- cells (which cannot assemble T4P) can be stimulated to assemble T4P by contact with *tgl*+ donor cells (Wall *et al.*, 1998). This stimulation involves the transfer of TgI protein from the *tgl*+ donor cells to the *tgl*- recipient cells (Nudleman *et al.*, 2005).

- Molecular mechanism of T4P biogenesis

To summarize the data above, the following model of the T4P biogenesis mechanism has been proposed (Pelicic, 2008). Prepilins are co-translationally targeted by the signal recognition particle to the Sec machinery, which is solely responsible for translocating them across the inner membrane. Due to their hydrophobic N-terminal *α*-helix, prepilins remain in the inner membrane as bitopic proteins, with the charged leader peptide in the cytoplasm and the C-terminal domain in the periplasm. This topology is required for the correct recognition and processing of prepilins by the prepilin peptidase, a polytopic inner membrane protein. The molecular mechanism of processing is not completely understood, but two conserved aspartate residues in the C-terminal cytoplasmic loop of prepilin peptidases are crucial (LaPointe and Taylor, 2000). The crystal structures of the assembly ATPases suggest that the extraction of pilin subunits from the inner membrane and their incorporation into the base of a growing pilus is powered by the mechanical force generated by domain rearrangements within the ATPases after ATP hydrolysis. This mechanical force would likely be transmitted through the inner membrane protein, specifically interacting with an assembly ATPase at the cytosolic face of the inner membrane. The emergence of T4P on the bacterial surface occurs via the PilQ complexes in the outer membrane (Carbonnelle *et al.*, 2005; Wolfgang *et al.*, 2000).

- T4P retraction

A fascinating feature that distinguishes the T4P from other types of bacterial appendages is their ability to be retracted through the cell wall, while the pilus tip remains firmly attached to a surface, allowing the pili to act as fishing rods or grappling hooks for translocation of the cell body (Burrows, 2005). Early electron microscopy work by Bradley demonstrated that the pili of *P. aeruginosa* could be retracted into the cell, as the susceptibility of bacteria to pilus-binding bacteriophages correlated with the presence of pili and anti-pilin antibodies inhibited cell motility (Bradley, 1972a, b).

T4P retraction has now been directly observed in three systems. Using a laser tweezers trap, Merz and colleagues (Merz *et al.*, 2000) found that pili of *N. gonorrhoeae* cells can form tethers between cells or between cells and inert objects, such as latex beads, and these tethers forcefully retract. Retraction requires PilT and is abolished by a point mutation in the PilT ATPase domain (Merz *et al.*, 2000). Quantitative experiments showed that the retraction occurs at average speeds of 1.2 µm/s and can generate tensile forces exceeding 80 pN per cell, which is substantially higher than the forces generated by eukaryotic motor proteins (Mahadevan and Matsudaira, 2000; Merz *et al.*, 2000).

Skerker and Berg (Skerker and Berg, 2001) covalently labeled pili of *P. aeruginosa* cells with a fluorescent dye and were able to directly observe individual pili using evanescent wave microscopy. They saw pili extend as well as retract, at speeds ~0.5 μm/s. It is important to note that in this study it was observed that individual pili extend and retract independently.

Studies in *M. xanthus* showed that WT cells, tethered by their T4P to a solid surface, exhibited a jiggling motion, bringing the cell body into the juxtaposition with the surface over time (Sun *et al.*, 2000). In contrast, mutants that were piliated but lacked T4P-dependent motility became tethered but were stationary and did not approach the surface (Sun *et al.*, 2000). Moreover, Clausen *et al*. reproduced the laser tweezers trap experiments with *M. xanthus* cells (Clausen *et al.*, 2009). In this study it was demonstrated that high-force generation is a conserved property of T4P systems, as the force generated by a single pilus of *M. xanthus* even exceeded the force generated by a single pilus in *N. gonorrhoeae*, approaching 150 pN (Clausen *et al.*, 2009).

Currently the molecular mechanism underlying T4P retraction is still fully speculative. Pilus depolymerization into the inner membrane is presumed to occur, but has not been demonstrated experimentally (Merz and Forest, 2002). However, several models were proposed for the mechanism of this process. In Brownian ratchet models, T4P melt spontaneously into the membranes and the retraction force is a consequence of the energy stored in the filament during an energy-consuming polymerization reaction. Consistent with this model, isolated T4P filaments are efficiently dissociated by gentle detergents that do not disassemble actin or tubulin filaments or the extremely stable type I pili (Merz and Forest, 2002). In this scenario, PilT could serve a regulatory function, such as catalyzing the removal of a stabilizing terminal cap from the pilus base and thereby triggering pilus retraction (Mahadevan and Matsudaira, 2000; Merz and Forest, 2002).

Pilus retraction might not be spontaneous. In alternative models T4P assembly is energetically favorable, or assembly and retraction are energetically equivalent. In these cases the T4P fiber would not store the useful energy, and PilT would be expected to participate more directly in the retraction process. In the facilitated ratchet scenario, PilT acts as an ATP-dependent chaperone, and peels pilin subunits off the fiber base one at a time. As subunits are removed, new hydrophobic patches are exposed at the fiber base, causing the base to sink into the membrane's hydrophobic interior. In this model PilT catalyzes disassembly, and disassembly causes T4P retraction (Merz and Forest, 2002).

Finally, in the power stroke models, suggested by Oster (Kaiser, 2000), PilT

walks up the filament, driving the filament into the membrane and thereby causing subunits to melt off the fiber's base. In these models, PilT catalyzes T4P retraction, and retraction causes disassembly. These models imply that PilT should "touch" the periplasm during its catalytic cycle; however, this has not been tested.

All the above models make clear that ATPase action is formally required during only one step of the cycle: during T4P extension if retraction is spontaneous, or during retraction if extension is spontaneous. Additional ATPase activities might be present for regulation, in cases where additional mechanical force is required, or to impart directionality if extension and retraction are energetically balanced (Merz and Forest, 2002).

1.4.2 Extracellular matrix

Second component required for T4P-dependent motility in *M. xanthus* is an extracellular matrix (ECM). *M. xanthus* cells are covered by ECM composed of exopolysaccharides (EPS) and proteins in a ratio of approximately 1:1 (Behmlander and Dworkin, 1994a). ECM was demonstrated to be important for *M. xanthus* motility, cell-cell cohesion and fruiting body formation (Lu *et al.*, 2005; Shimkets, 1986a, b). Specifically, the EPS portion of ECM was found to trigger T4P retraction (Li *et al.*, 2003) and the ECM zinc metalloprotease FibA has been proposed to be involved in regulation of motility (Kearns *et al.*, 2002). EPS of *M. xanthus* is composed of the five monosaccharides: galactose, glucosamine, glucose, rhamnose and xylose (Behmlander and Dworkin, 1994a); the ECM proteins identified in a proteomics-based approach comprise mostly hypothetical proteins, proteases, amidohydrolases and proteins coating the myxospores (Curtis *et al.*, 2007).

Accumulation of ECM is a tightly regulated process and involves several regulators (Konovalova *et al.*, 2010). The best-studied system involved in the regulation of ECM accumulation is the Dif chemosensory system (Yang *et al.*, 1998). The core proteins of Dif system are DifA, DifC and DifE, which are orthologs of methyl-accepting chemosensory proteins (MCP), CheW adaptor proteins and CheA histidine protein kinases, respectively (Yang *et al.*, 1998). These three proteins are encoded in an operon with three other genes, encoding DifB, DifD and DifG proteins. DifD is an ortholog of the CheY response regulator, DifG of the CheC phosphatase, and DifB is a hypothetical protein of unknown function (Black and Yang, 2004). Importantly, methyltransferase and methylesterase are absent in the Dif system. Mutants lacking DifA, DifC or DifE are defective in the T4P-dependent motility and development (Yang *et al.*, 1998). Interestingly, these mutants were also found to produce more pili compared to WT, but lacked EPS, leading to the hypothesis that the Dif system

regulates EPS accumulation, which is required for T4P-dependent motility (Yang *et al.*, 2000). In contrast to the *difACE* mutations, deletion of either *difD* or *difG* results in the overproduction of EPS, indicating that these loci negatively regulate the activity of the Dif chemosensory system (Black and Yang, 2004). Given that DifG is a CheC-like phosphatase (Szurmant *et al.*, 2004) capable of affecting the flow of the phosphoryl groups through the Dif signaling pathway, DifG is predicted to be the major contributor to adaptation for the Dif system, instead of a Dif-specific methylation system (Mignot and Kirby, 2008). Studies of Li and colleagues (Li *et al.*, 2003) suggest that components of EPS such as N-acetylglucosamine trigger pilus retraction and that pili are likely to bind EPS components directly. Moreover, the epistasis analysis indicated that pili act upstream of the Dif pathway for regulation of EPS production (Black *et al.*, 2006). The authors proposed a model in which T4P function as a sensory apparatus for the cell proximity, allowing cell contact to positively regulate EPS production, stimulate pilus retraction, and also regulate the relative position of cells within groups (Black *et al.*, 2006; Mignot and Kirby, 2008).

1.4.3 Lipopolysaccharide O-antigen

A third extracellular component required for the T4P-dependent motility in *M. xanthus* is the lipopolysaccharide (LPS) O-antigen. The *M. xanthus* LPS O-antigen is similar in overall structure to that in other Gram-negative bacteria. The carbohydrate moiety of *M. xanthus* LPS consists of glucose, mannose, rhamnose, arabinose, xylose, galactosamine, 2-keto-3-deoxyoctulosonic acid, 3-*O*-methylpentose and 6-*O*-methylgalactosamine (Yang *et al.*, 2008). Mutants deficient in LPS biosynthesis show defects in fruiting body formation (Bowden and Kaplan, 1998; Fink and Zissler, 1989). LPS mutants were also proposed to have a defect in A-motility (Fink and Zissler, 1989); however, detailed genetic analysis provided evidence that LPS mutants display defects in T4P-dependent motility (Bowden and Kaplan, 1998), although they still produce T4P. It has been proposed that the LPS mutants might be deficient in pilus retraction, because chains of LPS O-antigen completely cover the cell, and a retracting pilus may interact with the O-antigen chains as it slides through the covering (Kaiser, 2003). However, there are no experimental data confirming this hypothesis.

1.5 Reversing direction of cell movement

During colony expansion and fruiting body formation *M. xanthus* cells display directed movements. To be able to display directed movements, bacterial cells must regulate the frequency of direction changing. Bacteria that are propelled by flagella adjust directional bias of the flagella by controlling their rotation. *M. xanthus* lack

flagella and only move on surfaces in two dimensions. To control their directed movements, *M. xanthus* cells display cellular reversals (Jelsbak and Søgaard-Andersen, 2002). During a reversal a cell initially stops and then resumes movement in the opposite direction, so that the old leading pole becomes a new lagging pole and *vice versa* (Blackhart and Zusman, 1985) (Figure 8A and B).

Mutants that are unable to regulate the reversal frequency form abnormal spreading colonies and are unable to construct fruiting bodies (Bustamante *et al.*, 2004; Zusman, 1982). On average, cells undergo reversals every 5-10 min (Blackhart and Zusman, 1985). However, the reversal period is highly variable, and cells do not simply oscillate back and forth, but display net movements (Blackhart and Zusman, 1985). As previously described, T4P in *M. xanthus* are localized at the leading cell pole, where upon retraction they generate a force for pulling the cell forward (Mignot *et al.*, 2005; Sun *et al.*, 2000; Wu and Kaiser, 1995). Therefore, in order for cells to undergo a reversal, T4P need to change the direction in which they generate force and, thus, their polarity (Figure 8). A-motility system needs to change its polarity also (Figure 8). This phenomenon is referred to as polarity switching (Leonardy *et al.*, 2008). The cellular reversal frequency in *M. xanthus* is regulated by the Frz chemosensory system (Blackhart and Zusman, 1985; Leonardy *et al.*, 2008).

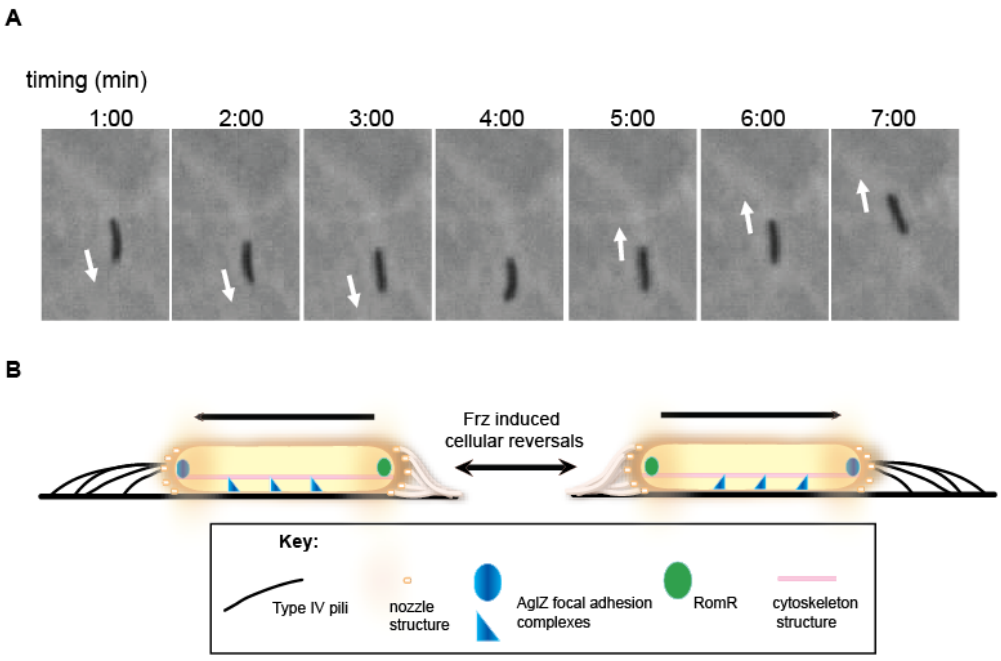

Figure 8. Cellular reversal is accompanied by the polarity switch of both motility systems

A) A sequence of phase-contrast images of a single *M. xanthus* cell moving on a solid surface for a period of 7 min. The white arrows indicate the direction of movement of the cell. The cell stopped from 3:00 to 4:00 and reversed its direction of movement from 4:00 to 5:00 min. **B**) Schematic representation of a reversing *M. xanthus* cell. Black arrows indicate the direction of gliding. After an Frz-induced cellular reversal the motility structures switch their polarity: T4P

and a large AglZ cluster switch to the new leading pole, whereas RomR cluster switches to the new lagging cell pole, where slime secretion is activated. Figure modified from Leonardy *et al*. (Leonardy et al., 2008).

1.5.1 Regulation of reversals by Frz chemosensory system

The *frz* (frizzy) genes (a cluster of seven genes) were discovered during a search for mutants that are defective in cellular aggregation. *frz* mutants rarely reverse, upon starvation they cannot aggregate into fruiting bodies and instead form 'frizzy' filaments (Blackhart and Zusman, 1985; Zusman, 1982). Genetic and protein sequence analyses revealed that the seven *frz* genes encode homologs to the chemosensory proteins found in many bacteria (McBride *et al.*, 1989; Zusman *et al.*, 2007). The Frz chemosensory system comprises a cytoplasmic methyl-accepting chemoreceptor FrzCD; two CheW homologs FrzA and FrzB; FrzE fusion protein, possessing both a CheA histidine kinase domain and a CheY-like receiver domain; methyltransferase FrzF which methylates FrzCD; methylesterase FrzG which demethylates FrzCD, and FrzZ, composed of two CheY-like response regulator domains that are connected by a linker region (Inclan *et al.*, 2008; Inclan *et al.*, 2007; Zusman *et al.*, 2007) (Figure 9). FrzCD, FrzA and the CheA domain of FrzE are the core components of the Frz pathway, as they are essential for responses to repellents and directed movements during both vegetative growth and development (Zusman *et al.*, 2007). The input signals that regulate the activity of the Frz system are unknown. Nevertheless, according to current models for how the Frz system works (Zusman *et al.*, 2007), signals are sensed by FrzCD or FrzF (Figure 9). This results in a change in FrzE autokinase activity. FrzE initially autophosphorylates on a conserved His residue (Inclan *et al.*, 2008). *In vitro* phosphorylation assays have demonstrated direct transfer of this phosphoryl group to either of the two receiver domains of FrzZ (Inclan *et al.*, 2007). Moreover, genetic evidence suggests that this phosphoryl group can also be transferred to the receiver domain of FrzE (FrzE-CheY) (Li *et al.*, 2005). Thus, three receiver domains compete for the phosphoryl group on the conserved His in FrzE (Figure 9). Accordingly, it has been proposed that the Frz system regulates cellular reversals in the A-motility and S-motility systems by a mechanism that depends on the competition for the phosphoryl group of the conserved His in FrzE (Li *et al.*, 2005). Phosphorylated FrzE-CheY results in the inhibition of reversals in the S-system and unphosphorylated FrzE-CheY stimulates reversals in the S-system (Figure 9). In contrast, phosphorylated FrzZ stimulates reversals in the A-system and unphosphorylated FrzZ results in the inhibition of reversals in the A-system (Figure 9). So, when the phosphoryl group on the conserved His residue in FrzE is directed to

FrzE-CheY (and away from FrzZ) (Figure 9, left panel), reversals are inhibited in both motility systems. On the other hand, when the phosphoryl group on the conserved His residue in FrzE is directed to FrzZ (and away from FrzE-CheY), reversals are stimulated in both motility systems (Figure 9, right panel). This model explains how both motility systems may switch polarity in parallel during a cellular reversal. However, it remains an open question how the phosphate flow from the conserved His in FrzE is regulated (Leonardy *et al.*, 2008; Zusman *et al.*, 2007).

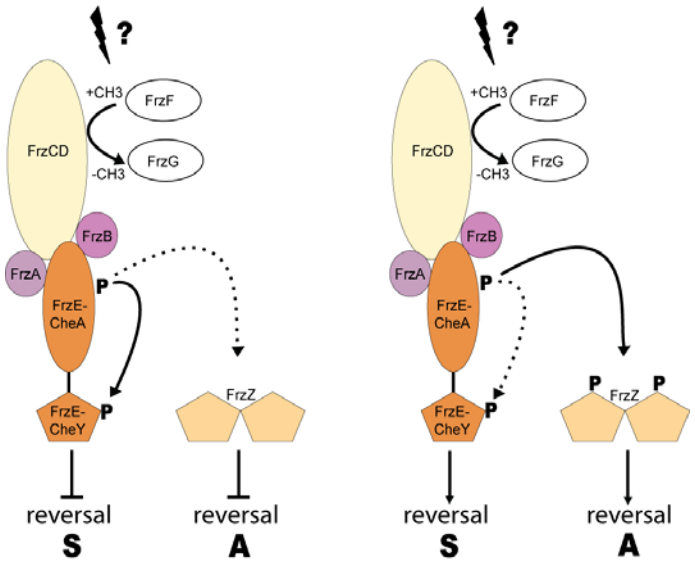

Figure 9. Model of the Frz chemosensory system

Two alternative phosphate flows from the kinase domain of FrzE (FrzE-CheA) to either the CheY domain in FrzE (FrzE-CheY) or to the two CheY-like domains in FrzZ. The signal that governs the direction of the phosphate flow is unknown. See the main text for details. The figure reproduced from Leonardy *et al*. (Leonardy *et al.*, 2008).

Recent localization studies demonstrated that FrzCD, a cytoplasmic chemoreceptor, does not form membrane-bound polar clusters typical for most bacteria, but rather forms cytoplasmic clusters that appear to be helically arranged and span the cell length (Mauriello *et al.*, 2009a). The distribution of FrzCD in living cells was found to be dynamic: FrzCD localized in clusters that continuously changed their size, number and position. Moreover, the number of FrzCD clusters correlated with cellular reversal frequency: fewer clusters were observed in hypo-reversing cells and additional clusters were observed in hyper-reversing cells. Interestingly, when moving cells made side-to-side contacts, FrzCD clusters in adjacent cells showed transient alignments; these events were frequently followed by one of the interacting cells reversing. Mauriello *et al.* (Mauriello *et al.*, 2009a) proposed a model, in which the FrzCD clusters track along a cytoskeletal filament, and continuous cluster rearrangement functions as a part of reversal clock, timing cell reversals. Stimulations

such as cell-cell contacts would speed up the clock, causing cluster re-localizations which in turn trigger reversals, thus suggesting a mechanism for the coordination of cell movements (Mauriello *et al.*, 2009a). Importantly, the Frz system has been shown to regulate the dynamic localization of three motility proteins, FrzS, RomR and AglZ (Leonardy *et al.*, 2007; Mignot *et al.*, 2005; Mignot *et al.*, 2007) (described in detail below).

1.5.2 Polarity switching of the A-engine

Only two A-motility proteins have been analyzed in detail to date, RomR and AglZ. As described in Chapter 1.3, the localization pattern of the two proteins is different, with AglZ localizing with the large cluster at the leading cell pole and in clusters along cell body (Mignot *et al.*, 2007), and RomR localizing in a bipolar asymmetric pattern with the large cluster at the lagging cell pole (Leonardy *et al.*, 2007). Thus, polarity switching of the A-engine has been addressed using AglZ and RomR proteins fused to fluorescent proteins as markers.

During cellular reversal AglZ protein initially becomes diffusely localized and then localizes with a large cluster to the new leading cell pole and smaller clusters along the cell body (Mignot *et al.*, 2007). In parallel, the large RomR cluster switches from the old lagging pole to the new lagging pole (Leonardy *et al.*, 2007). For both AglZ and RomR the dynamic localization during reversals involves the transfer of proteins between poles (Leonardy *et al.*, 2007; Mignot *et al.*, 2007). Therefore, AglZ and RomR oscillate between the poles in parallel with cellular reversals. Importantly, these oscillations depend on the Frz chemosensory system, as they were no longer observed in *frz* hypo-reversing mutants.

The localization and cell behavior studies of a RomR^{-} mutant, containing a D53E replacement of the phosphorylatable D53 residue in the receiver domain, demonstrated that this substitution bypassed a *frz* mutation for dynamic localization and cellular reversals, i.e. a mutant containing a *frz* mutation (causing hypo-reversals) and the *romR*^{D53E} mutation (causing frequent reversals) displayed dynamic RomR localization and cellular reversals (Leonardy *et al.*, 2007). These observations suggest that RomR acts downstream of Frz system to induce reversals in A-motility system, and that RomR is a master regulator of the A-engine polarity, because increasing pole-to-pole switching frequency of RomR (by D53E substitution) caused more frequent cellular reversals in the entire A-motility system (Leonardy *et al.*, 2008; Leonardy *et al.*, 2007).

1.5.3 Polarity switching of type IV pili

Because T4P in *M. xanthus* localize unipolarly at the leading cell pole, every time

the cell reverses, T4P must be disassembled at the old leading cell pole and reassembled at the new leading pole (Søgaard-Andersen, 2004; Sun *et al.*, 2000). To date, localization of three proteins important for T4P-dependent motility has been addressed.

Using immunofluorescence microscopy Nudleman and colleagues (Nudleman *et al.*, 2006) demonstrated that both the Tgl lipoprotein and the secretin PilQ are present in clusters at the cell poles. PilQ was found in equal amounts at both poles, whereas Tgl was only observed as a single condensed locus at one cell pole. On the basis of these observations, the authors suggested that T4P are assembled when Tgl is physically transferred from a donor cell to a recipient cell triggering PilQ multimerization at the new leading pole (Nudleman *et al.*, 2006). At the same time PilQ multimers at the old leading pole would disassemble. However, this model is difficult to reconcile with other experimental evidence. First, it seems very unlikely that PilQ multimers, which are resistant to boiling in 10% SDS for hours, could be disassembled within 1 min (a cellular reversal takes 30-60 s). Second, this model fails to explain how T4P polarity switching occurs in cells, which are not within contact distance of other cells (Sun *et al.*, 2000). The most plausible explanation of Tgl unipolar localization is that Tgl specifically accumulates at the new cell pole created by cell division to assist in the formation of functional PilQ multimers.

Ward and colleagues identified the FrzS protein as essential for T4P-dependent motility (Ward *et al.*, 2000). FrzS contains an N-terminal pseudo-receiver domain, i.e. a receiver domain without the conserved aspartate residue that receives a phosphoryl group from a histidine kinase, and a C-terminal coiled-coil domain. A *frzS* mutant still assembles functional T4P (Mignot *et al.*, 2005), thus, the specific function of FrzS is unknown. Mignot *et al*. (Mignot *et al.*, 2005) found that FrzS fused to GFP localized to the cell poles and, moreover, that FrzS oscillated between the poles in parallel with a cellular reversal and the large FrzS cluster always followed T4P localization. Importantly, FrzS localization was found to be no longer dynamic in *frz* hypo-reversing mutant, suggesting that Frz chemosensory system is required for FrzS (and T4P) polarity switching (Mignot *et al.*, 2005). This study revealed that at least some components of T4P-dependent motility oscillate between the poles during reversal, i.e. might be involved in the regulation of directed cell movement. However, the molecular mechanism underlying the T4P polarity switching during cellular reversals remains uncharacterized.

1.5.4 Regulation of polarity switching by Ras-like GTPase MglA

Taking advantage of the distinct localization patterns of FrzS and RomR,

Leonardy *et al*. (Leonardy *et al.*, 2007) used these two proteins as markers for the polarity of T4P and the A-motility system, respectively. In this study the two proteins were observed to relocate between poles independently of each other, but in synchrony during reversals (Leonardy *et al.*, 2007), suggesting the synchronous polarity switching of the two motility systems. Until recently, the mechanism underlying this synchronous polarity switching remained unclear.

The best candidate for a single spatial regulator in *M. xanthus* was the MglA protein, because it is the only protein required for both motility systems (Hodgkin and Kaiser, 1979b). Interestingly, MglA is homologous to small GTPases of the Ras-superfamily, which in eukaryotic systems act as regulatory proteins often by recruiting factors to their site of action (Charest and Firtel, 2007). The first line of evidence, suggesting that MglA in fact is required for establishment of the correct polarity of motility proteins, came from localization experiments described by Leonardy *et al*. (Leonardy *et al.*, 2007), who analyzed RomR localization in an *mglA* mutant. In the absence of MglA RomR localized in a unipolar pattern instead of a bipolar symmetric pattern characteristic for WT cells. Additionally, the RomR cluster in an *mglA* mutant colocalized with T4P, i.e. RomR was at the wrong pole and did not relocate between poles (Leonardy *et al.*, 2007).

Later, Mauriello and colleagues (Mauriello *et al.*, 2010) demonstrated that FrzS and AglZ localization was also affected in an *mglA* mutant. Moreover, this study revealed the importance of an actin-like protein MreB for both motility systems in *M. xanthus*, as blocking the MreB assembly with a specific drug A22 led to the inactivation of the T4P-dependent and A-motility (Mauriello *et al.*, 2010).

Finally, Leonardy *et al*. (Leonardy *et al.*, *in review*) analyzed several *mglA* mutants, containing substitutions of functionally important residues. In order to directly test the localization of A-motility proteins, RomR and AglZ were used as markers. The MglA^{G21V} mutant has a substitution in the phosphate-binding loop and corresponds to the oncogenic Ras^{G12V} mutant. Biochemical analyses showed that this mutant protein is permanently in the GTP-bound state (Leonardy *et al.*, *in review*) and, thus, thought to be permanently active (Scheffzek *et al.*, 1997; Vetter and Wittinghofer, 2001). *mglA*^{G21V} cells reversed on average every 4.5 min compared to *mglA*$^{+}$ cells, which reversed on average every 15 min. Moreover, RomR and AglZ hyper-switched in *mglA*^{G21V} cells. The MglA$^{T26/27N}$ mutant was designed based on the assumption that its properties are similar to the Ras^{S17N} mutant characterized by the reduced binding of nucleotides and tight binding to GEF (Cool *et al.*, 1999; Feig, 1999; John *et al.*, 1993; Leonardy *et al.*, *in review*). *mglA*$^{T26/27V}$ cells are unable to move, and both RomR and AglZ exhibited

altered localization. These observations led to a model, in which MglA/GTP stimulates A-motility by establishing the correct polarity of A-motility proteins and in which the GTP-bound state of MglA also stimulates reversals at the cellular level and pole-to-pole oscillations of motility proteins at the molecular level (Leonardy *et al.*, *in review*).

In eukaryotic cells, small GTPases are regulated by GEFs or GAPs (Bourne *et al.*, 1991). Based on sequence conservation, a search of the *M. xanthus* genome did not reveal eukaryotic-like GEFs or GAPs. However, genetic and/or biochemical evidence showed that MglA activity is controlled temporally and spatially by the Frz chemosensory system and by MglB protein, acting as MglA specific GEF and GAP, respectively (Leonardy *et al.*, *in review*).

To summarize, the full set of data on MglA clearly points towards MglA being an important spatial regulator in *M. xanthus* cells, which acts downstream of Frz system during cellular reversal and directs the A-motility proteins to the correct poles. Whether MglA is also regulating the dynamics of T4P remains an open question. Additionally, *M. xanthus* possesses two uncharacterized MglA paralogs, which might be also involved in the regulation of *M. xanthus* motility.

1.6 Scope of the study

More than 40 years ago Hodgkin and Kaiser revealed that gliding motility in *M. xanthus* is controlled by two multigene systems: the A-system and the S-motility. S-motility was shown to be powered by the T4P (Hodgkin and Kaiser, 1979a, b; Wu and Kaiser, 1995). In 1986 Blackhart and Zusman described cellular reversals, regulated by the Frz chemosensory system and leading to the polarity switching of *M. xanthus* cells (Blackhart and Zusman, 1985). Molecular mechanisms underlying A-motility function and Frz-regulated polarity switching have been extensively studied in the past five years (Leonardy *et al.*, 2007; Mauriello *et al.*, 2009b; Mignot *et al.*, 2007). However, in the T4P system, only the FrzS protein has been characterized in details with respect to localization (Mignot *et al.*, 2005). Thus, the molecular mechanisms of T4P-powered motility remain unelucidated.

In this study, I primarily addressed the molecular mechanisms underlying the T4P polarity switching during cellular reversal, as T4P in *M. xanthus* localize only at the leading cell pole, and thus switch pole during reversal (Mignot *et al.*, 2005; Sun *et al.*, 2000). For this, the localization of six highly conserved T4P components was investigated in parallel. The data obtained in this study suggest that the T4P polarity switching during reversals as well as T4P extension/retraction cycles are regulated by the dynamic disassembly and reassembly of the individual parts of the T4P molecular machine. Moreover, this study demonstrates the interdependency between T4P

components with respect to their stability and localization. Finally, regulation of the correct T4P localization at the leading cell pole by the small GTPase MglA and its paralog SofG was studied. This is the first comprehensive study of the molecular mechanisms of the T4P assembly and disassembly in *M. xanthus*.

2 Results

2.1 Characterization of *pilMNOPQ* gene cluster

The *pilMNOPQ* gene cluster encodes non-core T4P components, but is highly conserved with respect to both gene order and sequence identity among T4aP systems (Pelicic, 2008). In *P. aeruginosa*, *P. syringae, Neisseria* species and *M. xanthus* these proteins are essential for T4P biogenesis and twitching motility (Alm and Mattick, 1995; Ayers *et al.*, 2009; Carbonnelle *et al.*, 2006; Martin *et al.*, 1995; Nudleman *et al.*, 2006; Roine *et al.*, 1998). Moreover, in genera such as *Haemophilus* and *Thermus* this gene cluster (in *Haemophilus* annotated as *comABCDE*) is essential for T4P-mediated natural transformation (Bakaletz *et al.*, 2005; Rumszauer *et al.*, 2006). Additionally, a recent report showed that the PilM/N/O/P proteins from *P. aeruginosa* form an inner membrane complex required for optimal formation of the outer membrane PilQ multimers (Ayers *et al.*, 2009). In *M. xanthus pilM*, *pilN*, *pilO* and *pilP* point mutants are defective in Tgl lipoprotein donation, but assemble stable PilQ multimers (Nudleman *et al.*, 2006). We hypothesized that the PilM/N/O/P proteins also form an inner membrane complex in *M. xanthus* and that they might be required for the proper localization of the core T4P components, i.e. PilQ, PilC, PilD, PilT, PilB and PilA proteins (Figure 5). To explore this possibility, we decided to first confirm the reported phenotypes by generating non-polar, unmarked in-frame deletions in each of the *pilMNOP* genes.

2.1.1 *pilM*, *pilN*, *pilO*, *pilP* and *pilQ* genes constitute an operon

In *M. xanthus pilMNOPQ* genes are located in the *pil*-gene locus (Figure 6). It has been often assumed, but never tested whether these genes constitute an operon. Thus, first the *pilMNOPQ* transcriptional unit was mapped using a reverse transcription-PCR approach. For this purpose, total RNA was isolated from exponentially growing WT cultures, and cDNA was synthesized (Materials and Methods). Primer pairs were designed to generate PCR products covering the intergenic regions, as well as internal gene regions (Figure 10A). All PCR products were obtained with both genomic and cDNA as templates (Figure 10B), suggesting that *pilM*, *pilN*, *pilO*, *pilP* and *pilQ* genes constitute a single transcription unit.

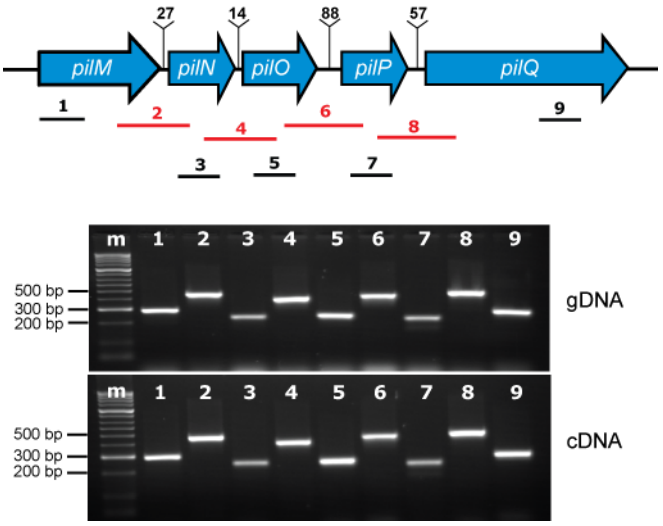

Figure 10. Operon mapping of *pil M/N/O/P/Q* gene cluster

A) Schematic representation of *pilM/N/O/P/Q* gene cluster. Numbers on top indicate distances between genes in bp. Black bars below correspond to the internal PCR products (odd numbers), red bars to the intergenic PCR products. **B)** Gel electrophoresis of PCR products received with internal (odd numbers) and intergenic (even numbers) primers. Genomic DNA and RNA were extracted from exponentially growing WT cells. cDNA was prepared as described in Materials and Methods. Top panel represents PCR products with genomic DNA as a template, bottom panel PCR products with cDNA as a template. M indicates a marker. Numbers on top correspond to the numbers in (A).

2.1.2 *pilM*, *pilN*, *pilO* and *pilP* in-frame deletions have S-motility defect

In-frame deletions of each of the *pilMNOP* genes were generated as described in Materials and Methods. PilQ has been shown to be required for T4P-dependent motility (Wall *et al.*, 1999). Thus, we predicted that deletions of each of the *pilMNOP* genes also may lead to the S-motility defects. To test A- and S-motility phenotypes of the generated mutants, colony morphologies on 1.5% and 0.5% agar plates were examined. On 1.5% agar, favoring A-motility, Δ*pilM*, Δ*pilN*, Δ*pilO* and Δ*pilP* colonies spread similarly to the WT colonies, and single cells were observed at the edge of each colony, which was not the case for the A^-S^+ control strain SA1128 (Figure 11).

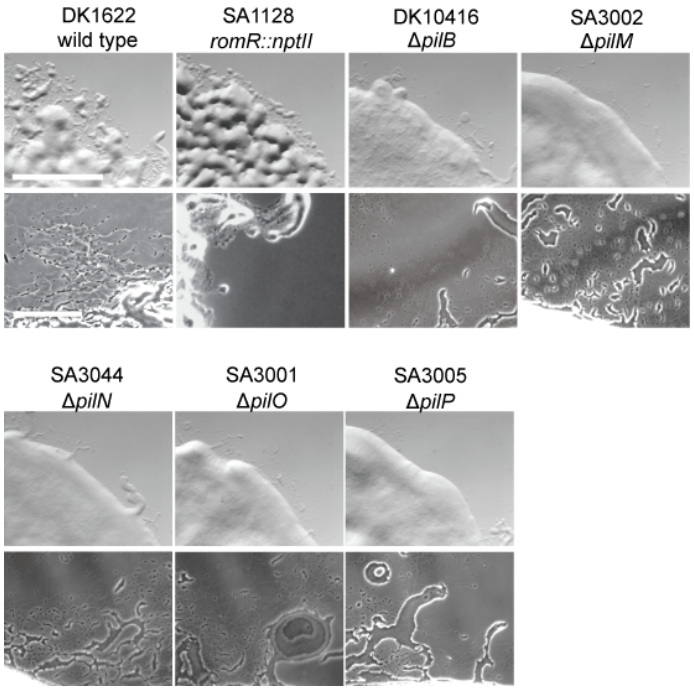

Figure 11. Individual in-frame deletions of *pilMNOP* genes do not affect A-motility

Motility phenotypes of Δ*pilM*, Δ*pilN*, Δ*pilO* and Δ*pilP* mutants. Cells were incubated at 32˚C for 24h on 1.5% agar supplemented with 0.5% CTT, and visualized with a stereomicroscope at 50-fold (top row) and 200-fold (bottom row) magnifications. Strain names and relevant genotypes are indicated. Scale bar for panels in top and bottom row: 5 mm and 50 µm, respectively.

On 0.5% agar, which favors T4P-dependent motility, in contrast to WT cells Δ*pilM*, Δ*pilN*, Δ*pilO* and Δ*pilP* colonies did not form rafts at the edge, but had rather a sharp edge (Figure 12). Therefore, we conclude that all of the PilM/N/O/P proteins are essential for T4P-dependent motility in *M.xanthus*.

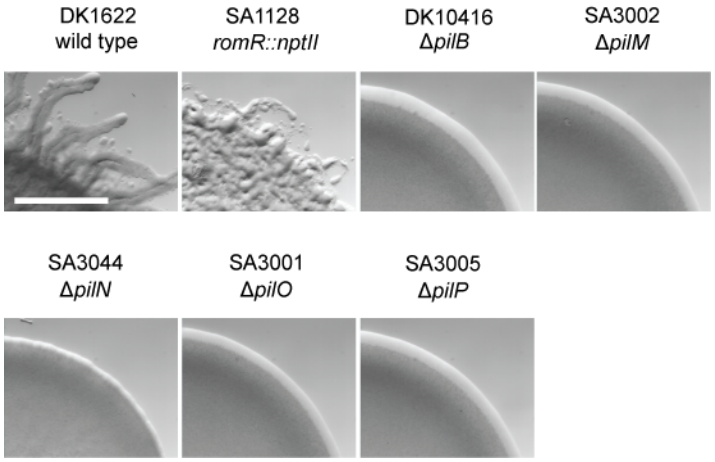

Figure 12. PilM, PilN, PilO and PilP are essential for T4P-dependent motility

Motility phenotypes Δ*pilM*, Δ*pilN*, Δ*pilO* and Δ*pilP* mutants. Cells were incubated at 32˚C for 24h on 0.5% agar supplemented with 0.5% CTT, and visualized with a stereomicroscope at 50-fold magnification. Strain names and relevant genotypes are indicated. Scale bar: 5 mm.

2.1.3 PilM, PilN, PilO and PilP are required for exopolysaccharides accumulation

It has been shown that genes required for T4P biogenesis are also required for accumulation of the exopolysaccharide (EPS) part of the extracellular matrix in

M. xanthus (Black *et al.*, 2006). To elucidate whether the Δ*pilM*, Δ*pilN*, Δ*pilO*, Δ*pilP* and Δ*pilQ* mutants are still able to accumulate EPS, qualitative Congo red binding assays were conducted, as Congo red binds to EPS of *M. xanthus* cells (Arnold and Shimkets, 1988; Colvin and Witter, 1983). Samples were prepared as for motility assays, and cells were spotted on 1.0% agar plates, supplemented with 0.5% CTT and 15 µg/ml Congo red. The Δ*dsp* (DK3470) strain was used as a control, because it is deficient in the exopolysaccharide (EPS) accumulation (Shimkets, 1986b), the Δ*digR* (SA1804) strain in contrast overaccumulates EPS (Overgaard *et al.*, 2006). After 24 h incubation at 32˚C, the changes in the color of the colonies were examined. In contrast to the WT colonies that turned orange or red after 24 h of the incubation, Δ*pilM*, Δ*pilN*, Δ*pilO*, Δ*pilP* and Δ*pilQ* colonies remained yellow resembling the Δ*dsp* mutant, i.e. they did not bind a dye (Figure 13). It is important to note, that the Δ*pilB* colonies, used as a control in this experiment, also remained yellow, whereas Δ*pilT* colonies (Δ*pilT mutant* assembles T4P) turned red.

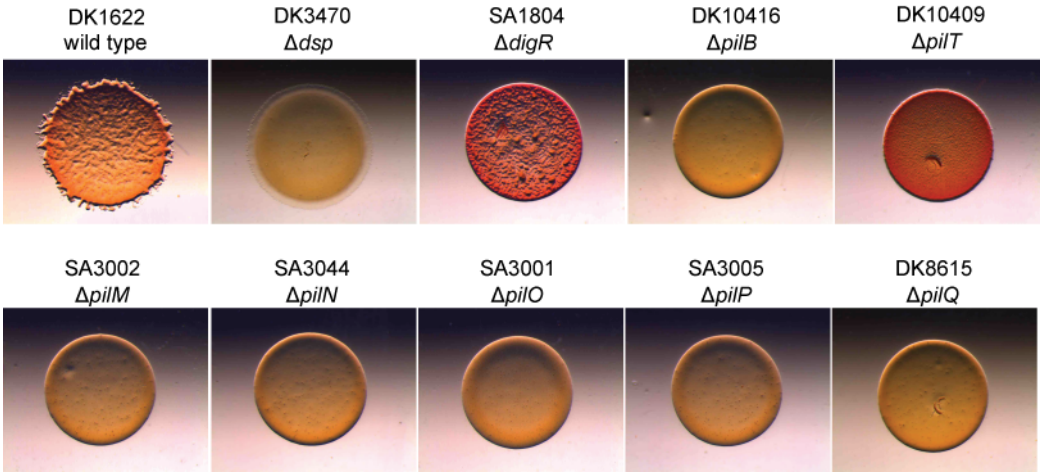

Figure 13. PilM, PilN, PilO and PilP are required for EPS production

Analysis of EPS production using qualitative Congo red binding assay. Cells were incubated at 32˚C for 24h on 0.5% agar supplemented with 0.5% CTT and 15 µg/ml Congo red dye, and visualized with a stereomicroscope at 12-fold magnification. Strain names and relevant genotypes are indicated. Δ*dsp* is deficient in EPS production, Δ*digR* overproduces EPS.

To examine the protein portion of ECM, the accumulation of the FibA metalloprotease was analyzed in total cell lysates. FibA is the most abundant protein in the ECM in *M. xanthus* (Behmlander and Dworkin, 1994b) and is recognized by monoclonal MAb 2105 antibody (Kearns *et al.*, 2002). The Δ*dsp* strain was used as a negative control in these experiments. A 66 kDa protein, which corresponds to full-length FibA (Kearns *et al.*, 2002) was detected in WT. However, this protein was not detected in the Δ*pilM*, Δ*pilN*, Δ*pilO*, Δ*pilP* and Δ*pilQ* mutants (Figure 14A).

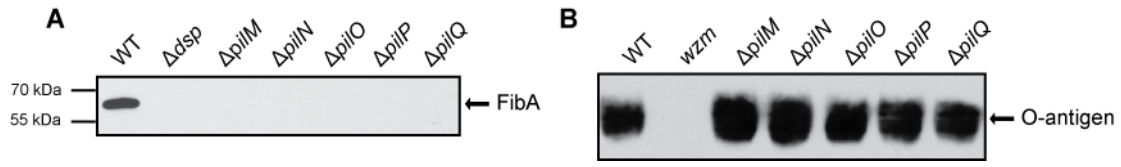

Figure 14. Accumulation of extracellular matrix and O-antigen in Δ*pil M*/*N*/*O*/*P* mutants

A) Immunoblot analysis of FibA metalloprotease accumulation. Cells from the exponentially growing cultures were harvested, total protein was separated by SDS–PAGE (protein from 7×10^7 cells loaded per lane), and analyzed by immunoblotting. Strains used (left to right): DK1622, DK3470 (Δ*dsp*), SA3002 (Δ*pilM*), SA3044 (Δ*pilN*), SA3001 (Δ*pilO*) SA3005 (Δ*pilP*) and DK8615 (Δ*pilQ*). Blot was probed with MAb 2105 monoclonal antibody. FibA protein is indicated on the right. Migration of molecular size markers is indicated on the left. **B)** Immunoblot analysis of total cell lysates with MAb 783 monoclonal antibody, specific to O-antigen portion of LPS. Cells from exponentially growing cultures were harvested and samples analyzed as in Figure 17A. Strains used as in panel (A), except for HK1321(*wzm*$^-$) strain, which is deficient in O-antigen synthesis.

To rule out that the S-motility defects of Δ*pilM*, Δ*pilN*, Δ*pilO*, Δ*pilP* and Δ*pilQ* mutants were caused by the absence of LPS O-antigen, which was previously demonstrated to be required for S-motility (Bowden and Kaplan, 1998), LPS O-antigen accumulation was determined by immunoblot analysis of total cell lysates with the monoclonal antibody (MAb 783) raised against *M. xanthus* O-antigen (Bowden and Kaplan, 1998). HK1321 strain carrying a mutation in *wzm* gene was used as a negative control. *wzm* encodes a subunit of an ABC transporter required for synthesis of the O-antigen. As depicted in Figure 14B, Δ*pilM*, Δ*pilN*, Δ*pilO*, Δ*pilP* and Δ*pilQ* mutants accumulated O-antigen at levels similar to WT. Thus, we conclude that each of the five PilM/N/O/P/Q proteins is dispensable for LPS O-antigen synthesis, but required for accumulation of EPS and of the protein fraction of ECM.

Similarities in ECM accumulation and S-motility defects of Δ*pilM*, Δ*pilN*, Δ*pilO*, Δ*pilP* and Δ*pilQ* mutants are consistent with a finding that these five genes constitute a single transcriptional unit. It has been demonstrated that Δ*pilQ* mutant does not assemble T4P (Wall *et al.*, 1999), but remains to be tested for Δ*pilM*, Δ*pilN*, Δ*pilO* and Δ*pilP* mutants.

2.1.4 PilQ multimeric complexes are stable in the absence of PilM/N/O/P proteins

Knowing that in *P. aeruginosa* PilM, PilN, PilO and PilP proteins are essential for a stable PilQ multimer formation in the outer membrane (Ayers *et al.*, 2009), we investigated whether this is also a case in *M. xanthus*. For this purpose a full-length PilQ (~98 kDa) was purified under denaturing conditions (described in Materials and Methods) and used for rabbit polyclonal antibody generation. In immunoblot analysis on cell lysates from WT and the Δ*pilQ* mutant (Figure 15), the anti-PilQ antibodies

recognized three proteins with sizes of >250 kDa, 98 kDa and 50 kDa in the WT, which were not present in the Δ*pilQ* mutant and correspond to the PilQ multimers, the PilQ monomer and a specific degradation product of PilQ, respectively (Nudleman *et al.*, 2006).

To address PilQ accumulation in the absence of PilM/N/O/P proteins, quantitative immunoblot analysis was performed with SA3002 (Δ*pilM*), SA3044 (Δ*pilN*), SA3001 (Δ*pilO*) and SA3005 (Δ*pilP*) total cell lysates (Figure 15). WT and DK10405 (Δ*tgl*) cells were used as controls, as Tgl lipoprotein was previously shown to be required for PilQ multimer formation (Nudleman *et al.*, 2006). Notably, the anti-PilQ antibodies recognized all three proteins, detected in WT, in the Δ*pilM*, Δ*pilN*, Δ*pilO* and Δ*pilP* mutants (Figure 15). The bands corresponding to the PilQ multimers and to the 50 kDa degradation product, however, were not detected in DK10405 (Δ*tgl*) cells, which is consistent with previously reported data (Nudleman *et al.*, 2006). To summarize these results, we conclude that PilM/N/O/P proteins are not essential for PilQ complex formation or stabilization in *M. xanthus*. Further experiments will be performed to elucidate whether deletion of Δ*pilM/N/O/P* affects Tgl donation as described for *pilM/N/O/P* mutants (Nudleman *et al.*, 2006).

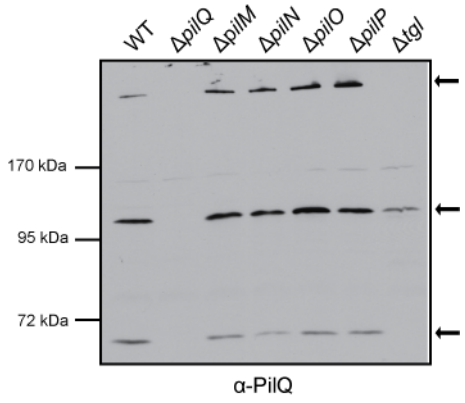

Figure 15. PilM, PilN, PilO and PilP are not required for PilQ multimers formation

Immunoblot analysis of PilQ accumulation. Cells from exponentially growing cultures were harvested and samples analyzed as in Figure 14A. Strains used (left to right): DK1622 (WT), DK3470 (Δ*pilQ*), SA3002 (Δ*pilM*), SA3044 (Δ*pilN*), SA3001 (Δ*pilO*) SA3005 (Δ*pilP*) and DK10405 (Δ*tgl*). Blot was probed with anti-PilQ antibodies. PilQ multimer (>250 kDa), PilQ monomer (~98 kDa) and PilQ degradation product (50 kDa) are indicated on the right. Migration of molecular size markers is indicated on the left.

2.1.5 PilN accumulation is affected in the absence of PilO and PilP

Recent studies in *P. aeruginosa* demonstrated that the accumulation levels of the PilM/N/O/P proteins are interdependent so that in the absence of one component, the accumulation of the others is significantly decreased or completely abolished (Ayers *et al.*, 2009; Sampaleanu *et al.*, 2009). We hypothesized that a similar interdependence could be present in *M. xanthus*. To test this idea, the accumulation of PilN protein was examined in all *pil* mutants by quantitative immunoblot analysis using anti-PilN antibodies (C. Schmidt, MPI Marburg).

As shown in Figure 16, PilN levels comparable to that in WT were observed in all mutants except for the Δ*pilO* and Δ*pilP* mutants. In Δ*pilP* mutant cells PilN accumulation was 2.5 fold lower than in WT cells, while in Δ*pilO* mutant cells PilN was barely detectable. These results suggest that in *M. xanthus* PilN accumulation depends on the accumulation of PilP and PilO but is independent of PilM.

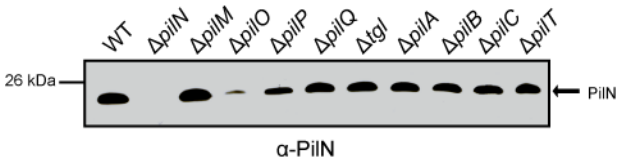

Figure 16. PilO and PilP proteins are required for PilN accumulation

Immunoblot of PilN accumulation. Cells from exponentially growing cultures were harvested and samples analyzed as in Figure 14A. Strains used (left to right): DK1622 (WT), SA3044 (Δ*pilN*), SA3002 (Δ*pilM*), SA3001 (Δ*pilO*), SA3005 (Δ*pilP*), DK8615 (Δ*pilQ*), DK10405 (Δ*tgl*), DK10410 (Δ*pilA*), DK10416 (Δ*pilB*), DK10417 (Δ*pilC*) and DK10409 (Δ*pilT*). Blot was probed with anti-PilN antibodies. PilN protein is indicated on the right. Migration of molecular size markers is indicated on the left.

2.2 Type IV pili machinery: localization and dynamics

It has been shown that the Frz chemosensory system controls the disassembly and reassembly of the T4P apparatus during reversal on the cellular level (Sun *et al.*, 2000). Moreover, it has been reported that the Frz system induces pole-to-pole relocation of two A-motility proteins (Leonardy *et al.*, 2007; Mignot *et al.*, 2007) and of a pseudo-response regulator FrzS which is required for S-motility (Mignot *et al.*, 2005). However, the exact function of FrzS remains unknown, and a *frzS* mutant still assembles functional T4P (Mignot *et al.*, 2005). Therefore, the molecular mechanism of T4P polarity switching during reversal remains unknown. We hypothesized that the localization of T4P proteins is a crucial parameter to determine at which pole T4P are assembled. To test this hypothesis, we analyzed the localization of six T4P proteins, which in combination localize to three different cellular compartments and were shown to be required for T4P biogenesis and retraction in *M. xanthus* (Jakovljevic *et al.*, 2008; Nudleman *et al.*, 2006; Wall *et al.*, 1999; Wu *et al.*, 1997). These six proteins have orthologs in all T4aP systems (Pelicic, 2008).

2.2.1 Outer membrane secretin PilQ localizes in a bipolar symmetric pattern

PilQ is a 901 amino acid protein with orthologs in all T4P systems (except for Gram-positive species) (Pelicic, 2008) that assembles into a heat-resistant multimeric complex functioning as a conduit for T4P in the outer membrane (Nudleman *et al.*,

2006; Wall *et al.*, 1999). To localize PilQ in *M. xanthus,* we attempted to construct an active fluorescent fusion protein in which PilQ was fused to mCherry. However, all attempts to generate active fusion proteins were unsuccessful as judged by the inability of the various constructs to complement the motility defect of the Δ*pilQ* mutant (DK8615). Therefore, in order to localize PilQ we performed the immunofluorescence microscopy with specific anti-PilQ antibodies.

For immunofluorescence microscopy *M. xanthus* cells were grown to a density of 7×10^8 cells per ml in liquid 1% CTT medium at 32°C, and fixed directly from suspension. Because T4P-dependent motility only functions in cells located on a surface, we also analyzed PilQ localization in moving cells. For this purpose, cells were grown to a density of 7×10^8 cells per ml, harvested, resuspended in 1% CTT medium to a calculated density of 7×10^9 cells/ml, and spotted (10 µl aliquots of cells) on a thin layer of 1.0% agar supplemented with 0.5% CTT. After 3-4 h incubation at 32°C, cells were harvested from the agar surface by washing with liquid 1% CTT medium mixed with a fixing solution. Under both conditions, affinity-purified anti-PilQ antibodies recognized PilQ clusters at the two cell poles (Figure 17A). These two polar PilQ clusters were of equal intensity (Figure 17A and B).

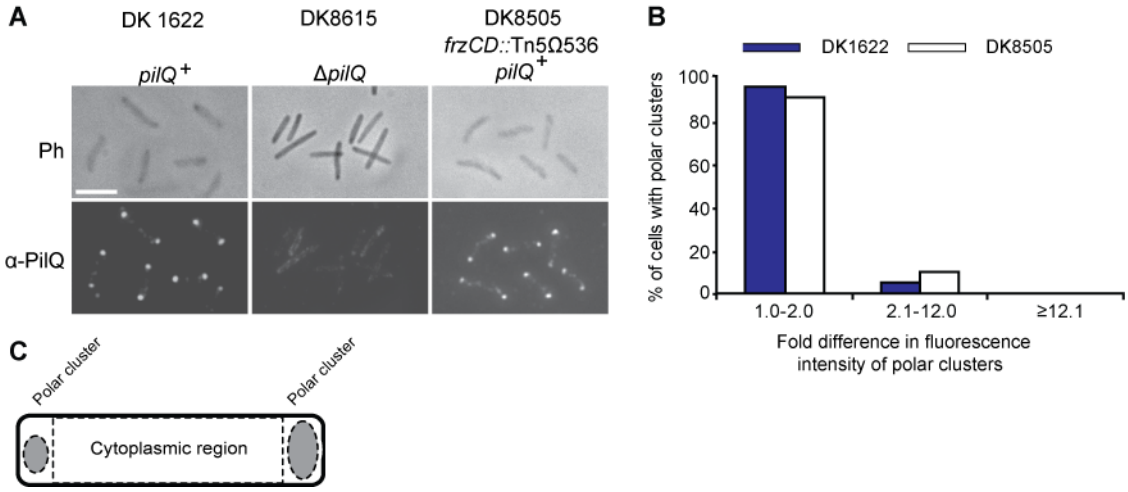

Figure 17. PilQ localizes in a bipolar symmetric pattern

A) Localization of PilQ by immunofluorescence microscopy using affinity-purified anti-PilQ antibodies in WT, Δ*pilQ* mutant, and *frz* mutant. Cells were harvested from the exponentially growing cultures, fixed, reacted with anti-PilQ antibodies and secondary antibodies, and imaged by fluorescence and phase-contrast microscopy. Top and bottom rows show phase-contrast and fluorescence images, respectively. Scale bar: 5 µm. **B)** Histogram of distribution of PilQ polar clusters WT and *frz* mutant. The integrated fluorescence intensities (arbitrary units) of the two background-subtracted polar clusters in a cell were measured and fold differences were calculated. Fold differences from 1.0 to 2.0 represent a bipolar symmetric pattern, fold differences between 2.1 and 12.0 represent a bipolar symmetric pattern, and differences more than 12.1 represent a unipolar pattern. In total N=100 cells were analyzed for each strain.

C) Schematic of the cell indicating the three regions for which fluorescence signals were quantified. Grey ovals indicate polar clusters.

Thus, in WT PilQ localizes in bipolar symmetric clusters as previously reported (Nudleman *et al.*, 2006). This localization pattern suggests that the two PilQ clusters are statically localized to the cell poles during cellular reversals. To further investigate this hypothesis, PilQ localization was determined in an *frz* mutant. The Frz chemosensory system regulates the cellular reversal frequency and *frz* mutants rarely reverse. In the strain DK8505, which contains the *frzCD*::Tn5lacΩ536 allele, PilQ also localized in a bipolar symmetric pattern. From these analyses, we conclude that native PilQ localizes in a bipolar symmetric pattern and that the polar PilQ clusters likely remain stationary during cellular reversals.

2.2.2 Inner membrane protein PilC localizes in a bipolar symmetric pattern

PilC is an integral membrane protein of 417 amino acids with orthologs in all T4P systems and essential for T4P assembly in *M. xanthus* (Wu *et al.*, 1997). PilC in *M. xanthus* is predicted to possess three transmembrane helices using the prediction tool TMHMM (Krogh *et al.*, 2001), two large cytoplasmic loops extending from residue 1 to 185 and 256 to 387, and two small periplasmic loops extending from 209 to 235 and 411 to 417. To verify that PilC in *M. xanthus* is an integral membrane protein we performed cell fractionation experiments with polyclonal anti-PilC antibodies generated against the first cytoplasmic loop of PilC protein extending from residue 1 to 185 (Bulyha *et al.*, 2009). In cell fractionation experiments total cell extracts were divided into fractions enriched for inner membrane proteins, outer membrane proteins and soluble proteins, which include cytoplasmic and periplasmic proteins. PilC was only detected in the fraction enriched for inner membrane proteins (Figure 18A).

Guided by the topology-model of PilC, we attempted to generate active mCherry and yellow fluorescent protein (YFP) fusion proteins. However, all attempts were unsuccessful as judged by the inability of the various constructs to complement the motility defect in a Δ*pilC* mutant (DK10417). Therefore, to localize native PilC immunofluorescence microscopy was performed. In WT cells fixed directly from suspension and cells fixed on a surface anti-PilC recognized PilC at the two cell poles, and the two polar clusters were of equal intensity (Figure 18B). We also observed the bipolar symmetric clusters in the hypo-reversing DK8505 strain, which contains the *frzCD*::Tn5lacΩ536 allele (Figure 18B). From these analyses we conclude that PilC is an integral inner membrane protein that localizes in a bipolar symmetric pattern, and that the polar PilC clusters likely remain stationary during cellular reversals.

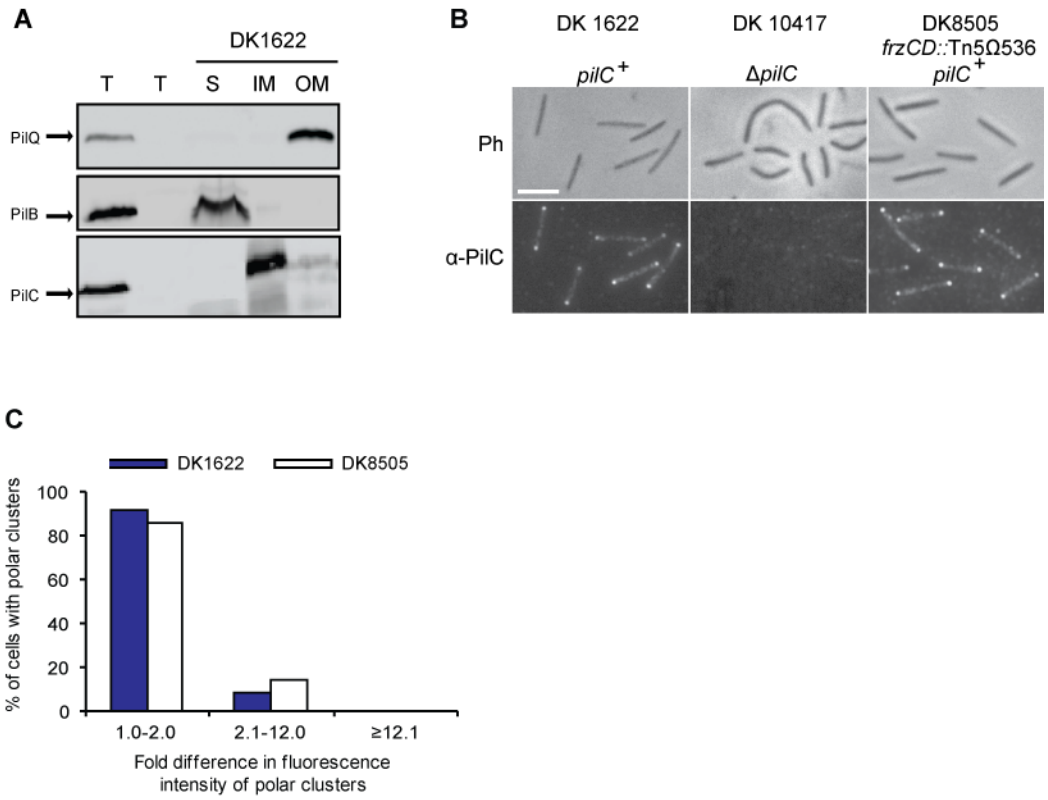

Figure 18. PilC localizes in a bipolar symmetric pattern

A) Subcellular localization of PilC in *M. xanthus*. Total cell extracts (T) were separated into fractions enriched for soluble (S), inner membrane (IM) and outer membrane (OM) proteins. The first lanes contain total cell extract from WT cells and the second lanes contain total cell extract from (top panel to bottom panel) DK8615 (Δ*pilQ*), DK10416 (Δ*pilB*), and DK10417 (Δ*pilC*) cells. Protein from 7×10^8 was loaded per lane and probed with anti-PilQ, anti-PilB or anti-PilC as indicated. **B)** Localization of PilC by immunofluorescence microscopy. Cells were harvested from the exponentially growing cultures and analyzed as described in Figure 14A using anti-PilC antibodies. Top and bottom rows show phase-contrast and fluorescence images, respectively. Scale bar: 5 µm. **C)** Histogram of distribution of PilC polar clusters WT and *frz* mutant. Data are presented as in Figure 17B. In total N=100 cells were analyzed for each strain.

2.2.3 PilN localizes in a bipolar symmetric pattern

PilN is 225 amino acid protein with orthologs in T4P systems of type IVa and is required for T4P assembly in *N. meningitidis* (Carbonnelle *et al.*, 2006), *M. xanthus* (Nudleman *et al.*, 2006) and *P. aeruginosa* (Alm and Mattick, 1995). PilN in *M. xanthus* is predicted to possess one transmembrane helix using the prediction tool TMHMM (Krogh *et al.*, 2001), a cytoplasmic loop extending from residue 1 to 26, and a periplasmic loop, extending from residues 43 to 225. PilN from *P. aeruginosa* was shown to localize predominantly in the inner membrane, forming a complex with PilO, PilP and PilM proteins (Ayers *et al.*, 2009; Sampaleanu *et al.*, 2009). We are currently testing whether this is also the case in *M. xanthus*.

To localize native PilN, immunofluorescence microscopy with specific anti-PilN antibodies, generated against the predicted periplasmic part of PilN (C. Schmidt, MPI

Marburg), was performed. In WT cells anti-PilN antibodies recognized PilN at both cell poles, and the two polar clusters were of equal intensity (Figure 19B). Similarly to the observations made previously for PilQ and PilC proteins, we also observed the bipolar symmetric PilN clusters in the hypo-reversing DK8505 strain, which contains the *frzCD*::Tn5lacΩ536 allele (Figure 19B). From these analyses we conclude that PilN localizes in a bipolar symmetric pattern, and that the polar PilN clusters likely remain stationary during cellular reversals.

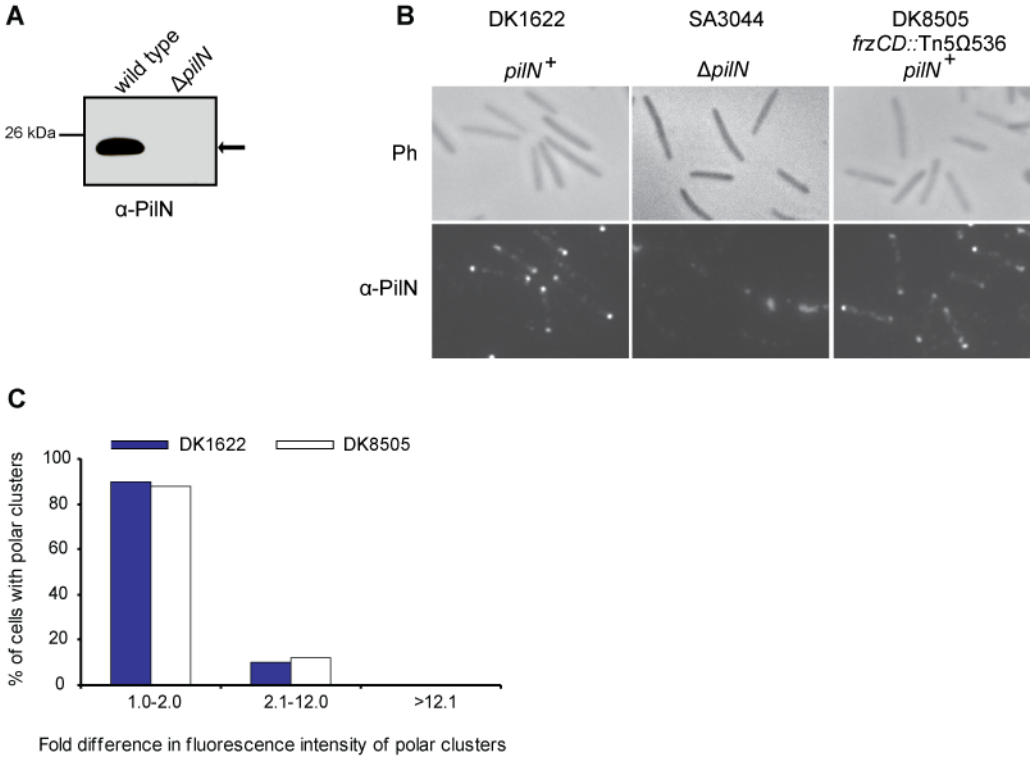

Figure 19. PilN localizes in a bipolar symmetric pattern

A) Immunoblot analysis of WT (left lane) and Δ*pilN* cell extracts. Cells from exponentially growing cultures were harvested and samples analyzed as in Figure 14A. PilN is indicated. Migration of molecular size markers is indicated on the left. **B)** Localization of PilN by immunofluorescence microscopy using anti-PilN antibodies in WT, Δ*pilN* mutant, and *frz* mutant. Cells from exponentially growing cultures were prepared and analyzed as described in Figure 17A. Top and bottom rows show phase-contrast and fluorescence images, respectively. Scale bar: 5 μm. **C)** Histogram of distribution of PilN polar clusters in WT and *frz* mutant. Data are presented as in Figure 17B. In total N=100 cells were analyzed for each strain.

2.2.4 MreB/FtsA-like protein PilM localizes in a bipolar symmetric pattern

PilM is 395 amino acid protein with orthologs in T4P systems of type IVa (Pelicic, 2008) and required for T4P assembly in *N. meningitides* (Carbonnelle *et al.*, 2006), *M. xanthus* (Nudleman *et al.*, 2006) and *P. aeruginosa* (Alm and Mattick, 1995). PilM neither contains a signal peptide nor transmembrane helices as predicted using SignalP (Bendtsen *et al.*, 2004) and TMHMM (Krogh *et al.*, 2001). Domain searches using the SMART domain database (Letunic *et al.*, 2004) showed that PilM contains an

MreB/FtsA domain (residues 43-199).

First, we verified that PilM is a cytoplasmic protein. For this, cell fractionation experiments with polyclonal anti-PilM antibodies generated against full-length PilM (Bulyha *et al.*, 2009) were carried out. In cell fractionation experiments in which total cell extracts were separated into fractions enriched for outer and inner membrane proteins, cytoplasmic and periplasmic proteins, respectively, PilM was only detected in the fraction enriched for soluble proteins (Figure 20). As PilM does not contain a signal peptide, we conclude that PilM is a cytoplasmic protein.

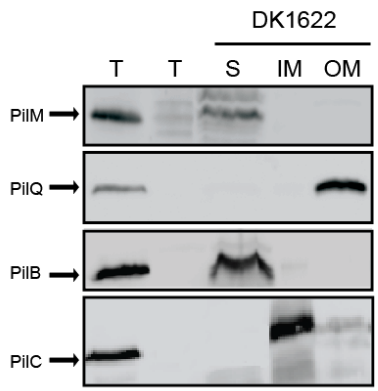

Figure 20. Subcellular localization of PilM in *M. xanthus*

Total cell extracts (T) were separated into fractions enriched for soluble (S), inner membrane (IM) and outer membrane (OM) proteins. The first lanes contain total cell extract from WT cells and the second lanes contain total cell extract from (top panel to bottom panel) SA3002 (Δ*pilM*), DK8615 (Δ*pilQ*), DK10416 (Δ*pilB*), and DK10417 (Δ*pilC*) cells. Protein from 10^8 cells was loaded per lane and probed with anti-PilM, anti-PilQ, anti-PilB or anti-PilC as indicated.

In order to localize PilM, the plasmid pSC8, which contains an *yfp-pilM* allele expressed from the *pilA* promoter, was generated. pSC8 was integrated via site-specific recombination at the chromosomal phage Mx8 attachment site in the strain SA3002 (Δ*pilM*) giving rise to strain SA3046. To verify whether YFP-PilM corrected the motility defect caused by the Δ*pilM* mutation in SA3002, motility assays on 0.5% agar plates favoring T4P-dependent motility (Figure 21B) were carried out. As depicted in Figure 21B, WT formed colonies with large rafts of cells at the edge typical of T4P-dependent motility, whereas SA3002 (Δ*pilM*) did not form rafts at the edge. Importantly, SA3046 (*ΔpilM/yfp-pilM*) displayed a motility phenotype similar to that of the WT.

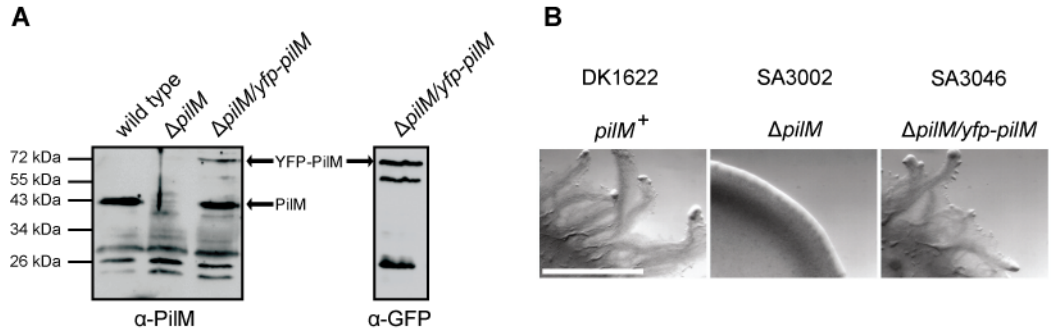

Figure 21. YFP-PilM accumulates at WT levels and restores S-motility defect in Δ*pilM*

A) Immunoblot of PilM and YFP-PilM accumulation. Cells from exponentially growing cultures were harvested and samples analyzed as in Figure 14A. Strains used (left to right): DK1622, SA3002, and SA3046. Blot on the left was probed with rabbit anti-PilM antibodies, and blot on the right with monoclonal anti-GFP antibodies, which also recognize YFP. PilM and YFP-PilM proteins are indicated with the arrows. Migration of molecular size markers is indicated on the left. **B)** YFP-PilM complements the motility defect in a Δ*pilM* mutant. Cells were incubated at 32˚ for 24h on 0.5% agar supplemented with 0.5% CTT, and visualized with a stereomicroscope. Scale bar: 5 mm.

Immunoblot analysis using anti-PilM and anti-GFP antibodies confirmed that YFP-PilM (calculated molecular mass 69.2 kDa) accumulated in SA3046 at a level similar to that of PilM in WT; however, a degradation product with a size similar to that of PilM was detected by anti-PilM and not by anti-GFP (Figure 21A) suggesting that a fraction of YFP-PilM is cleaved around the fusion site. Nevertheless, SA3046 strain was used to localize PilM.

Fluorescence microscopy showed that YFP-PilM localized to the two cell poles in a bipolar symmetric pattern in cells analyzed directly after growth in suspension (Figure 22A) as well as in cells moving on an agar surface (Figure 23A).

To confirm that the localization pattern observed for YFP-PilM reflected that of native PilM, immunofluorescence microscopy was performed on WT cells. As shown is Figure 22B and C, native PilM also localized in a bipolar symmetric pattern in cells analyzed directly after growth in suspension as well as in cells on a surface.

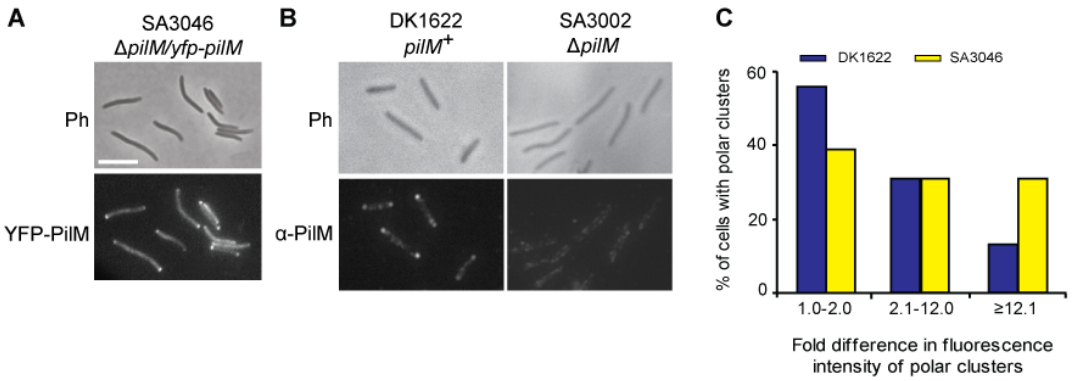

Figure 22. PilM localizes in a bipolar symmetric pattern

A) Localization of YFP-PilM. Cells were transferred from exponentially growing cultures to a thin 0.7% agar pad on a microscope slide, and imaged by fluorescence and phase-contrast microscopy. Top and bottom rows show phase-contrast and fluorescence images, respectively. Scale bar: 5 µm. **B)** Localization of PilM by immunofluorescence microscopy. Cells were harvested from the exponentially growing cultures and analyzed as described in Figure 17A using anti-PilM antibodies. Top and bottom rows show phase-contrast and fluorescence images, respectively. **C)** Histogram of distribution of PilM polar clusters. The data for WT (DK1622) are from immunofluorescence microscopy and for SA3046 from YFP-PilM localization. Data are presented as in Figure 17B. In total N=100 cells were analyzed for each strain.

Thus, YFP-PilM displays a localization pattern similar to that of the native PilM. We took advantage of this observation to analyze the localization of PilM during a cellular reversal. For this purpose cells containing YFP-PilM from the exponentially growing culture were placed on a thin agar pad on a microscope slide and immediately covered with a coverslip. After incubating the samples for 30 min at room temperature time-lapse recordings were performed. Cells were imaged for 15 min with 30 s intervals between frames. In total N=20 cells were followed, a representative cell is shown in Figure 23A. During the entire recording period, YFP-PilM localized in a bipolar symmetric pattern. Importantly, the cell depicted in Figure 23A stopped and reversed between 2:30 and 3:30 min, but the fluorescence intensity of the polar clusters remained unchanged. The quantifications of the polar signals are presented in Figure 23B.

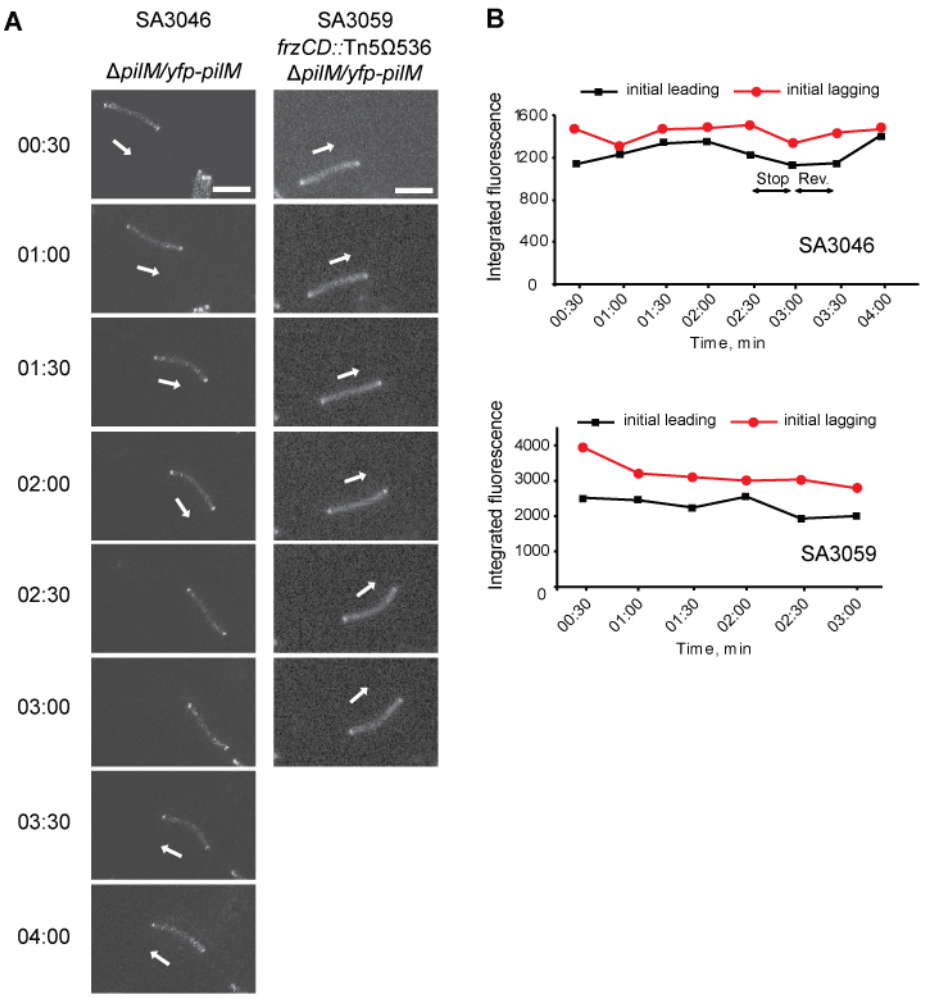

Figure 23. PilM does not relocate between the poles during a cellular reversal

A) Localization of YFP-PilM in moving cells. Cells of SA3046 and SA3059 were transferred from exponentially growing cultures to a thin 0.7% agar pad on a microscope slide, and imaged by fluorescence microscopy at 30 s intervals. Representative cells are shown. The SA3046 cell stopped and reversed between 2:30 and 3:30. White arrows indicate the direction of movement. Scale bar: 5 µm. **B)** Quantitative analysis of polar YFP-PilM fluorescence signals. Integrated fluorescence intensities (arbitrary units) of the two background-subtracted polar clusters in the cells in (A) are plotted as a function of time.

Similarly, the bipolar symmetric YFP-PilM clusters were observed in the hypo-reversing strain SA3059, which contains Δ*pilM* mutation and the *frzCD*::Tn5lacΩ536 mutation (Figure 23AB).

From these analyses we conclude that PilM is a cytoplasmic protein that localizes in a bipolar symmetric pattern and the polar PilM clusters remain static during cellular reversals.

2.2.5 The type IV pili extension motor PilB localizes in three polar patterns

The PilB ATPase energizes the T4P extension in *M. xanthus* upon ATP

hydrolysis (Jakovljevic *et al.*, 2008). PilB is one of the core T4P proteins with orthologs in all T4P systems (Pelicic, 2008). It is also one of the most challenging T4P proteins to analyse with respect to localization, because an active PilB protein fused to a fluorescent protein despite several attempts has not been obtained in *P. aeruginosa* (Chiang *et al*., 2005). Similarly, all our attempts to construct a functional PilB fusion protein in *M. xanthus* using GFP/YFP were unsuccessful as judged by the inability of the various constructs to complement the motility defect in a Δ*pilB* mutant (DK10409). Therefore, to localize PilB in *M. xanthus* immunofluorescence microscopy using anti-PilB antibodies raised against full-length PilB (Jakovljevic *et al.*, 2008) was carried out. Three distinct PilB localization patterns were observed in WT cells fixed directly after growth in suspension or on a surface (Figure 24A and B). 40% of WT cells displayed a unipolar localization pattern (calculated fold differences between the integrated fluorescence intensities of polar clusters >12.1); 35% a bipolar asymmetric pattern (fold differences between 2.1 and 12.0); and 25% a bipolar symmetric pattern (fold differences between 1.0 and 2.0).

Given that T4P in *M. xanthus* are localized in a unipolar pattern at the leading cell pole (Mignot *et al.*, 2005; Sun *et al.*, 2000), we hypothesized that the large PilB cluster localizes at the leading cell pole. In order to test this hypothesis, the immunofluorescence microscopy was conducted on a strain containing a RomR-GFP fusion (Leonardy et al., 2007). RomR-GFP localizes in a bipolar asymmetric pattern with a large cluster at the lagging cell pole, and oscillates from pole to pole during cellular reversals (Leonardy et al., 2007). Therefore, RomR-GFP was used as a marker for the lagging cell pole. As depicted in Figure 24C, a large PilB cluster localized at the pole opposite to that containing the large RomR-GFP cluster. Thus, as expected, the large PilB cluster is at the leading (piliated) cell pole.

The observed PilB localization patterns are consistent with a model in which PilB is dynamically localized and immediately after a reversal localizes to the leading cell pole. Between reversals PilB starts to build up at the opposite (lagging) cell pole giving rise to a bipolar asymmetric pattern, and later to a bipolar symmetric pattern. Upon induction of a reversal by the Frz chemosensory system PilB from the old leading pole completely relocates to the new leading cell pole giving rise - again - to a unipolar localization pattern (model is presented in details in Discussion). Importantly, this model suggests that the Frz chemosensory system is required for PilB relocation during reversals. A prediction from this model is that in a *frz* mutant PilB localization should shift towards a bipolar symmetric pattern. To test this prediction, PilB was localized using immunofluorescence microscopy in the hypo-reversing strain DK8505,

which contains the *frzCD*::Tn5lacΩ536 mutation. Indeed, a shift towards a bipolar symmetric PilB localization was observed in DK8505 cells (Figure 24A and B). 55% of the *frz* mutant cells displayed a bipolar symmetric pattern (compared to 25% in WT), 25% a bipolar asymmetric pattern (35% in WT) and 20% a unipolar localization pattern (40% in WT).

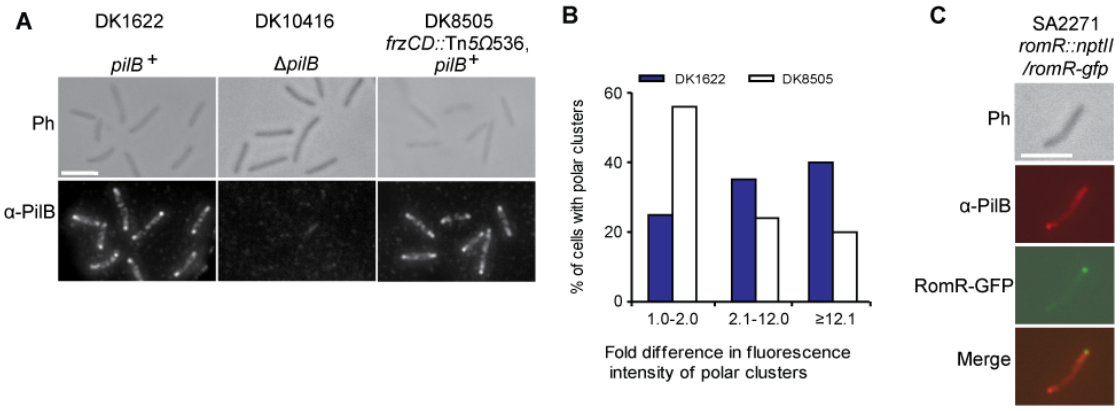

Figure 24. PilB localizes in three distinct polar patterns

A) Localization of PilB by microscopy. Cells were harvested from the exponentially growing cultures, fixed and analyzed as described in Figure 17A using anti-PilB antibodies. Top and bottom rows show phase-contrast and fluorescence images, respectively. Scale bar: 5 µm. **B)** Histogram of distribution of PilB polar clusters. Data are presented as in Figure 17B. In total N=100 cells were analyzed for each strain. **C)** Localization of PilB by immunofluorescence microscopy in RomR-GFP containing strain. Large PilB cluster localizes to the pole opposite to that of RomR-GFP. Cells were prepared and analyzed as described in (A). The top row shows phase-contrast image, middle rows fluorescence images, bottom row represents merged image. Scale bar: 5 µm.

In order to confirm that the mechanism underlying dynamic PilB localization involves the transfer of the protein from the old leading to the new leading pole the following experiments were conducted. *M. xanthus* WT cells were grown in 1% CTT liquid medium to an optical density of 7×10^8 cells/ml, then the culture was divided in two cultures of equal volume (20 ml) and 25 µg/ml chloramphenicol were added to one of the cultures to block protein synthesis. Both cultures were incubated at 32°C at 230 rpm on a shaker for 2 h. Samples (1 ml) were harvested at several time points, starting at 10 min, as we know from the previous research that chloramphenicol blocks protein synthesis in *M. xanthus* already 10 min upon addition (Anna Konovalova, MPI, unpublished data). All samples were precipitated with 10% trichloracetic acid (TCA) and immediately resuspended in SDS loading buffer to a calculated density of 7×10^9 cells/ml. Equal amounts of cells (7×10^7 cells/lane) were loaded for quantitative immunoblot analysis with anti-PilB antibodies. As shown in Figure 25, the amounts of PilB protein remained relatively constant up to 60 min after addition of chloramphenicol

and started to decrease only at 120 min. These data imply that the half-life of PilB is much longer than an average reversal period (15 min under our conditions). Thus, PilB that accumulates at the new leading pole just after reversal is not synthesized *de novo*, but must be transferred from the old leading pole.

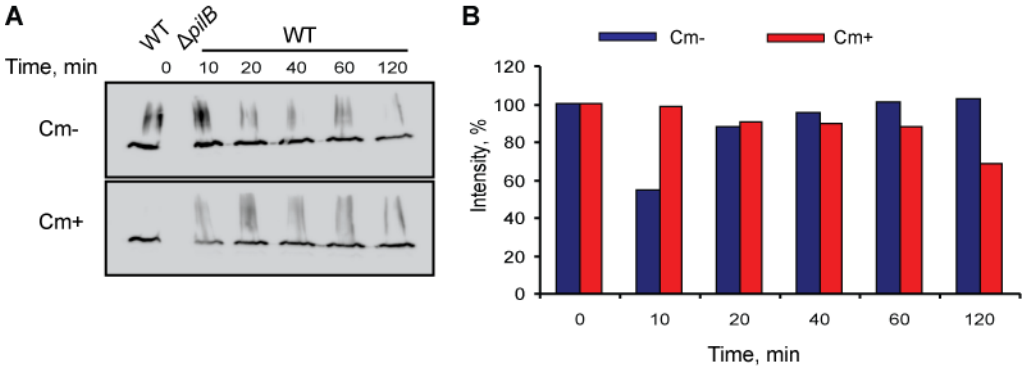

Figure 25. PilB levels are unchanged in presence of chloramphenicol for 60 min

A) Immunoblots of PilB accumulation. Total protein from 7×10^7 cells per lane was loaded. Top panel depicts PilB accumulation in untreated WT cells; bottom panel PilB accumulation in WT cells treated with chloramphenicol (Cm). **B)** Quantitative analysis of PilB accumulation. PilB levels in cells grown without Cm are shown in blue bars; in cells treated with Cm in red bars.

In summary, we found that PilB localizes predominantly at the leading cell pole and that PilB localization is likely dynamic with PilB being unipolar at the leading cell pole immediately after a cellular reversal, building up also at the lagging cell pole during a reversal period, and, finally, PilB relocating from the old leading pole to the new leading cell pole.

2.2.6 The type IV pili retraction motor PilT oscillates from pole to pole during reversal

PilT is a secretion ATPase, which upon ATP hydrolysis energizes T4P retraction in *M. xanthus* (Jakovljevic *et al.*, 2008). PilT orthologs are present in the majority of T4P systems (Pelicic, 2008). In order to localize PilT, the plasmid pIB75, which contains an *yfp-pilT* allele expressed from the *pilA* promoter, was generated. pIB75 was integrated at the chromosomal Mx8 attachment site in the strain DK10409 (Δ*pilT*) giving rise to strain SA3045. YFP-PilT fully corrected the S-motility defect caused by the Δ*pilT* mutation, as determined by motility assays on 0.5% agar favoring T4P-motility (Figure 26A). Furthermore, immunoblot analysis with anti-PilT antibodies generated against full-length PilT (Jakovljevic *et al.*, 2008) and anti-GFP antibodies showed that YFP-PilT (calculated molecular mass 67.6 kDa) accumulated at a level similar to that of PilT protein in WT cells (Figure 26B). However, a degradation product with a size of 50 kDa was also detected by both anti-PilT and anti-GFP antibodies

(Figure 26B, marked by grey arrow), suggesting that a fraction of YFP-PilT is cleaved.

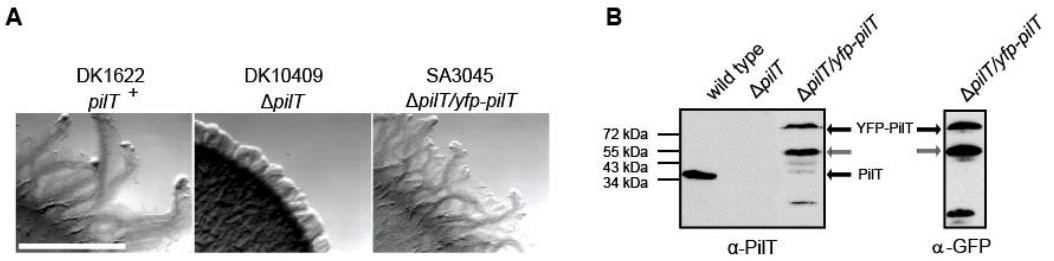

Figure 26. **YFP-PilT accumulates at WT levels and restores S-motility defect in Δ*pilT***

A) YFP-PilT complements the motility defect in a Δ*pilT* mutant. Cells were incubated at 32˚ for 24h on 0.5% agar supplemented with 0.5% CTT, and visualized with a stereomicroscope at 50-fold magnification. Scale bar: 5 mm. WT formed colonies with large rafts of cells at the edge typical of T4P-dependent motility whereas DK10409 (Δ*pilT*) did not form rafts at the edge. However, SA3045 (*ΔpilT/yfp-pilT*) displayed a motility phenotype similar to that of the WT. **B)** Immunoblot of PilT and YFP-PilT accumulation. Cells from exponentially growing cultures were harvested and samples analyzed as in Figure 14A. Strains used (left to right): DK1622, DK10409, and SA3045. Blot on the left was probed with rabbit anti-PilT antibodies, and blot on the right with monoclonal anti-GFP antibodies, which also recognize YFP. PilT and YFP-PilT proteins are indicated with the arrows. Grey arrows indicate the degradation product of YFP-PilT. Migration of molecular size markers is indicated on the left.

Therefore, we studied PilT localization using YFP-PilT as well as by immunofluorescence microscopy. In cells analyzed directly from suspension both YFP-PilT (Figure 27A and C) and a native PilT (Figure 27A and B) localized predominantly in a bipolar symmetric pattern. Surprisingly, in cells with bipolar asymmetric or unipolar PilT clusters, a large PilT cluster localized to the lagging, non-piliated cell pole, where it colocalized with the RomR-GFP - marker for the lagging cell pole (Figure 27D).

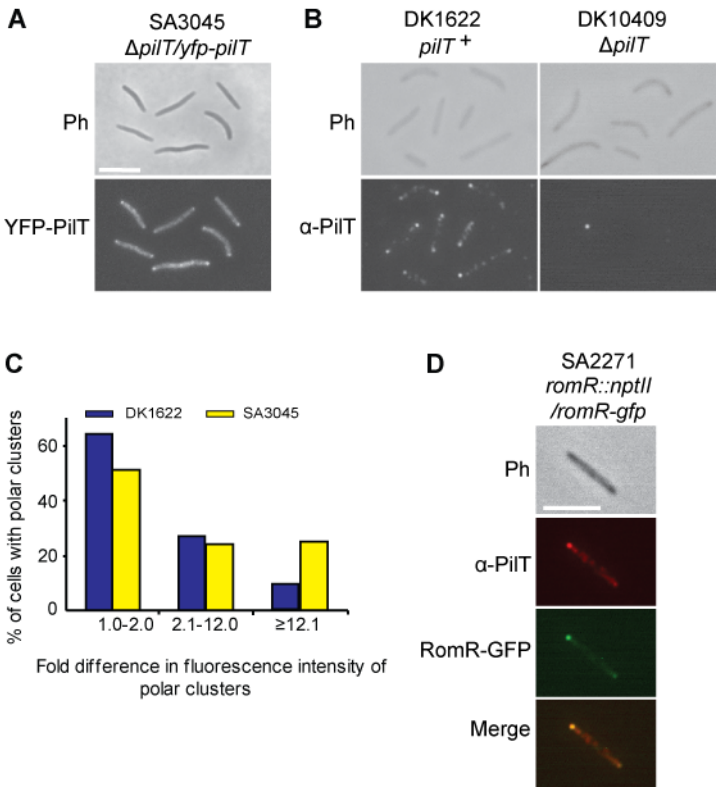

Figure 27. PilT localizes in a bipolar symmetric pattern in non-moving cells

A). Localization of YFP-PilT. Cells were transferred from exponentially growing cultures to a thin 0.7% agar pad on a microscope slide, and imaged by fluorescence and phase-contrast microscopy. Top and bottom rows show phase-contrast and fluorescence images, respectively. Scale bar: 5 µm. **B)**. Localization of PilT by immunofluorescence microscopy. Cells were harvested from the exponentially growing cultures and analyzed as described in Figure 17A using anti-PilT antibodies. Top and bottom rows show phase-contrast and fluorescence images, respectively. **C)**. Histogram of distribution of PilT polar clusters. The data for WT (DK1622) are from immunofluorescence microscopy and for SA3045 from YFP-PilT localization. Data are presented as in Figure 17B. In total N=100 cells were analyzed for each strain.**D)**. Localization of PilT by immunofluorescence microscopy in RomR-GFP containing strain. Large PilT cluster colocalizes with RomR-GFP. Cells were prepared and analyzed as described in (A). N=20 cells were examined. The top row shows phase-contrast image, middle rows fluorescence images, bottom row represents merged image. Scale bar: 5 µm.

Since native PilT and YFP-PilT localized similarly, we determined the localization of PilT in moving cells using YFP-PilT. In moving cells YFP-PilT localized in a unipolar or in a bipolar asymmetric pattern (Figure 28A and B).

Importantly, the large YFP-PilT cluster in moving cells also localized at the lagging cell pole. The YFP-PilT signal at the leading cell pole varied greatly over time in individual cells (Figure 28A: 1:00, 2:00, 2:30 and 4:00-5:00 min) and occasionally disappeared completely. Thus, PilT localization shifts from a predominantly bipolar symmetric pattern in cells analyzed directly from the liquid culture to an asymmetric polar pattern in cells moving on a surface.

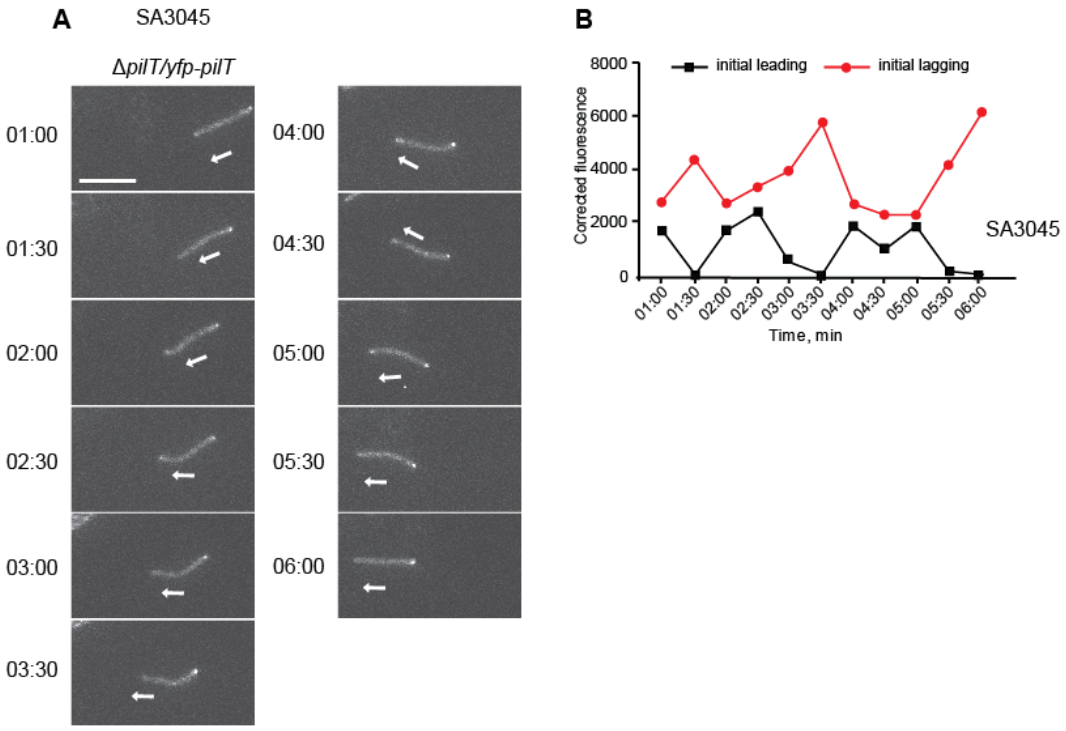

Figure 28. PilT localization is dynamic between reversals

A) Localization of YFP-PilT in moving cells. Cells of SA3045 were transferred from exponentially growing cultures to a thin 0.7% agar pad on a microscope slide, and imaged by fluorescence microscopy at 30 s intervals. Representative cell is shown. The cell moves in a direction indicated by white arrows and does not reverse. Scale bar: 5 µm. **B)** Quantitative analysis of polar YFP-PilT fluorescence signals. Integrated fluorescence intensities (arbitrary units) of the two background-subtracted polar clusters in the cells in (A) are plotted as a function of time.

To investigate whether PilT localization changes during reversals, YFP-PilT localization was followed in 20 reversing cells. All reversals were accompanied by relocation of the large YFP-PilT cluster from the old lagging pole to the new lagging pole (Figure 29A and B for a representative cell). Quantification of the fluorescence signal of the YFP-PilT clusters during reversals (Figure 29B) revealed that during a reversal the polar signals initially decreased in intensity (from 1:30 to 2:00 min for the cell depicted in Figure 29A) and at the same time the cell stopped moving. As the intensity of the cluster at the old lagging pole continued to decrease, the cell began to move in the opposite direction (at 2:30 for the cell shown in Figure 29A). Importantly, dynamic localization of PilT during reversals was also observed in the presence of 25 µg/ml chloramphenicol. In addition, in SA3045 cells displaying several reversals, large YFP-PilT cluster oscillated from the old lagging pole to the new lagging pole during each reversal (data not shown). Taken together, these observations strongly suggest that the YFP-PilT at the new, post-reversal lagging pole is not synthesized *de novo*, but originates from the YFP-PilT cluster at the old, pre-reversal lagging pole, i.e. the

mechanism underlying dynamic YFP-PilT localization involves the transfer of the protein from the old lagging to the new lagging cell pole.

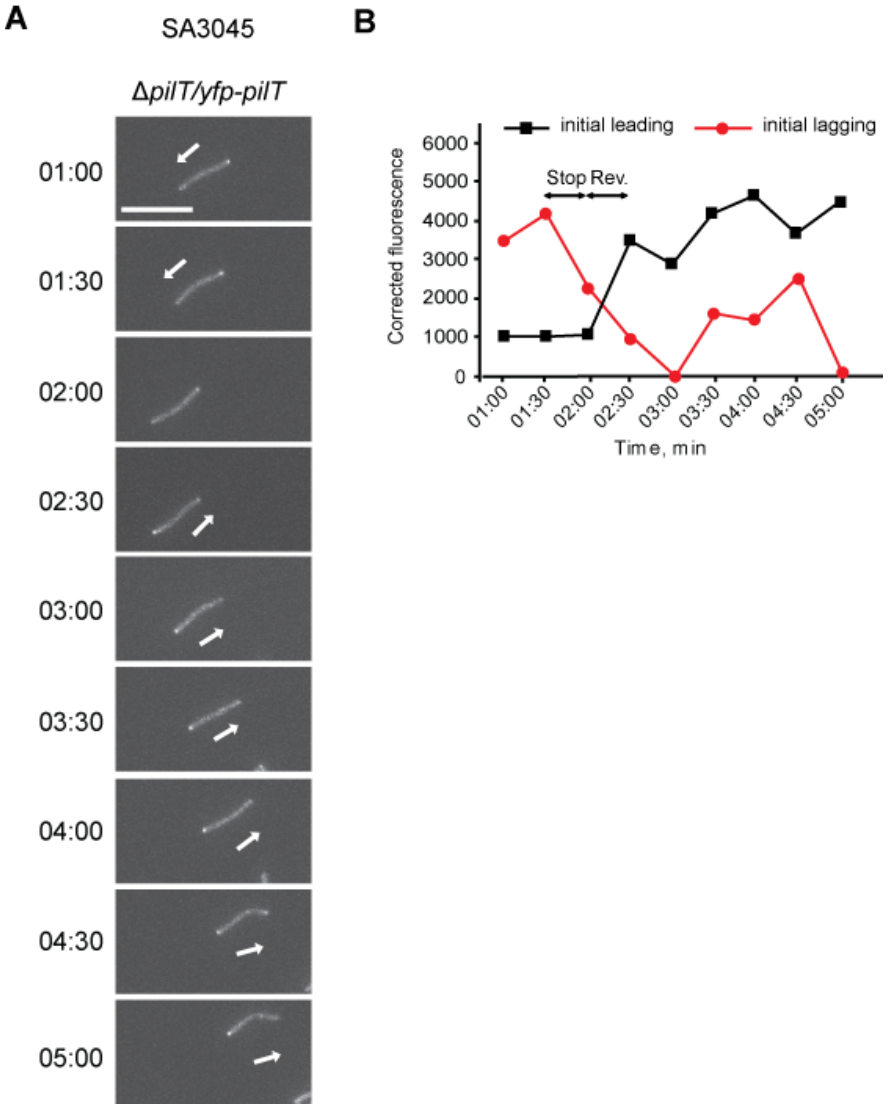

Figure 29. PilT localization is dynamic during reversals in WT

A) Localization of YFP-PilT in moving cells. Cells were prepared and analyzed as in Figure 28A. Representative cell is shown. Cell stops and reverses between 1:30 and 2:30 min. Scale bar: 5 µm. **B)** Quantitative analyses of polar YFP-PilT fluorescence signals. Integrated fluorescence intensities (arbitrary units) of the two background-subtracted polar clusters in the cells in (A) are plotted as a function of time.

To determine whether the dynamic localization of YFP-PilT depends on the Frz system, we analyzed its localization in moving cells in the hypo-reversing strain SA3029 (*frzCD*::Tn*5lac*Ω536, Δ*pilT*/*yfp-pilT*). In all SA3029 cells YFP-PilT also localized in unipolar and bipolar asymmetric patterns (N=20), and all cells contained the large YFP-PilT cluster at the lagging pole and displayed bursts of accumulation at the leading pole (Figure 30A and B). Cells of SA3029 did not reverse, and YFP-PilT did not relocate between poles. Therefore, Frz is dispensable for the unipolar and bipolar

asymmetric PilT localization but required for relocating PilT clusters during reversals.

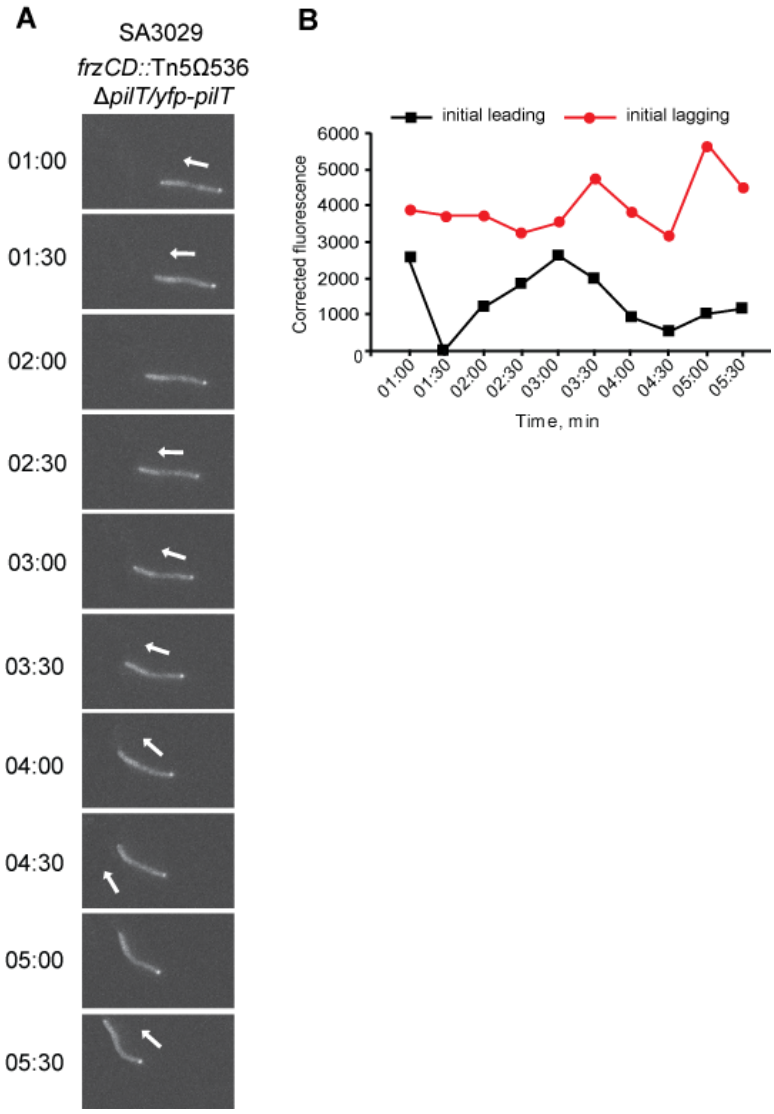

Figure 30. PilT dynamic localization during reversal depends on Frz system

A) Localization of YFP-PilT in hypo-reversing moving cells (SA3029). Cells were prepared and analyzed as in Figure 28A. Representative cell is shown. Scale bar: 5 µm. **B)** Quantitative analysis of polar YFP-PilT fluorescence signals in cells of SA3029. Integrated fluorescence intensities (arbitrary units) of the two background-subtracted polar clusters in the cells in (A) are plotted as a function of time.

2.2.7 PilT turns-over in the polar PilT clusters

Given that the PilT ATPase powers T4P retraction, it was surprising to find that the large PilT cluster localized at the lagging, non-piliated cell pole in moving cells. Notably, we detected YFP-PilT signal at the leading pole between reversals, but this signal varied over time and sometimes completely disappeared (Figure 28A and B). On the basis of these observations, we hypothesized that PilT molecules undergo rapid turnover in the polar clusters between reversals on a timescale much shorter than the average reversal period (15 min for WT cells), and this rapid turnover could

occasionally result in the noisy accumulation of PilT at the leading cell pole. At the leading pole PilT would be able to interact with the T4P machinery at the base of a T4P, thus, forming retraction machinery.

To test this hypothesis, we carried out Fluorescence Recovery After Photobleaching (FRAP) experiments with cells on a surface. For this purpose cells from an exponentially growing culture were spotted on a coverslip treated with polystyrene, which was then placed on a microscope slide and sealed. After 30 min incubation at room temperature samples were used for fluorescence microscopy and photobleaching. It is important to note that in the anti-PilT immunofluorescence microscopy of WT cells 58±8% of the total fluorescence signal is detected in the polar clusters (Figure 27B), whereas in SA3045 (Δ*pilT/yfp-pilT*) cells only 24±4% of the total fluorescence is detected in polar clusters (Figure 27A) (Figure 17C). We attribute the increased cytoplasmic signal in the SA3045 (Δ*pilT/yfp-pilT*) cells to degradation of YFP-PilT with the formation of a fluorescent degradation product that does not localize polarly (Figure 26B). Therefore, in FRAP experiments the background fluorescence was reduced by pre-bleaching the cytoplasmic region between the polar clusters. Subsequently, an area encompassing a polar region was bleached for 1 s and then fluorescence recovery and fluorescence loss were followed for 120 s. In these experiments, we specifically analyzed cells with two polar PilT clusters as we were interested in determining whether these clusters are exchanging molecules and are in a dynamic equilibrium. After bleaching of a polar region, the fluorescence signal at the bleached pole showed a recovery and stabilized after 50±10 s. Notably, the fluorescence signal at the non-bleached pole decreased in a manner resembling the increase in the fluorescence signal at the bleached pole (Figure 31A-C). The results were similar regardless whether a large cluster (Figure 31A and B) or a small cluster (Figure 31A and C) was bleached. Consistently, the total polar fluorescence and the fluorescent signal of the cytoplasmic region in both types of experiments remained nearly constant (Figure 31B and C). It is important to note that the fluorescent signals in the neighboring cells were not affected by the laser. Thus, there is a clear correlation between recovery of fluorescence at the bleached pole and loss of fluorescence at the non-bleached pole. From these analyses we conclude that PilT molecules undergo rapid turnover in the polar clusters, and that the PilT clusters are in a dynamic equilibrium and constantly exchange molecules.

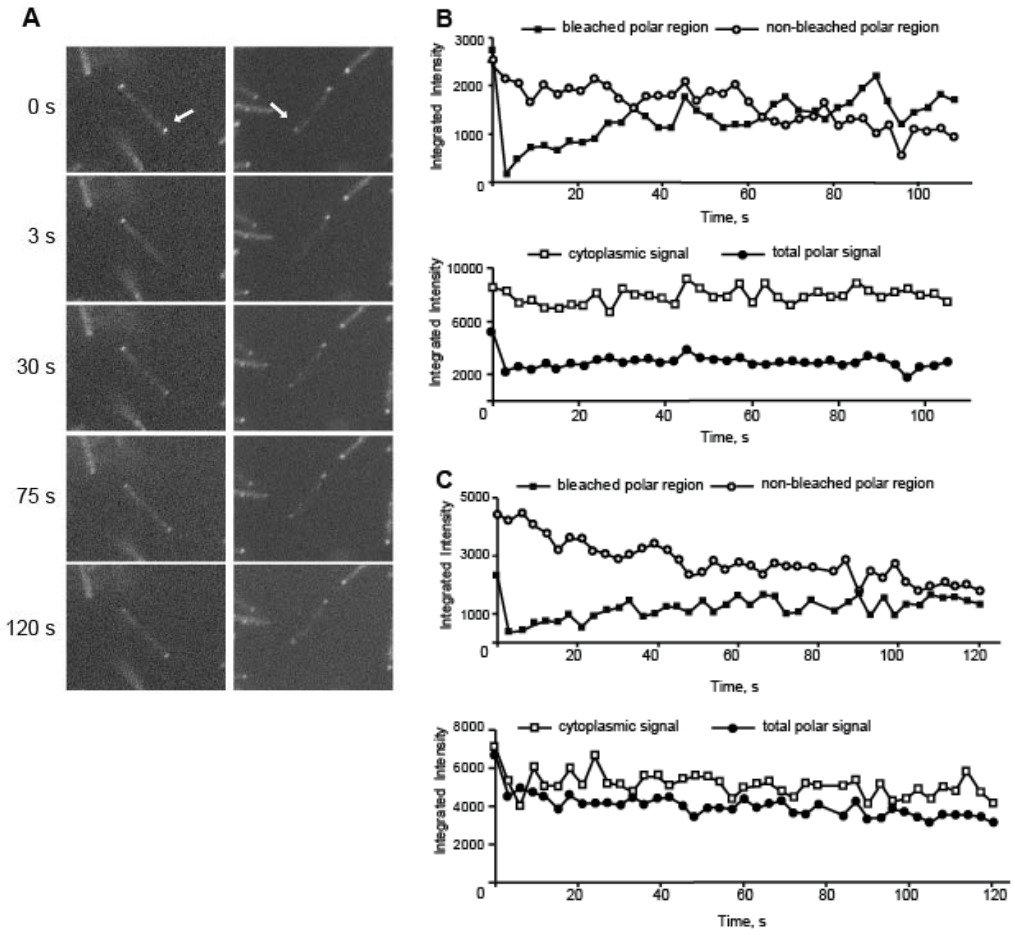

Figure 31. Polar PilT clusters are in a dynamic equilibrium

A) Successive fluorescence images of YFP-PilT cells (SA3045) before (0 s) and after bleaching (3 s to 120 s) of a polar region. The polar region was bleached for 1 s. Bleached polar regions are indicated by white arrows. In the cell on the left, polar region with a larger YFP-PilT cluster was bleached, and in the cell on the right, polar region with a smaller YFP-PilT cluster was bleached. **B)** and **C)** Quantitative analysis of recovery and loss of YFP-PilT fluorescence signals. Integrated fluorescence intensities (arbitrary units) of the polar clusters, the total polar signal (sum of the two polar cluster signals) and the total cytoplasmic signal in the cells in (A) were plotted as a function of time. Data in (B) and (C) are from the cell on the left and on the right panel in (A), respectively.

If T4P retraction depends on the noisy accumulation of PilT at the leading cell pole, we predicted that increased accumulation of PilT at the leading pole should result in cells with fewer T4P. To explore this possibility, strains that overproduce PilT were constructed. For this, plasmid pSL104, which expresses *pilT* allele from *pilA* promoter, plasmid pIB75, which expresses *yfp-pilT* allele from *pilA* promoter, were integrated by site-specific recombination at the Mx8 phage attachment site in the WT strain giving rise to SA3049 (*pilT*+/*pilT*+) and SA3064 (*pilT*+/*yfp-pilT*), respectively. Quantitative immunoblot analysis showed that PilT accumulated at a two-fold higher level in SA3049 compared to WT, and that both PilT and YFP-PilT in combination also

accumulated at a two-fold higher level compared to WT (Figure 32A). Next, YFP-PilT localization was examined. In moving cells of SA3064 (*pilT*+/*yfp-pilT*) YFP-PilT localized in a bipolar symmetric pattern (Figure 32B and C). Thus, two-fold increase in PilT concentration leads to the formation of the permanent PilT cluster at the leading cell pole.

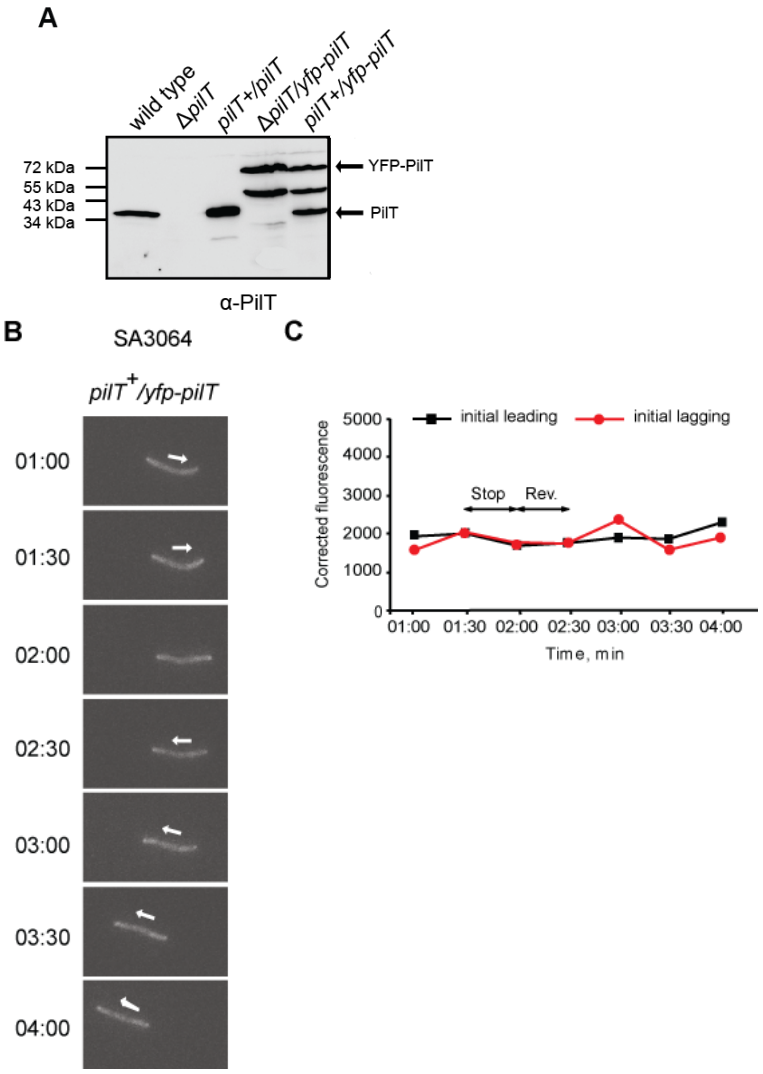

Figure 32. PilT accumulation at the leading pole is proportional to PilT expression level

A) Immunoblot of PilT and YFP-PilT accumulation. Cells from exponentially growing cultures were harvested and samples analyzed as in Figure 14A. Strains used (left to right): DK1622, DK10409, SA3049, SA3045 and SA3064. Blot was probed with rabbit anti-PilT antibodies. PilT and YFP-PilT proteins are indicated with the arrows. Migration of molecular size markers is indicated on the left. **B)** Localization of YFP-PilT in moving WT cells (SA3064). Cells were prepared and analyzed as in Figure 28A. Representative cell is shown. Scale bar: 5 µm. **C)** Quantitative analysis of polar YFP-PilT fluorescence signals in cells of SA3064. Integrated fluorescence intensities (arbitrary units) of the two background-subtracted polar clusters in the cells in (A) are plotted as a function of time.

In addition, transmission electron microscopy was used to determine the localization and number of T4P in WT and SA3049 cells. 20 cells of each strain were

analyzed for the presence of T4P. WT cells as well as SA3049 cells assembled T4P in unipolar patterns (Figure 33A and B) Importantly, WT cells contained significantly more T4P than *pilT+/pilT+* cells (6.5±3.0 and 3.2±2.4 T4P per piliated pole, respectively, P=0.0005). These findings confirm our hypothesis that an increase in the concentration of PilT at the leading pole leads to a decrease in the number of T4P at this pole.

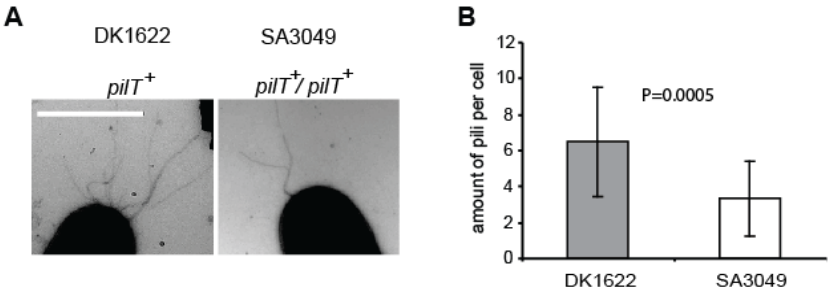

Figure 33. PilT overexpression leads to the reduction of T4P number

A) Cells from exponentially growing cultures of the indicated strains were directly transferred to a grid, stained with 2% (w/v) uranyl acetate, and visualized using transmission electron microscopy. Scale bar, 1.0 µm. **B)** Quantitative analysis of T4P number in WT and SA3049 cells. N=20 cells were analyzed for each strain.

2.3 Polar targeting of type IV pili components

All six T4P proteins investigated (PilQ, PilC, PilN, PilM, PilB and PilT) displayed polar localization. Moreover, these proteins localize in three different patterns: bipolar symmetric (PilQ, PilC, PilN and PilM), unipolar with a large cluster at the leading cell pole (PilB) and unipolar with a large cluster at the lagging cell pole (PilT). These localization patterns raise three questions: (i) How do T4P proteins become polarly localized? (ii) How do they localize to the “correct” pole? And (iii) how does localization change dynamically over time? To begin to address these questions two lines of experiments were carried out. First, we investigated if there is a potential interdependency in polar localization of these proteins. Second, using a candidate approach we searched for non-T4P proteins important for the localization of T4P proteins.

2.3.1 Localization of PilC in the absence of other type IV pili components

To address if the localization of a particular T4P protein depends on other T4P proteins, we focused on the localization of PilC, PilB and PilT. To determine the localization of PilC in the absence of PilQ/A/M/N/O/P/B/T and TgI, we determined PilC accumulation in strains lacking these proteins using anti-PilC quantitative immunoblot analysis. These analyses confirmed that PilC accumulated at WT levels in all mutants

tested (Figure 34A). Localization of PilC protein was determined by immunofluorescence microscopy with anti-PilC antibodies (Figure 34B). In the absence of PilB, PilT, PilM or PilP, PilC localized in a bipolar symmetric pattern as previously observed for WT (Figure 18) (Figure 34B). However, polar PilC clusters were rarely detected in the absence of PilA and PilQ. In the absence of these proteins, PilC localized in a patchy pattern with clusters distributed over the entire cell body (Figure 34B). In Δ*tgl*, Δ*pilN* and Δ*pilO* mutants PilC localized in a similar patchy pattern, but with slightly stronger PilC clusters at one or both poles (Figure 34B). Thus, we conclude that PilC polar localization is independent of the PilB, PilT, PilM and PilP proteins. In contrast, PilA, PilQ, and possibly Tgl, PilN and PilO proteins are required for proper PilC localization.

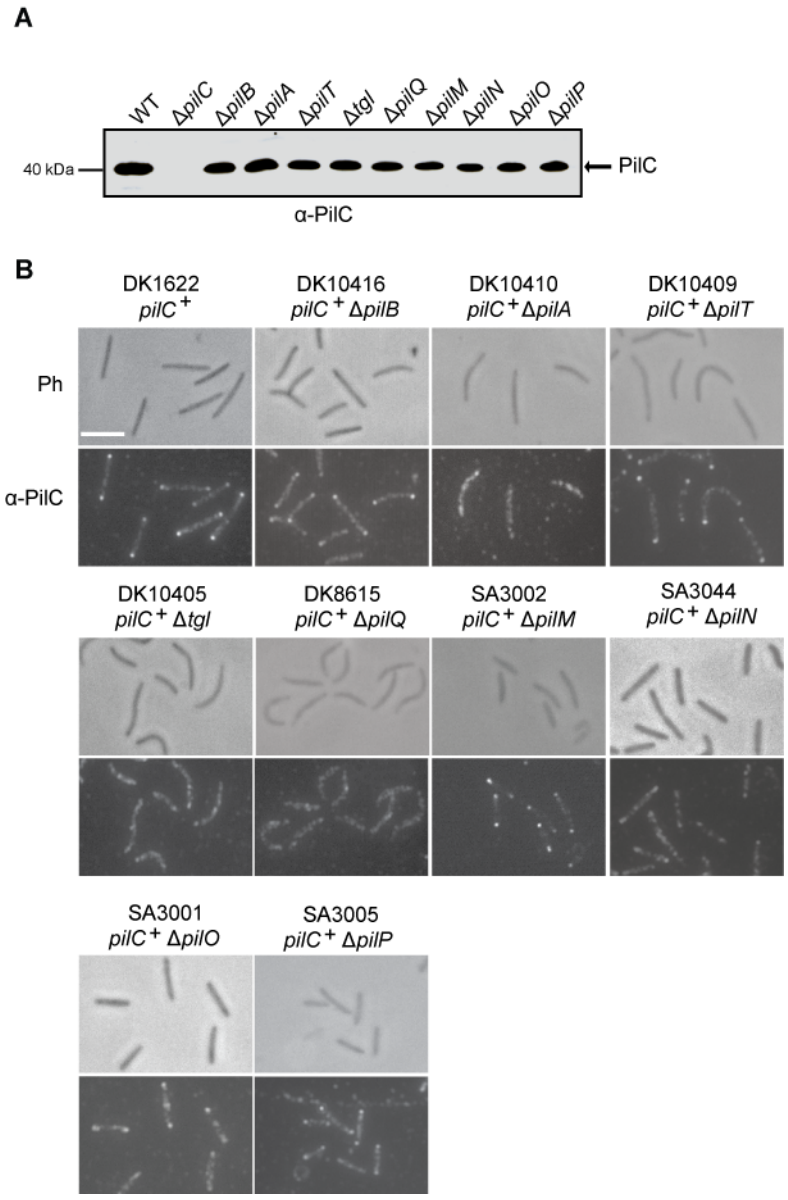

Figure 34. PilC localization in *pil* mutants

A) Immunoblot of PilC accumulation. Cells from exponentially growing cultures were harvested and samples analyzed as in Figure 14A. Strains used (left to right): DK1622 (WT), DK10417 (Δ*pilC*), DK10416 (Δ*pilB*), DK10410 (Δ*pilA*), DK10409 (Δ*pilT*), DK10405 (Δ*tgl*), DK8615 (Δ*pilQ*), SA3002 (Δ*pilM*), SA3044 (Δ*pilN*), SA3001 (Δ*pilO*) and SA3005 (Δ*pilP*). Blot was probed with anti-PilC antibodies. PilC protein is indicated on the right. Migration of molecular size markers is indicated on the left. **B)** Localization of PilC by immunofluorescence microscopy. Cells were harvested from the exponentially growing cultures and analyzed as described in Figure 17A using anti-PilC antibodies. Strain names and relevant genotypes are indicated. Top and bottom rows show phase-contrast and fluorescence images, respectively. Scale bar: 5 μm.

2.3.2 Localization of PilB in the absence of other type IV pili components

Quantitative immunoblot analyses demonstrated that PilB accumulated at WT levels in the absence of PilQ/A/C/M/N/O/P/T and Tgl proteins (Figure 35A). To explore PilB localization in the absence of other T4P proteins, immunofluorescence microscopy was conducted with anti-PilB antibodies (Figure 35B). In all mutants tested PilB localized in a pattern similar to that in WT, i.e. all three distinct PilB localization patterns were observed: bipolar symmetric, bipolar asymmetric and unipolar (Figure 35B). The detailed quantitative analysis of PilB polar signals in Δ*pilT* cells demonstrated that PilB clearly localized to the poles independently of PilT. We conclude therefore that PilQ/A/C/M/N/O/P/T and Tgl proteins are not required for polar PilB localization. However, careful statistical analysis of the PilB clusters in the strains lacking these proteins is required to find out if PilB clusters distribution is affected.

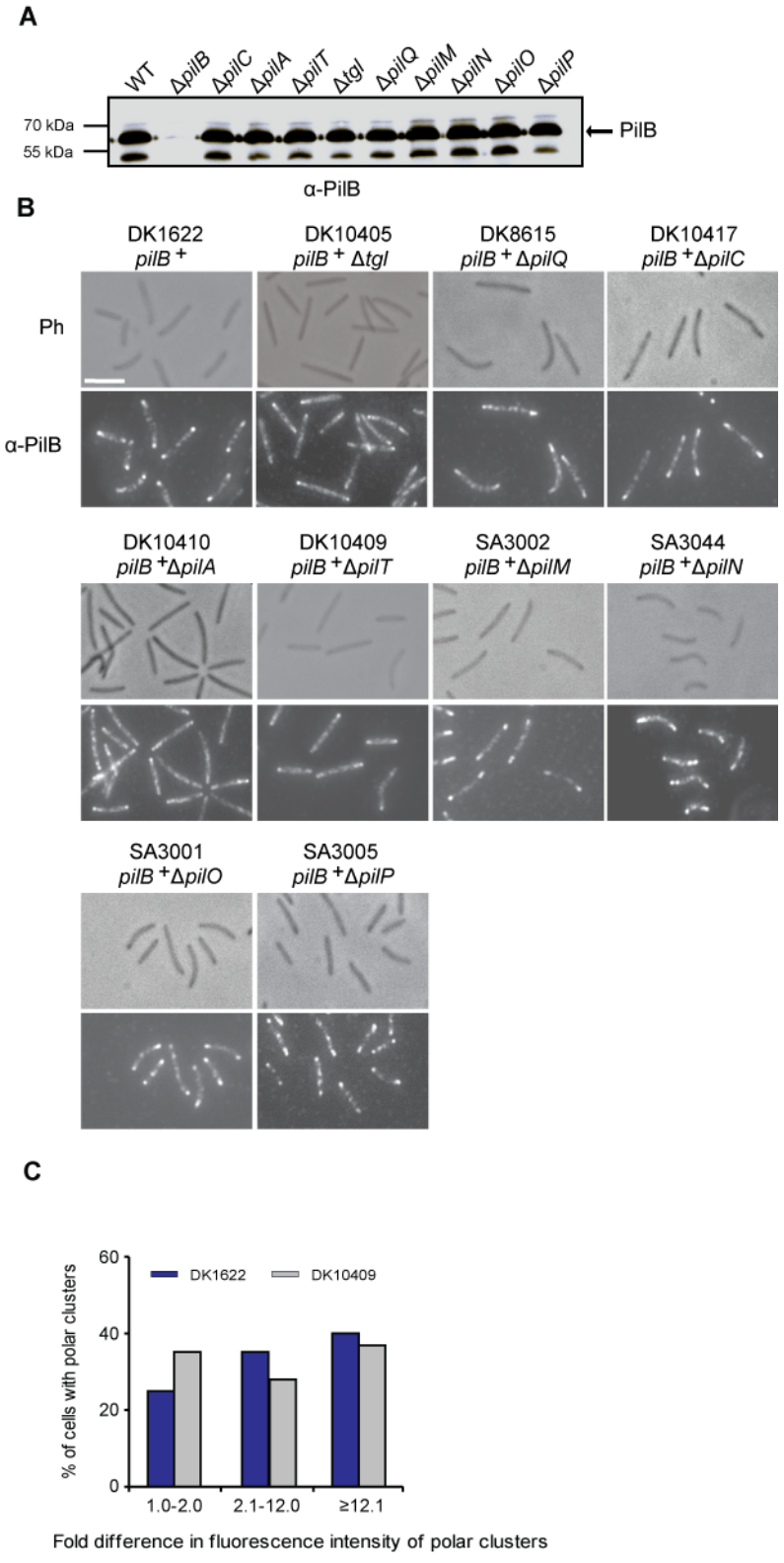

Figure 35. PilB localization in *pil*-mutants

A) Immunoblot of PilB accumulation. Cells from exponentially growing cultures were harvested and samples analyzed as in Figure 14A. Strains used (left to right): DK1622 (WT), DK10416 (Δ*pilB*), DK10417 (Δ*pilC*), DK10410 (Δ*pilA*), DK10409 (Δ*pilT*), DK10405 (Δ*tgl*), DK8615 (Δ*pilQ*), SA3002 (Δ*pilM*), SA3044 (Δ*pilN*), SA3001 (Δ*pilO*) and SA3005 (Δ*pilP*). Blot was probed with anti-PilB antibodies. PilB protein is indicated on the right. Migration of molecular size markers is indicated on the left. **B)** Localization of PilB by immunofluorescence

microscopy. Cells were harvested from the exponentially growing cultures and analyzed as described in Figure 17A using anti-PilB antibodies. Top and bottom rows show phase-contrast and fluorescence images, respectively. Scale bar: 5µm. **C)** Histogram of distribution of PilB polar clusters. Data are presented as in Figure 17B. In total N=100 cells were analyzed for each strain.

2.3.3 Localization of non-functional PilB^{E391A} mutant

PilB function depends on ATP binding and hydrolysis. To elucidate whether ATPase activity is important for PilB localization, the localization of the PilB protein that carries a substitution of the highly conserved Glu-391 residue to Ala in the Walker B box was determined. Based on the structures of several secretion ATPases (Savvides, 2007) Glu-391 in PilB is important for ATP hydrolysis, whereas ATP binding is unaffected. Consistently, PilB^{E391A} does not complement the motility defect of Δ*pilB* mutant, and purified PilB^{E391A} has a strong defect in ATP hydrolysis *in vitro* (Jakovljevic *et al.*, 2008). To determine the localization of PilB^{E391A} protein, the strain SA2415 (Δ*pilB*/*pilB*^{E391A}), containing *pilB*^{E391A} allele at the Mx8 phage attachement site expressed from *pilA* promoter, was used (Jakovljevic *et al.*, 2008). In SA2415 (Δ*pilB*/*pilB*^{E391A}), PilB^{E391A} accumulates at levels similar to that of PilB in WT (Jakovljevic *et al.*, 2008) and localizes in a patchy pattern with clusters distributed all over the entire cell body (Figure 36). From these analyses we conclude that PilB ATPase localizes at the cell poles in a manner that depends on ATPase activity.

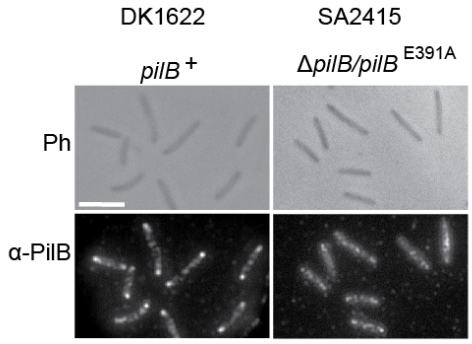

Figure 36. PilB localization depends on ATPase activity

Localization of PilB by immunofluorescence microscopy. Cells were harvested from the exponentially growing cultures and analyzed as described in Figure 17A using anti-PilB antibodies. Top and bottom rows show phase-contrast and fluorescence images, respectively. Scale bar: 5 µm.

2.3.4 Localization of PilT in the absence of other type IV pili components

To investigate PilT localization in the absence of PilB, PilQ, PilA and PilC, the plasmid pIB75, containing *yfp-pilT* allele expressed from *pilA* promoter, was integrated at the chromosomal Mx8 phage attachment site in the strains SA3054 (Δ*pilB* Δ*pilT*), DK8615 (Δ*pilQ*), DK10410 (Δ*pilA*) and DK10417 (Δ*pilC*), giving rise to the strains SA3043, SA3047, SA3061 and SA3063, respectively. Immunoblot analysis of total cell lysates showed that YFP-PilT accumulated in all strains tested except for SA3061

(Δ*pilA, pilT*$^+$/*yfp-pilT*) at levels similar to that of PilT protein in WT cells and YFP-PilT in SA3045 (Δ*pilT*/*yfp-pilT*) and SA3064 (*pilT*$^+$/*yfp-pilT*) cells (Figure 37A). A degradation product with a size of 50 kDa was also detected by both anti-PilT and anti-GFP antibodies. YFP-PilT was three-fold overproduced in SA3061 (Δ*pilA, pilT*$^+$/*yfp-pilT*) cells (Figure 37A, last lane). Clear polar YFP-PilT clusters were observed only in SA3043 (Δ*pilB* Δ*pilT*/*yfp-pilT*) cells (Figure 38A). Only 10% of SA3047 (Δ*pilQ, pilT*$^+$/*yfp-pilT*) and SA3063 (Δ*pilC, pilT*$^+$/*yfp-pilT*) cells contained YFP-PilT polar clusters, while the majority of these cells displayed diffused YFP-PilT localization (Figure 37B). SA3061 (Δ*pilA, pilT*$^+$/*yfp-pilT*) cells exhibited exclusively diffuse YFP-PilT localization (Figure 37B).

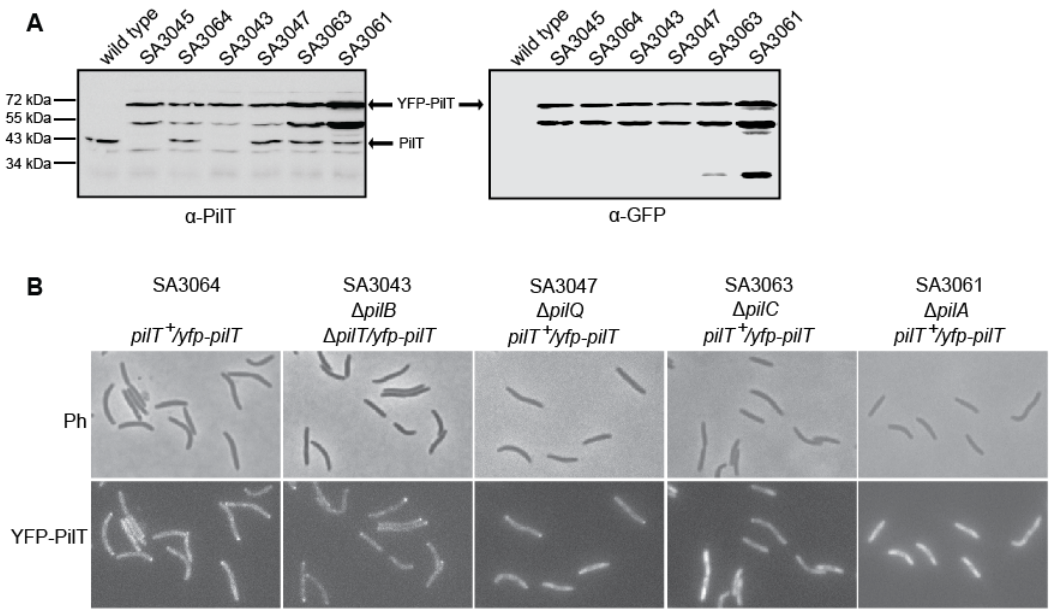

Figure 37. YFP-PilT localization in Δ*pilA*, Δ*pilB*, Δ*pilC* and Δ*pilQ* mutants

A) Immunoblots of PilT and YFP-PilT accumulation. Cells from exponentially growing cultures were harvested and samples analyzed as in Figure 14A. Strains used (left to right): DK1622 (WT), SA3045 (*ΔpilT/yfp-pilT*), SA3064 (*pilT*$^+$*/yfp-pilT*), SA3043 (*ΔpilBT/yfp-pilT*), SA3047 (*ΔpilQ,pilT*$^+$*/yfp-pilT*), SA3063 (*ΔpilC,pilT*$^+$*/yfp-pilT*) and SA3061 (*ΔpilC,pilT*$^+$*/yfp-pilT*). Relevant genotypes for the strains used are indicated in (B). Blot on the left was probed with rabbit anti-PilT antibodies, blot on the right with monoclonal anti-GFP antibodies, which also recognize YFP. PilT and YFP-PilT proteins are indicated with arrows. Migration of molecular size markers is indicated on the left. **B)** Localization of YFP-PilT. Cells were transferred from exponentially growing cultures to a thin 0.7% agar pad on a microscope slide, and imaged by fluorescence and phase-contrast microscopy. Top and bottom rows show phase-contrast and fluorescence images, respectively. Strain names and relevant genotypes are indicated. Scale bar: 5 µm.

Taken together, the observed YFP-PilT localization patterns suggest that proper PilT localization is independent of PilB, whereas PilQ, PilC and PilA appear to be required for PilT localization. However, we cannot rule out the possibility that mislocalization of PilT in SA3061 (Δ*pilA, pilT*$^+$/*yfp-pilT*) is caused by PilT

overproduction. Moreover, to elucidate whether PilQ and PilC are in fact required for PilT polar targeting, we need to verify YFP-PilT localization in the absence of an additional *pilT* copy, which affects PilT localization (Figure 32).

In order to find out whether PilB is required for PilT dynamic localization, YFP-PilT localization was determined in moving cells of SA3043 (Δ*pilB* Δ*pilT*/*yfp-pilT*) using time-lapse microscopy (Figure 38A and B). In moving SA3043 cells the large YFP-PilT cluster also localized at the lagging cell pole and relocated from the old lagging pole to the new lagging pole during each reversal (Figure 38 for the representative cell). Quantification of the fluorescence signal of the YFP-PilT clusters during reversals (Figure 38B) revealed that in SA3043 cells the YFP-PilT signal at the leading cell pole varied over time (Figure 38A: 2:00-3:00 min) and occasionally disappeared completely, resembling previously observed PilT behavior in SA3045 (Δ*pilT*/*yfp-pilT*) cells.

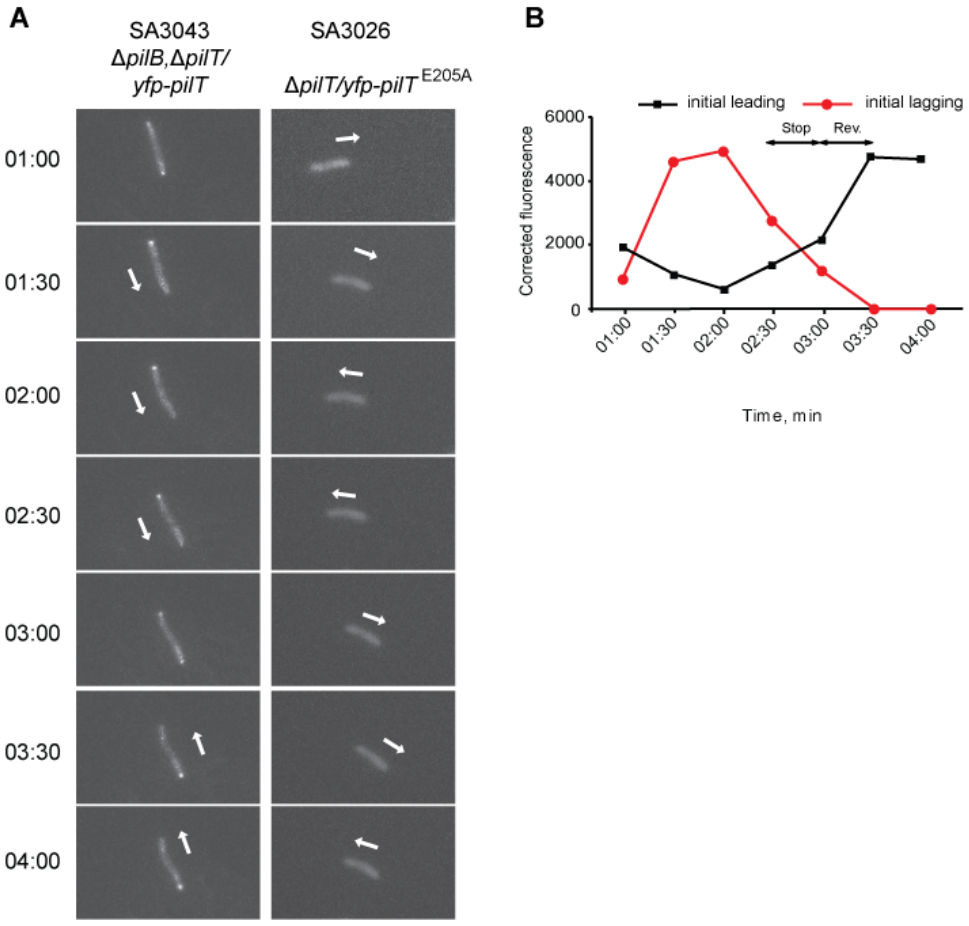

Figure 38. PilT localization does not depend on PilB localization, but on PilT ATPase activity

A) Localization of YFP-PilT in moving SA3043 (*ΔpilBT/yfp-pilT*) and SA3026 (*ΔpilT/yfp-pilT /yfp-pilT*^{E205A}) cells. Cells were prepared and analyzed as in Figure 28A. Representative cells are shown. **B)** Quantitative analysis of polar YFP-PilT fluorescence signals in cells of SA3043. Integrated fluorescence intensities (arbitrary units) of the two background-subtracted polar clusters in the cells in (A) are plotted as a function of time.

Thus, PilT dynamic localization between and during reversals is not controlled by PilB. These observations allow us to exclude a mutually exclusive mechanism, in which PilB would at least partially inhibit accumulation of PilT at the leading cell pole, and PilT would at least partially inhibit PilB accumulation at the lagging cell pole.

2.3.5 Localization of non-functional YFP-PilT^{E205A} mutant

PilT function depends on ATP binding and hydrolysis (Jakovljevic *et al.*, 2008). To address whether ATPase activity is important for PilT localization, the localization of YFP-PilT protein that carries a substitution of the highly conserved Glu-205 residue to Ala in the Walker B box was determined. As in the case of Glu391 in PilB, Glu-205 is important for ATP hydrolysis, whereas ATP binding is predicted to be unaffected (Jakovljevic *et al.*, 2008). Consistently, PilT^{E205A} does not complement the motility defect of Δ*pilT* mutant and purified PilT^{E205A} has a strong defect in ATP hydrolysis *in vitro* (Jakovljevic *et al.*, 2008). To localize PilT^{E205A} protein, the plasmid pIB74, containing *yfp-pilT*^{E205A} allele under control of *pilA* promoter, was integrated via site-specific recombination at the chromosomal Mx8 phage attachment site in DK10409 (Δ*pilT*) strain, giving rise to the SA3026 strain. In SA3026 (Δ*pilT/yfp-pilT*^{E205A}), YFP-PilT^{E205A} accumulated at levels similar to that of YFP-PilT in SA3045 (Δ*pilT/yfp-pilT*) (data not shown); however, YFP-PilT^{E205A} localized in a patchy pattern with clusters distributed over the entire cell body in both stalled and moving cells (Figure 38A). From these analyses we conclude that polar localization of PilT depends on its ATPase activity.

2.4 Regulation of the type IV pili oscillations

To search for non-T4P proteins important for the localization of T4P proteins, we used a candidate approach. Recent data suggest that the small GTPase of the Ras-superfamily MglA plays a pivotal role in establishing and maintaining the correct polarity of the A-motility proteins RomR and AglZ (Leonardy *et al.*, *in review*). We hypothesized that MglA may also regulate the polarity of T4P proteins.

2.4.1 Small Ras-like GTPase MglA is required for PilT dynamics during reversal

Genetic and cytological evidence suggests that MglA/GTP at a low concentration stmulates motility and that MglA/GTP at a higher concentration stimulates reversals (Leonardy *et al.*, *in review*). Moreover, MglA acts downstream of Frz system to control the dynamics of the motility proteins during reversal (Leonardy *et al.*, *in review*). Since we have previously observed that the Frz system induces the relocation of PilB and

PilT during cellular reversal, we hypothesized that MglA could also have an effect on the dynamics and/or polarity of T4P proteins.

To test this hypothesis, we focused on the analysis of the PilT localization as this is the only dynamic T4P protein that can be followed in living cells using a functional YFP-PilT fusion protein. For this, plasmids pSL51 and pSL52 containing *mglA*^{G21V} and *mglA*$^{T26/T27N}$ alleles, respectively, were used to replace *mglA* copy at the endogenous site via two-step homologous recombination in SA3045 (*ΔpilT/yfp-pilT*) strain. As described in Chapter 1.5.4, *mglA*^{G21V} cells reverse on average every 4.5 min compared to *mglA*$^{+}$ cells, which reversed on average every 15 min. Moreover, two A-motility proteins, RomR and AglZ, hyper-switch in *mglA*^{G21V} cells (Leonardy *et al.*, *in review*). *mglA*$^{T26/27V}$ cells are unable to move, and both RomR and AglZ exhibited altered localization (Leonardy *et al.*, *in review*).

Time-lapse microscopy was performed to follow YFP-PilT localization in the moving cells. As shown in Figure 39A, in *mglA*^{G21V} cells (N=20) YFP-PilT localized as in *mglA*$^{+}$ cells at the lagging cell pole. *mglA*^{G21V} cells reversed on average every 4.5 min, and the frequent reversals were accompanied by relocation of the large YFP-PilT cluster from the old lagging pole to the new lagging pole (Figure 39A and B). Thus, PilT hyper-switches between the poles in the *mglA*^{G21V} mutant.

In the non-moving *mglA*$^{T26/T27N}$ cells (N=100), 66% of the cells contained a single YFP-PilT cluster, and by T4P staining (data not shown) this pole was shown to be a non-piliated pole; 17% of cells contained YFP-PilT in the bipolar asymmetric pattern; and, finally, 17% of cells in a bipolar symmetric pattern (Figure 39C, black numbers). Thus, compared to the YFP-PilT localization in stalled *mglA*$^{+}$ cells (Figure 39C, blue numbers), YFP-PilT localization is shifted from bipolar symmetric to unipolar pattern in *mglA*$^{T26/T27N}$ cells. To summarize, these results demonstrate that the GTP-bound state of MglA is important for establishing PilT polarity, and that MglA regulates dynamic PilT localization.

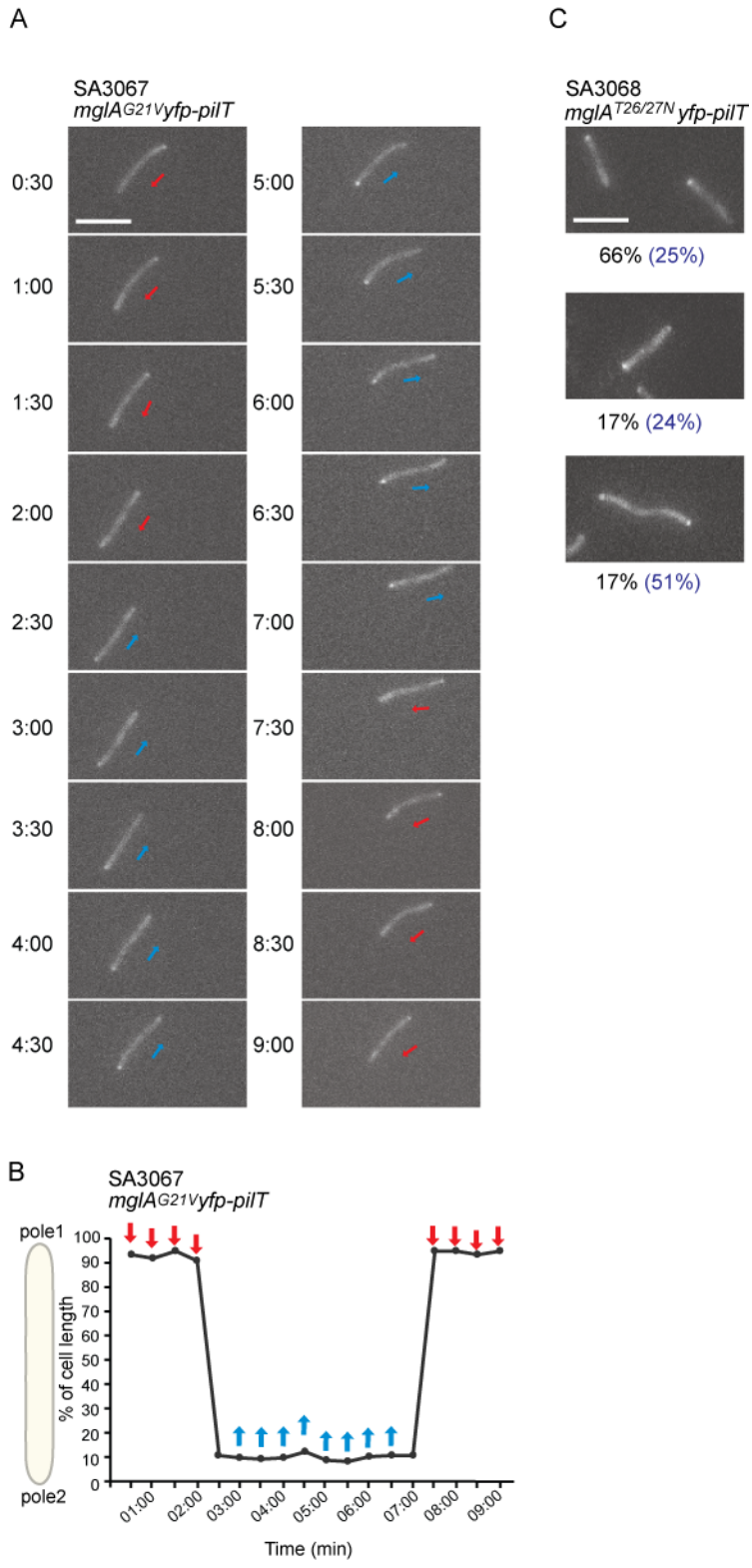

Figure 39. MglA/GTP establishes correct PilT polarity and regulates dynamic PilT localization

A) MglA^{G21V} regulates dynamic YFP-PilT localization. Cells were prepared and analyzed as in Figure 28A. Representative cell is shown. Red and blue arrows indicate opposite directions of movement. Cell reversed twice, between 2:00 and 2:30, 7:00 and 7:30. Scale bar: 4 µm. **B)** Quantitative analysis of polar YFP-PilT fluorescence signals in *mglA*^{G21V} cells. The localization as percentage of cell length of the maximum YFP-PilT fluorescence signal in the cell shown in (A) was plotted as a function of time. Red and blue arrows indicate opposite directions of

movement. **C)** MglA$^{T26/27N}$ is unable to establish correct YFP-PilT polarity. Cells were prepared and analyzed as in (A). Depicted cells did not move. The percentages of cells with unipolar, bipolar asymmetric and bipolar symmetric YFP-PilT localization are indicated below. Numbers in blue indicate the same percentages in stalled *mglA*$^{+}$ cells.

2.5 Characterization of a new S-motility component

MglA is the first small GTPase in prokaryotes shown to play a pivotal role in such fundamental processes as cell polarity establishment and cell movement (Leonardy *et al.*, *in review*). Two MglA paralogs were found in the *M. xanthus* genome, encoded by the genes *mxan_2694* and *mxan_6703*. We hypothesized that these MglA-like proteins could also be important for gliding motility and/or reversal frequency regulation. An in-frame deletion of *mxan_2694* did not cause any detectable defects in *M. xanthus* vegetative growth, motility or development (S. Brameyer, unpublished data). Thus, the focus of this study was the characterization of the second MglA paralog, encoded by *mxan_6703* gene, later named *sofG* (S-motility function GTPase).

2.5.1 Bioinformatics analyses of SofG (S-motility function GTPase)

To confirm that SofG belongs to the Ras-superfamily of GTPases, bioinformatics analyses were conducted. First, conserved domain searches were performed in order to identify known domains (Figure 40A). These analyses confirmed that SofG contains a Ras-like GTPase domain. Several conserved motifs were described to be required for the function of the GTPases of the Ras-superfamily (Bourne *et al.*, 1991; Saraste *et al.*, 1990). To determine whether these motifs are conserved in SofG, sequence alignments were generated (Figure 40B). A comparison of the primary sequence of SofG with MglA from *M. xanthus* and other characterized GTPases of the Ras-superfamily revealed that SofG contains the conserved residues in the P-loop (phosphate binding loop) required for GTP/GDP binding and GTP hydrolysis (Saraste *et al.*, 1990). In particular, the P-loop in SofG contains the residues G79 and T84, which are homologous to Ras residues G12 and T17 (Bourne *et al.*, 1991) and MglA residues G21 and T26 (Leonardy *et al.*, *in review*). In the switch I and switch II regions, which undergo major conformational changes in response to nucleotide binding (Vetter and Wittinghofer, 2001), SofG similarly to MglA lacks the conserved residue corresponding to Ras T35 in switch I region, but contains Q140 in switch II, which corresponds to Ras residue Q61 and is critical for GTPase activity (Vetter and Wittinghofer, 2001). Moreover, SofG also contains the highly conserved NKXD motif, required for specificity and affinity to the nucleotides (Vetter and Wittinghofer, 2001). Both SofG and MglA lack the conserved CAAX motif, at which many GTPases of the

Ras-superfamily are modified by attachment of a lipid moiety that facilitates the association of these proteins with the membrane (Karnoub and Weinberg, 2008). Finally, in contrast to MglA and other small GTPases of the Ras-superfamily, SofG possesses an additional N-terminal extension, which does not show significant similarities to any known domains or proteins.

MglA activity is controlled by the Frz chemosensory system and the MglB protein acting as MglA specific GEF and GAP, respectively (Leonardy *et al.*, *in review*). *mglB* and *mglA* genes constitute an operon (Stephens *et al.*, 1989), which is highly conserved among bacteria possessing MglA orthologs (Koonin and Aravind, 2000). The *sofG* gene is not adjacent to an *mglB* paralog, but might constitute a single transcription unit with a downstream gene *mxan_6702*, encoding an uncharacterized histidine kinase (Figure 40C). The closest SofG orthologs are found in other myxobacterial species *Stigmatella aurantiaca* and *Anaeromyxobacter dehalogenans* (S. Huntley, in preparation). Notably, in both genomes *sofG* is flanked by an *mxan_6702* ortholog.

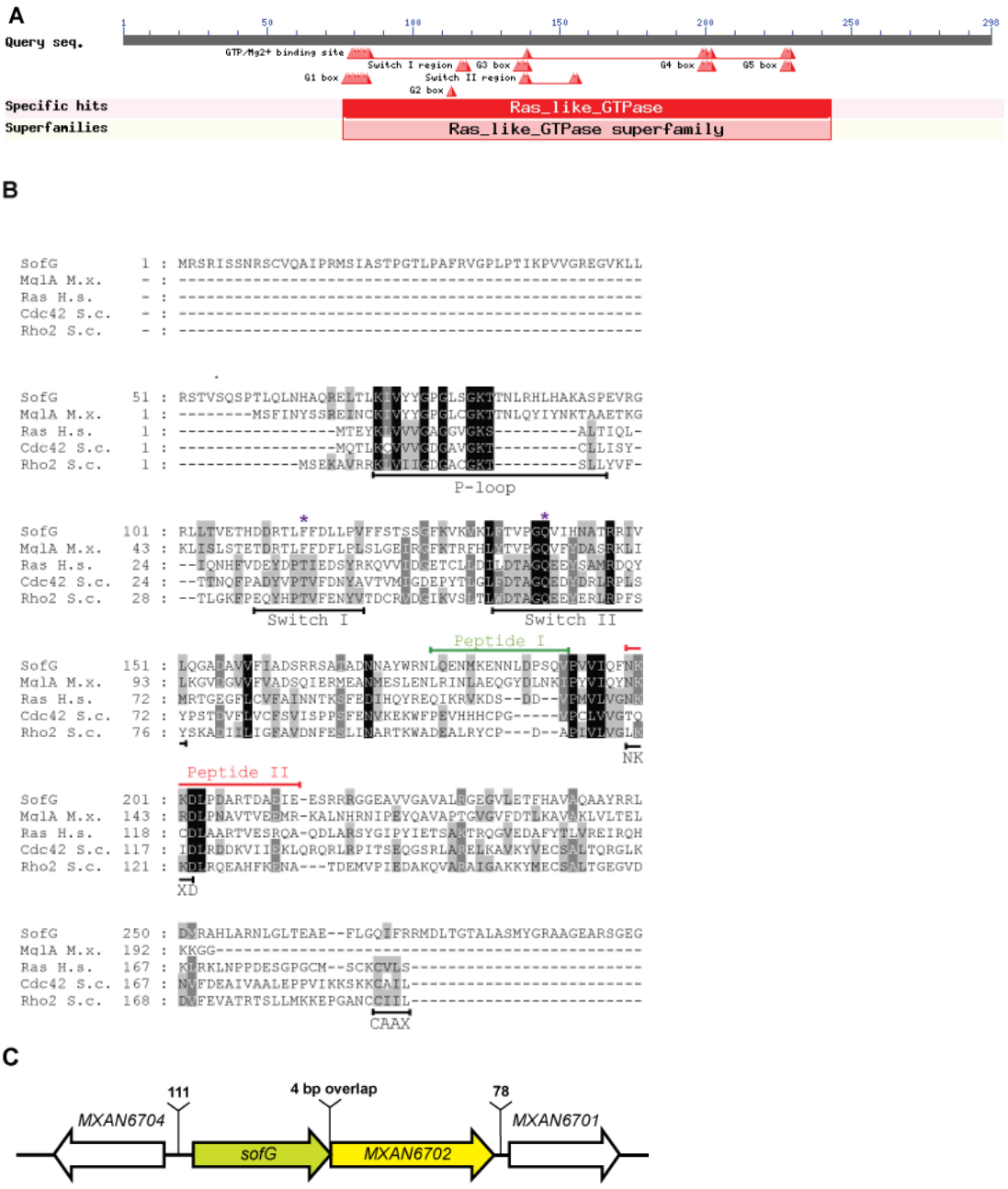

Figure 40. Bioinformatics analysis of SofG

A) Domain architecture of SofG according to Conserved Domain Search of NCBI. **B)** Sequence alignment of SofG with MglA from *M. xanthus* and characterized GTPases of the Ras-superfamily (Ras of *Homo sapiens*, Cdc42 and Rho2 of *S. cerevisiae*). Residues shaded black are 100% conserved; residues in white on gray are 80% conserved; residues in black on gray are 60% conserved. Conserved regions of small GTPases of the Ras-superfamily are indicated below each alignment block. Green asterisks mark the highly conserved residues in switch I (T35 in Ras) and switch II (Q61 in Ras) regions.Two peptides, used for anti-SofG antibodies generation are indicated in red and green. **C)** Schematic representation of *sofG* locus. Numbers on top indicate distances between start and stop codons of flanking genes in bp.

2.5.2 SofG is required for S- motility and development

To determine the function of SofG, a *sofG* in-frame deletion mutant was generated. As depicted in the top row in Figure 41A, the Δ*sofG* mutant did not form extended flares at the colony edge compared to WT cells, but also did not exhibit a completely smooth colony edge typical of the Δ*pilB* mutant. The motility phenotype of the Δ*sofG* mutant on 0.5% agar resembled the Δ*pilT* mutant phenotype. These observations suggest that SofG is required for T4P-dependent motility. On 1.5% agar, individual cells were observed at the colony edge of Δ*sofG* mutant (Figure 41A, bottom row) suggesting that SofG is dispensable for A-motility.

For development assays cells were harvested as for motility assays, but spotted on TPM starvation agar plates. After 24, 48, 72 and 120 h of incubation at 32°C the colonies were examined for a presence of aggregation centres and/or fruiting bodies. The *csgA*$^{-}$ mutant (DK5208), which is unable to produce the C-signal and therefore unable to fruit and sporulate (Kim and Kaiser, 1990a; Lobedanz and Sogaard-Andersen, 2003) and the *mglA9* mutant (DK3685), which fails to aggregate and to sporulate (Kim and Kaiser, 1990b) were used as controls. As shown in Figure 41B, WT cells formed compact fruiting bodies at 24 h, which darkened at 48 h, whereas *csgA*$^{-}$ cells formed loose translucent mounds, which did not turn into spore-filled dark fruiting bodies even after 120 h of starvation. The Δ*sofG* and *mglA9* mutants completely failed to aggregate and to fruit. Thus, SofG protein is required for the starvation-induced *M. xanthus* development. Importantly, developmental phenotype of Δ*sofG* mutant is most likely caused by the absence of SofG protein directly, as well characterized *pil* mutants deficient in S-motility are able to aggregate and to fruit (S. Brameyer, MPI, unpublished data). In this study we focused on the S-motility defect of Δ*sofG* mutant.

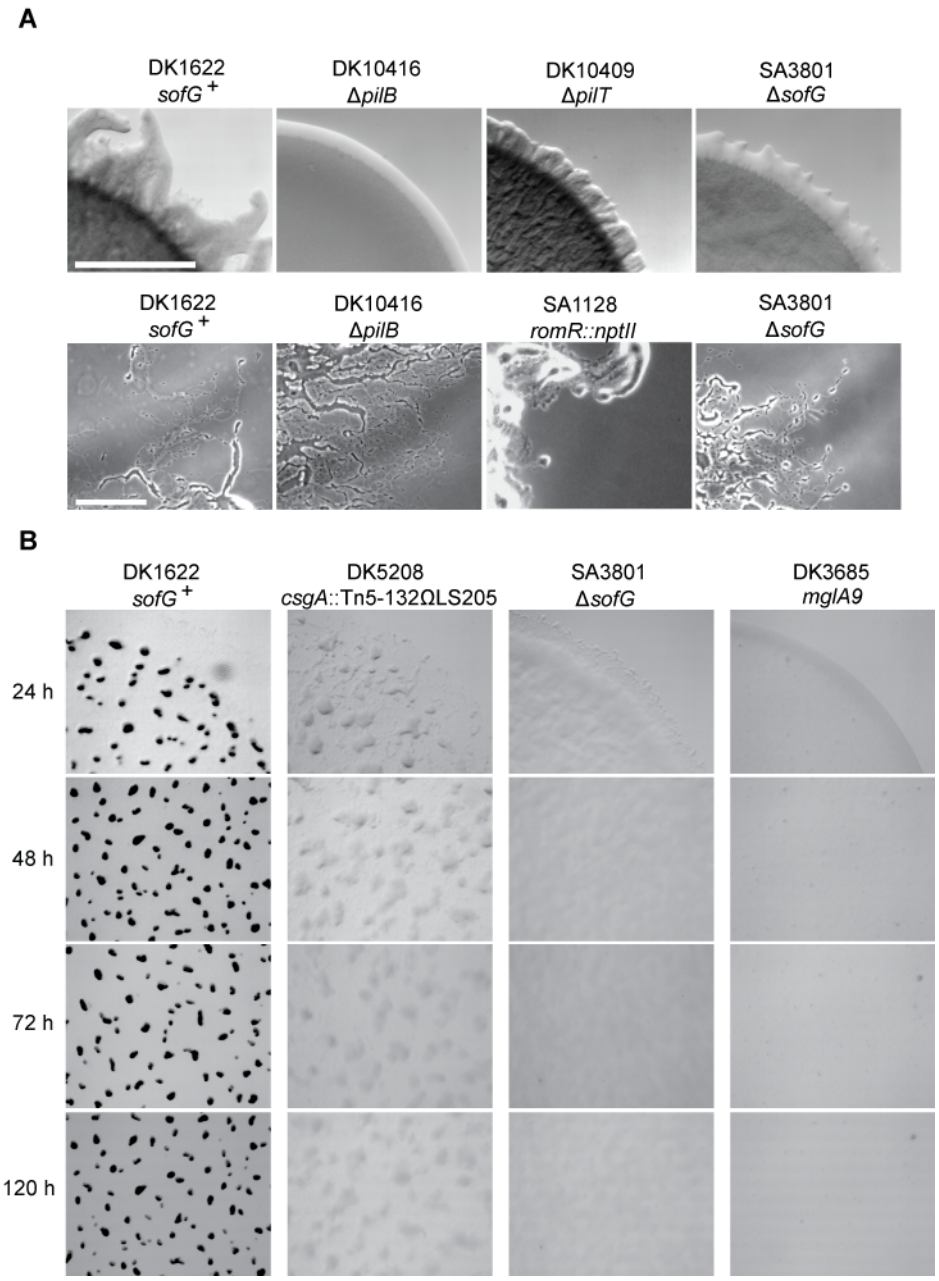

Figure 41. SofG is required for T4P-dependent motility and development

A) Motility phenotypes of *ΔsofG* mutant. Cells were incubated at 32˚C for 24h on 0.5% (top row) and 1.5% (bottom row) agar supplemented with 0.5% CTT, and visualized with a stereomicroscope. Strain names and relevant genotypes are indicated. Scale bars: 5 mm and 50 µm, respectively. **B)** Developmental phenotype of *ΔsofG* mutant. Cells were starved on TPM agar plates for the indicated on the left time periods (in hours) and visualized with a stereomicroscope. Strain names and relevant genotypes are indicated.

In order to confirm that the observed S-motility defect is caused by the deletion of the *sofG* gene, two complementation vectors were generated. In the pSB6 plasmid *sofG* allele was expressed from the *pilA* promoter, and in pSB10 500 bp upstream of *sofG* gene were used as a putative *sofG* promoter (S. Brameyer, MPI Marburg). Both pSB6 and pSB10 were introduced into the Δ*sofG* mutant at the Mx8 phage attachment

site, giving rise to the strains SA3810 and SA3813, respectively. Motility assays were conducted to verify restoration of the S-motility defect of the Δ*sofG* mutant by the introduction of an external copy of *sofG* (Figure 42). Only SA3813 cells expressing *sofG* from the *pilA* promoter formed extended flares at the colony edge comparable to the WT cells. SA3810 cells generated short flares at the colony edge suggesting that the 500 bp region upstream of *sofG* gene might not contain the native *sofG* promoter.

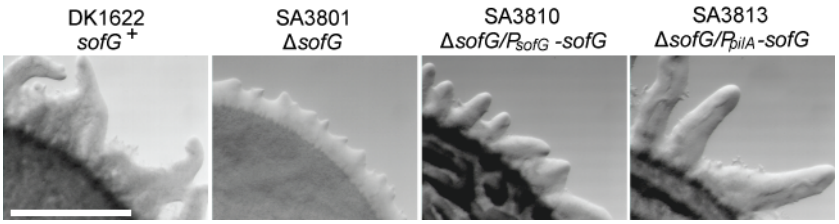

Figure 42. External *sofG* copy restores S-motility defect of Δ*sofG* mutant

Motility assays on 0.5% agar, favoring S-motility. Cells were incubated at 32˚C for 24h and visualized with a stereomicroscope. Strain names and relevant genotypes are indicated. Scale bar: 5 mm.

2.5.3 *ΔsofG* mutant assembles type IV pili at both poles

To determine the effect of lack of SofG on T4P assembly, T4P were visualized with negative staining electron microscopy. As depicted in Figure 43A, Δ*sofG* mutant assembled T4P. Strikingly, in 69% of Δ*sofG* cells T4P were detected at both poles (N=30 cells were analyzed for each strain), while only in 4% of WT cells a single pilus could be seen at the second pole (Figure 43B). Δ*sofG* cells possessed 6-10 T4P at one pole, which were comparable in length to WT T4P, and 3-5 T4P at the opposite pole, which were mostly shorter than WT T4P (Figure 43). 14% of Δ*sofG* cells assembled T4P only at one pole (76% in WT) and 17% cells of did not assemble T4P at any pole (comparable to 20% in WT) (Figure 43B). To summarize, these observations suggest that S-motility defect of the Δ*sofG* mutant is due to the T4P assembly at both poles and that SofG has an important function in inhibiting T4P assembly at the lagging pole. This is a first time that a mutant producing T4P at both poles has been identified.

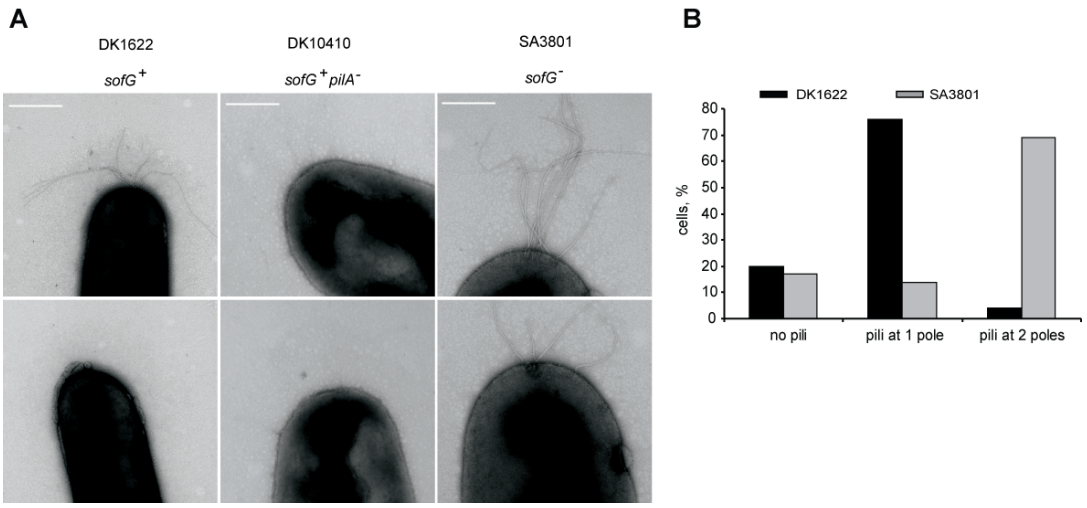

Figure 43. Δ*sofG* mutant assembles T4P at both poles

A) Cells from exponentially growing cultures of the indicated strains were directly transferred to a grid, stained with 2% (wt/vol) uranyl acetate, and visualized using transmission electron microscopy. The top row represents one pole, the bottom row the second pole for each strain. Scale bars: 0.5 µm for WT and 0.2 µm for Δ*pilA* and Δ*sofG* cells, respectively. **B)** Histogram of T4P distribution in WT and SA3801 cells. N=30 cells were analyzed for each strain.

2.5.4 Production ot exopolysaccharides in *ΔsofG* mutant

As described in Chapter 1.4.2, exopolysaccharides of the extracellular matrix (EPS) is one of the crucial components required for T4P-dependent motility. It is important to note that not only mutants unable to accumulate EPS (large group of *dsp* mutants) but also those that overproduce EPS (*ΔdigR* and *ΔsgmT* mutants) are impaired in T4P-dependent motility (Overgaard *et al.*, 2006; Shimkets, 1986b). Moreover, EPS appears to be essential for *M. xanthus* starvation-induced development (Li and Shimkets, 1993). Given the similarity of *mglA9* and Δ*sofG* mutants developmental phenotypes and the fact that all *mglA* mutants are deficient in production of EPS (Dana and Shimkets, 1993), we hypothesized that the S-motility and phenotype of *ΔsofG* mutant could be also due to a defect in EPS accumulation. To test this idea, quantitative dye-binding assays with Congo red were conducted as described by Black and Yang (Black and Yang, 2004). *Δdsp* and *ΔdigR* mutants were used as controls. The EPS accumulation was calculated as the percentage of the Congo red dye bound by cells.

ΔsofG mutant produced slightly decreased amounts of EPS compared to WT, but significantly more than the *Δdsp* mutant (Figure 44). We conclude that the S-motility defect in the *ΔsofG* mutant is caused not by the altered EPS accumulation, but rather by the T4P production at both poles.

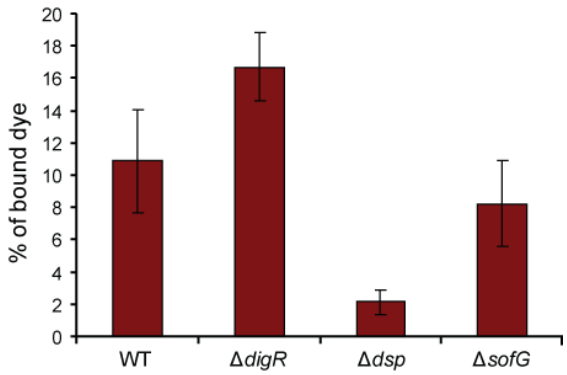

Figure 44. EPS production in Δ*sofG* mutant

Analysis of EPS production using quantitave Congo red binding assay. Cells mixed with Congo red solution were incubated at RT for 30 min in the dark, pelleted, and absorbances of the supernatants were measured at 490 nm. Strains used (from left to right): DK1622 (WT), SA1804 (Δ*digR*), DK3470 (Δ*dsp*) and SA3801 (Δ*sofG*).

2.5.5 Generation of YFP-SofG fusion proteins

To begin to understand how SofG affects T4P-dependent motility, we localized SofG. To this end, the plasmid pSB7, which contains an *yfp-sofG* allele expressed from the *pilA* promoter, was generated. pSB7 was integrated via site-specific recombination at the Mx8 phage attachment site in the strain SA3801 (Δ*sofG*), giving rise to the strain SA3811. To verify that the fusion protein is functional, motility assays on the 0.5% agar favoring S-motility were conducted. In contrast to the *sofG* allele expressed from *pilA* promoter (Figure 42), the YFP-SofG only partially corrected motility defect caused by the Δ*sofG* mutation in SA3801 (Figure 45A). To exclude possible negative effects of the 10 amino acid linker (from hereon, linker 1) inserted between YFP and SofG in order to improve YFP-SofG maturation, two other plasmids were generated. In the plasmid pIB97 the *yfp* gene was cloned in-frame with *sofG* gene without a linker sequence in between, and in the plasmid pIB99 *yfp* and *sofG* genes were separated by 60 bp, encoding a longer 20 amino acids linker (from hereon, linker 2). Both plasmids were integrated at the chromosomal Mx8 attachment site in the strain SA3801 (Δ*sofG*) giving rise to strains SA3074 and SA3076, respectively. However, all the YFP-SofG fusions generated only partially corrected SA3801 motility defect (Figure 45A).

To compare the expression levels of native SofG and different YFP-SofG proteins, antibodies against two peptides from the middle of SofG protein were raised (Figure 40). The anti-SofG antibodies did not detect any specific bands at the expected size (32.7 kDa) in WT cell lysates, which were not present in the Δ*sofG* mutant. However, the YFP-SofG proteins in the strains SA3811 (Δ*sofG/*P_{pilA}*-yfp-linker1-sofG*), SA3074 (Δ*sofG/*P_{pilA}*-yfp-sofG*) and SA3076 (Δ*sofG/*P_{pilA}*-yfp-linker2-sofG*) as well as SofG expressed from the *pilA* promoter in SA3810 were detected at the expected sizes (Figure 45B). These data suggest that the expression level of native SofG is too low to be recognized by the anti-peptide antibodies and that the expression from *pilA* promoter is higher compared to the native *sofG* promoter. Immunoblot analysis using anti-GFP antibodies confirmed the sizes of the YFP-SofG proteins. The anti-SofG

antibodies also detected a degradation product of YFP-SofG around 45 kDa, which was not recognized by anti-GFP antibodies, suggesting that this protein contains full-length SofG and only a small part of YFP. Anti-GFP antibodies detected in addition to the full-length YFP-SofG, two degradation products, around 50 kDa and 38 kDa, which were not recognized by anti-SofG antibodies (Figure 45B). These results demonstrate that full-length YFP-SofG proteins are expressed in all strains independently of the presence of a linker between YFP and SofG units. However, all fusions accumulate at the higher expression levels compared to the WT SofG protein.

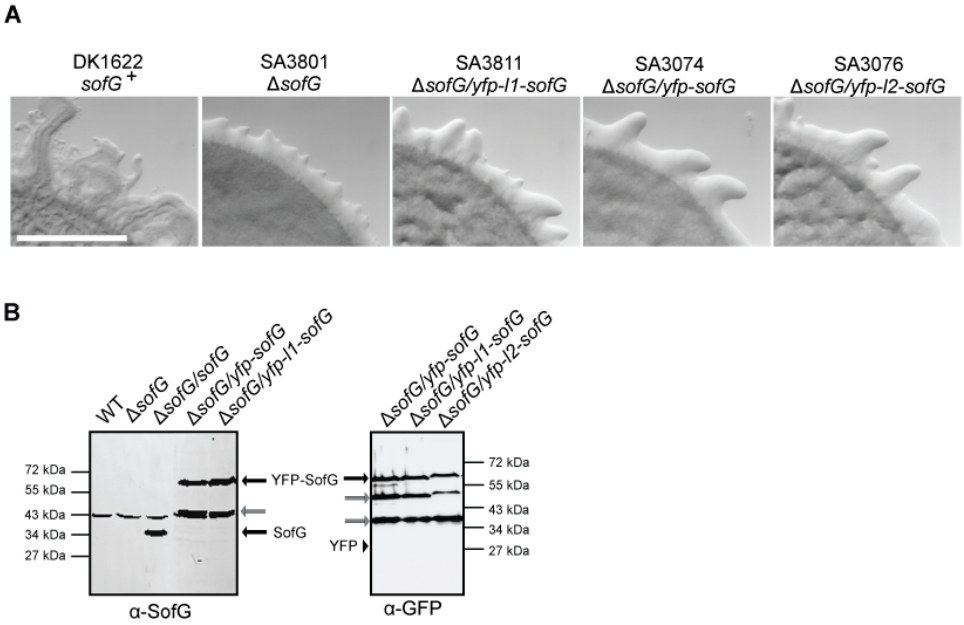

Figure 45. YFP-SofG fusions partially restore S-motility of Δ*sofG* mutant

A) Motility assays on 0.5% agar, favoring S-motility. Cells were incubated at 32˚C for 24h and visualized with a stereomicroscope. Strain names and relevant genotypes are indicated. Scale bar: 5 mm. **B)** Immunoblot analysis of SofG and YFP-SofG accumulation. Cells from exponentially growing cultures were harvested and samples analyzed as in Figure 14A. Strains used (left to right): DK1622 (WT), SA3801 (Δ*sofG*), SA3810 (Δ*sofG/sofG*), SA3811 (Δ*sofG/yfp-linker1-sofG*), SA3074 (Δ*sofG/yfp-sofG*) and SA3076 (Δ*sofG/yfp-linker2-sofG*). Blot on the left was probed with anti-SofG antibodies, blot on the left with anti-GFP antibodies. SofG and YFP-SofG proteins are marked with black arrows. Gray arrows indicate degradation products described in text. Black triangle indicates expected position of YFP protein.

In an attempt to optimize the SofG protein expression levels, several other fusions were generated. The plasmid pSB9 containing *yfp-linker1-sofG* expressed from the putative *sofG* promoter (500 bp upstream of *sofG* gene) was introduced via site-specific recombination at the chromosomal Mx8 phage attachment site in SA3801 (Δ*sofG*) strain, giving rise to the strain SA3812. In parallel, the plasmid pIB101 containing *yfp-linker1-sofG* was introduced via homologous recombination at the endogenous *sofG* locus on the chromosome in WT strain, giving rise to strain SA3083.

However, YFP-SofG in SA3812 and SA3083 strains were not detected by the immunoblot analysis with anti-SofG antibodies nor observed with fluorescence microscopy (data not shown). Hence, the YFP-SofG fusions expressed from the *sofG* native promoter appeared to be inefficient to produce detectable protein levels. Therefore, the YFP-SofG fusions expressed from *pilA* promoter were used to investigate SofG localization.

2.5.6 SofG has an unusual localization pattern

As no significant differences in the YFP-SofG expression levels and motility behavior were observed for SA3811 (Δ*sofG/P$_{pilA}$-yfp-linker1-sofG*), SA3074 (Δ*sofG/P$_{pilA}$-yfp-sofG*) and SA3076 (Δ*sofG/P$_{pilA}$-yfp-linker2-sofG*) strains, the SA3811 strain was used throughout all experiments. Fluorescence and phase-contrast microscopy were carried out to determine SofG localization. In all cells analyzed YFP-SofG accumulated in a single cluster found at various locations in a cell (Figure 46A). To determine the exact position of the single YFP-SofG cluster, statistical analysis was conducted. For this the maximal intensity of the fluorescent foci was measured using the linescan tool of Metamorph® v 7.5 as a function of the cell length in N=100 cells. This analysis revealed that in 82% of the cells YFP-SofG single cluster localized between 11 and 40% of a cell length, in 7% of the cells between 41 and 50% of a cell length (or in the middle cell region), and only in 11% of the cells between 1 and 10% of a cell length (or at the pole) (Figure 46).

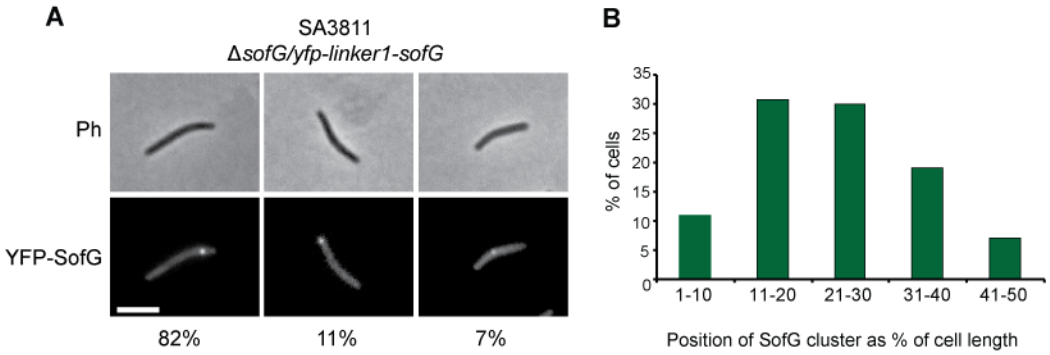

Figure 46. SofG has an unusual localization pattern

A) Localization of YFP-SofG at various locations in the cell. Cells were transferred from exponentially growing cultures to a thin 1.5% agar pad on a microscope slide, and imaged by fluorescence and phase-contrast microscopy. Top and bottom rows show phase-contrast and fluorescence images, respectively. Scale bar: 3 µm. **B)** Histogram of SofG cluster positioning in the cell. Position of the YFP-SofG cluster relative to the cell length (in %) was determined by linescan function of Metamorph® v 7.5 (maximum intensity) in N=100 cells. 1-10% of a cell length correspond to the cell pole, 41-50% to the middle cell region.

The observation that the YFP-SofG cluster was detected at various locations in the cell implyed that SofG localization might change over time. In order to study YFP-SofG cluster dynamics, time-lapse microscopy was performed. As SofG is a protein required for motility, moving cells were examined. Cells were followed for 15 min, with 30 s intervals between the frames. Movies of representative cells are shown in Figure 47-49. Quantitative analyses were carried out to elucidate whether there are any correlations between cell behavior and SofG cluster dynamics. Three distinct types of YFP-SofG cluster dynamics were observed.

In 30% of cells, YFP-SofG appeared to form a stationary cluster, which exhibit little if any dynamics (Figure 47A and B). Strikingly, reversals were also not accompanied by a change in the localization of a cluster. It is important to note that stationary YFP-SofG clusters were observed at different locations in the cell, i.e. at the pole, in the vicinity of the pole and at the middle cell region.

In 69% of cells the YFP-SofG cluster moved over the short distances. As can be seen in Figure 48A, the YFP-SofG cluster changed its position, moved from its original location towards the pole, remained there from 2:30 to 4:00 min, and then left the pole at 4:30 min. At 9:30 min, the YFP-SofG cluster was again at the pole, and left it at 10:00 min. At the beginning of a time-lapse recording those cells consistently displayed the YFP-SofG cluster localization in the vicinity of the pole, i.e. between 11 and 30% of the cell length.

Finally, in 1% of the YFP-SofG cluster traveled a longer distance (Figure 49A), so that the YFP-SofG cluster almost “relocated” from one pole or mid-cell to another pole. This “relocation” was consistently observed in the cells displaying the YFP-SofG cluster localization in the middle cell region, i.e. between 40 and 50% of the cell length, at the beginning of a time-lapse recording. We did not identify any correlations between cellular reversals and the YFP-SofG cluster oscillations.

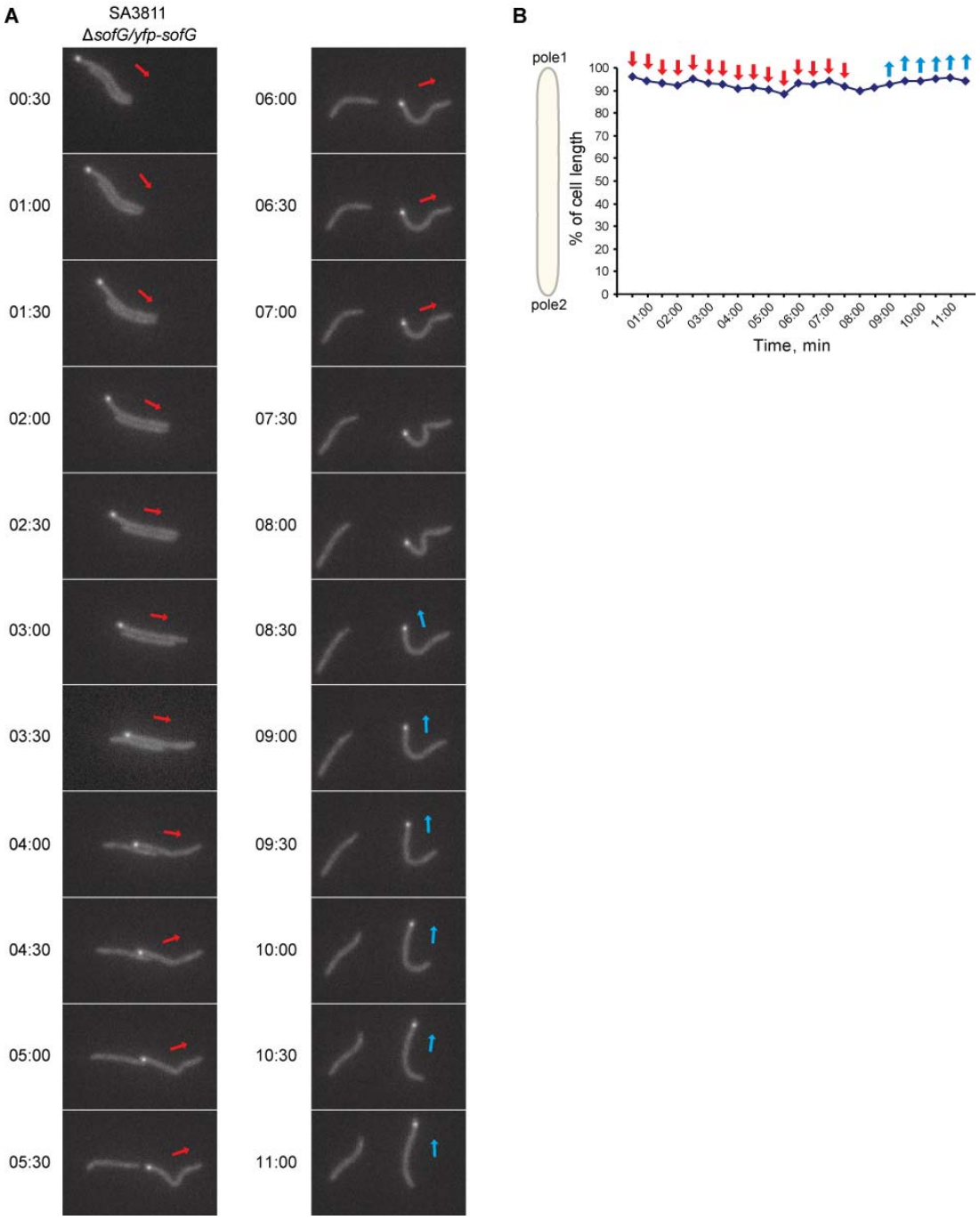

Figure 47. Stationary SofG cluster is observed in 30% of the cells

A) Localization of YFP-SofG in moving SA3811 cells. Cells were transferred from exponentially growing culture to the 1.5% thin agar pad and visualized with phase-contrast and fluorescence microscopy. Representative cell is shown. Red and blue arrows indicate opposite directions of movement. Cell stopped and reversed from 7:30 to 8:30. **B)** Quantitative analysis of polar YFP-SofG fluorescence signals in SA3811 cells. The localization as percentage of cell length of the maximum YFP-SofG fluorescence signal in the cell shown in (A) was plotted as a function of time. Red and blue arrows indicate opposite directions of movement.

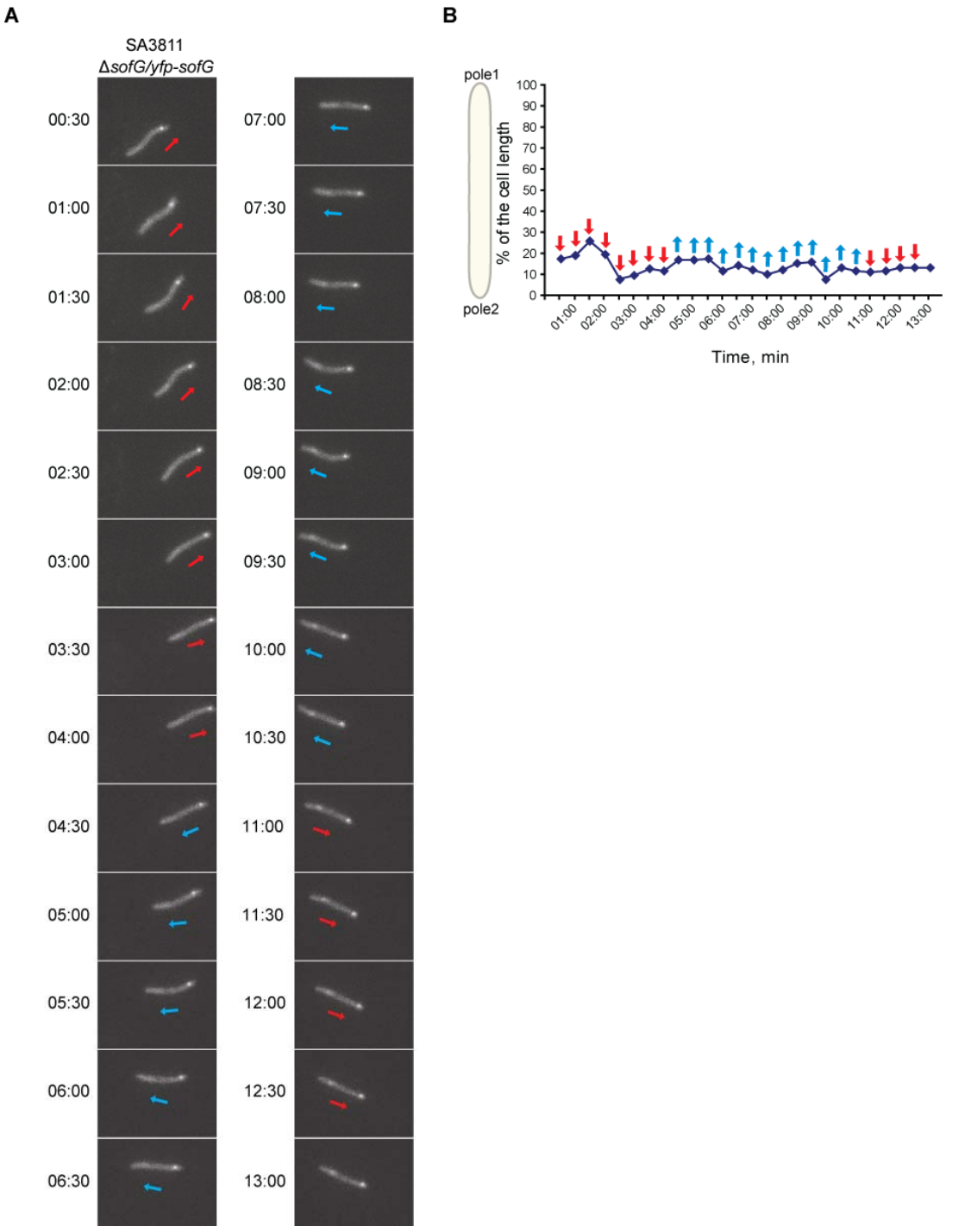

Figure 48. SofG cluster travels a short distance in 69% of the cells

A) Localization of YFP-SofG in moving SA3811 cells. Cells were were prepared and analyzed as in Figure 47A. Representative cell is shown. Red and blue arrows indicate opposite directions of movement. Cell reversed twice, between 4:00 and 4:30, 10:30 and 11:00. **B)** Quantitative analysis of polar YFP-SofG fluorescence signals in SA3811 cells. The localization as percentage of cell length of the maximum YFP-SofG fluorescence signal in the cell shown in (A) was plotted as a function of time. Red and blue arrows indicate opposite directions of movement.

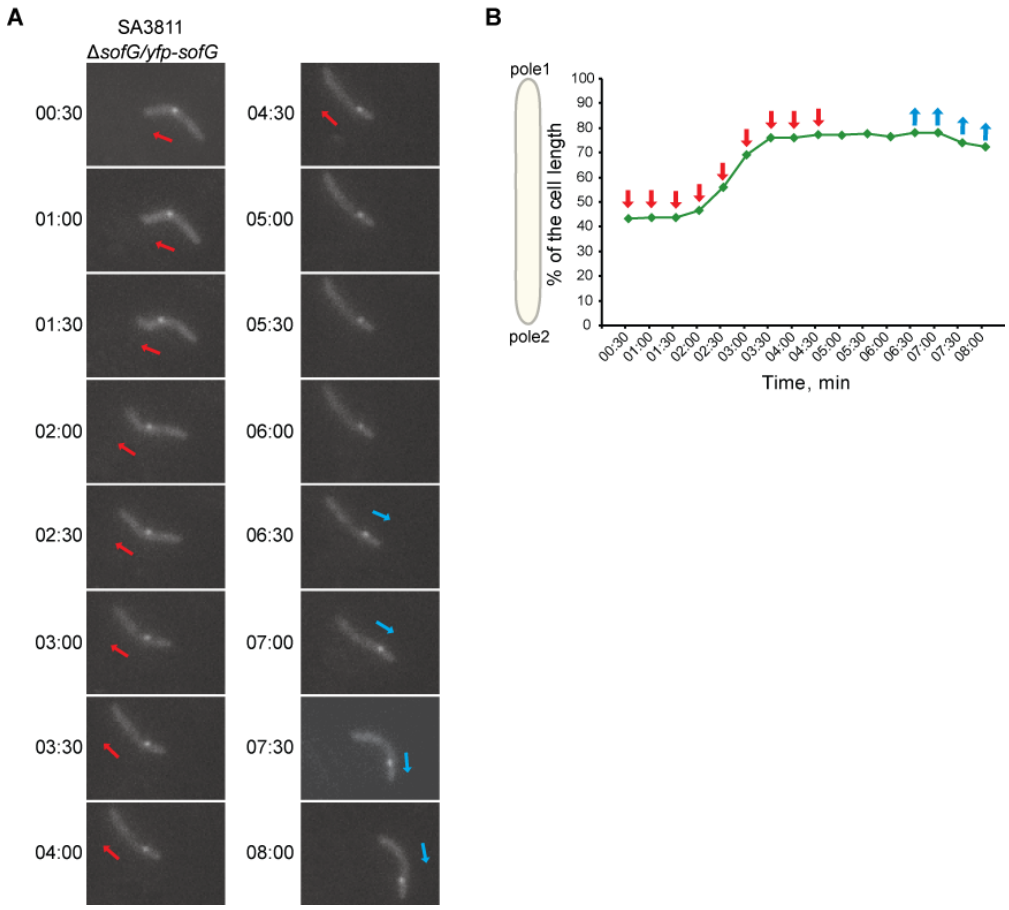

Figure 49. SofG cluster travels a long distance in 1% of the cells

A) Localization of YFP-SofG in moving SA3811 cells. Cells were were prepared and analyzed as in Figure 47A. Representative cell is shown. Red and blue arrows indicate opposite directions of movement. Cell stopped and reversed from 5:00 to 6:30. **B)** Quantitative analysis of polar YFP-SofG fluorescence signals in SA3811 cells. The localization as percentage of cell length of the maximum YFP-SofG fluorescence signal in the cell shown in (A) was plotted as a function of time. Red and blue arrows indicate opposite directions of movement.

2.5.7 Accumulation of type IV pili components is independent of SofG

We hypothesized that the defect in T4P dependent motility in the Δ*sofG* mutant could be due to an alteration in expression and/or localization of T4P proteins. To test this possibility, the accumulation levels of PilQ, PilC, PilB, PilM, PilT and PilA were examined using immunoblot analyses of whole cell lysates with specific antibodies (Figure 50). These analyses showed that the Δ*sofG* mutant accumulated all these proteins at WT levels (Figure 50). Next, we addressed the localization of three T4P components, namely of the stationary inner membrane protein PilC and the two dynamically localized ATPases PilB and PilT.

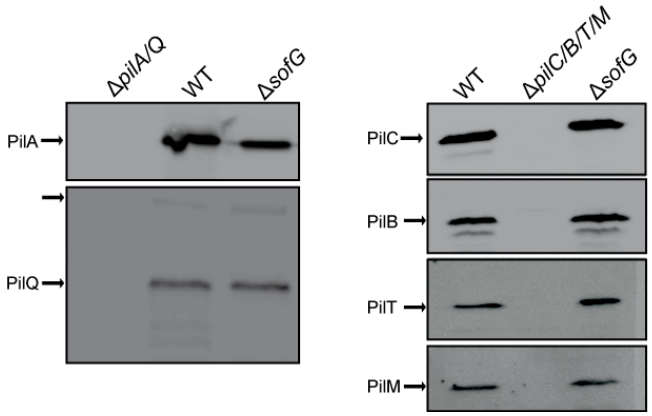

Figure 50. Δ*sofG* mutant expresses WT levels of T4P components

Immunoblot analyses of PilA, PilQ, PilC, PilB, PilT and PilM proteins accumulation. Relevant genotypes are indicated. Cells from exponentially growing cultures were harvested and samples analyzed as in Figure 14A. Blots were probed with corresponding antibodies. Proteins analyzed are indicated on the left. Additional arrow indicates PilQ multimers.

2.5.8 Localization of PilC in the absence of SofG

To elucidate PilC localization in the absence of SofG, immunofluorescence microscopy with anti-PilC antibodies was performed with SA3801 (Δ*sofG*). As depicted in Figure 51A, PilC localized in two polar clusters in SA3801 cells. Statistical analysis was performed in order to compare the PilC polar clusters ratios observed in WT and Δ*sofG* cells. The results of this analysis demonstrated that PilC localized independently of SofG (Figure 51B). Thus, the T4P-dependent motility defect of Δ*sofG* mutant is neither caused by the absence of PilC protein nor by PilC mislocalization.

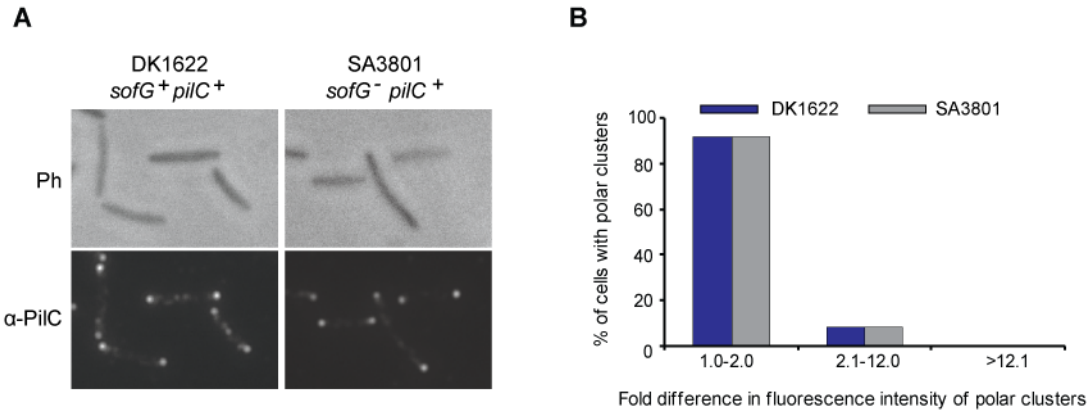

Figure 51. PilC localizes in a bipolar symmetric pattern in the absence of SofG

A) Localization of PilC by immunofluorescence microscopy using anti-PilC antibodies in WT and Δ*sofG* mutant. Cells from exponentially growing cultures were prepared and analyzed as described in Figure 17A. Top and bottom rows show phase-contrast and fluorescence images, respectively. Strain names and relevant genotypes are indicated. **B)** Histogram of distribution of PilC polar clusters in WT and Δ*sofG* mutant. Data are presented as in Figure 17B. In total N=100 cells were analyzed for each strain.

2.5.9 Localization of PilB ATPase in the absence of SofG

To localize PilB in the Δ*sofG* mutant, immunofluorescence microscopy with anti-PilB antibodies was conducted. In 80% of Δ*sofG* cells polar PilB clusters were observed (Figure 52A). To further compare PilB localization in the Δ*sofG* mutant and WT, statistical analysis of polar PilB clusters ration was carried out.

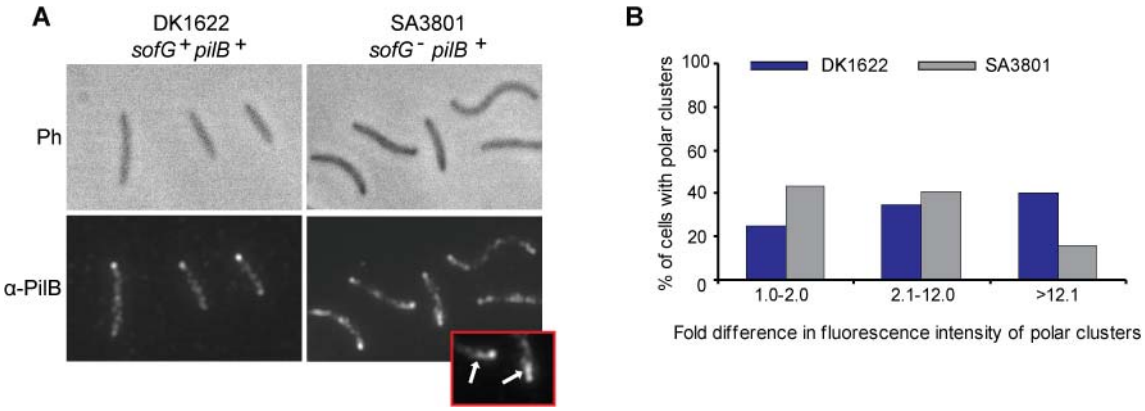

Figure 52. PilB localization is affected in the absence of SofG

A) Localization of PilB by immunofluorescence microscopy using anti-PilB antibodies in WT and Δ*sofG* mutant. Cells from exponentially growing cultures were prepared and analyzed as described in Figure 17A. Top and bottom rows show phase-contrast and fluorescence images, respectively. Strain names and relevant genotypes are indicated. Red rectangle depicts zoomed-in polar regions of two cells in the centre of the image. White arrows indicate additional PilB clusters. **B)** Histogram of distribution of PilB polar clusters in WT and Δ*sofG* mutant. Data are presented as in Figure 17B. In total N=100 cells were analyzed for each strain.

Although three distinct PilB localization patterns were detected in the Δ*sofG* mutant, the distribution of these patterns was clearly different from that in WT (Figure 52B). Only 16% of Δ*sofG* cells displayed unipolar PilB localization (40% in WT), 41% bipolar asymmetric pattern (comparable to 35% in WT) and 43% had a bipolar symmetric PilB localization (25% in WT). Moreover, in 80% of Δ*sofG* cells additional PilB accumulations/clusters were observed in the vicinity of the pole (Figure 52A, red rectangle). Also the cytoplasmic PilB signal in Δ*sofG* mutant cells was more intense and less homogenous compared to WT (Figure 52A). Thus, PilB localization is clearly altered in the absence of SofG suggesting that SofG might be involved in PilB polar targeting mechanism and/or PilB dynamics.

2.5.10 Localization of PilT ATPase in the absence of SofG

To further characterize the Δ*sofG* mutant, PilT localization was determined. For this, the Δ*sofG* mutation was generated in the Δ*pilT* mutant, giving rise to SA3819 strain. Next, the plasmid pIB75, containing *yfp-pilT* allele under control of the *pilA*

promoter, was integrated via site-specific recombination at the chromosomal Mx8 phage attachment site in SA3819 (Δ*sofG,* Δ*pilT*) strain, giving rise to the SA3069 strain. The YFP-PilT localization pattern in the Δ*sofG* mutant was very different from that observed in WT and similar to the localization of SofG (Figure 53).

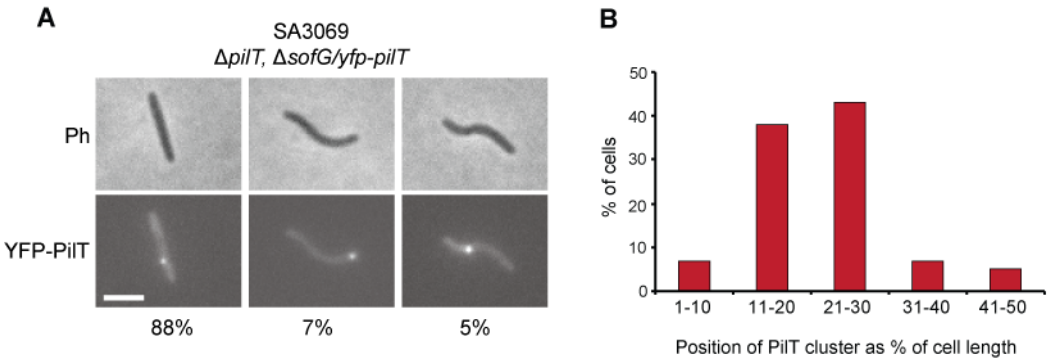

Figure 53. PilT localization is strongly impaired in the absence of SofG

A) Localization of YFP-PilT in SA3069. Cells were were prepared and imaged as in Figure 47A. Top and bottom rows show phase-contrast and fluorescence images, respectively. Scale bar: 3 μm. **B)** Histogram of PilT cluster positioning in the cell. Position of the YFP-PilT cluster relative to the cell length was determined by linescan function of Metamorph® v 7.5 (maximum intensity) in N=100 cells.

To determine the exact PilT position in SA3069 (Δ*sofG,* Δ*pilT/yfp-pilT*) cells, the statistical analysis previously used for YFP-SofG was conducted, i.e. the maximal intensity of the fluorescent foci was measured using the linescan tool of Metamorph® v 7.5 as a function of the cell length in N=100 cells. This analysis revealed that similarly to SofG localization (Figure 46A) in 88% of Δ*sofG* cells, PilT cluster localized between 11 and 40% of a cell length, in 5% of the cells between 41 and 50% of a cell length (or in the middle cell region), and only in 7% of the cells between 1 and 10% of a cell length (or at the pole) (Figure 53A and B).

To examine the dynamics of YFP-PilT localization in the Δ*sofG* strain, 15 min time-lapse recordings with 30 s intervals between frames were made. These experiments demonstrated that in 80% of cells (independently of the YFP-PilT cluster position in the cell), the YFP-PilT cluster did not display any significant dynamics (a representative cell is depicted in Figure 54A and B). Also no changes in YFP-PilT localization were observed during cellular reversal (from 4:00 to 4:30 min for the cell shown in Figure 54A).

In 20% of cells, the YFP-PilT cluster moved a short distance. As shown in the representative cell in Figure 55A, the YFP-PilT cluster constantly moved. From 1:30 to 10:30 min, the YFP-PilT cluster moved in the direction from mid-cell to the pole, at 11:00 min it started to move in the opposite direction. There were no significant changes in YFP-PilT cluster behavior during a reversal, which occurs between 7:30

and 8:30 (Figure 55A). At the beginning of a time-lapse recording those cells consistently displayed the YFP-PilT cluster localization in the vicinity of the pole, i.e. between 11 and 30% of the cell length.

Thus, we conclude that PilT localization is severely impaired in the absence of SofG. Although in 20% of cells YFP-PilT cluster is dynamic, it does not localize to the poles. These findings together with the data obtained for PilB localization in the Δ*sofG* mutant strongly suggest that SofG regulates the localization of both T4P ATPases PilB and PilT.

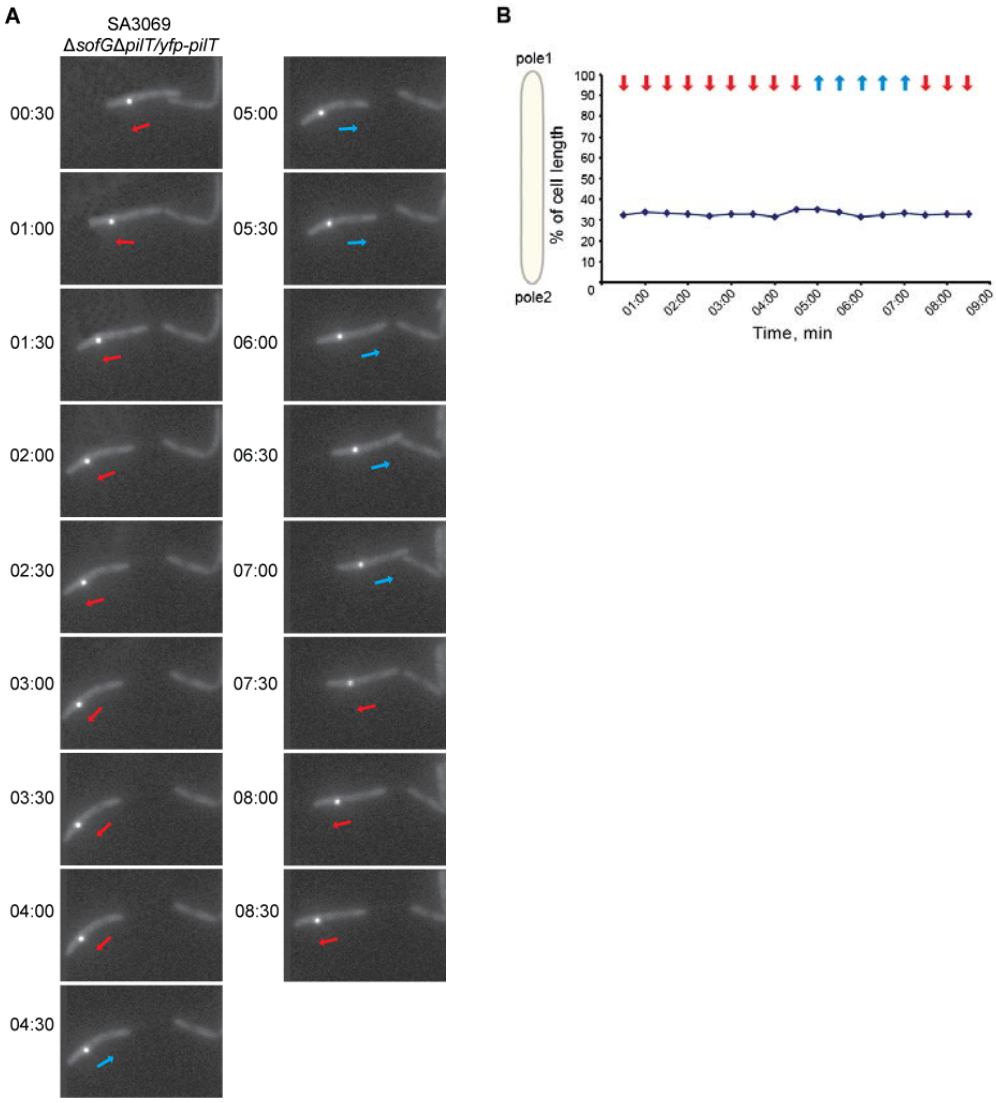

Figure 54. Non-moving PilT cluster is observed in 80% of Δ*sofG* cells

A) Localization of YFP-PilT in moving SA3069 (Δ*sofG,ΔpilT/yfp-pilT*) cells. Cells were were prepared and imaged as in Figure 47A. Representative cell is shown. Red and blue arrows indicate opposite directions of movement. Cell reversed from 4:00 to 4:30. **B)** Quantitative analysis of polar YFP-PilT fluorescence signals in SA3069 cells. The localization as percentage of cell length of the maximum YFP-PilT fluorescence signal in the cell shown in (A) was plotted as a function of time. Red and blue arrows indicate opposite directions of movement.

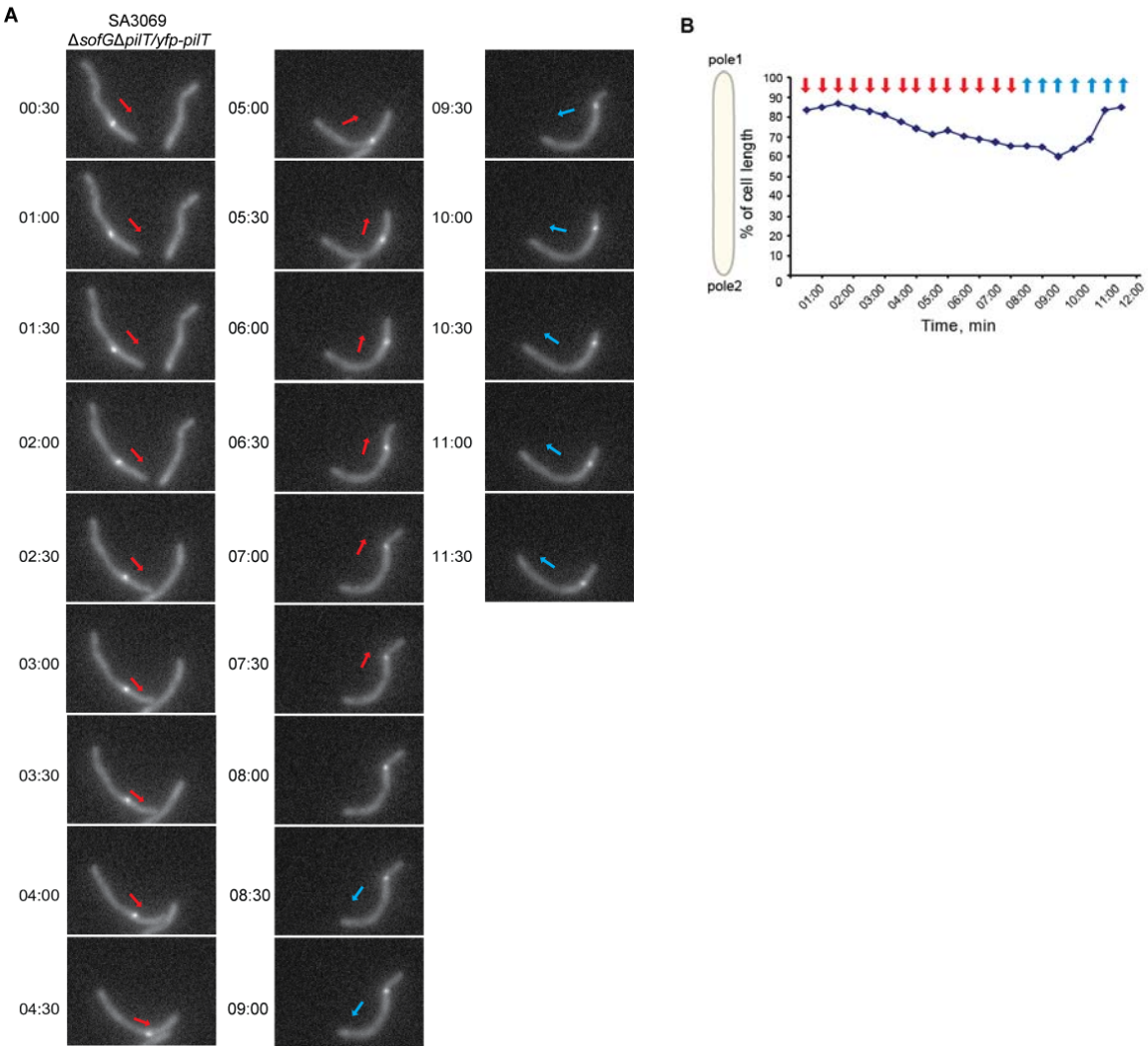

Figure 55. PilT travels on a short distance in 20% of Δ*sofG* cells

A) Localization of YFP-PilT in moving SA3069 (Δ*sofG,*Δ*pilT/yfp-pilT*) cells. Cells were were prepared and imaged as in Figure 47A. Representative cell is shown. Red and blue arrows indicate opposite directions of movement. Cell stopped and reversed from 7:30 to 8:30. **B)** Quantitative analysis of polar YFP-PilT fluorescence signals in SA3069 cells. The localization as percentage of cell length of the maximum YFP-PilT fluorescence signal in the cell shown in (A) was plotted as a function of time. Red and blue arrows indicate opposite directions of movement.

3 Discussion

Coordinated cell movement plays a pivotal role during *M. xanthus* vegetative growth, predation on other bacteria and fruiting body formation. The ability of cells to actively move depends on two distinct motility systems: S-motility, powered by retraction of type IV pili (T4P) at the leading cell pole; and A-motility, which has been suggested to depend on two distinct units, slime secretion at the lagging cell pole, and focal adhesions along the cell body (Hodgkin and Kaiser, 1979a, b; Leonardy *et al.*, 2007; Mignot *et al.*, 2007; Wall and Kaiser, 1999). The event required for regulated movements is cellular reversals, which allow cells to change their direction of movement. During the periodical reversals, cell polarity is inverted so that the old leading pole becomes the new lagging pole and *vice versa* (Blackhart and Zusman, 1985). The Frz chemosensory system regulates the reversal frequency by an unknown mechanism (Blackhart and Zusman, 1985). The mechanisms that target motility proteins to the poles and underly the inversion of cell polarity (or polarity switching) during reversal are being extensively studied for both S- and A-motility systems.

In this study we provide evidence for the first time that T4P polarity switching during reversal relies on the dynamic behavior of the two motor proteins, PilB and PilT. Moreover, we demonstrate that the spatial separation of these two motors provides a mechanism for temporal regulation of T4P extension and retraction in *M. xanthus*. Finally, our data indicate that correct T4P localization and pole-to-pole oscillations are regulated by the Frz chemosensory system, Ras-like GTPase MglA and its paralog SofG.

3.1 Mechanism underlying type IV pili pole-to-pole oscillations during reversal

To address the mechanism underlying T4P oscillations during reversal we examined the localization of six T4P components, conserved in all bacteria producing T4aP (Pelicic, 2008). The localization patterns of these six proteins provide evidence that not only T4P pole-to-pole oscillations during reversal, but also T4P extension/retraction cycles depend on dynamic disassembly/re-assembly of the T4P machinery.

3.1.1 Stationary type IV pili components

Immunofluorescence microscopy data and YFP-PilM fusion protein localization studies provide evidence that four T4P proteins - PilQ in the outer membrane, PilC and PilN in the inner membrane, and PilM in the cytoplasm - localize in bipolar symmetric clusters and that these clusters likely remain stationary during reversals (Figure 56C).

In support of this idea, we demonstrated that the PilQ, PilC, PilN and PilM bipolar symmetric localization was not affected in a hypo-reversing *frz* mutant. It should be noted that the subcelular localization of PilN was deduced from the homology to PilN from *P. aeruginosa*, which has been shown to localize to the inner membrane (Ayers *et al.*, 2009), but remains to be demonstrated experimentally. We also observed that PilN stability depends on PilO and PilP proteins suggesting that these proteins may interact in *M. xanthus* as was recently suggested in *P. aeruginosa* (Ayers *et al.*, 2009). It, therefore, remains a possibility that PilO and PilP are also localized in stationary, bipolar and symmetric clusters.

3.1.2 Dynamic type IV pili components

In contrast to PilQ, PilC, PilN and PilM localization pattern, the localization patterns observed for the PilB ATPase in WT and hypo-reversing *frz* mutant cells using immunofluorescence microscopy suggest a model in which PilB is dynamic between and during reversals (Figure 56A). According to this model, PilB is localized to the leading cell pole after reversal. Between two reversals PilB starts to accumulate at the lagging cell pole initially giving rise to a bipolar asymmetric pattern, and then to bipolar symmetric pattern. Finally, when cell reverses, the remaining PilB from the old leading pole relocates to the new leading pole, thus giving rise to a unipolar pattern. Because a reversal period (15 min under our experimental conditions) is much shorter than the generation time of *M. xanthus* (4-5 h), only about 5% of the total PilB protein is synthesized during a reversal period. Furthermore, our chloramphenicol experiments let us estimate a half-life of PilB in the order of 200 min. Taken together, these observations suggest that most of PilB that accumulates at the lagging cell pole is not synthesized *de novo*, but derived from PilB released from the cluster at the leading cell pole. Following the proposed model (Figure 56A), the Frz system, which regulates the reversal frequency, would function to reset PilB localization from a bipolar symmetric to a unipolar pattern. In a *frz* mutant this resetting mechanism would be disabled, which explains the predominantly bipolar symmetric PilB localization pattern, observed in *frz* hypo-reversing mutant. Accordingly, Frz system is not a pole-targeting determinant of PilB *per se*, but is required to reset the system to asymmetry upon reversal.

Furthermore, we directly observed that PilT localization is dynamic between and during reversals (Figure 56B). PilT localizes in two polar patterns in moving cells, unipolar and bipolar asymmetric. Unexpectedly, the large PilT cluster localizes to the lagging cell pole. In individual cells, the cluster at the leading cell pole was highly variable and appeared and disappeared over time (discussed in detail later). Notably, in *frz* hypo-reversing mutant PilT asymmetry has been maintained. Thus, PilT does not

progressively accumulate at the leading cell pole during a reversal period as suggested for PilB at the lagging pole. During reversals the large PilT cluster relocates from the old lagging pole to the new lagging pole, also in cells treated with chloramphenicol, confirming that PilT cluster at the new lagging pole derives from PilT cluster at the old lagging pole.

3.1.3 Model of the type IV pili polarity switching during reversal

The localization patterns of PilQ, PilC, PilN, PilM, PilB, PilT and FrzS proteins (Mignot *et al.*, 2005) suggest that T4P proteins can be divided into two groups. One group is represented by PilQ, PilC, PilN and PilM, and these proteins are localized in bipolar symmetric clusters, which remain stationary during reversals forming a pre-assembled part of T4P machinery. The second group is represented by PilB, PilT and FrzS, and these proteins relocate from pole to pole during reversals. PilB and FrzS are predominantly found at the leading cell pole and PilT at the lagging cell pole. On the basis of these data, we suggest a model (Figure 56C) in which pole-to-pole oscillations of T4P involve the disassembly at the leading pole of the T4P extension machinery with a release of PilB and FrzS, and reassembly of the new T4P extension machinery at the new leading cell pole with the binding of PilB and FrzS to pre-assembled stationary T4P proteins. In parallel, PilT is released from the old lagging pole and relocates to the new lagging pole. Thus, the pre-assembled parts of T4P machine at both poles would be activated in an alternating manner depending on the localization of the PilB and PilT motor proteins.

PilB, PilT and FrzS may not be the only T4P proteins oscillating between the poles during reversals. Notably, even though PilB starts to accumulate at the lagging pole between reversals, and in some WT and Δ*pilT* cells localizes in a bipolar symmetric pattern, T4P are assembled only at one (leading) pole (Jakovljevic *et al.*, 2008; Wu *et al.*, 1997). These observations demonstrate that PilT does not simply function to retract pili at the lagging cell pole (otherwise, we would expect Δ*pilT* mutant to assemble T4P at both poles). We hypothesize that a yet to be identified protein(s) required for T4P assembly may relocate during reversals. Alternatively, an inhibitor of T4P assembly at the lagging pole could also relocate from the old lagging to the new lagging pole during reversals. This point is further discussed in Chapter 3.4.

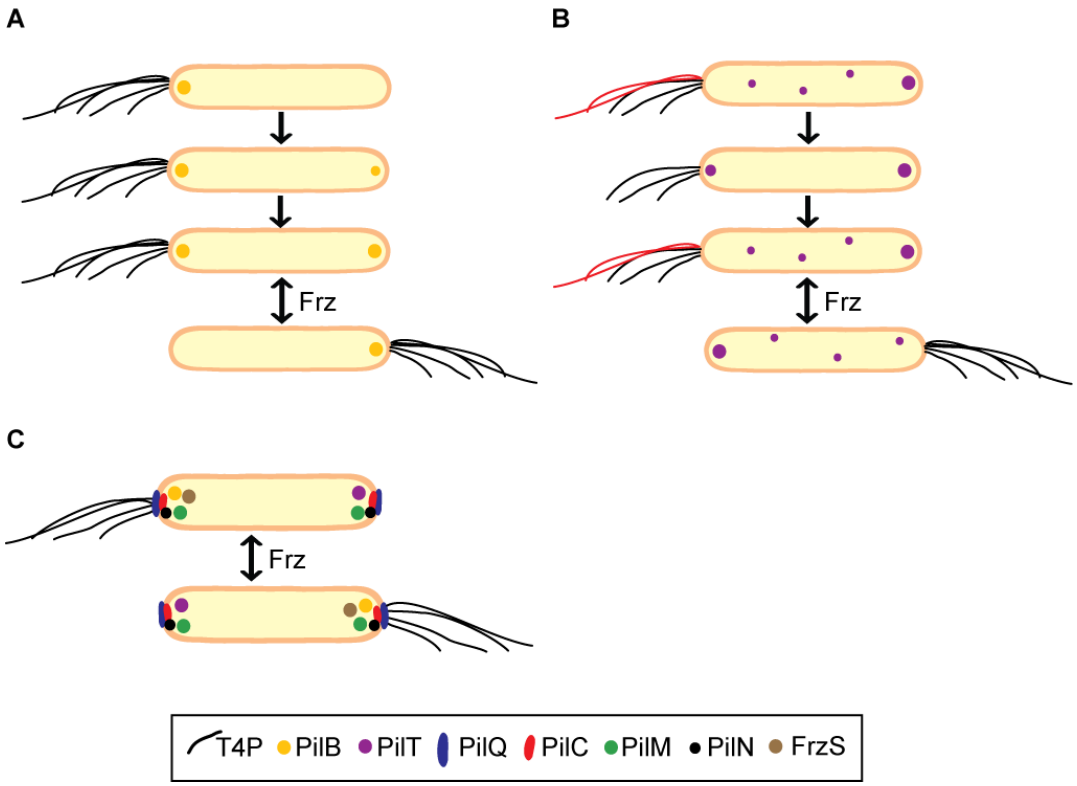

Figure 56. Type IV pili function depends on disassembly and reassembly processes

A) Model for PilB localization. Immediately after reversal, PilB is unipolarly localized at T4P (leading) pole. During reversal period, PilB also builds up at non-piliated pole giving rise to bipolar asymmetric and bipolar symmetric pattern. In response to Frz activity, PilB localization is reset to unipolar pattern with PilB at the new leading pole. **B)** Model for PilT localization. Majority of PilT is localized in a large cluster at the lagging cell pole with some PilT in the cytoplasm. PilT is rapidly turned over in the cluster resulting in the stochastic accumulation of PilT at the leading pole followed by retraction of T4P (retracted pili marked in red). In absence of PilT at the leading pole, T4P extension is catalysed by PilB. In response to Frz activity, PilT cluster from the old lagging pole relocates to the new lagging pole. **C)** Pole switching of T4P involves disassembly and reassembly of T4P molecular machine. PilQ, PilC, PilM and PilN are present in symmetric clusters that remain stationary during reversals. PilB and FrzS are predominantly localized at the T4P pole, PilT predominantly at the lagging pole, and these three proteins relocate during reversal in response to Frz activity.

3.2 Mechanism regulating temporal separation of type IV pili extension and retraction

T4P function depends on the temporal separation of extension and retraction. It has remained an open question how the activities of PilB and PilT ATPases are regulated to allow the temporal separation of extension and retraction. Our PilB and PilT localization data provide a solution to this question. As expected, PilB asymmetry is strongly biased towards the piliated, leading cell pole where it would energize T4P extension. Unexpectedly, the large PilT cluster localized to the lagging cell pole with bursts of accumulation at the leading pole.

In FRAP experiments we demonstrated that PilT molecules in the polar clusters

are rapidly turned over, and that PilT molecules in the polar clusters are in dynamic equilibrium on a timescale that is much shorter than an average reversal period. In the absence of evidence supporting the active transport of PilT between the poles, we analyzed the diffusion of PilT in the cytoplasm. For a freely diffusible cytoplasmic protein with a molecular mass of 72 kDa, the experimentally determined diffusion coefficient (D_a) is 2.5±0.6 $\mu m^2/s$ (Elowitz *et al.*, 1999). YFP-PilT has a molecular mass 67.6 kDa and, thus, is expected to have a diffusion coefficient in the order of 2.5 $\mu m^2/s$. From the Stoke-Einstein relation it follows that the diffusion coefficient for a PilT hexamer is 1.5 $\mu m^2/s$. Using these coefficients and an average *M. xanthus* cell length of 6 µm, we can estimate that PilT monomers and hexamers would need ~7 s and ~12 s, respectively, to relocate between the poles by diffusion. However, our FRAP data show that it takes 60-80 s for PilT molecules after the release from non-bleached polar cluster to bind to the opposite pole. This suggests that the dynamic exchange of PilT molecules between the poles is not diffusion-limited but is likely limited by the on- and off-events, i.e. binding and unbinding from the poles. In fact, detailed quantitative analysis, performed by Peter Lenz (Bulyha *et al.*, 2009), demonstrated that dissociation from the poles is slower than association. Furthermore, our FRAP data proved that PilT clusters are highly dynamic structures. From quantitative immunoblots (data not shown) we estimated that individual *M. xanthus* cells contain 1800 PilT molecules which is equivalent to 300 hexamers. Given that 58±8% of PilT is bound at the poles (estimated from immunofluorescence microscopy data analysis), approximately 1080 molecules (or 180 hexamers) are at the poles and 720 molecules (120 hexamers) are in the cytoplasm. It is not known whether PilT in the polar clusters and in the cytoplasm is present as monomer or hexamer. Nevertheless, given these low protein numbers of protein and slow binding and unbinding dynamics of PilT at the poles, the accumulation of PilT at the leading pole is expected to be heavily influenced by the stochasticity of the single protein binding processes. Therefore, PilT accumulation at the leading pole is expected to be noisy and show variation over time. Once at the leading pole, PilT would interact with T4P machinery to energize retraction. One scenario how PilT would promote retraction is that it could displace PilB at the base of T4P. Alternatively, PilB and PilT could interact in parallel with T4P machinery. The observation that PilB and PilT targeting to the pole does not involve a mutually exclusive mechanism suggests that PilB and PilT interact with T4P machinery in parallel.

One prediction from a model in which PilT noisy accumulations at the leading pole are caused by PilT binding kinetics is that the overproduction of PilT should lead to an increased number of PilT molecules at the leading cell pole, and, therefore, to

result in cells with fewer pili. Consistently, we observed that in moving cells containing an additional *pilT* copy on the chromosome, YFP-PilT is found in bipolar symmetric clusters. Additionally, two-fold increase in the accumulation of PilT results in cells with approximately two-fold fewer pili. Therefore, we suggest that the spatial separation of PilB and PilT in combination with noisy PilT accumulation at the leading cell pole allows the temporal separation of T4P extension and retraction. According to this model, PilB in the absence of PilT at the leading pole is able to energize pilus extension. The occasional accumulation of PilT at the leading cell pole would allow PilT to intermittently cause retractions. Consistent with this model, it was observed that T4P are retracted at a reduced frequency in a *N. gonorrhoeae* mutant that accumulates reduced levels of PilT (Maier *et al.*, 2004). Interestingly, *M. xanthus* Δ*pilT* mutant contains the same number of T4P as WT (Jakovljevic *et al.*, 2008), suggesting that in a WT T4P assembly occurs close to the maximum rate and that retraction (PilT activity) is low.

Polar localization appears to be a shared property of T4P motor ATPases. In bundle-forming pili of enteropathogenic *E. coli*, PilT ortholog BfpF was shown to localize unipolarly by immunofluorescence microscopy (Hwang *et al.*, 2003). A non-active PilB-YFP fusion and an active YFP-PilT fusion both localize in bipolar symmetric pattern in *P. aeruginosa*, whereas an active YFP-PilU fusion (PilU is a paralog of PilT and required for T4P retraction in *P. aeruginosa*) localizes in a unipolar pattern at the piliated pole (Chiang *et al.*, 2005). However, in these analyses cells were observed under conditions where they could not display T4P-dependent motility (in liquid media, not on solid surfaces). In *M. xanthus* PilT localizes in a bipolar symmetric pattern under similar conditions but redistributes into the asymmetric pattern when cells are placed on a surface that allows T4P-dependent motility. Thus, it remains unclear whether the model we suggest for *M. xanthus* which allows temporal separation of PilB and PilT activities is applicable to *P. aeruginosa*.

3.3 Polar targeting and polar retention of type IV pili components

To identify polar targeting determinants for the two T4P ATPases PilB and PilT and the inner membrane protein PilC, we used a cell biological approach. Recent studies in *P. aeruginosa* (Ayers *et al.*, 2009; Sampaleanu *et al.*, 2009) demonstrated that the PilM/N/O/P proteins, which are so far the least characterized T4P components, form an inner membrane complex (Figure 57) functionally similar to that described for *V. cholerae* type II secretion system (Lybarger *et al.*, 2009). This inner membrane complex is absolutely required in *P. aeruginosa* for the optimal formation of the outer membrane PilQ complex, as PilQ stability is negatively affected in its absence (Ayers *et*

al., 2009). Our data revealed several similarities as well as some differences between *P. aeruginosa* and *M. xanthus* T4P systems.

Our fractionation experiments suggest that PilM in *M. xanthus* is a cytoplasmic protein. However, we can not rule out a possibility of a transient association of PilM with inner membrane. Notably, PilM and PilN proteins in *M. xanthus* as well as PilQ and PilC proteins localize in a similar bipolar symmetric pattern, suggesting that these proteins may interact to generate stationary membrane-spanning protein complexes that could also include other T4P proteins. Several lines of evidence support this hypothesis. First, similarly to the *P. aeruginosa* system PilP and PilO proteins of *M. xanthus* are required for accumulation of PilN. We do not have data on the subcellular localization of these proteins, but sequence analyses suggest that both PilN and PilO proteins localize to the inner membrane, and that PilP is a lipoprotein (data not shown). Thus, we speculate that the model proposed for the *P. aeruginosa* inner membrane complex also applies to *M. xanthus*. Second, the mislocalization of PilC in the absence of PilA, PilQ, PilN, PilO and Tgl proteins strongly supports the idea of a membrane-spanning complex that could include PilC. Examining the localization of PilA, PilO, PilQ, PilN and Tgl proteins in other mutants may provide further insights on protein-protein interactions among T4P proteins. We speculate that Tgl, PilP and PilQ proteins form an outer membrane complex, whereas PilC, PilN and PilO proteins compose an inner membrane complex. In these complexes, individual proteins are required for stability and/or proper localization of their interaction partners, and the proper formation of one complex is required for the proper formation of another one. The role of PilA protein remains to be elucidated but it remains an interesting idea that PilA assists in connecting these two complexes.

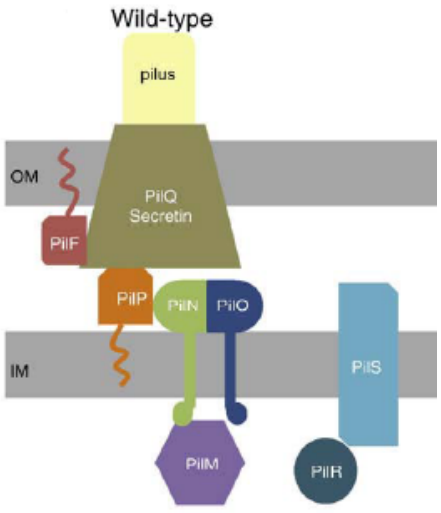

Figure 57. Model of type IVa pili in *P. aeruginosa*

Model depicts the inner membrane complex, composed of PilM/N/O/P proteins that links with an outer membrane composed of PilQ and PilF (Tgl ortholog). PilS/R two-component system is proposed to negatively affect the stability of the inner membrane complex. Figure modified from Ayers *et al*. (Ayers *et al.*, 2009).

We observed that in contrast to *P. aeruginosa* PilQ multimers in *M. xanthus* are stable in the absence of the PilM/N/O/P proteins. This suggests that the T4P-dependent motility defects of Δ*pilM*, Δ*pilN,* Δ*pilO* and Δ*pilP* mutants are caused either by the mislocalization of PilQ complexes (to be tested *in vivo*) or by the requirement of PilM/N/O/P proteins for aligning the inner membrane T4P components with PilQ outer membrane complexes for the successful T4P extrusion as proposed by Ayers *et al*. (Ayers *et al.*, 2009).

Interestingly, we found that PilT polar localization is partially impaired in Δ*pilQ* and Δ*pilC* mutants, suggesting that PilT may interact with the inner membrane protein PilC (or the inner membrane complex), which as discussed above needs PilQ secretin (or the outer membrane complex) for a proper localization. On the other hand, PilB localization is independent of PilC and PilQ. Thus, it is not clear whether PilT and PilB possess the same polar targeting determinants within T4P machinery. To further explore which T4P proteins are required for PilB and PilT localization to the poles, PilT and PilB localization will be examined in Δ*pilM*, Δ*pilN,* Δ*pilO*, Δ*pilP* and Δ*tgl* mutants.

Notably, both mutant PilB and PilT proteins that can bind but cannot hydrolyze ATP, no longer localize to the cell poles suggesting that polar targeting of PilB and PilT depends on a particular protein conformation or that polar localization is actively maintained and depends on ATP hydrolysis. Interestingly, in *P. aeruginosa* mutant PilT and PilU proteins that contain amino acid substitutions similar but not identical to those described here for PilB and PilT, still display normal polar localization (Chiang *et al.*, 2008), suggesting that the mechanisms by which motor ATPases are targeted to the poles are different in different species.

3.4 Regulation of type IV pili localization and oscillations by Ras-like GTPase MglA and its paralog SofG

In our study we show that similarly to eukaryotic systems, polarity of motility proteins in *M. xanthus* depends on the function of small Ras-like GTPase MglA and its paralog SofG. Leonardy *et al*. (Leonardy *et al.*, *in review*) analyzed three different versions of MglA protein ($MglA^{WT}$, $MglA^{G21V}$ and $MglA^{T26,27N}$) and showed that MglA is a nucleotide-dependent molecular switch, which at low concentration of MglA/GTP stimulates motility and at high concentration of MglA/GTP stimulates cellular reversals. Moreover, MglA establishes correct polarity of the A-motility RomR protein and regulates the pole-to-pole oscillations of RomR and AglZ proteins (Leonardy *et al.*, 2007; Leonardy *et al.*, *in review*).

3.4.1 MglA regulates correct PilT polarity and oscillations during reversal

To investigate whether MglA also regulates the correct polarity of S-motility proteins, we analyzed PilT localization in different *mglA* mutants. We found that MglA establishes the correct polarity of PilT, as PilT localization in non-moving *mglA*$^{-}$ and *mglA*^{T26,27N} cells is significantly shifted towards a unipolar localization pattern in comparison to stalled *mglA*$^{+}$ cells. Additionally, MglA regulates the dynamic PilT localization as PilT hyper-switches in *mglA*^{G21V} cells, which undergo reversals every 4.5 min. These data suggest that not only dynamically localized A-motility proteins but also dynamically localized S-motility proteins depend on MglA for dynamic localization. Such “one-for-all” mechanism would ensure that once established, the correct polarity of dynamically localized proteins is maintained over time guaranteeing that the two motility systems generate force in the same direction. The localization patterns of MglA and PilT suggest that MglA does not recruit PilT to the correct pole, as MglA/GTP localizes to the leading cell pole (Leonardy *et al.*, *in review*), whereas the large PilT cluster localizes to the lagging cell pole. Most likely MglA interacts with some effector proteins to direct PilT to the lagging cell pole. Currently the effector proteins of MglA are not known. However, Mauriello *et al*. recently observed that localization of FrzS and AglZ depends on the actin-like protein MreB, which forms a helix spanning the length of the cell (Mauriello *et al.*, 2010). Thus, it is possible that MglA regulates the polarity of MreB or some other cytoskeletal element in order to direct motility proteins to the correct poles.

3.4.2 SofG establishes correct polarity of two type IV pili motors and regulates their dynamic localization

MglA regulates the correct polarity and dynamic localization of PilT, but is not required for PilT polar localization *per se*. We speculated that the two MglA paralogs, encoded by genes *mxan_2694* and *mxan_6703* could be involved in regulation of proper localization of motility proteins. Deletion of *mxan_2694* did not affect vegetative growth, motility or development of *M. xanthus* (S. Brameyer, MPI, unpublished data), whereas deletion of *mxan_6703* (hereafter *sofG*) caused an S-motility defect. Δ*sofG* mutant also failed to aggregate and to form fruiting bodies similarly to *mglA* mutants (Dana and Shimkets, 1993). Strikingly, Δ*sofG* mutant assembled T4P at both poles, but synthesized WT levels of EPS suggesting that the S-motility defect and the inability to aggregate of Δ*sofG* mutant are caused by a direct impact on T4P assembly. The finding that Δ*sofG* mutant did not display any reversal frequency defects implies that SofG is not involved in the regulation of reversals unlike its paralog MglA. Moreover, Δ*sofG* cells were able to move as single, isolated cells, suggesting that SofG is

required for T4P-dependent (S-) motility only.

To test whether SofG is required for T4P function, we first examined the accumulation levels of the conserved T4P components. Δ*sofG* mutant synthesized WT levels of all proteins tested (PilQ, PilC, PilA, PilM, PilB and PilT). To elucidate whether localization of T4P proteins is perturbed in the absence of SofG, we analyzed the localization of PilC, PilB and PilT proteins in a Δ*sofG* mutant. Our findings demonstrate that SofG is not required for the proper PilC localization. We speculate that the localization of other inner and outer membrane T4P components is also not altered in Δ*sofG* cells, since SofG is predicted to be a cytoplasmic protein.

Strikingly, both PilB and PilT localization are affected in Δ*sofG* mutant. The localization pattern of PilB was shifted from predominantly unipolar in WT to bipolar in Δ*sofG* mutant. Interestingly, apart from the polar regions, PilB accumulations were observed in the vicinity of both poles (Figure 58A), sometimes even giving rise to the additional, pre-polar clusters.

Remarkably, PilT did not localize to the poles in Δ*sofG* cells. Instead, a single PilT cluster was found predominantly between 11 and 30% of the cell length (either in the vicinity of the leading or of the lagging pole) (Figure 58B). In the majority of the cells this cluster did not display any significant dynamics.

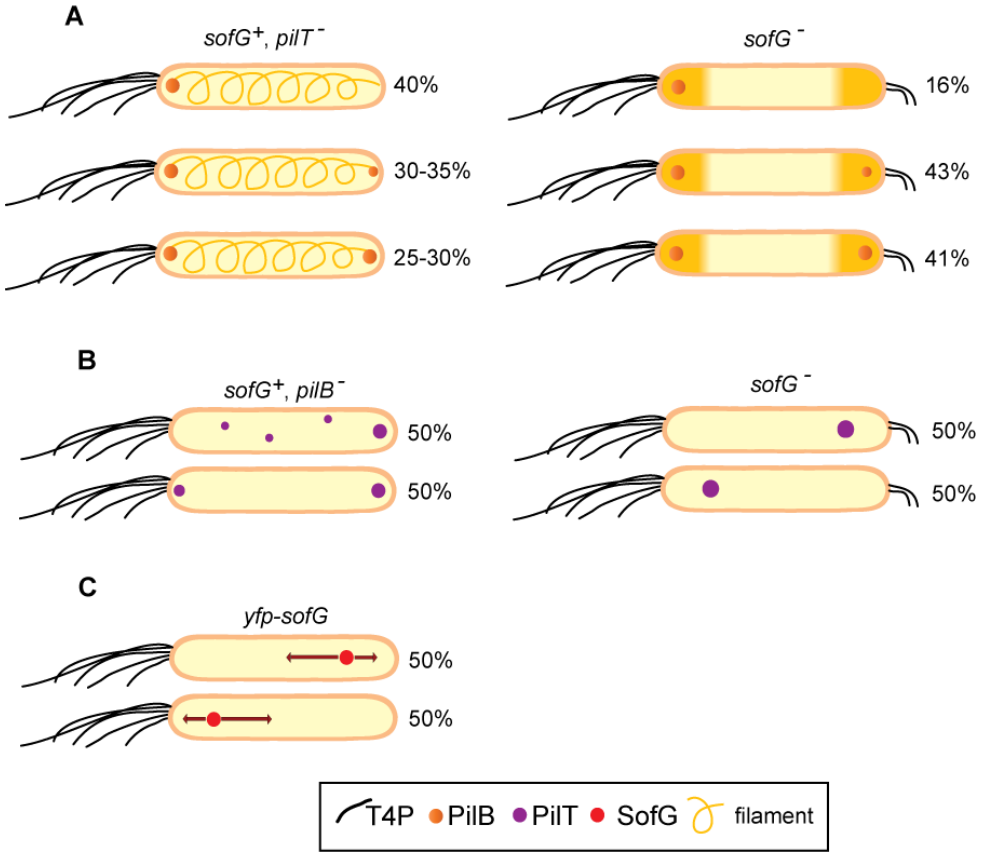

Figure 58. SofG is required for dynamic localization of PilB and polar localization of PilT

A) Model of PilB localization in WT, Δ*pilT* and Δ*sofG*. In WT and Δ*pilT* PilB localizes predominantly to the leading cell pole and is gradually transferred to the lagging cell pole. Filament represents a cytoskeletal element with which PilB molecules interact. In Δ*sofG* cells PilB does not interact with a cytoskeletal element, but concentrates at the poles. **B)** Model of PilT localization patterns in moving WT, Δ*pilB* and Δ*sofG* cells. In WT and Δ*pilB* PilT localizes predominantly to the lagging cell pole and stochastically accumulates at the leading cell pole. In Δ*sofG* cells PilT localizes in the vicinity of one pole and does not relocate between poles. **C)** SofG localization patterns in moving WT cells. SofG cluster localizes in the vicinity of one (leading or lagging) pole, travels between pole and mid-cell but does not relocate to the opposite pole. Arrows indicate directions of movement of SofG cluster.

Thus, SofG is involved in the establishment of the correct polarity and in the dynamic localization of both T4P ATPases. To determine whether SofG can directly bring PilB and PilT to the cell poles, localization of SofG was examined using a YFP-SofG fusion protein. Notably, a single SofG cluster localized between 11 and 30% of the cell length in the majority of cells (Figure 58C). Moreover, the SofG cluster moved between one of the poles and mid-cell, but these irregular oscillations did not correlate with cellular reversals (Figure 58C). Only in a few cells the SofG cluster from one cell half passed mid-cell and approached the opposite pole. Again, these SofG cluster movements did not correlate with reversals.

As both PilB and PilT are found at the poles in WT cells, we assume that they do not colocalize with SofG in the majority of cells. In some cells, however, we observed that the SofG cluster transiently localized to one of the poles. These observations suggest that PilB and PilT can transiently colocalize with SofG. Notably, PilT localization in the Δ*sofG* mutant almost mirrored SofG localization in WT cells (Figure 58B and C). Our findings imply that SofG targets PilT to the poles. Our current data allow us to speculate about the following functions for SofG.

- <u>SofG regulates PilB dynamic localization</u>

Given that PilB is found at both poles in Δ*sofG* mutant, most likely SofG is not a protein that targets PilB to the pole. Moreover, the pole-targeting determinant of PilB localization likely still localizes to the poles in the absence of SofG, because *sofG* cells assemble pili. The accumulation of PilB in the pre-polar regions in a Δ*sofG* mutant indicates that the dynamic localization of PilB is impaired. The mechanism underlying PilB transfer from pole to pole is not known. Recently MreB, a major bacterial cytoskeletal element, forming a helix spanning the cell body (Gitai *et al.*, 2005; Kruse *et al.*, 2003), has been shown to be required for both A- and S-motility in *M. xanthus* (Mauriello *et al.*, 2010). In addition, Mauriello *et al*. (Mauriello *et al.*, 2010) demonstrated that the correct polar localization and dynamic localization of two motility proteins, FrzS and AglZ, strongly depends on the presence of intact MreB. Furthermore, AglZ protein was shown to directly interact with MreB (Mauriello *et al.*,

2010). Based on these observations, we propose that PilB pole-to-pole oscillations could similarly depend on the presence of intact MreB (or another cytoskeletal element).

According to this model, one reason for PilB mislocalization in the Δ*sofG* mutant could be the absence of a cytoskeletal element required for PilB dynamic localization. MreB is an essential protein in *M. xanthus* (Mauriello *et al.*, 2010) and depletion of MreB from *E. coli*, *Bacillus subtilis*, *Caulobacter crescentus* and *M. xanthus* causes cells to round up and lyse (Figge *et al.*, 2004; Gitai *et al.*, 2004; Kruse *et al.*, 2003; Mauriello *et al.*, 2010; Varley and Stewart, 1992). A Δ*sofG* mutant, however, does not display any cell shape perturbations, suggesting that MreB is intact. Thus, our data on PilB localization in the absence of SofG rather imply that in these cells PilB is not able to interact with MreB - or another cytoskeletal element - required for its dynamic localization. In total, we speculate that SofG regulates PilB dynamic localization by mediating PilB interaction with a cytoskeletal element.

- SofG regulates polar and dynamic PilT localization

In contrast to PilB, PilT does not localize to the poles in a Δ*sofG* mutant. Thus, SofG may be a protein that brings PilT to the pole. Moreover, in the absence of SofG PilT localizes in a pattern strikingly similar to that of SofG suggesting that SofG acts to inhibit PilT localization in clusters away from the poles. The data on SofG localization in WT and PilT localization in Δ*sofG* mutant allow us to propose two scenarios.

In one scenario, SofG directly interacts with PilT, transports it to the poles and then leaves, whereas PilT interacts at the poles with the T4P machinery. We found that PilT clusters are rarely observed in Δ*pilC* and Δ*pilQ* mutants, which supports this model. It is not clear, however, how SofG can transport PilT to both poles as SofG localized only in one half of the cell and no correlations between SofG localization and cellular reversals were observed, while the large PilT cluster was shown to relocate between the poles during reversal.

A different possibility is that SofG is required only for the delivery of PilT to one of the poles, where it interacts not only with the T4P components, but also with a cytoskeletal element responsible for PilT pole-to-pole oscillations. In this case the function of SofG would be to regulate PilT transport indirectly via mediating its interaction with a cytoskeletal element.

Finally, we cannot exclude that YFP-SofG fusion protein localization does not reflect the localization of native SofG due to the overproduction of YFP-SofG. In fact, overproduction of certain proteins can drastically affect their localization as it has been recently demonstrated for Soj protein of *B. subtilis* (Murray and Errington, 2008). The

localization of the native SofG protein will help to address this question. Nevertheless, we conclude that PilT interaction with other T4P components is not sufficient for PilT polar localization and SofG is a key protein regulating this localization.

Interestingly, Kuhn *et al* (Kuhn *et al.*, 2010) described a new class of cytoskeletal elements named bactofilins that are widely conserved among bacteria. Bactofilins are able to polymerize *in vitro* spontaneously, forming rod-like structures. Kuhn *et al*. identified four genes encoding bactofilins in *M. xanthus*. Deletion of all four genes led to an S-motility defect (Kuhn *et al.*, 2010). Moreover, all four *M. xanthus* bactofilins formed filaments *in vitro* and three out of four formed filaments *in vivo* that were localized in the middle regions of the cells, i.e. did not reach the cell poles (Kuhn *et al.*, 2010). These localization patterns suggest the intriguing possibility that SofG may interact with bactofilins and move along the cell body on these filaments and/or that bactofilins are required for proper PilT land PilB ocalization.

- SofG inhibits T4P assembly at the lagging pole

The most unexpected finding of this study is that Δ*sofG* mutant assembles T4P at both poles. We know from our previous observations that PilB protein in 25-30% of the WT and Δ*pilT* cells localizes in a bipolar symmetric pattern. Furthermore, we showed that PilT^{E205A} mutant protein which is unable to hydrolyze ATP localizes diffusely. However, all these cells assemble T4P only at one (leading) cell pole (Jakovljevic *et al.*, 2008; Wu *et al.*, 1997), indicating that bipolar symmetric localization of PilB and mislocalization of PilT *per se* are not causing T4P assembly at both poles. Taken together, these data imply that T4P assembly is positively or negatively controlled by a third protein. We propose that SofG is this protein. If SofG positively regulated T4P assembly, we would expect Δ*sofG* mutant to be unable to produce T4P. Hence, most likely regulation of T4P assembly by SofG involves an inhibitory mechanism. Whether SofG directly interacts with T4P components in order to inhibit T4P assembly at the lagging pole is still an open question. A different intriguing possibility is that this inhibitory mechanism involves different nucleotide-bound states of SofG, as SofG shows significant similarities to MglA and eukaryotic Ras-like GTPases, which function as nucleotide-dependent molecular switches. Finally, it is tempting to speculate that a crosstalk as observed for many eukaryotic GTPases (Iden and Collard, 2008) can also occur in *M. xanthus* between SofG and MglA, which both regulate correct polarity and dynamic localization of T4P proteins in *M. xanthus*.

3.5 Conclusions

To summarize, we have demonstrated that T4P proteins in *M. xanthus* can be divided in two groups: stationary localized components (PilQ, PilC, PilM and PilN),

which do not relocate between the poles during cellular reversals, and dynamic components (FrzS, PilB and PilT), which oscillate from pole to pole during cellular reversals. Thus, previously reported T4P pole-to-pole oscillations in *M. xanthus* (Sun et al., 2000) depend on the dynamic localization of the two motor proteins PilB and PilT. PilB and PilT localize to the opposite cell poles and relocate between poles during reversal. Furthermore, we propose that the spatial separation of PilB and PilT localization to the opposite poles provides an elegant strategy for the temporal regulation of T4P extension/retraction. Importantly, the Frz chemosensory system and Ras-like GTPase MglA and its paralog SofG regulate PilB and PilT localization. Additionally, MglA and SofG regulate the correct polarity of PilT.

Remarkably, unipolar T4P assembly at the leading cell pole appears to be negatively regulated in *M. xanthus* by SofG. Such a mechanism ensuring the T4P assembly at the leading cell pole only is of a great importance for directed cell movement, essential for the social life style of *M. xanthus*.

4 Materials and Methods

4.1 Chemicals and equipment

Reagents, enzymes and antibiotics used in this study as well as their suppliers are listed in Table 2. Technical equipment and its manufacturers are listed in Table 3. Specific software applied for data analysis is listed in Table 4.

Table 2. Reagents, enzymes, antibiotics and kits

Reagent	Supplier
Media components, agar	Roth (Karlsruhe), Merck (Darmstadt), Difco (Heidelberg), Invitrogen (Darmstadt)
Pure chemicals	Roth (Karlsruhe), Merck (Darmstadt), Sigma-Aldrich (Taufkirchen)
SDS-PAGE size standards	MBI Fermentas (St. Leon-Rot)
Agarose gel electrophoresis size standards	Bioline (Luckenwalde)
Oligonucleotides	Eurofins MWG Operon (Ebersberg), Thermo Scientific (Dreieich)
Rabbit antisera	Eurogentec (Seraing, Belgium)
Anti-GFP monoclonal antibody	Roche (Mannheim)
Rabbit anti-mouse IgG	DakoCytomation (Glostrup, Denmark)
Goat anti-rabbit IgG, goat anti-rabbit IgG DyLight 549	Pierce/Thermo Scientific (Dreieich)
SuperSignal chemiluminescence detection	Pierce/Thermo Scientific (Dreieich)
Uranyl acetate	PLANO (Wetzlar)
Enzymes	
Eppendorf® MasterMix	Eppendorf (Hamburg)
*PfuUltra*TMII-polymerase	Stratagene (Amsterdam)
Other nucleic acid modifying enzymes (restriction endonucleases, T4 DNA ligase, Antarctic phosphatase)	New England Biolabs (Frankfurt a. M.) MBI Fermentas (St. Leon-Rot)
Antibiotics	
Kanamycin sulfate, chloramphenicol, ampicillin sodiumsulfate, gentamycin, oxytetracycline dehydrate, tetracycline	Roth (Karlsruhe)
Kits	
DNA&RNA purification, gel extraction, plasmid preparation	Qiagen (Hilden), Hiss Diagnostics (Freiburg)
MasterPure DNA purification kit	Epicentre Biotechnologies (Madison, USA)
SlowFade antifade kit	Molecular Probes/Invitrogen (Darmstadt)
cDNA Archive kit	Applied Biosystems (Darmstadt)

Table 3. Equipment used in this study

Application	Device	Manufacturer
Cell disruption	Branson sonifier	Heinemann (Schwäbisch Gmünd)
Centrifugation	RC 5B plus, Ultra Pro 80, Multifuge 1 S-R, Biofuge frasco, Biofuge pico	Sorvall/Thermo Scientific (Dreieich), Heraeus/Thermo Scientific (Dreieich),
PCR	MasteCycler personal MasteCycler epgradient	Eppendorf (Hamburg)
Electroporation	GenePulser Xcell	Bio-Rad (Munchen)
Protein electrophoresis	Mini-PROTEAN® 3 cell	Bio-Rad (Munchen)
Western blotting	TE77 semi-dry transfer unit	Amersham Biosciences (Munchen)
Chemiluminescence detection	Fuji Photo Film FPM 100A Luminescent image analyzer LAS-4000	Fujifilm (Düsseldorf)
Immunofluorescence microscopy	Diagnostic microscope slides 12 well	Thermo Scientific (Dreieich)
Electron microscopy	Carbon-film covered grids	PLANO (Wetzlar)
Imaging	Leica DM6000B and DM IRE2 light microscopes MZ75 stereomicroscope Nikon Eclipse TE 2000-E light microscope Philips EM 301 electron microscope	Leica Microsystems (Wetzlar) Nikon (Düsseldorf) Eindhoven (Netherlands)
Determination of optical densities	Ultrospec 2100 pro spectrophotometer	Amersham Biosciences (Munchen)
Determination of nucleic acids absorption	Nanodrop ND-1000 UV-Vis spectrophotometer	Nanodrop (Wilmington)
DNA illumination and documentation	UVT 20 LE UV table	Herolac (Wiesloch)

Table 4. Software for data analysis

Application	Program	Vendor
Fluorescence microscopy data analysis	Metamorph® v 7.5 Image-Pro® 6.2	Molecular Devices (Union city, CA) MediaCybernetics (Bethesda, MD)
Checking sequences, sequence alignments	Vector NTI advance software, suite 11	Invitrogen (Darmstadt)
Stereomicroscopy	IM50	Leica Microsystems (Wetzlar)

4.2 Media

Culture media for *E. coli* were prepared as desribed in Sambrook & Rassel, 2000 (Table 5). *M. xanthus* strains were grown in 1% CTT media (Table 5). Antibiotics were added when needed (Table 6).

Table 5. Growth media for *E. coli* and *M. xanthus*

Medium	Composition
E. coli	
Luria-Bertani (LB)	1% (w/v) tryptone, 0.5% (w/v) yeast extract, 1% (w/v) NaCl
LB agar plates	LB medium, 1% (w/v) agar
2YT	16 g bacto tryptone, 5 g yeast extract, 5 g NaCl, pH 7.2
M. xanthus	
1% CTT	1% (w/v) BactoTM casitone, 10 mM Tris-HCl pH 8.0, 1 mM potassium phosphate buffer pH 7.6, 8 mM $MgSO_4$
1% CTT-YE	1% (w/v) BactoTM casitone, 10 mM Tris-HCl pH 8.0, 1 mM KH_2PO_4 pH 7.6, 8 mM $MgSO_4$, 0.2% yeast extract pH 7.6
1% CTT agar plates	1% CTT medium, 1.5% agar
CTT soft agar	1% CTT medium, 0.75% agar

Table 6. Additives for *E. coli* and *M. xanthus* liquid cultures and plates

Additive	Final concentration	Dissolved in
E. coli		
Ampicillin sodium sulfate	100 µg/mL	H_2O
Chloramphenicol	50 µg/mL	99.99% ethanol
Kanamycin sulfate	100 µg/mL	H_2O
Tetracyclin	15 µg/mL	99.99% ethanol
M. xanthus		
Kanamycin sulfate	50 µg/mL	H_2O
Oxytetracycline	10 µg/mL	99.99% methanol

For *M. xanthus* motility and development assays and time-lapse microscopy media were prepared as described in Table 7.

Table 7. Media for *M. xanthus* assays

Medium	Composition
A-motility plates (Hodgkin and Kaiser, 1977)	0.5% CTT, 1.5% agar
S-motility plates (Hodgkin and Kaiser, 1977)	0.5% CTT, 0.5% agar
TPM development agar (Kuner and Kaiser, 1982)	10 mM Tris-HCl pH 7.6, 1 mM KH_2PO_4 pH 7.6, 8 mM $MgSO_4$, 1.5% (w/v) agar
A50 microscopy agar	10 mM MOPS pH 7.2, 10 mM $CaCl_2$, 10 mM $MgCl_2$, 50 mM NaCl, 1.5% or 0.7% (w/v) agar

4.3 Microbiological methods

4.3.1 *E. coli* strains

Table 8. *E. coli* strains used in this study

Strain	Relevant characteristics	Source or reference
Top10	F- *mcrA* Δ (*mrr-hsdRMS-mcrBC*), 80*lacZ*ΔM15Δ*lacX74 recA1 deoR araD139* Δ(*ara-leu*)7697 *galU galK rpsL strR endA1 nupG*	Invitrogen (Darmstadt)
Rosetta 2 (DE3)	F^- *ompT hsdS*$_B$(r_B-m_B) *gal dcm*(DE3) pRARE2(Cm^R)	Novagen/Merck (Darmstadt)

4.3.2 *M. xanthus* strains

Table 9. *M. xanthus* strains used in this study

Strain	Relevant characteristics[1]	Source or reference
DK1622	WT	(Kaiser, 1979)
DK8505	*frzCD*::Tn*5lac* Ω536, Km^R	(Sager and Kaiser, 1994)
DK8506	*frzCD*::Tn*5lac* Ω224, Km^R	(Sager and Kaiser, 1994)
DK8615	Δ*pilQ*	(Wall *et al.*, 1999)
DK10405	Δ*tgl*	(Rodriguez-Soto and Kaiser, 1997)
DK10409	Δ*pilT*	(Jakovljevic *et al.*, 2008; Wu *et al.*, 1997)
DK10410	Δ*pilA*	(Wu and Kaiser, 1996)
DK10416	Δ*pilB*	(Jakovljevic *et al.*, 2008; Wu *et al.*, 1997)
DK10417	Δ*pilC*	(Wu *et al.*, 1997)
DK3685	*mglA*::Tn5-132 Ω1901 (*mglA9*), Tet^R	(Kroos *et al.*, 1988)
DK5208	*csgA*::Tn5-*132* ΩLS205	(Kroos and Kaiser, 1987)
SA1128	*romR*::nptII, Km^R	(Leonardy *et al.*, 2007)
SA1804	Δ*digR*	(Overgaard *et al.*, 2006)
DK3470	Δ*dsp*	(Overgaard *et al.*, 2006)
SA2415	Δ*pilB*/P_{pilA}-*pilB*^{E391A} (pSL105BWalkerB), Km^R	(Jakovljevic *et al.*, 2008)
SA3001	Δ*pilO*	This study
SA3002	Δ*pilM*	This study
SA3005	Δ*pilP*	This study
SA3025	WT/P_{pilA}-*yfp- linker1-pilT*^{E205A} (pIB74)[2], Km^R	This study
SA3026	Δ*pilT*/P_{pilA}-*yfp- linker1-pilT*^{E205A} (pIB74), Km^R	This study
SA3027	*frzCD*::Tn*5lac* Ω536 Δ*pilT*, Km^R	This study
SA3028	*frzCD*::Tn*5lac* Ω224 Δ*pilT*, Km^R	This study
SA3029	*frzCD*::Tn*5lac* Ω536 Δ*pilT*/P_{pilA}-*yfp- linker1-pilT* (pIB75), Km^R Tet^R	This study

SA3030	*frzCD*::Tn*5lac* Ω224 Δ*pilT*/P_{pilA}-*yfp- linker1-pilT* (pIB75), Km^R Tet^R	This study
SA3043	Δ*pilB* Δ*pilT*/ P_{pilA}-*yfp- linker1-pilT* (pIB75), Tet^R	This study
SA3044	Δ*pilN*	This study
SA3045	Δ*pilT*/P_{pilA}-*yfp- linker1-pilT* (pIB75), Tet^R	This study
SA3046	Δ*pilM*/P_{pilA}-*yfp- linker1-pilM* (pCS8), Tet^R	This study
SA3047	Δ*pilQ*/P_{pilA}-*yfp- linker1-pilT* (pIB75), Tet^R	This study
SA3049	WT/P_{pilA}-*pilT* (pSL104), Km^R	This study
SA3050	Δ*tgl*/P_{pilA}-*yfp- linker1-pilT* (pIB75), Tet^R	This study
SA3054	Δ*pilB* Δ*pilT*	V. Jakovljevic
SA3056	*frzCD*::Tn*5lac* Ω224 Δ*pilM*, Km^R	This study
SA3057	*frzCD*::Tn*5lac* Ω536 Δ*pilM*, Km^R	This study
SA3058	*frzCD*::Tn*5lac* Ω224 Δ*pilM*/P_{pilA}-*yfp- linker1-pilM* (pCS8), Km^R Tet^R	This study
SA3059	*frzCD*::Tn*5lac* Ω536 Δ*pilM*/P_{pilA}-*yfp- linker1-pilM* (pCS8), Km^R Tet^R	This study
SA3061	Δ*pilA*/P_{pilA}-*yfp- linker1-pilT* (pIB75) , Tet^R	This study
SA3063	Δ*pilC*/P_{pilA}-*yfp- linker1-pilT* (pIB75), Tet^R	This study
SA3064	WT/P_{pilA}-*yfp- linker1-pilT* (pIB75), Tet^R	This study
SA3067	Δ*pilT,mglA*-G21V/ P_{pilA}-*yfp-pilT* (pIB75), Tet^R	This study
SA3068	Δ*pilT*, *mglA*-T26/27N/ P_{pilA}-*yfp- linker1-pilT* (pIB75), Tet^R	This study
SA3801	Δ*sofG*	This study
SA3810	Δ*sofG*/P_{pilA}-*sofG* (pSB6), Km^R	S. Brameyer
SA3812	Δ*sofG*/P_{sofG}-*yfp-linker1-sofG* (pSB9), Tet^R	S. Brameyer
SA3813	Δ*sofG*/P_{sofG}-*sofG* (pSB10), Tet^R	S. Brameyer
SA3811	Δ*sofG*/P_{pilA}-*yfp-linker1-sofG* (pSB7), Km^R	S. Brameyer
SA3819	Δ*sofG*, Δ*pilT*	This study
SA3069	Δ*sofG*, Δ*pilT*/ P_{pilA}-*yfp-linker1-pilT* (pIB75), Tet^R	This study
SA3074	Δ*sofG*/P_{pilA}-*yfp-sofG* (pIB97), Km^R	This study
SA3076	Δ*sofG*/P_{pilA}-*yfp-linker2 -sofG* (pIB99)[3], Km^R	This study
SA3083	*yfp-sofG* at endogenous locus	This study

[1] Km^R and Tet^R indicate kanamycin and tetracycline resistance, respectively

[2] linker1: 5'-ggatcggccggctccgccgccggctccggctctgga-3'

[3] linker2: 5'-ggtaccacaagatctcgagctccggagaatacgaacgttacgcgtcaccggtcggccacc-3'

4.3.3 Cultivation of bacteria

All media and solutions were autoclaved for 20 min at 121˚C and 1 bar over pressure. Antibiotic solutions were filtered using 0.22 µm pore size filters (Millipore, Schwalbach) and added to the pre-cooled to 55˚C media.

E. coli cells were grown aerobically on LB agar plates at 37˚C. *E. coli* liquid cultures were incubated on horizontal shakers at 37˚C and 230 rpm. The optical density was determined at 600 nm (OD_{600}).

M. xanthus cells were cultivated aerobically on 1% CTT agar plates at 32˚C in the dark. For *M. xanthus* liquid cultures single *M. xanthus* colonies were first resuspended in 1 ml of 1% liquid CTT medium. Liquid cultures were incubated on horizontal shakers at 32˚C and 230 rpm in the dark. The optical density was determined at 550 nm (OD_{550}).

4.3.4 Storage of transformed *E. coli* and *M. xanthus* strains

E. coli and *M. xanthus* cultures on plates were stored for up to four weeks at 4˚C and 18˚C, respectively. For long term storage, *M. xanthus* cultures were grown until OD_{550}=0.8-1.2, 1 ml of the culture was mixed with glycerol (4% final concentration), fast frozen in the liquid nitrogen and stored at -80˚C. *E. coli* glycerol stocks were prepared from overnight cultures by adding glycerol to 10%, fast frozen in the liquid nitrogen and stored at -80˚C.

4.3.5 Motility assays of *M. xanthus*

To investigate motility phenotypes, *M. xanthus* cells from exponentially growing cultures were harvested at OD_{550}=0.7-0.9 (corresponding to 7×10^8 cells/ml) by centrifugation at 4,700 rpm for 10 min and resuspended in 1% CTT liquid medium without antibiotica to a calculated cell density of 7×10^9 cells/ml. 5 µl aliquots of cell suspension were spotted on 0.5% and 1.5% agar motility plates. 0.5% agar plates favour S-motility and 1.5% agar plates favour A-motility (Hodgkin and Kaiser, 1977). After 24 h incubation at 32˚C in the dark, colony morphology and colony edges were examined with Leica MZ75 stereomicroscope at 8× and 50× magnifications, and Leica IRE2 inverted microscope at 400× magnification. Images were recorded with Leica DFC280 camera and processed with IM50 software from Leica Microsystems (Wetzlar).

4.3.6 Congo red dye-binding assays

To determine the ability of *M. xanthus* cells to bind Congo red dye (which binds to the EPS portion of the extracellular matrix), dye binding plate assays were carried out. For this, cells were grown and samples prepared as for motility assays, and 5 µl

aliquots were spotted on 1.5% agar motility plates, supplemented with 20 μg/ml Congo red. After 24 h incubation at 32˚C in the dark, changes in colony color were examined with Leica MZ75 stereomicroscope and visualized with Leica DFC280 camera.

In order to quantify the amount of Congo red bound to *M. xanthus* cells, a dye binding liquid assay was performed (adapted from Black and Yang, 2004). For this, a total of 7×10^8 cells from mid-exponential *M. xanthus* cultures were harvested, washed once and resuspended in 900 μl MOPS buffer. The cell suspensions were mixed with 100 μl of Congo red stock solution (150 μg/ml) to final cell density of 7×10^8 cells/ml and 15 μg of Congo red/ml. Control sample containing Congo red in MOPS buffer only was included, triplicate assays were performed for all samples. All samples were mixed briefly and incubated undisturbed in the dark at room temperature for 30 min. Then cell suspensions were pelleted at 13,000 rpm for 5 min, and the absorbancies of supernatants were measured at 490 nm. Percentage of Congo red bound by each sample was calculated from the quotient obtained by dividing the absorbance of each sample by the absorbance of the control.

4.3.7 Development assay of *M. xanthus*

To analyze developmental phenotypes, *M. xanthus* cells were grown to OD_{550}=0.5-0.9, harvested and resuspended in TPM buffer (10 mM Tris-HCl, pH 7.6, 1 mM KH_2PO_4, pH 7.6, 8 mM $MgSO_4$) to a calculated density of 7×10^9 cells/ml. 20 μl aliquots were spotted on TPM agar plates (TPM buffer, supplemented with 1.5% (w/v) agar) and incubated at 32˚C in the dark for 72 h. Aggregation and fruiting body formation were evaluated at 24, 48, 72 and 120 h with a Leica MZ75 stereomicroscope and visualized with Leica DFC280 camera.

4.4 Molecular biological methods

4.4.1 Oligonucleotides and plasmids

All oligonucleotides and plasmids used in this study are listed in Table 10-13. Underlined sequences indicate sequences in the respective genes. Additional sequences required for cloning are not underlined. Red sequences indicate restriction sites used for cloning, blue sequences indicate complementary sequences that were used to fuse PCR products. Green sequences indicate the addition of a linker.

Table 10. Oligos used for in-frame deletion constructs

Name	Description	Sequence (5'→ 3')
pilM deletion		
oPilM-A	Primer A forward	ATCGGAAGCTTGGGCTCACCGCAGAGGCC

oPilM-B	Primer B reverse	GCCCGGGCGGTGCCTGGAGCCCGCCTG
oPilM-C	Primer C forward	TCCAGGCACCGCCCGGGCGACAAGCTG
oPilM-D	Primer D reverse	ATCGGGAATTCTGCTGTCTTGCTGTCCCG
oUpstM-1	Primer E forward	TCAACCGCGAGCTGAACCGAG
oDownM-1	Primer F reverse	ATCTTGAACTCGACCAGGATC
pilN deletion		
oPilN-A	Primer A forward	ATCGGAAGCTTTCATCTCCAACGGCGCGA
oPilN-B-Xba	Primer B reverse	ATCGGTCTAGAACGCTTCTTCACCGCCCG
oPilN-C-Xba	Primer C forward	ATCGGTCTAGACAACTACGCCATCTGACA
oPilN-D	Primer D reverse	ATCGGGAATTCGTTCTTGAGTTTGGCCGA
oUpstPilN	Primer E forward	CTCGGTGGTGAACATCAA
oDownPilN	Primer F reverse	CTCGCTCTGCAAGACGAC
pilO deletion		
oPilO-A	Primer A forward	ATCGGAAGCTTGTCGCTTCAACCAAGGCG
oPilO-B	Primer B reverse	GGCCTTCTGGAATTGATCCAGGTACTT
oPilO-C	Primer C forward	GATCAATTCCAGAAGGCCGCTGCGTCG
oPilO-D	Primer D reverse	ATCGGGAATTCGAACACCTCTGTCACCGT
pilP deletion		
oPilP-A	Primer A forward	ATCGGAAGCTTGAAATCGGTTGGGCGGTG
oPilP-B	Primer B reverse	GTTGTAGGCCGGCTCCTCGCACGCAGC
oPilP-C	Primer C forward	GCTGCGTGCCAGGACCCCGCCTACAAC
oPilP-D	Primer D reverse	ATCGGGAATTCCGACGCGGTCATGCGTTC
oDownPilP	Primer F reverse	CCATCCGCACGAATGCTG
sofG deletion		
oSB_10	Primer A forward	TAGCCAAGCTTAGGATGTTGCCCAGGCCCTTGC
oSB_11-1	Primer B reverse	AATCTGCCCCGGCAGGGTGCCAGGCGTGG
oSB_12-1	Primer C forward	ACCCTGCCGGGGCAGATTTTCCGGCGCATGG
oSB_13	Primer D reverse	TAGCCTCTAGAAAGTCCGCCAGCTCCTCCGGC
oSB_14-1	Primer E forward	GCTCACCGCGGGCGAGTTGG
oSB_15	Primer F reverse	CATGCGCGCGCGACAGGTCC
oSB_10	Primer G forward	GGGCGCGCATGTCGAGCCG
oSB_10	Primer H reverse	ATGCCCAGCGAGAGCTGACGC

Table 11. Primers used for generation of YFP-PilT and YFP-SofG fusions

Name	Description	Sequence (5'→ 3')
YFP primers		
oYFP-1	forward	ATCACTAGTATGGTGAGCAAGGGCGAG

oYFP-2	reverse	ATCGAATTCCTTGTACAGCTCGTCCAT
oYFP-5	reverse	ATCAAGCTT**CTA**CTTGTACAGCTCGTCCAT
oYFP-6	forward	ATCGAATTCATGGTGAGCAAGGGCGAG
oYFP-7	reverse	ATCGATATCCTTGTACAGCTCGTCCAT
oYFP-8	reverse	ATCGATATCGGTACCACAAGATCTCGAGCTCCGGA GAATACGAACGTTACGCGTCACCGGTCGGCCACC CTTGTACAGCTCGTCCAT
oYFP-10	forward	ATCGGATCCATGGTGAGCAAGGGCGAG
pilT primers		
oPilT-4	reverse	ATCGGAAGCTTCTAACGACCACCCGCTCC
oPilT-7	forward	ATCGAATTCGGATCGGCCGGCTCCGCCGCCGGCT CCGGCTCTGGA
sofG primers		
o6703-4	forward	ATCGATATCGTGAGGAGCCGGATTTCGTCG
oSofG-7	reverse	ATCGGATCCCAGCGGAGAGGAGGGCCT
oSB_21	reverse	TAGCCAAGCTTTCATCGCCCTTCTCCGCTGCG
oSB_26	forward	TAGCCGAATTCTCCCGGGCCGCCTTCAGCGC

Table 12. Primers used for generation of PilQ overexpression construct

Name	Description	Sequence (5'→ 3')
oPilQ-7	forward	ATCGGCTGCAGATGCCGACCTTTACCGTG
oPilQ-8	reverse	ATCGGAAGCTTTTACAGAGTCTGCGCAAT

Table 13. Primers used to map *pilM/N/O/P/Q* locus

Name	Description	Sequence (5'→ 3')
pilM primers		
oPilM-6	Internal region of *pilM*, forward	CAGGACCTGATGTCCGAGCTGAA
oPilM-7	Internal region of *pilM*, reverse	GGAGACCACCGTGGTGTAGTCGT
oPilM-8	Intergenic region *pilM-pilN*, forward	CCGACTCGAACTTCAGCAAGGTC
pilN primers		
oPilN-5	Intergenic region *pilM-pilN*, reverse	GCAATCCTCGCCTTGGTTGAAGC
oPilN-6	Internal region of *pilN*, forward	AACACCCGGAAGGCCGAAGTGGA
oPilN-7	Internal region of *pilN*, reverse	TTGGGTGTCCACACCACACCGTT
oPilN-8	Intergenic region *pilN-pilO*, forward	GGGACAGCAAGACAGCACGAGTC
pilO primers		
oPilO-5	Intergenic region *pilN-pilO*, reverse	ACTCTTGTCCGCCAGTTCCAGGT
oPilO-6	Internal region of *pilO*, forward	AATGAGCGTCGGCGCGAGATGGA
oPilO-7	Internal region of *pilO*, reverse	GAGCGCAATCTCGTGGTAGTTGC

oPilO-8	Intergenic region *pilO-pilP*, forward	AGATGGCCAACATGCGCCGCATC
pilP primers		
oPilP-5	Intergenic region *pilO-pilP*, reverse	TCGATCGGACTCCGGAAAGGGTC
oPilP-6	Internal region of *pilP*, forward	CCTCTGCTCGTTCGACTTGGATC
oPilP-7	Internal region of *pilP*, reverse	CCGGATTCTTGATGATCTCTCCG
oPilP-8	Intergenic region *pilP-pilQ*, forward	GTGACAGAGGTGTTCTCCGGCAA
pilQ primers		
oPilQ-12	Intergenic region *pilP-pilQ*, reverse	AGAGCCCTCGTGGTGTCCCTTGA
oPilN-13	Internal region of *pilQ*, forward	ACGTGGTGGCTGCCGAGGCTGAT
oPilN-14	Internal region of *pilQ*, reverse	CCAGCACCAGGCGAACCTTGTCT

Table 14. Primers used to verify integration at Mx8 phage attachment site

Name	Description	Sequence (5'→ 3')
attB right	Genome specific *attB* forward primer	GGAATGATCGGACCAGCTGAA
attB left	Genome specific *attB* reverse primer	CGGCACACTGAGGCCACATA
attP right	Plasmid specific *attP* forward primer	GCTTTCGCGACATGGAGGA
attP left	Plasmid specific *attP* reverse primer	GGGAAGCTCTGGGTACGAA

Table 15. Primers used for sequencing

Name	Description	Sequence (5'→ 3')
M13 fwd	General sequencing primer, forward	GTCGTGACTGGGAAAACCCTGGCG
M13 rev	General sequencing primer, reverse	CTGGGGTGCCTAATGAGTGAGCTA
pCC1fwd	Sequencing pSWU30, forward	ATGTGCTGCAAGGCGATTAAGTT
GFy045	Sequencing pSWU30, reverse	TTTACACTTTATGCTTCCGGCT
pSW105fwd	Sequencing pSW105, forward	GGCTTGGAGTGCGCACCT
pSW105rev	Sequencing pSW105, reverse	ACGACGTTGTAAAACGAC
T7-Pm	Sequencing pET45b+, forward	TAATACGACTCACTATAGGG
T7-rev	Sequencing pET45b+, reverse	GCTAGTTATTGCTCAGCGG
oYFP-3	Internal sequencing primer, forward	CGCCGAGGTGAAGTTCGAGGGC
oYFP-4	Internal sequencing primer, reverse	CTCGATGCGGTTCACCAGGGTGTC
oSofG-IntForw	Internal sequencing primer, forward	CCAGGTCATCCACAACGC
oSofG-IntRev	Internal sequencing primer, reverse	TTCACCTTCACCTTGAAG

Table 16. List of plasmids used in this study

Plasmid	Relevant characteristics[1]	Source or reference
pBluescript II SK-	Vector for cloning, blue/white selection, Ap^R	Fermentas (St. Leon-Rot)
pBJ114	Vector for in-frame deletion constructs, Km^R	(Julien *et al.*, 2000)
pBJ113	Vector for in-frame deletion constructs, Km^R	(Julien *et al.*, 2000)
pSWU30	Vector for integration at *attB* site, Tet^R	(Wu *et al.*, 1997)
pSW105	Vector for integration at *attB* site, containing *pilA* promoter, Km^R	S. Weiss (MPI, Marburg)
pET45b+	Expression vector, T7 promoter, N-term. His_6-tag, Ap^R	Novagen/Merck (Darmstadt)
pSW105-YFP	pSW105-*yfp*	V. Jakovljevic (MPI, Marburg)
pCS8	pSW105-yfp-linker1-pilM [2], Km^R	(Bulyha *et al.*, 2009)
pSL104	pSW105-*pilT*, Km^R	S. Leonardy (MPI, Marburg)
pSL107	pSW105-gfp-linker1-pilT, Km^R	S. Leonardy (MPI, Marburg)
pSB6	pSW105-*sofG*, Km^R	S. Brameyer (MPI, Marburg)
pSB7	pSW105-*yfp-linker1-sofG*, Km^R	S. Brameyer (MPI, Marburg)
pSB9	pSWU30-P_{sofG}-*yfp-linker1-sofG*, Tet^R	S. Brameyer (MPI, Marburg)
pSB10	pSWU30-*sofG*, Tet^R	S. Brameyer (MPI, Marburg)
pSB13	pBJ114- *sofG* in-frame deletion, Km^R	S. Brameyer (MPI, Marburg)
pSL104TWalkerB	pSW105- $pilT^{E205A}$	(Jakovljevic *et al.*, 2008)
pIB18	pBJ114- *pilO* in-frame deletion, Km^R	This study
pIB20	pBJ113- *pilM* in-frame deletion, Km^R	This study
pIB21	pBJ113- *pilP* in-frame deletion, Km^R	This study
pIB49	$pET45b^+$-*pilQ*, Ap^R	This study
pIB59	pBJ113- *pilN* in-frame deletion, Km^R	This study
pIB71	pSK^--*linker1-pilT*, Ap^R	This study
pIB72	pSK^--yfp-linker1-pilT, Ap^R	This study
pIB73	pSW105-*yfp-linker1-pilT*, Km^R	This study
pIB74	pSW105-*yfp-linker1-*$pilT^{E205A}$, Km^R	This study
pIB75	pSWU30- *yfp-linker1-pilT*, Tet^R	This study
pIB92	pSK^--*sofG*, Ap^R	This study
pIB94	pSK^--yfp-*linker2*-sofG, Ap^R	This study
pIB96	pSK^--*yfp-sofG*, Ap^R	This study
pIB97	pSW105-*yfp-sofG*, Km^R	This study
pIB99	pSW105-*yfp-linker2-sofG* [3], Km^R	This study
pIB101	pSW105-P_{sofG}-*yfp-sofG*, Km^R	This study

pIB113	pBJ113-P_{sofG}-*yfp-sofG*, Km^R	This study

[1] Ap^R, Km^R and Tet^R indicate ampicillin, kanamycin and tetracycline resistance, respectively.

[2] linker1: 5'-ggatcggccggctccgccgccggctccggctctgga-3'

[3] linker2: 5'-ggtaccacaagatctcgagctccggagaatacgaacgttacgcgtcaccggtcggccacc-3'

4.4.2 Construction of plasmids

Purified *M. xanthus* genomic DNA was used as a template to amplify chromosomal regions for cloning. Plasmid DNA was used as a template to amplify YFP fusions. Unless otherwise stated, *E. coli* Top10 cells were used for cloning. Isolated plasmids were sequenced to confirm the inserts were error-free, and subsequently correct plasmids were introduced into *M. xanthus* cells.

Plasmids pIB18, pIB20, pIB21, and pIB59 (in-frame deletion constructs): Those plasmids are derivatives of pBJ113 and pBJ114 and were used for the generation of the markerless in-frame deletions of *pilO, pilM, pilP,* and *pilN* genes, respectively, as described in Chapter 4.4.3.

pIB49 (PilQ overexpression): To construct pIB49, which encodes His_6-tagged full-length PilQ protein *pilQ* fragment was generated from WT genomic DNA with the primers oPilQ-7 and oPilQ-8, digested with *PstI* and *HindIII* and cloned into pET45b+. Verified by sequencing correct plasmid was then introduced into *E. coli* Rosetta 2 cells for overexpression.

Plasmids pIB71, pIB72, pIB73 and pIB75 (fluorescence labeling of PilT): To construct pIB71, the *pilT* gene was amplified with primers oPilT-4 and oPilT-7 using pSL107 plasmid (S. Leonardy, MPI Marburg) as a template, giving rise to the full-length *pilT* with an additional 10 aa linker (linker1 in the Table 16) at the 5'-end. The corresponding PCR product was digested with *EcoRI* and *HindIII*, and cloned into pBluescript II SK-, giving rise to pIB71. The *yfp* gene was amplified by PCR using primers oYFP-1 and oYFP-2 and pSW105-YFP (V. Jakovljevic, MPI Marburg) as a template. The yielding PCR product was digested with *SpeI* and *EcoRI* and cloned in-frame upstream of *pilT* gene in pIB71 generating pIB72. The *SpeI-HindIII* fragment from pIB72 was then re-cloned into pSW105, which contains the *pilA* gene promoter giving rise to pIB73. Finally, the *NdeI-HindIII* fragment of pIB73, containing P_{pilA}-*yfp-pilT*, was cloned into pSWU30, generating pIB75.

pIB74 (fluorescence labeling of $PilT^{E205A}$): To construct pIB74, *pilT* ^{E205A} copy from pSL104TWalkerB plasmid (V. Jakovljevic, MPI Marburg) was re-cloned using *XbaI-HindIII* restriction sites into pIB73 plasmid instead of WT *pilT* copy.

Plasmids pIB92, pIB94, pIB96, pIB97, pIB99, pIB101 and pIB113 (fluorescence labeling of SofG): To construct pIB92, the *sofG* gene was amplified with primers o6703-4 and oSB_21 WT genomic DNA as a template. The corresponding PCR product, containing the full-length *sofG* gene, was digested with *EcoRV* and *HindIII*, and cloned into pBluescript II SK-, giving rise to pIB92. The *yfp* gene was amplified by PCR using primer pairs oYFP-6-oYFP-7 and oYFP-6-oYFP-8 and pSW105-YFP (V. Jakovljevic, MPI Marburg) as a template. The oYFP-6-oYFP-8 PCR product, containing *yfp* gene with 20 aa linker at 5'-end, encoded by oYFP-7 primer (linker2 in Table 16), was digested with *EcoRI* and *EcoRV* and cloned in-frame upstream of *sofG* gene in pIB92 generating pIB94. The oYFP-6-oYFP-7 PCR product, containing *yfp* gene without any linker was digested with *EcoRI* and *EcoRV* and cloned in-frame upstream of *sofG* gene in pIB92 giving rise to pIB96. The *EcoRI-HindIII* fragments from pIB94 and pIB96 containing *yfp-linker2-sofG* and *yfp-sofG*, respectively, were re-cloned into pSW105, generating pIB99 and pIB97, respectively. To construct pIB101, the region encompassing *yfp-sofG* was amplified using primers oYFP-10 and oSB_21 and pIB97 as a template. The corresponding PCR product was digested with *BamHI* and *HindIII* and cloned into pBJ113, generating pIB101. Finally, region containing 500 bp upstream of *sofG* gene, was amplified with primers o6703-7 and oSB_26, digested with *EcoRI-BamHI* and cloned into pIB101, giving rise to pIB113.

4.4.3 Generation of in-frame deletions

In-frame deletions of specific genomic regions were generated as previously described (Shi *et al.*, 2008). In brief, approximately 500 bp fragments directly up- and downstream of the target gene were amplified by PCR using primers designated as A, B, C and D. The primers A and D contain restriction sites for cloning into the plasmids pBJ113 and pBJ114. The primers B and C were designed to possess compatible ends which allow fusing the AB and CD fragments in a second PCR reaction or restriction sites for cloning. The fragments AB and CD were used for generating the full-length in-frame deletion fragment either by direct cloning or by fusing two PCR products in a second PCR reaction with primers A and D and AB-CD fragments as templates (Figure 59). Plasmids proved to be error-free by sequencing were introduced into *M. xanthus* WT cells. The plasmids pBJ113/pBJ114 cannot replicate autonomously in *M. xanthus* but confer kanamycin resistance when integrated into the chromosome by homologous recombination. Thus, *M. xanthus* transformants growing on kanamycin possess a plasmid integrated up- or downstream of the target gene. Insertions were mapped by

PCR and both, up- and downstream integration transformants were isolated if possible.

To obtain markerless in-frame deletion, a second round of homologous recombination has to take place to excise the plasmid. pBJ113/pBJ114 vectors also contain the counter-selection marker *galK* (galactokinase-encoding gene from *E. coli*). The product of *galK* gene converts galactose into its phosphorylated form. *M. xanthus* is not able to metabolize galactose phosphate, which accumulates in the cells to the toxic levels when the cells are grown on galactose-containing media. Therefore, only cells that have undergone the second round of homologous recombination, resulting in the excision of the plasmid, are viable. After excision of the plasmid only 50% of the transformants will contain in-frame deletion, whereas another 50% will restore the original (WT) genomic situation (Figure 59).

For the second round of homologous recombination ("loop-out"), transformants containing up- and downstream integration were grown in liquid CTT medium containing kanamycin to mid-log phase. Then, cultures were diluted 1/100 with CTT medium without antibiotics and grown to the OD_{550}=0.5-0.7. 50, 100, 200 and 400 µl aliquots from those cultures were mixed with 3 ml of CTT soft agar and plated on CTT agar plates, containing 2.5% (w/v) galactose. Transformants from those plates were transferred in parallel to CTT plates containing kanamycin and CTT plates without antibiotics. Colonies, growing on CTT plates, but not on kanamycin, were used to verify in-frame deletions by PCR.

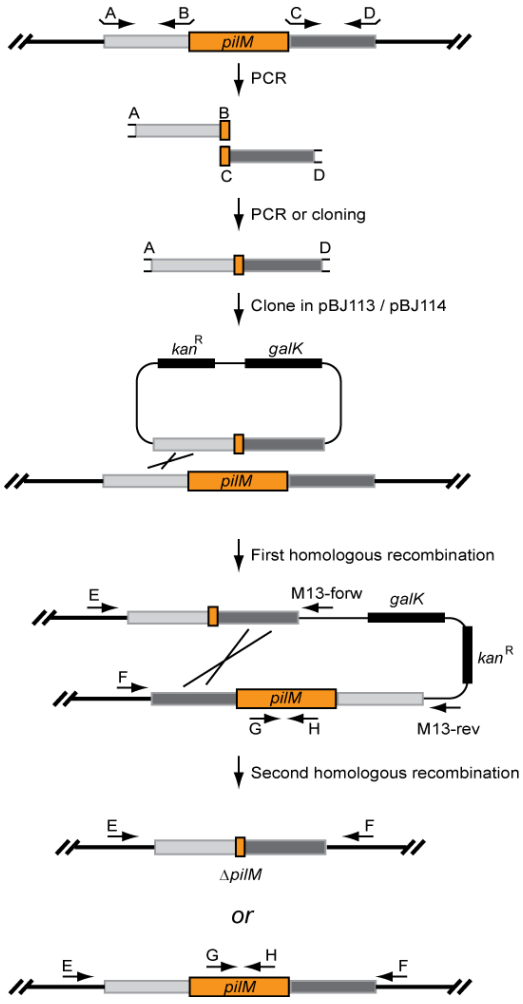

Figure 59. In-frame deletion generation strategy

First homologous recombination leads to plasmid integration up- or downstream of the genomic region to be deleted. Second recombination event allows excision of the vector together with the target region (in-frame deletion) or only the vector (reconstitution). Details in text. Figure modified from Shi *et al*. (Shi *et al.*, 2008).

4.4.4 DNA preparation from *E. coli* and *M. xanthus* cells

Plasmid DNA from *E. coli* was isolated using QIAprep Spin Miniprep Kit (Qiagen). *M. xanthus* genomic DNA was prepared using MasterPure DNA preparation Kit (Epicentre) according to the instructions of the manufacturer. Concentration and purity of DNA was determined with the Nanodrop ND-1000 spectrophotometer (Nanodrop, Wilmington). Crude genomic DNA preparations for verification of the insertions by PCR were prepared by boiling cell samples for 5 min in 50 µl H_2O followed by brief sedimantetion of cell debris.

4.4.5 Polymerase Chain Reaction (PCR)

Amplification of specific DNA fragments was performed in 50 µl reaction volume using *PfuUltra*™II-polymerase (Strategene, Amsterdam). To test the plasmid integration, colony PCR was conducted in 20 µl reaction volume using Eppendorf® MasterMix (Eppendorf), containing *Taq* polymerase. PCR mixtures were prepared as described in Table 17.

Table 17. PCR reaction mixes for cloning (50 µl) and for check PCR (20 µl)

Component	Volume	Final concentration
PCR for cloning		
Genomic DNA or plasmid DNA	1 µl	40-100 ng
10 µM primer	1.5 µl each	0.3 µM each
10 mM (each) dNTPs	1.5 µl	0.2 mM each
10× *PfuUltra* II buffer	5 µl	1×
DMSO	5 µl	10% (v/v)
PfuUltra ™II polymerase	0.5 µl	0.5 units
Sterile deionized water	34 µl	-
Check PCR		
Crude genomic DNA	1 µl	100 ng
10 µM primer	1 µl each	0.5 µM each
Eppendorf MasterMix	8 µl	-
DMSO	2 µl	10% (v/v)
Sterile deionized water	6.5 µl	-

The PCR programs used in this study are represented in Table 18. PCR conditions were modified based on the predicted primer annealing temperature, expected product sizes and polymerase used.

Table 18. PCR programs used in this study

Step	Temperature	Time
Standard PCR program[1]		
Initial denaturation	94˚C	3 min
Denaturation	94˚C	30 s
Primer annealing	5˚C below predicted melting temperature	30 s
Elongation	72˚C	30 s
		×30
Final elongation	72˚C	5 min
Hold	4˚C	∞
Touch down PCR program		
Initial denaturation	94˚C	3 min
Denaturation	94˚C	30 s
Primer annealing	70˚C	30 s
Elongation	72˚C	30 s
		×9
Denaturation	94˚C	30 s
Primer annealing	60˚C	30 s
		×9

Elongation	72˚C	30 s	×9
Denaturation	94˚C	30 s	
Primer annealing	55˚C	30 s	×20
Elongation	72˚C	30 s	
Final elongation	72˚C	5 min	
Hold	4˚C	∞	
Check PCR program			
Initial denaturation	94˚C	3 min	
Denaturation	94˚C	30 s	
Primer annealing	51˚C	30 s	×9
Elongation	72˚C	1 min per kb	
Hold	4˚C	∞	

[1] Standard and touch down PCR programs were used for amplifying PCR products for cloning, performed with *PfuUltra* II polymerase; check PCR program was used to verify integration of the plasmids, performed with Eppendorf MasterMix (*Taq* polymerase).

PCR product size was verified by agarose gel electrophoresis. Correct PCR products were either directly purified using DNA Clean&Concentrator-5 kit or extracted from the agarose gel and purified with Gel Recovery Kit (ZymoResearch Hiss Diagnostics).

4.4.6 Reverse transcription PCR

Total RNA was isolated from cell pellets using hot-phenol method (Overgaard *et al.*, 2006). Briefly, approximately 7×10^8 *M. xanthus* cells were harvested and transferred to a tube containing $^1/_{10}$ volume of ice-cold ethanol/phenol stop solution (5% saturated acid phenol pH<6.0 in 96% ethanol) and spun down at 4700 rpm and 4˚C for 10 min. The pellet was resuspended in 600 µl ice-cold solution 1 (0.3 M sucrose, 0.01 M NaAc, pH 4.5) and 300 µl aliquots were transferred into 1.5 ml tubes, each containing 300 µl hot (65˚C) solution 2 (2% SDS, 0.01 M NaAc, pH 4.5). The cell lysis was performed twice with equal volume of hot phenol extraction (saturated acid phenol pH<6.0 at 65˚C), once with equal volume of phenol: chloroform extraction (5:1), and once with equal volume of chloroform: isoamyl alcohol extraction (24:1). RNA was precipitated with $^1/_{10}$ volume of 3 M NaAc, pH 4.5 and two volumes of 96% ethanol for 20 min at -20˚C. RNA pellet was centrifuged at 10000×g at 4˚C and washed twice with equal volumes of ice-cold 75% ethanol. The final pellet was dried briefly at room temperature and resuspended in 50 µl RNase-free H_2O. RNA was stored at -80˚C.

cDNA was synthesized using the cDNA Archive kit (Applied Biosciences) from 1 µg of DNA-free total RNA following protocol of the manufacturer. To map *pilMNOPQ* locus PCR was performed using cDNA as a template and primers listed in Table 13.

4.4.7 Agarose gel electrophoresis

Nucleic acid fragments were separated by size using agarose gel electrophoresis at 120 V in TAE buffer (Invitrogen). Ethidium bromide was added to agarose in the final concentration of 0.01% (v/v). DNA samples were mixed with 5× sample loading buffer (Bioline). Agarose gels were imaged using 2UV transilluminator (UVP-Bio-Doc-It-System, UniEquip) at 365 nm.

4.4.8 Restriction and ligation of DNA fragments

For restriction, DNA (0.5-2 µg) was incubated with restriction endonucleases for 2 h according to the specific requirements for the enzyme used. Restricted DNA was purified with DNA Clean&Concentrator-5 kit (ZymoResearch Hiss Diagnostics).

Ligation reactions were performed with T4 DNA ligase. DNA fragments were ligated into vectors applying 3-5-fold molar excess of insert DNA. Normally, 10 fmol of insert and 30 fmol of vector DNA were ligated for 2 h at room temperature, followed by the inactivation of the enzyme at 65˚C for 15 min.

4.4.9 Preparation and transformation of electrocompetent *E. coli* cells

To prepare electrocompetent *E. coli* cells, overnight cultures were used to inoculate 1 L of LB medium. Cells were grown at 37˚C on horizontal shakers at 230 rpm. At OD_{600}=0.6 cells were harvested by centrifugation at 5,000×g for 20 min at 4˚C. The cell pellet was resuspended in 500 ml ice-cold sterile deionized water and centrifuged again. The washing steps were repeated with 100 ml, 50 ml and 10 ml volumes. Final cell pellet was resuspended in 2 ml sterile deionized water, 50 µl aliquots were fast frozen in liquid nitrogen and stored at -80˚C for later use.

For electroporation, 5 µl of heat-inactivated ligation reaction were first dialysed against sterile water for 30 min and then added to 50 µl electrocompetent *E. coli* cells on ice. The mixture was transferred into an electroporation cuvette (Bio-Rad, Munchen) and pulsed with 1.8 kV, 25 µF and 200 Ω. 1 ml LB medium was added; the suspension was transferred into a sterile plastic tube and incubated for 1 h at 37˚C shaking at 230 rpm. After 1 h incubation cells were harvested at by centrifugation at 2,000×g for 5 min, resuspended in 100 µl of LB medium and plated on LB agar plates containing appropriate antibiotics. The plates were incubated at 37˚C overnight; grown colonies were transferred onto fresh agar plates and screened for the presence of the plasmid containing the insert by restriction digestion with subsequent agarose gel electrophoresis. For sequencing obtained constructs were sent to Microfins MWG Operon; received DNA sequences were analyzed using Vector NTI Advance suite 11 (Invitrogen).

4.4.10 Preparation and transformation of electrocompetent *M. xanthus* cells

M. xanthus cells were grown in 5 ml CTT medium to an OD_{550}=0.5-0.8, 2 ml of this culture were centrifuged at 13,000 rpm for 2 min at room temperature. The cell pellet was resuspended in 1 ml of sterile deionized water and centrifuged as above. Washing step was repeated twice. The final cell pellet was resuspended in 40 µl of sterile deionized water.

For electroporation, 0.1 µg (for the integration at the chromosomal Mx8 attachment site) or 1 µg (for the integration at the endogenous site) of plasmid DNA or 5 µg of the chromosomal DNA were dialysed against sterile deionized water (VSWP membrane from Millipore was used). Next, dialysed DNA was added to the suspension of electrocompetent *M. xanthus* cells, the mixture was transferred into an 0.1 cm electroporation cuvette (Bio-Rad, Munchen) and pulsed with 0.65 kV, 25 µF and 400 Ω. 1 ml CTT-YE medium was added immediately; the suspension was transferred into a sterile Erlenmeyer flask and incubated for 6-8 h at 32˚C and 230 rpm in the dark. Then the suspension was mixed with 4 ml of CTT soft agar and plated on CTT agar plates containing appropriate antibiotics. The plates were incubated at 32˚C for 5 to 10 days; grown colonies transferred onto fresh agar plates. The integration of the plasmids was verified by PCR described in Table 17 and Table 18.

4.5 Biochemical methods

4.5.1 Purification of *M. xanthus* PilQ and PilT proteins

To overexpress the His_6-tagged PilQ protein, plasmid pIB49 was propagated in *E. coli* Rosetta 2 (DE3)/pLysS strain (Novagen). To purify His_6-tagged PilT, previously generated JM109/pMS421 strain containing pSL4 plasmid (Jakovljevic *et al.*, 2008) was used. JM109/pMS421 and Rosetta 2 cells were grown to OD_{600}=0.5 in 1 L 2YT medium at 37˚C and 230 rpm. For induction, IPTG was added to a final concentration of 1 mM and cultivation was continued for 4 h 37˚C. The cells were harvested by centrifugation at 5,000×g for 20 min, resuspended in the native lysis buffer (300 mM NaCl, 50 mM Tris-HCl, 10% glycerol, 5 mM β-mercaptoethanol, 10 mM imidazole, pH 8.0) with protease inhibitor tablet (Roche). The cell suspensions were sonicated 6x 20 s with microtip, output 3 and duty 50%. The lysates were centrifuged at 13,000 ×g for 30 min at 4°C. The supernatants were saved as soluble fractions, whereas the pellets were resuspended in the lysis buffer and saved as insoluble fractions. When the soluble and insoluble fractions were examined by SDS-PAGE both PilT and PilQ proteins were present only in the insoluble fraction. Therefore, for PilT/PilQ purification the pellet of the cell lysate containing His_6-PilT/His_6-PilQ was

resuspended in 30 ml of the denaturing buffer (8 M urea, 0.1 M Tris-HCl pH 8.0), incubated for 1 h at room temperature with shaking to dissolve inclusion bodies and centrifuged for 30 min at 13,000×g and 4°C. The supernatant was incubated with 1 ml of Ni-NTA agarose slurry (Qiagen) shaking at 4°C for 1 h, and denatured His_6-PilT/His_6-PilQ were purified according to the recommendations of the supplier. Purity of His_6-PilT/His_6-PilQ proteins was confirmed by SDS-PAGE. 2 mg of pure His_6-PilQ were used for rabbit immunization in order to produce anti-PilQ antibodies.

4.5.2 Determination of protein concentration

To determine protein concentrations Bio-Rad protein assay kit (Bio-Rad, München) based on Bradford method (Bradford, 1976) was used according to the instructions of the manufacturer. Bovine serum albumin (BSA) was used as a protein standard for standard curves preparation. Sample protein concentrations were determined in duplicates in 1 ml total reaction volume. Samples were incubated with Bradford reagent for 15 min at room temperature in the dark. Finally, absorbance was measured at 595 nm with Ultrospec 2100 pro spectrophotometer (Amersham Biosciences, München). Protein concentrations were calculated based on the slope value of the standard curve.

4.5.3 SDS polyacrylamide gel electrophoresis (SDS-PAGE)

To monitor heterologous protein expression, to separate and purify proteins under denaturing conditions SDS-PAGE (Laemmli, 1970) with 8% (for PilQ protein) and 14% gels was performed. To denature proteins, samples were mixed with 5× loading buffer (50% (v/v) glycerol, 250 mM Tris-HCl pH 6.8, 10 mM EDTA, 10% (w/v) SDS, 0.5 M DTT, 1% (w/v) bromphenol blue) and heated at 96°C for 5 min prior to loading the gel. Gel electrophoresis was carried out in Bio-Rad electrophoresis chambers (Bio-Rad, München) at 120-150 V in 1× Tris/Glycine SDS (TGS) running buffer from Bio-Rad. To estimate molecular weight of proteins prestained protein markers from Fermentas (St. Leon-Rot) were used. Proteins were visualized by staining for 20 min at room temperature in Coomassie brilliant blue (Sambrook *et al.*, 1989).

4.5.4 Immunoblot analysis

Immunoblot analysis was conducted using standard protocol (Sambrook *et al.*, 1989). Equal amounts of protein (between 5 and 15 µg protein or protein from approximately 7×10^7 cells per lane) were loaded onto SDS-PAGE and protein transfer to the nitrocellulose membrane was performed using Hoefer TE77 semi-dry blotting apparatus (Amersham Biosciences, Munchen) with constant current 0.8 mA/cm^2. Buffers used for the transfer are listed in Table 19. After transfer, nitrocellulose

membranes were blocked using 1× TTBS buffer (0.05% (v/v) Tween 20, 20 mM Tris-HCl, 137 mM NaCl pH 7) supplemented with 5% (w/v) non-fat milk powder overnight shaking at 4˚C. Next, membranes were washed twice with 1×TTBS buffer and subsequently incubated with the proper dilution of primary antibodies (Table 20) in 1×TTBS buffer containing 2% (w/v) non-fat milk powder for 2 h at 4˚C. After incubation with primary antibodies, membranes were washed 2×5 min with 1×TTBS buffer and finally incubated with 1:15000 dilution of secondary anti-rabbit IgG or 1:2500 dilution of secondary anti-mouse IgG horseradish peroxidase (HPR) coupled antibodies (Pierce/Thermo Scientific, DakoCytomation). After 1 h incubation at 4˚C with secondary antibodies, membranes were washed twice with 1×TTBS buffer, then chemiluminescence substrate (Pierce/Thermo Scientific) was added for 1 min and finally signals were visualized using luminescent image analyzer LAS-4000 (Fujifilm).

Table 19. Transfer buffers for immunoblot analysis

Membrane side (anode)		**Gel side (kathode)**	
Chemical/ 1 liter H_20	**Final concentration**	**Chemical/ 1 liter H_20**	**Final concentration**
3,03 g Tris	25 mM	6,06 g Tris	50 mM
14,4 g glycine	192 mM	28,8 g glycine	384 mM
0,1 g SDS	0,01%	2,0 g SDS	0,2%
250 ml methanol	25%	100 ml methanol	10%

Table 20. Dilutions of primary antibodies used for immunoblot analysis

Antibody	PilQ	PilC	PilM	PilN	PilB	PilT	GFP	SofG
Fold dilution	10000	5000	2000	5000	6000	1000	500	500

4.5.5 Affinity purification of antibodies

To prevent unspecific binding of anti-PilT and anti-PilQ antibodies, they were subjected to affinity purification based on the protocol from Michael Koelle, Yale University. To purify 2 ml of the antiserum, 1-2 mg of purified protein were loaded on SDS-PAGE and transferred to the nitrocellulose membrane. Protein was visualized using Ponceau S, the protein band of interest was cut out and washed twice with sterile H_2O to remove remaining stain from the membrane. The membrane was washed with 100 mM glycine/HCl, pH 2.5 for 5 min to remove poorly bound protein, washed 2×2 min with TBS buffer and blocked by soaking it in TBS-BSA buffer (TBS, supplemented with 3% (w/v) of bovine serum albumine) for 1 h at room temperature with gentle rocking. After blocking, the membrane was washed 2×2 min with TBS buffer. 2 ml of

antiserum were diluted with 8 ml of TBS and incubated with the washed membrane overnight at 4˚C on a rocker. The supernatant was recovered, and the membrane was washed 2×5 min with TBS buffer, followed by washing 2×5 min with PBS buffer (137 mM NaCl, 2.7 mM KCl, 10 mM Na_2HPO_4, 1.8 mM KH_2PO_4, pH 7.4). The bound antibodies were eluted from the membrane by incubation for 10 min with 1 ml of 100 mM glycine/HCl, pH 2.5 and occasional vortexing. The eluate was transferred to a tube containing 100 µl of 1 M Tris, pH 8.0 in order to bring the final pH to 7. The elution step was done twice, and the eluates were pooled together. Purified antibodies were stabilized by adding sodium azide (to 5 mM final concentration) and BSA (to 1 mg/ml final concentration), and stored at 4˚C.

4.5.6 Cell fractionation

Biochemical fractionation of cells was performed as previously described (Thomasson *et al.*, 2002). In brief, 100 ml of exponentially growing *M. xanthus* WT cells were grown in 1% CTT liquid medium to a cell density of 7×10^8 cells/ml, harvested by centrifugation at 8,000 rpm for 10 min and resuspended in 10 ml of 50 mM Tris-HCl pH 7.6, supplemented with protease inhibitors tablet (Roche). Cells were lysed by sonication 8x 15 s with middle-sized tip, output 2.5 and duty 50%. The supernatant was separated from the cell debris by centrifugation at 5,000 rpm for 10 min at 4˚C. The cleared lysate was subjected to ultracentrifugation at 45,000×g for 1 h at 4˚C to separate soluble (periplasmic and cytoplasmic) proteins from the insoluble, membrane-enriched fraction. The membrane-enriched pellet was solubilized in 10 ml of Tris-buffer containing detergent and magnesium (50 mM Tris-HCl pH 7.6, 2% (v/v) Triton X-100, 10 mM $MgCl_2$) by stirring the samples on Labinco LD-79 Rotator at 4˚C overnight. The resulting supernatant, enriched for inner membrane proteins, was separated from the pellet, enriched in the outer membrane proteins by ultracentrifugation at 45,000×g for 1 h at 4˚C. All fractions (soluble, inner and outer membrane-enriched) were precipitated with 4 volumes of ice-cold acetone at -20˚C overnight, resuspended in SDS-PAGE loading buffer, separated by SDS-PAGE and analyzed in immunoblots.

4.6 Microscopy

4.6.1 Live-cell imaging and data analysis

For phase-contrast and fluorescence microscopy, exponentially growing cultures of *M. xanthus* were grown to a density of 7×10^8 cells/ml in liquid CTT medium at 32°C, transferred to a microscope slide and immediately observed in a Leica DM6000B microscope, using a Leica Plan Apo×100/NA 1.40 phase-contrast oil objective. Cells

were visualized with a Roper Photometrics® Cascade II 1024 camera. For fluorescence microscopy, a Leica YFP filter (excitation range 490–510 nm, emission range 520–550 nm) was used. Images were recorded and processed with Image-Pro® 6.2 (MediaCybernetics). Processed images were arranged in Adobe Photoshop 6 (Adobe Systems).

For time-lapse recordings, cells were spotted on a thin 0.7% agar-pad buffered with A50 starvation buffer (10 mM MOPS, pH 7.2, 10 mM $CaCl_2$, 10 mM $MgCl_2$, 50 mM NaCl) on a glass slide and immediately covered with a coverslip. After 30 min at room temperature, cells were imaged at 30 s intervals between frames.

Quantification of fluorescence was done as follows. The average fluorescence intensities (arbitrary units) of polar clusters and the average fluorescence intensity of the intracellular background between the polar regions were measured using the region measurement tool in Metamorph® v 7.5 (Molecular Devices). The average fluorescence intensity of the intracellular background was subtracted from the average fluorescence intensities of the polar clusters. The background subtracted values were used to calculate ratios of polar signals. For each strain 100 cells were analyzed.

To determine the exact position of the single YFP-SofG/YFP-PilT clusters in the cell, the maximal intensity of the fluorescent foci was measured using the linescan tool of Metamorph® v 7.5 (Molecular Devices) as a function of the cell length in N=100 cells.

4.6.2 Immunofluorescence microscopy and data analysis

Immunofluorescence microscopy was performed as described essentially (Mignot *et al.*, 2005). Briefly, *M. xanthus* cells were grown to a density of 7×10^8 cells per ml in liquid CTT medium at 32°C and either fixed directly from suspension or harvested, resuspended in 1% CTT medium to a calculated density of 7×10^9 cells/ml, and placed (10 µl aliquots of cells) on 1.0% agar supplemented with 0.5% CTT in order to analyze cells on a surface. After 3-4 h incubation at 32°C, cells were harvested from the plate by washing with 1% CTT medium mixed with fixing solution. Cells were fixed with 3.2% (PilC, PilN and PilM) or 1.6% paraformaldehyde (PilQ, PilB and PilT) and 0.008% glutaraldehyde for 20 min on freshly prepared poly L-Lysine treated 12-well diagnostic slides (Thermo Scientific). Cells were permeabilized with GTE buffer (50 mM glucose, 20 mM Tris, 10 mM EDTA, pH 7.5) for 4 min and probed with relevant affinity-purified polyclonal antibodies (Table 21) at 4°C overnight in PBS buffer (137 mM NaCl, 2.7 mM KCl, 10 mM Na_2HPO_4, 1.8 mM KH_2PO_4, pH 7.4) supplemented with 2% BSA. DyLight 549-conjugated goat anti-rabbit antibodies (Pierce/Thermo Scientific) were used as a secondary antibody. SlowFade AntiFade Reagent (Molecular Probes/Invitrogen) was added to each well. Cells were observed in a Leica DM6000B microscope, using a

Leica Plan Apo 100x/NA 1.40 phase contrast oil objective and visualized with a Leica DFC 350FX camera. For fluorescence microscopy, a Leica Y3 filter (excitation range 530-560 nm, emission range 570-650 nm) and a Leica GFP filter (excitation range 450–490 nm, emission range 500–550 nm) were used. Processed images were arranged in Adobe Photoshop 6. Quantification of fluorescence signals was performed as described in Chapter 4.6.1. For each strain 100 cells were analyzed.

Table 21. Dilutions of primary antibodies used for immunofluorescence microscopy

Antibody	PilQ	PilC	PilM	PilN	PilB	PilT
Fold dilution	100	3000	2000	2000	2500	2000

4.6.3 Fluorescence recovery after photobleaching (FRAP) experiments and data analysis

For FRAP microscopy *M. xanthus* cells were grown to a density of 7×10^8 cells per ml in liquid CTT medium at 32°C, transferred to a microscope slide, covered with a polystyrene-covered coverslip and sealed. After 30-60 min at room temperature cells were observed in a Nikon Eclipse TE 2000-E microscope (Nikon) with a Nikon CFI Plan Fluor 100x/NA1.30 oil immersion objective. For photobleaching, a 514 nm laser beam of an argon ion laser (Melles Griot Laser Group) was focussed in the image plane of the microscope. The cytoplasmic region was prebleached for 3 s in order to decrease non-polar fluorescence signals. Subsequently, a polar region was bleached for 1 s, and recovery of the fluorescence signal followed for 120 s, with time intervals of 3 s between frames. Images were recorded with a Roper Photometrics® Cascade II 512 camera. Images were processed with NIS Elements AR 2.30 (Nikon). Data analysis was performed as follows. Fluorescence intensity of the intercellular background was measured using the linescan tool in Metamorph® v 7.5, and the average values subtracted from all images to minimize background fluorescence. Then integrated fluorescence intensities (arbitrary units) of polar YFP-PilT clusters as well as the integrated fluorescence intensity of the cytoplasmic region were measured using the region measurement tool in Metamorph® v 7.5. For each region measured inside a cell I determined the integrated fluorescence intensity of a similar region outside the cell and subtracted this value from the inside value to obtain background-subtracted integrated intensities. Final values were plotted as a function of time. Because the total fluorescence signal over individual cells did not change over time after bleaching of a polar region, the data were not corrected for continuous bleaching. A total of 10 cells were analyzed.

4.6.4 Transmission electron microscopy

For electron microscopy *M. xanthus* overnight cultures were diluted 1:10 with 1% liquid CTT medium and grown on horizontal shaker at 32˚C in the dark for 2-4 h. After 2-4 h incubation, 50 µl of *M. xanthus* culture was placed on parafilm. A small piece of carbon-coated mica was dipped into the drop for 30 s, allowing cells to adsorb to the surface of the carbon film. The carbon film was picked with a copper grid (PLANO), excess liquid was soaked off, the film was placed briefly on a drop of distilled water, excess liquid was soaked off again, and the film was transferred on a drop of 2% uranyl acetate (wt/vol) for 2 seconds and blotted dry. Transmission electron microscopy was performed on a Philips EM 301 electron microscope at calibrated magnifications.

4.7 Bioinformatics analyses

M. xanthus genes and protein sequences were obtained online from TIGR (http://cmr.jcvi.org/tigr-scripts/CMR/CmrHomePage.cgi) and analyzed using the Blastn (against non-redundant database), Blastp and psiBlastp algorithms from NCBI (http://blast.ncbi.nlm.nih.gov/) or the SMART algorithm from EMBL (http://smart.embl-heidelberg.de/). Protein sequences for the alignments generation were obtained from NCBI (http://www.ncbi.nlm.nih.gov/). Selected sequences were aligned and analyzed using Vector NTI Advance suite 11 (Invitrogen).

5 References

Abendroth, J., Murphy, P., Sandkvist, M., Bagdasarian, M., and Hol, W.G. (2005). The X-ray structure of the type II secretion system complex formed by the N-terminal domain of EpsE and the cytoplasmic domain of EpsL of *Vibrio cholerae*. *J Mol Biol* **348**, 845-855.

Alm, R.A., and Mattick, J.S. (1995). Identification of a gene, pilV, required for type 4 fimbrial biogenesis in Pseudomonas aeruginosa, whose product possesses a pre-pilin-like leader sequence. *Mol Microbiol* **16**, 485-496.

Arnold, J.W., and Shimkets, L.J. (1988). Inhibition of cell-cell interactions in Myxococcus xanthus by congo red. *J Bacteriol* **170**, 5765-5770.

Audette, G.F., Irvin, R.T., and Hazes, B. (2004). Crystallographic analysis of the *Pseudomonas aeruginosa* strain K122-4 monomeric pilin reveals a conserved receptor-binding architecture. *Biochemistry* **43**, 11427-11435.

Ayers, M., Sampaleanu, L.M., Tammam, S., Koo, J., Harvey, H., Howell, P.L., and Burrows, L.L. (2009). PilM/N/O/P proteins form an inner membrane complex that affects the stability of the *Pseudomonas aeruginosa* type IV pilus secretin. *J Mol Biol* **394**, 128-142.

Bakaletz, L.O., Baker, B.D., Jurcisek, J.A., Harrison, A., Novotny, L.A., Bookwalter, J.E., Mungur, R., and Munson, R.S., Jr. (2005). Demonstration of Type IV pilus expression and a twitching phenotype by Haemophilus influenzae. *Infect Immun* **73**, 1635-1643.

Baker, M.D., Wolanin, P.M., and Stock, J.B. (2006). Signal transduction in bacterial chemotaxis. *Bioessays* **28**, 9-22.

Behmlander, R.M., and Dworkin, M. (1994a). Biochemical and structural analyses of the extracellular matrix fibrils of *Myxococcus xanthus*. *J Bacteriol* **176**, 6295-6303.

Behmlander, R.M., and Dworkin, M. (1994b). Integral proteins of the extracellular matrix fibrils of *Myxococcus xanthus*. *J Bacteriol* **176**, 6304-6311.

Bendtsen, J.D., Nielsen, H., von Heijne, G., and Brunak, S. (2004). Improved prediction of signal peptides: SignalP 3.0. *J Mol Biol* **16**, 783-795.

Berleman, J.E., Chumley, T., Cheung, P., and Kirby, J.R. (2006). Rippling is a predatory behavior in Myxococcus xanthus. *J Bacteriol* **188**, 5888-5895.

Berleman, J.E., and Kirby, J.R. (2007). Multicellular development in Myxococcus xanthus is stimulated by predator-prey interactions. *J Bacteriol* **189**, 5675-5682.

Bhaya, D., Bianco, N.R., Bryant, D., and Grossman, A. (2000). Type IV pilus biogenesis and motility in the cyanobacterium *Synechocystis* sp. PCC6803. *Mol Microbiol* **37**, 941-951.

Black, W.P., Xu, Q., and Yang, Z. (2006). Type IV pili function upstream of the Dif chemotaxis pathway in *Myxococcus xanthus* EPS regulation. *Mol Microbiol* **61**, 447-456.

Black, W.P., and Yang, Z. (2004). *Myxococcus xanthus* chemotaxis homologs DifD and DifG negatively regulate fibril polysaccharide production. *J Bacteriol* **186**, 1001-1008.

Blackhart, B.D., and Zusman, D.R. (1985). "Frizzy" genes of *Myxococcus xanthus* are involved in control of frequency of reversal of gliding motility. *Proc Natl Acad Sci U S A* **82**, 8771-8774.

Bourne, H.R., Sanders, D.A., and McCormick, F. (1991). The GTPase superfamily: conserved structure and molecular mechanism. *Nature* **349**, 117-127.

Bowden, M.G., and Kaplan, H.B. (1998). The *Myxococcus xanthus* lipopolysaccharide O-antigen is required for social motility and multicellular development. *Mol Microbiol* **30**, 275-284.

Bradford, M.M. (1976). A rapid and sensitive method for the quantitation of microgram quantities of protein utilizing the principle of protein-dye binding. *Anal Biochem* **72**, 248-254.

Bradley, D.E. (1972a). Evidence for the retraction of *Pseudomonas aeruginosa* RNA phage pili. *Biochem Biophys Res Commun* **47**, 142-149.

Bradley, D.E. (1972b). Shortening of *Pseudomonas aeruginosa* pili after RNA-phage adsorption. *J Gen Microbiol* **72**, 303-319.

Bulyha, I., Schmidt, C., Lenz, P., Jakovljevic, V., Hone, A., Maier, B., Hoppert, M., and Sogaard-Andersen, L. (2009). Regulation of the type IV pili molecular machine by dynamic localization of two motor proteins. *Mol Microbiol* **74**, 691-706.

Burrows, L.L. (2005). Weapons of mass retraction. *Mol Microbiol* **57**, 878-888.

Bustamante, V.H., Martinez-Flores, I., Vlamakis, H.C., and Zusman, D.R. (2004). Analysis of the Frz signal transduction system of *Myxococcus xanthus* shows the importance of the conserved C-terminal region of the cytoplasmic chemoreceptor FrzCD in sensing signals. *Mol Microbiol* **53**, 1501-1513.

Camberg, J.L., and Sandkvist, M. (2005). Molecular analysis of the *Vibrio cholerae* type II secretion ATPase EpsE. *J Bacteriol* **187**, 249-256.

Carbonnelle, E., Helaine, S., Nassif, X., and Pelicic, V. (2006). A systematic genetic analysis in Neisseria meningitidis defines the Pil proteins required for assembly, functionality, stabilization and export of type IV pili. *Mol Microbiol* **61**, 1510-1522.

Carbonnelle, E., Helaine, S., Prouvensier, L., Nassif, X., and Pelicic, V. (2005). Type IV pilus biogenesis in *Neisseria meningitidis*: PilW is involved in a step occurring after pilus assembly, essential for fibre stability and function. *Mol Microbiol* **55**, 54-64.

Charest, P.G., and Firtel, R.A. (2007). Big roles for small GTPases in the control of directed cell movement. *Biochem J* **401**, 377-390.

Chiang, P., Habash, M., and Burrows, L.L. (2005). Disparate subcellular localization patterns of Pseudomonas aeruginosa Type IV pilus ATPases involved in twitching motility. *J Bacteriol* **187**, 829-839.

Chiang, P., Sampaleanu, L.M., Ayers, M., Pahuta, M., Howell, P.L., and Burrows, L.L. (2008). Functional role of conserved residues in the characteristic secretion NTPase motifs of the *Pseudomonas aeruginosa* type IV pilus motor proteins PilB, PilT and PilU. *Microbiology* **154**, 114-126.

Clausen, M., Koomey, M., and Maier, B. (2009). Dynamics of type IV pili is controlled by switching between multiple states. *Biophys J* **96**, 1169-1177.

Collins, R.F., Frye, S.A., Balasingham, S., Ford, R.C., Tonjum, T., and Derrick, J.P. (2005). Interaction with type IV pili induces structural changes in the bacterial outer membrane secretin PilQ. *J Biol Chem* **280**, 18923-18930.

Collins, R.F., Saleem, M., and Derrick, J.P. (2007). Purification and three-dimensional electron microscopy structure of the *Neisseria meningitidis* type IV pilus biogenesis protein PilG. *J Bacteriol* **189**, 6389-6396.

Colvin, J.R., and Witter, D.E. (1983). Congo Red and Calcofluor White Inhibition of Acetobacter-Xylinum Cell-Growth and of Bacterial Cellulose Microfibril Formation - Isolation and Properties of a Transient, Extracellular Glucan Related to Cellulose. *Protoplasma* **116**, 34-40.

Cool, R.H., Schmidt, G., Lenzen, C.U., Prinz, H., Vogt, D., and Wittinghofer, A. (1999). The Ras mutant D119N is both dominant negative and activated. *Mol Cell Biol* **19**, 6297-6305.

Craig, L., and Li, J. (2008). Type IV pili: paradoxes in form and function. *Curr Opin Struct Biol* **18**, 267-277.

Craig, L., Pique, M.E., and Tainer, J.A. (2004). Type IV pilus structure and bacterial pathogenicity. *Nat Rev Microbiol* **2**, 363-378.

Craig, L., Taylor, R.K., Pique, M.E., Adair, B.D., Arvai, A.S., Singh, M., Lloyd, S.J., Shin, D.S., Getzoff, E.D., Yeager, M.*, et al.* (2003). Type IV pilin structure and assembly: X-ray and EM analyses of *Vibrio cholerae* toxin-coregulated pilus and *Pseudomonas aeruginosa* PAK pilin. *Mol Cell* **11**, 1139-1150.

Crowther, L.J., Anantha, R.P., and Donnenberg, M.S. (2004). The inner membrane subassembly of the enteropathogenic *Escherichia coli* bundle-forming pilus machine. *Mol Microbiol* **52**, 67-79.

Crowther, L.J., Yamagata, A., Craig, L., Tainer, J.A., and Donnenberg, M.S. (2005). The ATPase activity of BfpD is greatly enhanced by zinc and allosteric interactions with other Bfp proteins. *J Biol Chem* **280**, 24839-24848.

Curtis, P.D., Atwood, J., 3rd, Orlando, R., and Shimkets, L.J. (2007). Proteins associated with the *Myxococcus xanthus* extracellular matrix. *J Bacteriol* **189**, 7634-7642.

Dana, J.R., and Shimkets, L.J. (1993). Regulation of cohesion-dependent cell interactions in Myxococcus xanthus. *J Bacteriol* **175**, 3636-3647.

Dubnau, D. (1999). DNA uptake in bacteria. *Annu Rev Microbiol* **53**, 217-244.

Dworkin, M. (1996). Recent advances in the social and developmental biology of the *Myxobacteria*. *Microbiol Rev* **60**, 70-102.

Elowitz, M.B., Surette, M.G., Wolf, P.E., Stock, J.B., and Leibler, S. (1999). Protein mobility in the cytoplasm of *Escherichia coli*. *J Bacteriol* **181**, 197-203.

Feig, L.A. (1999). Tools of the trade: use of dominant-inhibitory mutants of Ras-family GTPases. *Nat Cell Biol* **1**, E25-27.

Figge, R.M., Divakaruni, A.V., and Gober, J.W. (2004). MreB, the cell shape-determining bacterial actin homologue, co-ordinates cell wall morphogenesis in *Caulobacter crescentus*. *Mol Microbiol* **51**, 1321-1332.

Fink, J.M., and Zissler, J.F. (1989). Defects in motility and development of *Myxococcus xanthus* lipopolysaccharide mutants. *J Bacteriol* **171**, 2042-2048.

Gitai, Z., Dye, N., and Shapiro, L. (2004). An actin-like gene can determine cell polarity in bacteria. *Proc Natl Acad Sci U S A* **101**, 8643-8648.

Gitai, Z., Dye, N.A., Reisenauer, A., Wachi, M., and Shapiro, L. (2005). MreB actin-mediated segregation of a specific region of a bacterial chromosome. *Cell* **120**, 329-341.

Hansen, J.K., and Forest, K.T. (2006). Type IV pilin structures: insights on shared architecture, fiber assembly, receptor binding and type II secretion. *J Mol Microbiol Biotechnol* **11**, 192-207.

Harshey, R.M. (1994). Bees aren't the only ones: swarming in gram-negative bacteria. *Mol Microbiol* **13**, 389-394.

Hartzell, P.L., and Youderian, P. (1995). Genetics of gliding motility and development in *Myxococcus xanthus*. *Arch Microbiol* **164**, 309-323.

Hazes, B., Sastry, P.A., Hayakawa, K., Read, R.J., and Irvin, R.T. (2000). Crystal structure of *Pseudomonas aeruginosa* PAK pilin suggests a main-chain-dominated mode of receptor binding. *J Mol Biol* **299**, 1005-1017.

Henrichsen, J. (1972). Gliding and twitching motility of bacteria unaffected by cytochalasin B. *Acta Pathol Microbiol Scand B Microbiol Immunol* **80**, 623-624.

Henrichsen, J. (1983). Twitching motility. *Annu Rev Microbiol* **37**, 81-93.

Herdendorf, T.J., McCaslin, D.R., and Forest, K.T. (2002). *Aquifex aeolicus* PilT, homologue of a surface motility protein, is a thermostable oligomeric NTPase. *J Bacteriol* **184**, 6465-6471.

Hodgkin, J., and Kaiser, D. (1977). Cell-to-cell stimulation of movement in nonmotile mutants of *Myxococcus*. *Proc Natl Acad Sci U S A* **74**, 2938-2942.

Hodgkin, J., and Kaiser, D. (1979a). Genetics of gliding motility in *Myxococcus xanthus* (Myxobacterales) : genes controlling movement of single cells. *Mol Gen Genet* **171**, 167-176.

Hodgkin, J., and Kaiser, D. (1979b). Genetics of Gliding Motility in *Myxococcus xanthus* (Myxobacterales): Two gene systems control movement. *Mol Gen Genet* **171**, 177-191.

Hoiczyk, E. (2000). Gliding motility in cyanobacterial: observations and possible explanations. *Arch Microbiol* **174**, 11-17.

Hwang, J., Bieber, D., Ramer, S.W., Wu, C.Y., and Schoolnik, G.K. (2003). Structural and topographical studies of the type IV bundle-forming pilus assembly complex of enteropathogenic *Escherichia coli*. *J Bacteriol* **185**, 6695-6701.

Iden, S., and Collard, J.G. (2008). Crosstalk between small GTPases and polarity proteins in cell polarization. *Nat Rev Mol Cell Biol* **9**, 846-859.

Inclan, Y.F., Laurent, S., and Zusman, D.R. (2008). The receiver domain of FrzE, a CheA-CheY fusion protein, regulates the CheA histidine kinase activity and downstream signalling to the A- and S-motility systems of *Myxococcus xanthus*. *Mol Microbiol* **68**, 1328-1339.

Inclan, Y.F., Vlamakis, H.C., and Zusman, D.R. (2007). FrzZ, a dual CheY-like response regulator, functions as an output for the Frz chemosensory pathway of *Myxococcus xanthus*. *Mol Microbiol* **65**, 90-102.

Insall, R., and Andrew, N. (2007). Chemotaxis in *Dictyostelium*: how to walk straight using parallel pathways. *Curr Opin Microbiol* **10**, 578-581.

Jakovljevic, V., Leonardy, S., Hoppert, M., and Sogaard-Andersen, L. (2008). PilB and PilT are ATPases acting antagonistically in type IV pilus function in *Myxococcus xanthus*. *J Bacteriol* **190**, 2411-2421.

Jelsbak, L., and Søgaard-Andersen, L. (2002). Pattern formation by a cell surface-associated morphogen in *Myxococcus xanthus*. *Proc Natl Acad Sci USA* **99**, 2032-2037.

John, J., Rensland, H., Schlichting, I., Vetter, I., Borasio, G.D., Goody, R.S., and Wittinghofer, A. (1993). Kinetic and structural analysis of the Mg(2+)-binding site of the guanine nucleotide-binding protein p21H-ras. *J Biol Chem* **268**, 923-929.

Julien, B., Kaiser, A.D., and Garza, A. (2000). Spatial control of cell differentiation in *Myxococcus xanthus*. *Proc Natl Acad Sci U S A* **97**, 9098-9103.

Kaiser, D. (1979). Social gliding is correlated with the presence of pili in *Myxococcus xanthus*. *Proc Natl Acad Sci USA* **76**, 5952-5956.

Kaiser, D. (2000). Bacterial motility: how do pili pull? *Curr Biol* **10**, R777-780.

Kaiser, D. (2003). Coupling cell movement to multicellular development in myxobacteria. *Nature Rev Microbiol* **1**, 45-54.

Kaiser, D. (2006). A microbial genetic journey. *Annu Rev Microbiol* **60**, 1-25.

Kaiser, D., and Crosby, C. (1983). Cell movements and its coordination in swarms of *Myxococcus xanthus*. *Cell Motil* **3**, 275-284.

Karnoub, A.E., and Weinberg, R.A. (2008). Ras oncogenes: split personalities. *Nat Rev Mol Cell Biol* **9**, 517-531.

Kearns, D.B., Bonner, P.J., Smith, D.R., and Shimkets, L.J. (2002). An extracellular matrix-associated zinc metalloprotease is required for dilauroyl phosphatidylethanolamine chemotactic excitation in *Myxococcus xanthus*. *J Bacteriol* **184**, 1678-1684.

Kim, S.K., and Kaiser, D. (1990a). C-factor: a cell-cell signaling protein required for fruiting body morphogenesis of *Myxococcus xanthus*. *Cell* **61**, 19-26.

Kim, S.K., and Kaiser, D. (1990b). Cell motility is required for the transmission of C-factor, an intercellular signal that coordinates fruiting body morphogenesis of *Myxococcus xanthus*. *Genes Dev* **4**, 896-904.

Kirn, T.J., Bose, N., and Taylor, R.K. (2003). Secretion of a soluble colonization factor by the TCP type 4 pilus biogenesis pathway in *Vibrio cholerae*. *Mol Microbiol* **49**, 81-92.

Klausen, M., Aaes-Jorgensen, A., Molin, S., and Tolker-Nielsen, T. (2003). Involvement of bacterial migration in the development of complex multicellular structures in *Pseudomonas aeruginosa* biofilms. *Mol Microbiol* **50**, 61-68.

Konovalova, A., Petters, T., and Sogaard-Andersen, L. (2010). Extracellular biology of *Myxococcus xanthus*. *FEMS Microbiol Rev* **34**, 89-106.

Koonin, E.V., and Aravind, L. (2000). Dynein light chains of the Roadblock/LC7 group belong to an ancient protein superfamily implicated in NTPase regulation. *Curr Biol* **10**, R774-776.

Krogh, A., Larsson, B., von Heijne, G., and Sonnhammer, E.L. (2001). Predicting transmembrane protein topology with a hidden Markov model: application to complete genomes. *J Mol Biol* **305**, 567-580.

Kroos, L., Hartzell, P., Stephens, K., and Kaiser, D. (1988). A link between cell movement and gene expression argues that motility is required for cell-cell signaling during fruiting body development. *Genes Dev* **2**, 1677-1685.

Kroos, L., and Kaiser, D. (1987). Expression of many developmentally regulated genes in *Myxococcus* depends on a sequence of cell interactions. *Genes & Dev* **1**, 840-854.

Kruse, T., Moller-Jensen, J., Lobner-Olesen, A., and Gerdes, K. (2003). Dysfunctional MreB inhibits chromosome segregation in *Escherichia coli*. *Embo J* **22**, 5283-5292.

Kuhn, J., Briegel, A., Morschel, E., Kahnt, J., Leser, K., Wick, S., Jensen, G.J., and Thanbichler, M. (2010). Bactofilins, a ubiquitous class of cytoskeletal proteins mediating polar localization of a cell wall synthase in *Caulobacter crescentus*. *Embo J* **29**, 327-339.

Kuner, J.M., and Kaiser, D. (1982). Fruiting body morphogenesis in submerged cultures of *Myxococcus xanthus*. *J Bacteriol* **151**, 458-461.

Kuspa, A., Kroos, L., and Kaiser, D. (1986). Intercellular signaling is required for developmental gene expression in *Myxococcus xanthus*. *Dev Biol* **117**, 267-276.

Laemmli, U.K. (1970). Cleavage of structural proteins during the assembly of the head of bacteriophage T4. *Nature* **227**, 680-685.

Laird, D.J., von Andrian, U.H., and Wagers, A.J. (2008). Stem cell trafficking in tissue development, growth, and disease. *Cell* **132**, 612-630.

LaPointe, C.F., and Taylor, R.K. (2000). The type 4 prepilin peptidases comprise a novel family of aspartic acid proteases. *J Biol Chem* **275**, 1502-1510.

Leonardy, S., Bulyha, I., and Sogaard-Andersen, L. (2008). Reversing cells and oscillating motility proteins. *Mol Biosyst* **4**, 1009-1014.

Leonardy, S., Freymark, G., Hebener, S., Ellehauge, E., and Sogaard-Andersen, L. (2007). Coupling of protein localization and cell movements by a dynamically localized response regulator in *Myxococcus xanthus*. *EMBO J* **26**, 4433-4444.

Leonardy, S., Miertzchke, M., Bulyha, I., Sperling, E., Wittinghofer, A., and Sogaard-Andersen, L. (*in review*). Regulation of dynamic polarity switching in bacteria by a Ras-like G-protein and its cognate GAP.

Letunic, I., Copley, R.R., Schmidt, S., Ciccarelli, F.D., Doerks, T., Schultz, J., Ponting, C.P., and Bork, P. (2004). SMART 4.0: towards genomic data integration. **32 Database issue**, D142-D144.

Li, S.F., and Shimkets, L.J. (1993). Effect of dsp mutations on the cell-to-cell transmission of CsgA in Myxococcus xanthus. *J Bacteriol* **175**, 3648-3652.

Li, Y., Bustamante, V.H., Lux, R., Zusman, D., and Shi, W. (2005). Divergent regulatory pathways control A and S motility in *Myxococcus xanthus* through FrzE, a CheA-CheY fusion protein. *J Bacteriol* **187**, 1716-1723.

Li, Y., Sun, H., Ma, X., Lu, A., Lux, R., Zusman, D., and Shi, W. (2003). Extracellular polysaccharides mediate pilus retraction during social motility of *Myxococcus xanthus*. *Proc Natl Acad Sci U S A* **100**, 5443-5448.

Lobedanz, S., and Sogaard-Andersen, L. (2003). Identification of the C-signal, a contact-dependent morphogen coordinating multiple developmental responses in *Myxococcus xanthus*. *Genes Dev* **17**, 2151-2161.

Lu, A., Cho, K., Black, W.P., Duan, X.Y., Lux, R., Yang, Z., Kaplan, H.B., Zusman, D.R., and Shi, W. (2005). Exopolysaccharide biosynthesis genes required for social motility in *Myxococcus xanthus*. *Mol Microbiol* **55**, 206-220.

Lybarger, S.R., Johnson, T.L., Gray, M.D., Sikora, A.E., and Sandkvist, M. (2009). Docking and assembly of the type II secretion complex of *Vibrio cholerae*. *J Bacteriol* **191**, 3149-3161.

Mahadevan, L., and Matsudaira, P. (2000). Motility powered by supramolecular springs and ratchets. *Science* **288**, 95-100.

Maier, B., Koomey, M., and Sheetz, M.P. (2004). A force-dependent switch reverses type IV pilus retraction. *Proc Natl Acad Sci U S A* **101**, 10961-10966.

Maier, B., Potter, L., So, M., Long, C.D., Seifert, H.S., and Sheetz, M.P. (2002). Single pilus motor forces exceed 100 pN. *Proc Natl Acad Sci U S A* **99**, 16012-16017.

Martin, P.R., Watson, A.A., McCaul, T.F., and Mattick, J.S. (1995). Characterization of a five-gene cluster required for the biogenesis of type 4 fimbriae in Pseudomonas aeruginosa. *Mol Microbiol* **16**, 497-508.

Mattick, J.S. (2002). Type IV pili and twitching motility. *Ann Rev Microbiol* **56**, 289-314.

Mauriello, E.M., Astling, D.P., Sliusarenko, O., and Zusman, D.R. (2009a). Localization of a bacterial cytoplasmic receptor is dynamic and changes with cell-cell contacts. *Proc Natl Acad Sci U S A* **106**, 4852-4857.

Mauriello, E.M., Mouhamar, F., Nan, B., Ducret, A., Dai, D., Zusman, D.R., and Mignot, T. (2010). Bacterial motility complexes require the actin-like protein, MreB and the Ras homologue, MglA. *EMBO J* **29**, 315-326.

Mauriello, E.M., Nan, B., and Zusman, D.R. (2009b). AglZ regulates adventurous (A-) motility in *Myxococcus xanthus* through its interaction with the cytoplasmic receptor, FrzCD. *Mol Microbiol* **72**, 964-977.

McBride, M.J. (2001). Bacterial gliding motility: multiple mechanisms for cell movement over surfaces. *Annu Rev Microbiol* **55**, 49-75.

McBride, M.J., Weinberg, R.A., and Zusman, D.R. (1989). "Frizzy" aggregation genes of the gliding bacterium *Myxococcus xanthus* show sequence similarities to the chemotaxis genes of enteric bacteria. *Proc Natl Acad Sci U S A* **86**, 424-428.

Merz, A.J., and Forest, K.T. (2002). Bacterial surface motility: slime trails, grappling hooks and nozzles. *Curr Biol* **12**, R297-303.

Merz, A.J., So, M., and Sheetz, M.P. (2000). Pilus retraction powers bacterial twitching motility. *Nature* **407**, 98-102.

Mignot, T. (2007). The elusive engine in *Myxococcus xanthus* gliding motility. *Cell Mol Life Sci* **64**, 2733-2745.

Mignot, T., and Kirby, J.R. (2008). Genetic circuitry controlling motility behaviors of *Myxococcus xanthus*. *Bioessays* **30**, 733-743.

Mignot, T., Merlie, J.P., Jr., and Zusman, D.R. (2005). Regulated pole-to-pole oscillations of a bacterial gliding motility protein. *Science* **310**, 855-857.

Mignot, T., Shaevitz, J.W., Hartzell, P.L., and Zusman, D.R. (2007). Evidence that focal adhesion complexes power bacterial gliding motility. *Science* **315**, 853-856.

Murray, H., and Errington, J. (2008). Dynamic control of the DNA replication initiation protein DnaA by Soj/ParA. *Cell* **135**, 74-84.

Nakasugi, K., Alexova, R., Svenson, C.J., and Neilan, B.A. (2007). Functional analysis of PilT from the toxic cyanobacterium Microcystis aeruginosa PCC 7806. *J Bacteriol* **189**, 1689-1697.

Nariya, H., and Inouye, M. (2008). MazF, an mRNA interferase, mediates programmed cell death during multicellular Myxococcus development. *Cell* **132**, 55-66.

Nudleman, E., Wall, D., and Kaiser, D. (2005). Cell-to-cell transfer of bacterial outer membrane lipoproteins. *Science* **309**, 125-127.

Nudleman, E., Wall, D., and Kaiser, D. (2006). Polar assembly of the type IV pilus secretin in Myxococcus xanthus. *Mol Microbiol* **60**, 16-29.

O'Connor, K.A., and Zusman, D.R. (1991a). Behaviour of peripheral rods and their role in the life cycle of *Myxococcus xanthus*. *Journal of Bacteriology* **173**, 3342-3355.

O'Connor, K.A., and Zusman, D.R. (1991b). Development in *Myxococcus xanthus* involves differentiation into two cell types, peripheral rods and spores. *J Bacteriol* **173**, 3318-3333.

O'Toole, G.A., and Kolter, R. (1998). Flagellar and twitching motility are necessary for *Pseudomonas aeruginosa* biofilm development. *Mol Microbiol* **30**, 295-304.

Okamoto, S., and Ohmori, M. (2002). The cyanobacterial PilT protein responsible for cell motility and transformation hydrolyzes ATP. *Plant Cell Physiol* **43**, 1127-1136.

Overgaard, M., Wegener-Feldbrugge, S., and Sogaard-Andersen, L. (2006). The orphan response regulator DigR is required for synthesis of extracellular matrix fibrils in *Myxococcus xanthus*. *J Bacteriol* **188**, 4384-4394.

Parge, H.E., Forest, K.T., Hickey, M.J., Christensen, D.A., Getzoff, E.D., and Tainer, J.A. (1995). Structure of the fibre-forming protein pilin at 2.6 A resolution. *Nature* **378**, 32-38.

Peabody, C.R., Chung, Y.J., Yen, M.R., Vidal-Ingigliardi, D., Pugsley, A.P., and Saier, M.H., Jr. (2003). Type II protein secretion and its relationship to bacterial type IV pili and archaeal flagella. *Microbiology* **149**, 3051-3072.

Pelicic, V. (2008). Type IV pili: e pluribus unum? *Mol Microbiol* **68**, 827-837.

Pugsley, A.P. (1993). The complete general secretory pathway in Gram-negative bacteria. *Microbiol Rev* **57**, 50-108.

Ramboarina, S., Fernandes, P.J., Daniell, S., Islam, S., Simpson, P., Frankel, G., Booy, F., Donnenberg, M.S., and Matthews, S. (2005). Structure of the bundle-forming pilus from enteropathogenic *Escherichia coli*. *J Biol Chem* **280**, 40252-40260.

Ramer, S.W., Schoolnik, G.K., Wu, C.Y., Hwang, J., Schmidt, S.A., and Bieber, D. (2002). The type IV pilus assembly complex: biogenic interactions among the bundle-forming pilus proteins of enteropathogenic *Escherichia coli*. *J Bacteriol* **184**, 3457-3465.

Robien, M.A., Krumm, B.E., Sandkvist, M., and Hol, W.G. (2003). Crystal structure of the extracellular protein secretion NTPase EpsE of *Vibrio cholerae*. *J Mol Biol* **333**, 657-674.

Rodriguez-Soto, J.P., and Kaiser, D. (1997). Identification and localization of the Tgl protein, which is required for *Myxococcus xanthus* social motility. *J Bacteriol* **179**, 4372-4381.

Roine, E., Raineri, D.M., Romantschuk, M., Wilson, M., and Nunn, D.N. (1998). Characterization of type IV pilus genes in Pseudomonas syringae pv. tomato DC3000. *Mol Plant Microbe Interact* **11**, 1048-1056.

Rosenberg, E., Keller, K.H., and Dworkin, M. (1977). Cell density-dependent growth of *Myxococcus xanthus* on casein. *J Bacteriol* **129**, 770-777.

Rosenbluh, A., Nir, R., Sahar, E., and Rosenberg, E. (1989). Cell-density-dependent lysis and sporulation of Myxococcus xanthus in agarose microbeads. *J Bacteriol* **171**, 4923-4929.

Rumszauer, J., Schwarzenlander, C., and Averhoff, B. (2006). Identification, subcellular localization and functional interactions of PilMNOWQ and PilA4 involved in transformation competency and pilus biogenesis in the thermophilic bacterium Thermus thermophilus HB27. *FEBS J* **273**, 3261-3272.

Sager, B., and Kaiser, D. (1994). Intercellular C-signaling and the traveling waves of *Myxococcus*. *Genes Dev* **8**, 2793-2804.

Sakai, D., Horiuchi, T., and Komano, T. (2001). ATPase activity and multimer formation of PilQ protein are required for thin pilus biogenesis in plasmid R64. *J Biol Chem* **276**, 17968-17975.

Sambrook, J., Fritsch, E.F., and Maniatis, T. (1989). Molecular cloning. A laboratory manual (Cold Spring Harbor, N.Y., Cold Spring Harbor Laboratory Press).

Sampaleanu, L.M., Bonanno, J.B., Ayers, M., Koo, J., Tammam, S., Burley, S.K., Almo, S.C., Burrows, L.L., and Howell, P.L. (2009). Periplasmic domains of *Pseudomonas aeruginosa* PilN and PilO form a stable heterodimeric complex. *J Mol Biol* **394**, 143-159.

Sandkvist, M., Bagdasarian, M., Howard, S.P., and DiRita, V.J. (1995). Interaction between the autokinase EpsE and EpsL in the cytoplasmic membrane is required for extracellular secretion in *Vibrio cholerae*. *Embo J* **14**, 1664-1673.

Saraste, M., Sibbald, P.R., and Wittinghofer, A. (1990). The P-loop--a common motif in ATP- and GTP-binding proteins. *Trends Biochem Sci* **15**, 430-434.

Satyshur, K.A., Worzalla, G.A., Meyer, L.S., Heiniger, E.K., Aukema, K.G., Misic, A.M., and Forest, K.T. (2007). Crystal structures of the pilus retraction motor PilT suggest large domain movements and subunit cooperation drive motility. *Structure* **15**, 363-376.

Savvides, S.N. (2007). Secretion superfamily ATPases swing big. *Structure* **15**, 255-257.

Savvides, S.N., Yeo, H.J., Beck, M.R., Blaesing, F., Lurz, R., Lanka, E., Buhrdorf, R., Fischer, W., Haas, R., and Waksman, G. (2003). VirB11 ATPases are dynamic hexameric assemblies: new insights into bacterial type IV secretion. *Embo J* **22**, 1969-1980.

Scheffzek, K., Ahmadian, M.R., Kabsch, W., Wiesmuller, L., Lautwein, A., Schmitz, F., and Wittinghofer, A. (1997). The Ras-RasGAP complex: structural basis for GTPase activation and its loss in oncogenic Ras mutants. *Science* **277**, 333-338.

Shi, X., Wegener-Feldbrugge, S., Huntley, S., Hamann, N., Hedderich, R., and Sogaard-Andersen, L. (2008). Bioinformatics and experimental analysis of proteins of two-component systems in *Myxococcus xanthus*. *J Bacteriol* **190**, 613-624.

Shimkets, L.J. (1986a). Correlation of energy-dependent cell cohesion with social motility in *Myxococcus xanthus*. *J Bacteriol* **166**, 837-841.

Shimkets, L.J. (1986b). Role of cell cohesion in *Myxococcus xanthus* fruiting body formation. *J Bacteriol* **166**, 842-848.

Shimkets, L.J. (1999). Intercellular signaling during fruiting-body development of Myxococcus xanthus. *Annu Rev Microbiol* **53**, 525-549.

Shimkets, L.J., Gill, R.E., and Kaiser, D. (1983). Developmental cell interactions in *Myxococcus xanthus* and the *spoC* locus. *Proc Natl Acad Sci USA* **80**, 1406-1410.

Shimkets, L.J., and Kaiser, D. (1982). Induction of coordinated movement of *Myxococcus xanthus* cells. *J Bacteriol* **152**, 451-461.

Shiue, S.J., Kao, K.M., Leu, W.M., Chen, L.Y., Chan, N.L., and Hu, N.T. (2006). XpsE oligomerization triggered by ATP binding, not hydrolysis, leads to its association with XpsL. *EMBO J* **25**, 1426-1435.

Skerker, J.M., and Berg, H.C. (2001). Direct observation of extension and retraction of type IV pili. *Proc Natl Acad Sci USA* **98**, 6901-6904.

Sliusarenko, O., Neu, J., Zusman, D.R., and Oster, G. (2006). Accordion waves in Myxococcus xanthus. *Proc Natl Acad Sci U S A* **103**, 1534-1539.

Sliusarenko, O., Zusman, D.R., and Oster, G. (2007). The motors powering A-motility in *Myxococcus xanthus* are distributed along the cell body. *J Bacteriol* **189**, 7920-7921.

Søgaard-Andersen, L. (2004). Cell polarity, intercellular signalling and morphogenetic cell movements in *Myxococcus xanthus*. *Curr Opin Microbiol* **7**, 587-593.

Sogaard-Andersen, L., Slack, F.J., Kimsey, H., and Kaiser, D. (1996). Intercellular C-signaling in *Myxococcus xanthus* involves a branched signal transduction pathway. *Genes Dev* **10**, 740-754.

Soto, G.E., and Hultgren, S.J. (1999). Bacterial adhesins: common themes and variations in architecture and assembly. *J Bacteriol* **181**, 1059-1071.

Spormann, A.M. (1999). Gliding motility in bacteria: insights from studies of *Myxococcus xanthus*. *Microbial Mol Biol Rev* **63**, 621-641.

Stephens, K., Hartzell, P., and Kaiser, D. (1989). Gliding motility in *Myxococcus xanthus*: *mgl* locus, RNA, and predicted protein products. *J Bacteriol* **171**, 819-830.

Sun, H., Zusman, D.R., and Shi, W. (2000). Type IV pilus of *Myxococcus xanthus* is a motility apparatus controlled by the frz chemosensory system. *Curr Biol* **10**, 1143-1146.

Szurmant, H., Muff, T.J., and Ordal, G.W. (2004). *Bacillus subtilis* CheC and FliY are members of a novel class of CheY-P-hydrolyzing proteins in the chemotactic signal transduction cascade. *J Biol Chem* **279**, 21787-21792.

Thomasson, B., Link, J., Stassinopoulos, A.G., Burke, N., Plamann, L., and Hartzell, P.L. (2002). MglA, a small GTPase, interacts with a tyrosine kinase to control type IV pili-mediated motility and development of *Myxococcus xanthus*. *Mol Microbiol* **46**, 1399-1413.

Tripathi, S.A., and Taylor, R.K. (2007). Membrane association and multimerization of TcpT, the cognate ATPase ortholog of the *Vibrio cholerae* toxin-coregulated-pilus biogenesis apparatus. *J Bacteriol* **189**, 4401-4409.

Varley, A.W., and Stewart, G.C. (1992). The *divIVB* region of the *Bacillus subtilis* chromosome encodes homologs of *Escherichia coli* septum placement (*minCD*) and cell shape (*mreBCD*) determinants. *J Bacteriol* **174**, 6729-6742.

Vetter, I.R., and Wittinghofer, A. (2001). The guanine nucleotide-binding switch in three dimensions. *Science* **294**, 1299-1304.

Vlamakis, H., Aguilar, C., Losick, R., and Kolter, R. (2008). Control of cell fate by the formation of an architecturally complex bacterial community. *Genes Dev* **22**, 945-953.

Wall, D., and Kaiser, D. (1999). Type IV pili and cell motility. *Mol Microbiol* **32**, 01-10.

Wall, D., Kolenbrander, P.E., and Kaiser, D. (1999). The *Myxococcus xanthus pilQ (sglA*) gene encodes a secretin homolog required for type IV pilus biogenesis, social motility, and development. *J Bacteriol* **181**, 24-33.

Wall, D., Wu, S.S., and Kaiser, D. (1998). Contact stimulation of Tgl and type IV pili in *Myxococcus xanthus*. *J Bacteriol* **180**, 759-761.

Ward, M.J., Lew, H., and Zusman, D.R. (2000). Social motility in *Myxococcus xanthus* requires FrzS, a protein with an extensive coiled-coil domain. *Mol Microbiol* **37**, 1357-1371.

Ward, M.J., and Zusman, D.R. (1997). Regulation of directed motility in *Myxococcus xanthus. Mol Microbiol* **24**, 885-893.

Welch, R., and Kaiser, D. (2001). Pattern formation and traveling waves in myxobacteria: Experimental demonstration. *Proc Natl Acad Sci USA* **98**, 14907-14912.

Wireman, J.W., and Dworkin, M. (1977). Developmentally induced autolysis during fruiting body formation by *Myxococcus xanthus*. *J Bacteriol* **129**, 798-802.

Wolfgang, M., Lauer, P., Park, H.S., Brossay, L., Hebert, J., and Koomey, M. (1998). PilT mutations lead to simultaneous defects in competence for natural transformation and twitching motility in piliated *Neisseria gonorrhoeae*. *Mol Microbiol* **29**, 321-330.

Wolfgang, M., van Putten, J.P., Hayes, S.F., Dorward, D., and Koomey, M. (2000). Components and dynamics of fiber formation define a ubiquitous biogenesis pathway for bacterial pili. *Embo J* **19**, 6408-6418.

Wolgemuth, C., Hoiczyk, E., Kaiser, D., and Oster, G. (2002). How myxobacteria glide. *Curr Biol* **12**, 369-377.

Wolgemuth, C.W., and Oster, G. (2004). The junctional pore complex and the propulsion of bacterial cells. *J Mol Microbiol Biotechnol* **7**, 72-77.

Wu, S.S., and Kaiser, D. (1995). Genetic and functional evidence that Type IV pili are required for social gliding motility in *Myxococcus xanthus*. *Mol Microbiol* **18**, 547-558.

Wu, S.S., and Kaiser, D. (1996). Markerless deletions of *pil* genes in *Myxococcus xanthus* generated by counterselection with the *Bacillus subtilis sacB* gene. *J Bacteriol* **178**, 5817-5821.

Wu, S.S., Wu, J., and Kaiser, D. (1997). The *Myxococcus xanthus pilT* locus is required for social gliding motility although pili are still produced. *Mol Microbiol* **23**, 109-121.

Yang, R., Bartle, S., Otto, R., Stassinopoulos, A., Rogers, M., Plamann, L., and Hartzell, P. (2004). AglZ is a filament-forming coiled-coil protein required for adventurous gliding motility of *Myxococcus xanthus*. *J Bacteriol* **186**, 6168-6178.

Yang, Z., Duan, X., Esmaeiliyan, M., and Kaplan, H.B. (2008). Composition, structure, and function of the *Myxococcus xanthus* cell envelope. In *Myxobacteria: Multicellularity and Differentiation*, W. DE, ed. (ASM Press, Washington, DC).

Yang, Z., Geng, Y., Xu, D., Kaplan, H.B., and Shi, W. (1998). A new set of chemotaxis homologues is essential for *Myxococcus xanthus* social motility. *Mol Microbiol* **30**, 1123-1130.

Yang, Z., Ma, X., Tong, L., Kaplan, H.B., Shimkets, L.J., and Shi, W. (2000). *Myxococcus xanthus dif* genes are required for biogenesis of cell surface fibrils essential for social gliding motility. *J Bacteriol* **182**, 5793-5798.

Yeo, H.J., Savvides, S.N., Herr, A.B., Lanka, E., and Waksman, G. (2000). Crystal structure of the hexameric traffic ATPase of the *Helicobacter pylori* type IV secretion system. *Mol Cell* **6**, 1461-1472.

Yoshida, T., Kim, S.R., and Komano, T. (1999). Twelve *pil* genes are required for biogenesis of the R64 thin pilus. *J Bacteriol* **181**, 2038-2043.

Youderian, P. (1998). Bacterial motility: secretory secrets of gliding bacteria. *Curr Biol* **8**, R408-411.

Youderian, P., Burke, N., White, D.J., and Hartzell, P.L. (2003). Identification of genes required for adventurous gliding motility in *Myxococcus xanthus* with the transposable element mariner. *Mol Microbiol* **49**, 555-570.

Yu, R., and Kaiser, D. (2007). Gliding motility and polarized slime secretion. *Mol Microbiol* **63**, 454-467.

Zusman, D.R. (1982). "Frizzy" mutants: a new class of aggregation-defective developmental mutants of *Myxococcus xanthus*. *J Bacteriol* **150**, 1430-1437.

Zusman, D.R., and McBride, M.J. (1991). Sensory transduction in the gliding bacterium *Myxococcus xanthus*. *Mol Microbiol* **5**, 2323-2329.

Zusman, D.R., Scott, A.E., Yang, Z., and Kirby, J.R. (2007). Chemosensory pathways, motility and development in *Myxococcus* xanthus. *Nat Rev Microbiol* **5**, 862-872.

Acknowledgments

I would like to express my sincere gratitude to my supervisor, Prof. MD, PhD Lotte Søgaard-Andersen not only for her guidance and advice throughout my research, but above all for her constructive criticism prompting my academic advancement.

I am deeply indebted to my thesis and defense committee members, Prof. Dr. Martin Thanbichler, Prof. Dr. Michael Feldbrügge, Prof. Dr. Uwe Maier, Dr. Kai Thormann, and Prof. Dr. Gero Steinberg for their time and valuable suggestions from which I have benefited. Especially I would like to thank Prof. Dr. Martin Thanbichler for his time in reviewing this work and for all the productive discussions during my research.

My sincere thanks go to Dr. Simone Leonardy, Dr. Kryssia Aguiluz and Edina Hot for crucial comments on my thesis, helpful discussions and support during my stay here. I would also wish to make a grateful acknowledgment to Carmen Schmidt for producing anti-PilM and anti-PilN antibodies and all her contribution on my work.

I would like to thank our collabotarors Prof. Dr. Berenike Maier for giving me an opportunity to carry out FRAP experiments in her lab and Andrea Höne for her excellent assistance with FRAP experiments.

I am grateful to International Max Planck Research School for Environmental, Cellular and Molecular Microbiology and the Intra- and Intercellular Transport and Communication Research School for providing financial support during my research. I would like to extend my thanks to Susanne Rommel and Christian Bengelsdorff for taking care of all the documents and helping so much during my stay in Marburg.

I would like to gratefully acknowledge all colleagues from Department of Ecophysiology for providing a friendly working environment. I am especially indebted to the people in our lab including previous lab members, who gave so much assistance and enjoyable time during my stay.

In a special way I would like to thank all my friends, particularly Simone, Yuliya and Christian for their understanding and enormous support. Finally, I would like to take this opportunity to thank my mom for her endless love and faith in me, which encourage me every day.

Curriculum Vitae

Personal data

Name	Iryna M. Bulyha
Date of birth	June 23rd 1983
Place of birth	Minsk, Belarus

Education

10/2006 – 03/2010	PhD (Dr. rer. nat.) Philipps-University Marburg Max-Planck-Institute for Terrestrial Microbiology, Marburg, Germany Supervisor: Prof. MD, PhD Lotte Søgaard-Andersen PhD thesis: Regulation of type IV pili localization in *Myxococcus xanthus*
09/2005 – 09/2006	Master of natural sciences Subjects: Genetics & Microbiology Belarusian State University, Minsk, Belarus Faculty of Biology, Department of Genetics Supervisor: Prof. Dr. Marina A. Titok Master thesis: Characteristics of naphthalene-utilizing bacteria, isolated on the territory of Belarus
09/2000 – 06/2005	Diploma of Biologist Subjects: Biology & Chemistry Belarusian State University, Minsk, Belarus Faculty of Biology, Department of Genetics Supervisor: Prof. Dr. Marina A. Titok Diploma thesis: Description of Nah-plasmids from natural strains of *Pseudomonas*
06/1996-05/2000	High school certificate Jacub Kolas National State Lyceum for Humanities, Minsk, Belarus

List of publications:

Leonardy S., Miertzschke M., **Bulyha I.**, Sperling E., Wittinghofer A., Søgaard-Andersen L., (2010) Regulation of dynamic polarity switching in bacteria by a Ras-like G-protein and its cognate GAP. *in review*

Bulyha I., Schmidt C., Lenz P., Jakovljevic V., Höne A., Maier B., Hoppert M., , Søgaard-Andersen L., (2009) Regulation of the type IV pili molecular machine by dynamic localization of two motor proteins. *Mol Microbiol.* 74: 691-706.

Leonardy, S., **Bulyha I**., Søgaard-Andersen L., (2008) Reversing cells and oscillating motility proteins. *Mol Biosyst* 4: 1009-1014.

Leuchuk AA, **Bulyga IM**, Izmalkova TIu, Sevast'ianovich IaR, Kosheleva IA, Thomas CM, Titok MA (2006) Nah plasmids of the IncP-9 group in natural *Pseudomonas* strains. Mol Biol (Mosk) 40: 835-843. Russian

Leuchuk AA, Vasilenko SL, **Bulyga IM**, Titok MA, Thomas KM (2005) Characteristics of natural strains of naphthalene-utilizing bacteria of the genus *Pseudomonas*. Izv Akad Nauk Ser Biol 2, 162-167. Russian

Erklärung

Hiermit versichere ich, dass ich die vorliegende Dissertation mit dem Titel „Regulation of type IV pili localization in *Myxococcus xanthus*“ selbstständig verfasst, keine anderen als die im Text angegebenen Hilfsmittel verwendet und sämtliche Stellen, die im Wortlaut oder dem Sinn nach anderen Werken entnommen sind, mit Quellenangaben kenntlich gemacht habe.

Die Dissertation wurde in der jetzigen oder einer ähnlichen Form noch bei keiner anderen Hochschule eingereicht und hat noch keinen sonstigen Prüfungszwecken gedient.

Iryna Bulyha

Ort, Datum

Einverständniserklärung

Ich erkläre mich damit einverstanden, dass die vorliegende Dissertation

Regulation of type IV pili localization in *Myxococcus xanthus*

in Bibliotheken allgemein zugänglich gemacht wird. Dazu gehört, dass sie

- von der Bibliothek der Einrichtung, in der ich meine Arbeit anfertigt habe, zur Benutzung in ihren Räumen bereit gehalten wird;
- in konventionellen und maschinenlesbaren Katalogen, Verzeichnissen und Datenbanken verzeichnet wird;
- im Rahmen der urheberrechtlichen Bestimmungen für Kopierzwecke genutzt werden kann.

Marburg, den

(Unterschrift des Autors) (Unterschrift des betreuendenHochschullehrers)